

Electronic Thesis and Dissertation Repository

---

7-12-2012 12:00 AM

## Brain connectivity studied by fMRI: homologous network organization in the rat, monkey, and human

R. Matthew Hutchison, *The University of Western Ontario*

Supervisor: Dr. L. Stan Leung, *The University of Western Ontario*

Joint Supervisor: Dr. Seyed M. Mirsattari, *The University of Western Ontario*

A thesis submitted in partial fulfillment of the requirements for the Doctor of Philosophy degree in Neuroscience

© R. Matthew Hutchison 2012

Follow this and additional works at: <https://ir.lib.uwo.ca/etd>



Part of the [Systems Neuroscience Commons](#)

---

### Recommended Citation

Hutchison, R. Matthew, "Brain connectivity studied by fMRI: homologous network organization in the rat, monkey, and human" (2012). *Electronic Thesis and Dissertation Repository*. 637.  
<https://ir.lib.uwo.ca/etd/637>

This Dissertation/Thesis is brought to you for free and open access by Scholarship@Western. It has been accepted for inclusion in Electronic Thesis and Dissertation Repository by an authorized administrator of Scholarship@Western. For more information, please contact [wlsadmin@uwo.ca](mailto:wlsadmin@uwo.ca).

BRAIN CONNECTIVITY STUDIED BY FMRI: HOMOLOGOUS NETWORK  
ORGANIZATION IN THE RAT, MONKEY, AND HUMAN

(Spine title: Functional network homologies of the rat, monkey, and human)

(Thesis format: Integrated Article)

by

R. Matthew Hutchison

Graduate Program in Neuroscience

A thesis submitted in partial fulfillment  
of the requirements for the degree of  
Doctor of Philosophy

The School of Graduate and Postdoctoral Studies  
The University of Western Ontario  
London, Ontario, Canada

© R. Matthew Hutchison 2012

**CERTIFICATE OF EXAMINATION**

Supervisors

Examiners

\_\_\_\_\_  
Dr. L. Stan Leung

\_\_\_\_\_  
Dr. Bruce Morton

\_\_\_\_\_  
Dr. Seyed M. Mirsattari

\_\_\_\_\_  
Dr. Stefan Köhler

Supervisory Committee

\_\_\_\_\_  
Dr. Charles McKenzie

\_\_\_\_\_  
Dr. Rob Bartha

\_\_\_\_\_  
Dr. Daniel Margulies

\_\_\_\_\_  
Joseph S. Gati

\_\_\_\_\_  
Dr. Stefan Everling

The thesis by

**R. Matthew Hutchison**

entitled:

**Brain connectivity studied by fMRI: homologous network  
organization in the rat, monkey, and human**

is accepted in partial fulfillment of the  
requirements for the degree of  
**Doctor of Philosophy**

\_\_\_\_\_  
Date

\_\_\_\_\_  
Chair of the Thesis Examination Board

# Abstract

The mammalian brain is composed of functional networks operating at different spatial and temporal scales — characterized by patterns of interconnections linking sensory, motor, and cognitive systems. Assessment of brain connectivity has revealed that the structure and dynamics of large-scale network organization are altered in multiple disease states suggesting their use as diagnostic or prognostic indicators. Further investigation into the underlying mechanisms, organization, and alteration of large-scale brain networks requires homologous animal models that would allow neurophysiological recordings and experimental manipulations. My current dissertation presents a comprehensive assessment and comparison of rat, macaque, and human brain networks based on evaluation of intrinsic low-frequency fluctuations of the blood oxygen-level-dependent (BOLD) fMRI signal. The signal fluctuations, recorded in the absence of any task paradigm, have been shown to reflect anatomical connectivity and are presumed to be a hemodynamic manifestation of slow fluctuations in neuronal activity. Importantly, the technique circumvents many practical limitations of other methodologies and can be compared directly between multiple species. Networks of all species were found underlying multiple levels of sensory, motor, and cognitive processing. Remarkable homologous functional connectivity was found across all species, however network complexity was dramatically increased in primate compared to rodent species. Spontaneous temporal dynamics of the resting-state networks were also preserved across species. The results demonstrate that rats and macaques share remarkable homologous network organization with humans, thereby providing strong support for their use as an animal model in the study of normal and abnormal brain connectivity as well as aiding the interpretation of electrophysiological recordings within the context of large-scale brain networks.

**Keywords:** functional connectivity, resting-state, fMRI, animal models, networks, macaque, rat, homology, network dynamics.

## Co-Authorship

The current thesis contains published material that has been co-authored by R. Matthew Hutchison, L. Stan Leung, Seyed M. Mirsattari, Stefan Everling, Joseph S. Gati, Ravi S. Menon, Craig K. Jones, and Thilo Womelsdorf. Dr. Leung and Dr. Mirsattari served as supervisors throughout the completion of all projects contained within this thesis dissertation (e.g. experimental design, data analysis, interpretation, writing of manuscripts). In addition, Dr. Everling and Dr. Menon served an additional supervisory role in Projects 2 and 3 (Chapters 3 and 4), respectively. Dr. Jones helped with computer programming necessary for data analysis in all projects. Dr. Womelsdorf assisted with data analysis strategies and interpretation for Project 3 (Chapter 4). Mr. Gati was instrumental in data collection for all projects. All project authors provided assistance in editing and revising early versions of the submitted manuscripts. The written material in this thesis represents my own work, but, as my advisors, Dr. Leung and Dr. Mirsattari provided assistance in editing and revising all of the material contained within this thesis.

## Epigraph

It makes no sense to read a newspaper with a microscope.

-Valentino Braitenberg, neuroanatomist

## Dedication

To my wife and parents, for letting me live out my dream to become a doctor –  
“the research kind”

## Acknowledgments

My years completing this doctorate degree have been filled with both challenges and conquests - doubt and discovery. In this time I have transformed from a naive and wide-eyed undergraduate into a naive and wide-eyed scientist. I am grateful to all those who have lead and walked beside me on this academic journey. I owe them everything because without them it would not have been possible.

It is with the utmost gratitude that I thank Dr. Leung who gave me the opportunity to step out of the lecture room and into the laboratory. His pursuit of excellence has motivated me to do more than I thought possible. To deal with my over-zealous ambitions Stan recruited Dr. Mirsattari to be my co-supervisor, a clinician and scientist that opened the doors to the imaging research that I was so eager to pursue. Both allowed me the freedom to explore my diverse interests that included work with mice, rats, monkeys, and humans. I believe their greatest difficulty was not keeping me interested in my project, but keeping me focused on only one of them. I thank you both.

Journeying into the world of functional imaging at Robarts Research Institute, I met colleagues that fulfilled the roles not only of collaborators, but friends and mentors. Each put up with incessant questions about life and research, though at this point the line between the two is almost transparent. It will be difficult to conduct research anywhere else. I hope the work presented here warrants their time and dedication. Joe “the Magician” Gati is Robarts’ secret weapon and catalyst for all things imaging; my success hung in the balance of his technical wizardry. Craig Jones took me under his wing during the early days when everything seemed impossible. He instilled in me a confidence in signal processing that I never thought possible with no previous computer skills. Stefan Everling first introduced me to monkey research and later became my career coach. The advice he has given me is truly invaluable (though I am sure we could try to negotiate a price...). Ravi Menon, a tough love principal investigator with a knack for exposing false assumptions and inadequate analysis, has helped prepare me for the challenges ahead on the academic battleground. Thilo Womelsdorf’s enthusiasm for research has been infectious and I hope we can continue to collaborate.

I would like to acknowledge my advisory committee members and comprehensive examiners not included above, Dr. Rob Bartha, Dr. Raj Rajakumar, Dr. Paul Gribble, and Dr. Rick? McLachlan. I have learned so much from all you and appreciate your support. This is particularly true of Dr. Gribble. The lessons we covered are applied within this thesis and all of my ongoing projects. If there is a question he does not know the answer too, I still have not found it.

Fighting can break apart a group, though when training to fight, it can bring turn a group into a family. I wish to thank my teammates and coaches, both at Team Tompkins/Adrenaline Training Centre and Western Varsity Wrestling for countless hours of training, numerous bruises, and a few scars. It is my time here that has defined me as a person and given me the confidence to succeed in all aspects of my life.

I thank my rock, my light, my wife - Melina Hutchison. Though you would probably much rather have an apology for all the late-night Robarts trips, non-stop research talk, and an inability to go an entire day without making it abundantly clear I am a science geek. I love you. This love also extends to my two beagles, Soda Pop and Kingsley, the only ones that cannot judge a person for staying home on Friday nights to run pilot analysis in order to add another project to the list.

And finally, I would like to acknowledge those that were there from the very beginning, Mom and Dad. You gave me the opportunity to be whatever I wanted to be. I am where I want to be, I made it because of you. I love you both.

# Table of Contents

<b>CERTIFICATE OF EXAMINATION</b> .....	ii
Abstract.....	iii
Co-Authorship .....	iv
Epigraph .....	v
Dedication.....	vi
Acknowledgments .....	vii
Table of Contents .....	ix
List of Tables .....	xiv
List of Figures.....	xv
List of Appendices.....	xxxiv
List of Abbreviations .....	xxxv
Chapter 1 .....	1
1 General Introduction .....	1
1.1 Preamble .....	1
1.1.1 Why study the brain?.....	1
1.1.2 Focus and scale.....	1
1.2 Networks.....	4
1.2.1 Graph theory .....	7
1.2.2 Complex networks.....	10
1.3 Brain networks.....	13
1.4 Brain Connectivity.....	16
1.5 Network communication: Oscillations and synchrony.....	19
1.6 Methodologies .....	20
1.7 Resting-state fMRI (RS-fMRI).....	24

1.7.1	Resting-state signal.....	29
1.7.1.1	Correlate.....	30
1.7.2	Methodology.....	31
1.7.2.1	Seed-region analysis.....	32
1.7.2.2	Independent component analysis (ICA).....	32
1.7.3	Resting-state networks (RSNs).....	34
1.7.4	The relationship between function and structure.....	38
1.7.5	Applying graph analysis to resting-state fMRI .....	39
1.7.6	Resting-state networks and disease .....	40
1.8	Resting-state investigations of animal models .....	42
1.9	Summary and current projects.....	43
1.10	References .....	45
Chapter 2 .....		60
2	<b>Functional Networks in the Anesthetized Rat Brain Revealed by Independent Component Analysis of Resting-State fMRI.....</b>	<b>60</b>
2.1	Introduction .....	60
2.2	Methods .....	62
2.2.1	Animal usage and preparation.....	62
2.2.2	MRI acquisition .....	63
2.2.3	Image analysis .....	64
2.3	Results .....	65
2.4	Discussion.....	73
2.4.1	Connectivity patterns.....	75
2.4.2	Anesthesia.....	79
2.4.3	Physiological fluctuations .....	80
2.5	Conclusions .....	80

2.6	References .....	81
Chapter 3	.....	87
3	Resting-state networks in the macaque at 7 T .....	87
3.1	Introduction .....	87
3.2	Methods .....	89
3.2.1	Animal preparation .....	89
3.2.2	Data acquisition .....	90
3.2.3	Image preprocessing .....	91
3.2.4	Group independent component analysis .....	91
3.2.5	RSN identification and visualization .....	93
3.2.6	Single-subject ICA .....	95
3.2.7	Functional network connectivity .....	95
3.3	Results .....	95
3.3.1	Resting-state networks .....	95
3.3.2	Single subject ICA .....	104
3.3.3	Functional network connectivity .....	113
3.4	Discussion .....	115
3.5	Conclusions .....	120
3.6	References .....	121
Chapter 4	.....	129
4	Resting-state networks show dynamic functional connectivity in awake humans and anesthetized macaques .....	129
4.1	Introduction .....	129
4.2	Methods .....	132
4.2.1	Macaque monkeys .....	132
4.2.1.1	Data acquisition and preprocessing of monkey scans .....	133

4.2.1.2	Oculomotor network identification in monkeys .....	134
4.2.1.3	Ventral premotor network identification in monkeys .....	136
4.2.2	Human participants .....	136
4.2.2.1	Data acquisition and preprocessing of human scans .....	137
4.2.2.2	Oculomotor network identification in humans .....	138
4.2.3	Sliding window correlation analysis .....	140
4.2.4	Graph analysis .....	140
4.3	Results .....	141
4.3.1	Monkey OCM and vPM network identification .....	141
4.3.2	Human OCM network identification .....	148
4.3.3	Transient network states .....	152
4.3.4	Fluctuating connectivity dynamics during awake and anaesthetized states .....	163
4.3.5	Hyper-synchronization .....	168
4.4	Discussion .....	177
4.4.1	Dynamic RSN connectivity occurs in the absence of cognition .....	177
4.4.2	Electrophysiological correlates .....	179
4.4.3	Anti-correlations .....	183
4.4.4	Evolutionarily preserved mechanism .....	183
4.4.5	Controls and limitations .....	184
4.4.6	Implications for future work .....	186
4.5	Conclusions .....	187
4.6	References .....	187
Chapter 5	.....	199
5	General discussion .....	199
5.1	Comparative biology .....	200

5.2 Homologous connectivity patterns .....	205
5.2.1 Fronto-parietal networks .....	210
5.2.2 Default-mode network .....	215
5.2.3 Expanding network investigations .....	222
5.2.4 Summary of comparative biology .....	224
5.3 The relationship between function and structure revisited .....	226
5.4 Function of spontaneous fluctuations and synchronization .....	231
5.5 Anesthesia and States .....	233
5.6 Future Directions .....	234
5.7 Conclusions .....	237
5.8 References .....	237
Appendix A: Documentation of Ethics Approval. ....	248
Appendix B: Permissions from Publishers .....	251
Curriculum Vitae .....	261

## List of Tables

Table 1.1. Network Measures.....	8
Table 2.1. Number of rats in isoflurane and ketamine/xylazine anesthesia groups that had independent spatial components corresponding to anatomical locations (Paxinos & Watson, 1986) in both hemispheres (bilaterally synchronous), or in the left or right hemisphere. ....	68
Table 2.2. Distribution of rats (N=20, combining 10 rats under isoflurane and 10 under ketamine/xylazine anesthetic) that had unilateral and bilateral components corresponding to anatomical locations (Paxinos & Watson, 1986). ....	69
Table 2.3. Previously identified resting-state networks of the rat corresponding to anatomical locations (Paxinos & Watson, 1986). ....	74
Table 3.1. Spatial correlations of single subject ICA derived networks to group-ICA derived networks.....	112

## List of Figures

- Figure 1.1. The multiple levels of brain organization. .... 3
- Figure 1.2. Wiring diagrams for complex networks across multiple disciplines. A. Food web of Little Rock Lake, Wisconsin, currently the largest food web in the primary literature. Nodes are functionally distinct ‘trophic species’ containing all taxa that share the same set of predators and prey. Height indicates trophic level with mostly phytoplankton at the bottom and fishes at the top. Cannibalism is shown with self-loops, and omnivory (feeding on more than one trophic level) is shown by different coloured links to consumers. B. New York State electric power grid. Generators and substations are shown as small blue bars. The lines connecting them are transmission lines and transformers. Line thickness and colour indicate the voltage level: red, 765 kV and 500 kV; brown, 345 kV; green, 230 kV; grey, 138 kV and below. Pink dashed lines are transformers. C. Connectivity backbone of human brain. Kamada-Kawai force-spring layout of the connectivity backbone. Labels indicating anatomical subregions are placed at their respective centers of mass. Nodes (individual ROIs) are coded according to strength and edges are coded according to connection weight. D. A portion of the molecular interaction map for the regulatory network that controls the mammalian cell cycle. Colours indicate different types of interactions: black, binding interactions and stoichiometric conversions; red, covalent modifications and gene expression; green, enzyme actions; blue, stimulations and inhibitions. Modified with permission from Kohn, 1999; Strogatz, 2001; Hagmann et al., 2008. .... 6
- Figure 1.3. Features of a graph upon which network topology is assessed. Measures of integration are based on shortest path lengths (green), while measures of segregation are often based on triangle counts (blue) but also include more sophisticated decomposition into modules (ovals). Measures of centrality may be based on node degree (red) or on the length and number of shortest paths between nodes. Hub nodes (black) often lie on a high number of shortest paths and consequently often have high betweenness centrality. Patterns of local

connectivity are quantified by network motifs (yellow). An example three-node and four-link anatomical motif contains six possible functional motifs, of which two are shown—one motif containing dashed links, and one motif containing crossed links. Modified with permission from Rubinov & Sporns, 2010. ....9

Figure 1.4. The emergence of small world networks. (A) A random rewiring procedure starts with a regular ring lattice with edges connecting node with probability  $p$ . As  $p$  increases, the graph becomes increasingly disordered until for  $p = 1$ , all edges are rewired randomly. For intermediate values of  $p$ , the graph is a small-world network: highly clustered like a regular graph, yet with small characteristic path length, like a random graph. (B) The characteristic path length  $L(p)$  and clustering coefficient  $C(p)$  for the family of randomly rewired graphs described in A. Note that a logarithmic ..... 11

Figure 1.5. Parcellation of the human cortex. Lateral views of (A) Gall’s phrenology map and cytoarchitecture cortical maps of (B) Brodmann, (C) von Economo and Koskinas, and (D) Sarkisov. Modified with permission from Zilles & Amunts, 2010. Original images from Phillips & Hunt 1879; Brodmann, 1910; von Economo & Koskinas, 1925; Sarkisov, Filimonoff & Preobrashenskaya, 1949. .... 14

Figure 1.6. Structural connectivity of human (A) and monkey (B) brain. A. Dorsal and lateral views of the human connectivity backbone. Labels indicating anatomical subregions are placed at their respective centers of mass. Nodes (individual ROIs) are coded according to strength and edges are coded according to connection weight. B. Macaque brain long-distance network in which each vertex of the network corresponds to a brain region in the hierarchical brainmap and each edge encodes the presence of long-distance connection between corresponding brain regions. A colorwheel is used for better discrimination amongst brain regions. Modified with permission from Hagmann et al., 2008 and Modha & Singh, 2010. .... 18

Figure 1.7. Neuroscience techniques differ in their spatial and temporal resolution. Functional MRI provides a good balance of spatial and temporal resolution and thus is appropriate for a wide range of experimental questions. Other approaches,

including electrophysiology, lesion studies, and drug manipulations, can provide complementary information. Reprinted with permission from Huettel, Song, & McCarthy, 2004. ....22

Figure 1.8. Traditional fMRI analysis and BOLD noise. Unaveraged blood oxygen level dependent (BOLD) time course (magenta) from a region in the primary visual cortex during a simple task paradigm that requires subjects to open and close their eyes. The paradigm is shown in blue (delayed to account for the hemodynamic response). Traditional functional magnetic resonance imaging (fMRI) analysis involves correlating BOLD data with a stimulation time-course across multiple blocks. This in effect averages across each condition and performs a subtraction, minimizing ‘noise’ in the BOLD signal and highlighting regions that are modulated by the task paradigm. In this case, subtraction of the eyes-closed condition from the eyes-open condition identifies a BOLD signal intensity difference in the primary visual cortex (shown below). Modified with permission from Fox & Raichle, 2007. ....25

Figure 1.9. The first comparison of task-based and resting-state functional maps. A. fMRI task-activation response to bilateral left and right finger movement, superimposed on an anatomical image. B. Correlation map derived using a resting-state scan. Red is positive correlation, and yellow is negative. Reprinted with permission from Biswal, Yetkin, Haughton, & Hyde, 1995. ....28

Figure 1.10. Eight of the most common and consistent RSNs identified by ICA. Sagittal, coronal, and axial views of different spatial maps associated with low-frequency resting patterns estimated from a group of 10 subjects. All images have been coregistered into the space of the MNI template. The coordinates refer to mm distances from the anterior commissure and images are shown in radiological convention. Reprinted with permission from Beckmann, DeLuca, Devlin, & Smith, 2005. ....36

Figure 2.1. Homologous resting-state networks of representative isoflurane and ketamine/xylazine (Ket/Xy) anesthetized rats derived using independent component analysis (ICA) of blood-oxygen-level-dependent (BOLD) functional

time courses overlaid on the respective anatomical images (Paxinos and Watson 1986). Except for the hypothalamus, horizontal slices were obtained from 1 rat, anesthetized with isoflurane or Ket/Xy, with distance (mm) ventral to bregma shown in the left lower corner. The hypothalamus component map was derived from a different rat for each anesthetic, and is displayed in a coronal orientation referenced posterior to bregma (mm), to allow better anatomical localization. Reprinted with permission from Hutchison, Mirsattari, Jones, Gati, & Leung (2010)..... 67

Figure 2.2. Frequency analysis of the hippocampus component isolated by independent component analysis in a representative rat under isoflurane anesthesia, showing spatial connectivity map (A), time course (B), time-frequency analysis of the time course (C), and amplitude spectrum in arbitrary units (a.u.) of the entire time course (D). Reprinted with permission from Hutchison, Mirsattari, Jones, Gati, & Leung (2010). ..... 71

Figure 2.3. Resting-state connectivity of representative ketamine/xylazine (Ket/Xy; rats 1 and 2) and isoflurane (rats 3 and 4) anesthetized rats derived using seed-region analysis. Cross-correlation coefficient (CCC) maps were calculated by correlating the time course of all voxels with the average time course of a spherical seed region (0.5 mm radius) in the medial frontal cortex (MFC; A), primary somatosensory cortex (SSI; B), hippocampus (Hp; C), caudate-putamen (CPu; D), thalamus (Th; E), or hypothalamus (Ht; F). Different CCC thresholds were used for each image, as indicated by the color bar below each image. Coronal images are displayed and distance (mm) from bregma is shown at the right lower corner of each image (positive anterior, negative posterior to bregma). Reprinted with permission from Hutchison, Mirsattari, Jones, Gati, & Leung (2010)..... 72

Figure 2.4. Spatially asymmetrical cortical resting-state networks derived using independent component analysis of BOLD functional time courses overlaid on the respective anatomical images (Paxinos and Watson, 1986). Left or right network dominance (defined as the hemisphere with the greater voxel spatial extent) in four rats is

shown to vary within animals (columns), within networks (rows), and within anesthesia groups (isoflurane anesthetized animal in the two left columns; ketamine/xylazine anesthetized animals in the two right columns). The distance of the slice (mm) ventral to bregma is shown in the left lower corner. Reprinted with permission from Hutchison, Mirsattari, Jones, Gati, & Leung (2010). ..... 78

Figure 3.1. Cerebrospinal fluid related artifact decomposed from resting-state functional data using independent component analysis. Overlaid color maps represent thresholded z-scores displayed on the MR image of the F99 atlas (Van Essen, 2004; see <http://sumsdb.wustl.edu.proxy1.lib.uwo.ca:2048/sums/macaquemore.do>). Numerical values indicate the distance (mm) from the anterior commissure. Reprinted with permission from Hutchison, Leung, Mirsattari, Gati, Menon, & Everling (2011). ..... 94

Figure 3.2. Cortical representation of eleven resting-state networks (RSNs) identified by independent component analysis of fMRI data acquired from isoflurane-anesthetized macaque monkeys (N=6). Overlaid color maps represent thresholded z-scores. All images have been normalized to the space of the F99 template (Van Essen, 2004; see <http://sumsdb.wustl.edu/sums/macaquemore.do>). For each RSN, the left images depict lateral and medial views of left hemisphere, the center images depict the dorsal view of both hemispheres, and the right images depict the lateral and medial views of right hemisphere. Potential functional roles of each network are discussed in the text. Reprinted with permission from Hutchison, Leung, Mirsattari, Gati, Menon, & Everling (2011). ..... 97

Figure 3.3. The eleven resting-state networks (RSNs) presented in Fig. 3.2 projected onto a flattened brain. RSNs were identified by group independent component analysis of fMRI data from six isoflurane-anesthetized macaque monkeys. Overlaid color maps represent thresholded z-scores. All images have been normalized to the space of the F99 template (Van Essen, 2004; see <http://sumsdb.wustl.edu.proxy1.lib.uwo.ca:2048/sums/macaquemore.do>). The left

and right images correspond to the left and right hemispheres, respectively. Sulci and color bar are shown in the bottom right quadrant. as, arcuate sulcus; cas, calcarine sulcus; cis, cingulate sulcus; cs, central sulcus; hs, hippocampal sulcus; ips, intraparietal sulcus; los, lateral orbital sulcus; ls, lingual sulcus; ots, occipito-temporal sulcus; sf, sylvian fissure; sts, superior temporal sulcus; pos, parieto-occipital sulcus; ps, principal sulcus. Reprinted with permission from Hutchison, Leung, Mirsattari, Gati, Menon, & Everling (2011). ..... 98

Figure 3.4. Cortical coverage of eleven resting-state networks (RSNs) identified by group independent component analysis of fMRI data from six isoflurane-anesthetized macaque monkeys. All images have been normalized to the space of the F99 template (Van Essen, 2004; see <http://sumsdb.wustl.edu.proxy1.lib.uwo.ca:2048/sums/macacuemore.do>). (A) The left images depict lateral and medial views of left hemisphere, the center images depict the dorsal view of both hemispheres, and the right images depict the lateral and medial views of right hemisphere. (B) Cortical coverage of (A) projected onto a flattened brain. Reprinted with permission from Hutchison, Leung, Mirsattari, Gati, Menon, & Everling (2011). ..... 103

Figure 3.5. Resting-state networks (RSN) of all monkeys (M1–M6) following single-subject independent component analysis (ICA) that were most spatially correlated to group-ICA identified RSN B (fronto-parietal). Overlaid color maps represent thresholded z-scores. All images have been normalized to the space of the F99 template (Van Essen, 2004; see <http://sumsdb.wustl.edu/sums/macacuemore.do>). For each RSN, the left images depict lateral and medial views of left hemisphere, the center images depict the dorsal view of both hemispheres, and the right images depict the lateral and medial views of right hemisphere. Reprinted with permission from Hutchison, Leung, Mirsattari, Gati, Menon, & Everling (2011). ..... 105

Figure 3.6. Resting-state networks (RSN) of monkey M1 identified by single-subject independent component analysis (ICA) that were most spatially correlated to group-ICA identified networks seen in Fig. 3.2 and Fig. 3.3. The networks are

projected onto a flattened brain. Overlaid color maps represent thresholded z-scores. All images have been normalized to the space of the F99 template (Van Essen, 2004; see <http://sumsdb.wustl.edu.proxy1.lib.uwo.ca:2048/sums/macaquemore.do>). The left and right images correspond to the left and right hemispheres, respectively. Sulci and color bar are shown in the bottom right quadrant; as, arcuate sulcus; cas, calcarine sulcus; cis, cingulate sulcus; cs, central sulcus; hs, hippocampal sulcus; ips, intraparietal sulcus; los, lateral orbital sulcus; ls, lingual sulcus; ots, occipito-temporal sulcus; sf, sylvian fissure; sts, superior temporal sulcus; pos, parieto-occipital sulcus; ps, principal sulcus. Reprinted with permission from Hutchison, Leung, Mirsattari, Gati, Menon, & Everling (2011). ..... 106

Figure 3.7. Resting-state networks (RSN) of monkey M2 identified by single-subject independent component analysis (ICA) that were most spatially correlated to group-ICA identified networks seen in Fig. 3.2 and Fig. 3.3. The networks are projected onto a flattened brain. Overlaid color maps represent thresholded z-scores. All images have been normalized to the space of the F99 template (Van Essen, 2004; see <http://sumsdb.wustl.edu.proxy1.lib.uwo.ca:2048/sums/macaquemore.do>). The left and right images correspond to the left and right hemispheres, respectively. Sulci and color bar are shown in the bottom right quadrant; as, arcuate sulcus; cas, calcarine sulcus; cis, cingulate sulcus; cs, central sulcus; hs, hippocampal sulcus; ips, intraparietal sulcus; los, lateral orbital sulcus; ls, lingual sulcus; ots, occipito-temporal sulcus; sf, sylvian fissure; sts, superior temporal sulcus; pos, parieto-occipital sulcus; ps, principal sulcus. Reprinted with permission from Hutchison, Leung, Mirsattari, Gati, Menon, & Everling (2011). ..... 107

Figure 3.8. Resting-state networks (RSN) of monkey M3 identified by single-subject independent component analysis (ICA) that were most spatially correlated to group-ICA identified networks seen in Fig. 3.2 and Fig. 3.3. The networks are projected onto a flattened brain. Overlaid color maps represent thresholded z-scores. All images have been normalized to the space of the F99 template (Van Essen, 2004; see

<http://sumsdb.wustl.edu.proxy1.lib.uwo.ca:2048/sums/macaquemore.do>). The left and right images correspond to the left and right hemispheres, respectively. Sulci and color bar are shown in the bottom right quadrant; as, arcuate sulcus; cas, calcarine sulcus; cis, cingulate sulcus; cs, central sulcus; hs, hippocampal sulcus; ips, intraparietal sulcus; los, lateral orbital sulcus; ls, lingual sulcus; ots, occipito-temporal sulcus; sf, sylvian fissure; sts, superior temporal sulcus; pos, parieto-occipital sulcus; ps, principal sulcus. Reprinted with permission from Hutchison, Leung, Mirsattari, Gati, Menon, & Everling (2011). ..... 108

Figure 3.9. Resting-state networks (RSN) of monkey M4 identified by single-subject independent component analysis (ICA) that were most spatially correlated to group-ICA identified networks seen in Fig. 3.2 and Fig. 3.3. The networks are projected onto a flattened brain. Overlaid color maps represent thresholded z-scores. All images have been normalized to the space of the F99 template (Van Essen, 2004; see

<http://sumsdb.wustl.edu.proxy1.lib.uwo.ca:2048/sums/macaquemore.do>). The left and right images correspond to the left and right hemispheres, respectively. Sulci and color bar are shown in the bottom right quadrant; as, arcuate sulcus; cas, calcarine sulcus; cis, cingulate sulcus; cs, central sulcus; hs, hippocampal sulcus; ips, intraparietal sulcus; los, lateral orbital sulcus; ls, lingual sulcus; ots, occipito-temporal sulcus; sf, sylvian fissure; sts, superior temporal sulcus; pos, parieto-occipital sulcus; ps, principal sulcus. Reprinted with permission from Hutchison, Leung, Mirsattari, Gati, Menon, & Everling (2011). ..... 109

Figure 3.10. Resting-state networks (RSN) of monkey M5 identified by single-subject independent component analysis (ICA) that were most spatially correlated to group-ICA identified networks seen in Fig. 3.2 and Fig. 3.3. The networks are projected onto a flattened brain. Overlaid color maps represent thresholded z-scores. All images have been normalized to the space of the F99 template (Van Essen, 2004; see

<http://sumsdb.wustl.edu.proxy1.lib.uwo.ca:2048/sums/macaquemore.do>). The left and right images correspond to the left and right hemispheres, respectively. Sulci and color bar are shown in the bottom right quadrant; as, arcuate sulcus; cas,

calcarine sulcus; cis, cingulate sulcus; cs, central sulcus; hs, hippocampal sulcus; ips, intraparietal sulcus; los, lateral orbital sulcus; ls, lingual sulcus; ots, occipito-temporal sulcus; sf, sylvian fissure; sts, superior temporal sulcus; pos, parieto-occipital sulcus; ps, principal sulcus. Reprinted with permission from Hutchison, Leung, Mirsattari, Gati, Menon, & Everling (2011). ..... 110

Figure 3.11. Resting-state networks (RSN) of monkey M6 identified by single-subject independent component analysis (ICA) that were most spatially correlated to group-ICA identified networks seen in Fig. 3.2 and Fig. 3.3. The networks are projected onto a flattened brain. Overlaid color maps represent thresholded z-scores. All images have been normalized to the space of the F99 template (Van Essen, 2004; see [http://sumsdb.wustl.edu.proxy1.lib.uwo.ca:2048/sums/macaquemore.do](http://sumsdb.wustl.edu.proxy1.lib.uwo.ca:2048/sums/macaque/sums/macaquemore.do)). The left and right images correspond to the left and right hemispheres, respectively. Sulci and color bar are shown in the bottom right quadrant; as, arcuate sulcus; cas, calcarine sulcus; cis, cingulate sulcus; cs, central sulcus; hs, hippocampal sulcus; ips, intraparietal sulcus; los, lateral orbital sulcus; ls, lingual sulcus; ots, occipito-temporal sulcus; sf, sylvian fissure; sts, superior temporal sulcus; pos, parieto-occipital sulcus; ps, principal sulcus. Reprinted with permission from Hutchison, Leung, Mirsattari, Gati, Menon, & Everling (2011). ..... 111

Figure 3.12. Average functional network connectivity of macaque resting-state networks (RSNs). Lines and numerical values indicate functional connectivity between two RSNs in which there was a significant temporal correlation of their respective time-courses (one-sample Student t-test,  $p < 0.05$ , corrected for multiple comparisons between 55 pairs, with a time lead/lag of  $\pm 3$  s). Network letters refer to spatial representations shown in Fig. 1. Reprinted with permission from Hutchison, Leung, Mirsattari, Gati, Menon, & Everling (2011). ..... 114

Figure 4.1. Monkey Seed locations. Spherical seeds ( $r = 1.5$  mm) are displayed to scale on coronal slices of the F99 atlas (Van Essen, 2004) overlaid with the group-averaged “oculomotor” network. Coordinates in F99 atlas space are indicated above below the brain area label. Abbreviations are indicated in the text.

Reprinted with permission from Hutchison, Womelsdorf, Gati, Everling & Menon (2012). ..... 135

Figure 4.2. Human Seed locations. Spherical seeds ( $r = 5$  mm) are displayed to scale on coronal slices of the MNI template atlas overlaid with the group-averaged “oculomotor” network. Coordinates in MNI atlas space are indicated above below the brain area label. Abbreviations are indicated in the text. Reprinted with permission from Hutchison, Womelsdorf, Gati, Everling & Menon (2012). ..... 139

Figure 4.3. Group-averaged “oculomotor” network following correlation analysis of isoflurane-anesthetized macaques ( $N = 6$ ) with a seed placed in the anterior bank of the arcuate sulcus corresponding to the left frontal eye fields (FEF; black asterisks). The lateral, medial, and flattened cortical views of the left (column 1) and right (column 3) hemisphere in addition to the dorsal and ventral views (column 2) are overlaid with thresholded correlation maps normalized to the space of the F99 template (Van Essen, 2004). No negative correlations were present at  $r < -0.2$ . Labels indicate prominent sulci. as, arcuate sulcus; cas, calcarine sulcus; cis, cingulate sulcus; cs, central sulcus; hs, hippocampal sulcus; ios, inferior occipital sulcus; ips, intraparietal sulcus; ls, lateral sulcus, lus, lunate sulcus; ots, occipito-temporal sulcus; sf, sylvian fissure; sts, superior temporal sulcus; pos, parieto-occipital sulcus; ps, principal sulcus. Reprinted with permission from Hutchison, Womelsdorf, Gati, Everling & Menon (2012). ..... 142

Figure 4.4. Single-subject (averaged across both scans) “oculomotor” networks of all isoflurane-anesthetized macaques (M1-M6). The lateral medial, and flattened cortical views of the left (column 1) and right (column 3) hemisphere in addition to the dorsal and ventral views (column 2) are overlaid with thresholded correlation maps normalized to the space of the F99 template (Van Essen, 2004). Reprinted with permission from Hutchison, Womelsdorf, Gati, Everling & Menon (2012). ..... 143

Figure 4.5. Group-averaged ventral premotor network following correlation analysis of isoflurane-anesthetized macaques ( $N = 6$ ) with a seed placed in the ventral motor area (area 1/F1; black asterisks). The lateral medial, and flattened cortical views

of the left (column 1) and right (column 3) hemisphere in addition to the dorsal and ventral views (column 2) are overlaid with thresholded correlation maps normalized to the space of the F99 template (Van Essen, 2004). No negative correlations were present at  $r < -0.2$ . Labels indicate prominent sulci. as, arcuate sulcus; cas, calcarine sulcus; cis, cingulate sulcus; cs, central sulcus; hs, hippocampal sulcus; ios, inferior occipital sulcus; ips, intraparietal sulcus; ls, lateral sulcus; lus, lunate sulcus; ots, occipito-temporal sulcus; sf, sylvian fissure; sts, superior temporal sulcus; pos, parieto-occipital sulcus; ps, principal sulcus. Reprinted with permission from Hutchison, Womelsdorf, Gati, Everling & Menon (2012). ..... 145

Figure 4.6. Average pair-wise correlation matrix of resting-state BOLD time-courses from 16 “oculomotor” (OCM) network, 10 ventral premotor (vPM) network, and 8 white matter (WM) seeds for isoflurane-anesthetized macaques (N = 6). Abbreviations are indicated in the text. Reprinted with permission from Hutchison, Womelsdorf, Gati, Everling & Menon (2012). ..... 147

Figure 4.7. Group-averaged “oculomotor” network following correlation analysis of awake human subjects (N = 12) with a seed placed in the left frontal eye fields (black asterisks). The lateral, medial, and flattened cortical views of the left (column 1) and right (column 3) hemisphere in addition to the dorsal and ventral views (column 2) are overlaid with thresholded correlation maps normalized to the space of the PALS-B12 template (Van Essen, 2005). No negative correlations were present at  $r < -0.3$ . Labels indicate prominent sulci. Note that the correlation threshold differs between human and monkey maps shown in Fig 4.3. cas, calcarine sulcus; cis, cingulate sulcus; cs, central sulcus; ifs, inferior frontal sulcus; ls, lateral sulcus; lus, lunate sulcus; mfs, middle frontal sulcus; pos, parieto-occipital sulcus; pocs, posterior central sulcus; prcs, precentral sulcus; sfs, superior frontal sulcus; sts, superior temporal sulcus. Reprinted with permission from Hutchison, Womelsdorf, Gati, Everling & Menon (2012). ..... 149

Figure 4.8. Single-subject “oculomotor” networks of all awake human subjects (S-S12). The flattened cortical views of the both hemispheres are overlaid with thresholded

correlation maps normalized to the space of the PALS-B12 template (Van Essen, 2005). Reprinted with permission from Hutchison, Womelsdorf, Gati, Everling & Menon (2012). ..... 150

Figure 4.9. Average pair-wise correlation matrix of resting-state BOLD time-courses from 16 “oculomotor” (OCM) network and 8 white matter (WM) seeds for awake human subjects (N = 12). Abbreviations are indicated in the text. Reprinted with permission from Hutchison, Womelsdorf, Gati, Everling & Menon (2012). ..... 151

Figure 4.10. Network changes across time with a sliding-window correlation size of 60s for a representative isoflurane-anesthetized monkey (M2, scan 2). The top five rows represent a single windowed correlation between the times. The bottom row displays the average for the entire run. Column 1 shows the pairwise correlation matrix of “oculomotor” network seeds in the same fashion as the blue bounded box in Fig. 4.6. Column 2 and 3 display the flattened cortical views of the left and right hemisphere, respectively, overlaid with voxel-wise correlation maps for the left FEF seed normalized to the space of the F99 template (Van Essen, 2004). Column 4 displays the graph representation of the functional “oculomotor” network connectivity in which each seed represents a node and pair-wise correlation  $r < 0.4$  represented by an edge. The size of the node represents its degree centrality. For window sizes of 30, 120, and 240, see Supplementary Figs. 4.11, 4.12, and 4.13 respectively. For all time points of pair-wise correlations, see Supplementary Movie 1. For all time points of voxel-wise left FEF correlation see Supplementary Movie 2. Reprinted with permission from Hutchison, Womelsdorf, Gati, Everling & Menon (2012). ..... 154

Figure 4.11. Network changes across time with a sliding-window correlation size of 30s for a representative isoflurane-anesthetized monkey (M2, scan 2). The top five rows represent a single windowed correlation between the times. The bottom row displays the average for the entire run. Column 1 shows the pairwise correlation matrix of “oculomotor” network seeds in the same fashion as the blue bounded box in Fig. 4.6. Column 2 and 3 display the flattened cortical views of the left and right hemisphere, respectively, overlaid with voxel-wise correlation maps for

the left FEF seed normalized to the space of the F99 template (Van Essen, 2004). Column 4 displays the graph representation of the functional “oculomotor” network connectivity in which each seed represents a node and pair-wise correlation  $r < 0.4$  represented by an edge. The size of the node represents its degree centrality. Reprinted with permission from Hutchison, Womelsdorf, Gati, Everling & Menon (2012). ..... 156

Figure 4.12. Network changes across time with a sliding-window correlation size of 120s for a representative isoflurane-anesthetized monkey (M2, scan 2). The top five rows represent a single windowed correlation between the times. The bottom row displays the average for the entire run. Column 1 shows the pairwise correlation matrix of “oculomotor” network seeds in the same fashion as the blue bounded box in Fig. 4.6. Column 2 and 3 display the flattened cortical views of the left and right hemisphere, respectively, overlaid with voxel-wise correlation maps for the left FEF seed normalized to the space of the F99 template (Van Essen, 2004). Column 4 displays the graph representation of the functional “oculomotor” network connectivity in which each seed represents a node and pair-wise correlation  $r < 0.4$  represented by an edge. The size of the node represents its degree centrality. Reprinted with permission from Hutchison, Womelsdorf, Gati, Everling & Menon (2012). ..... 158

Figure 4.13. Network changes across time with a sliding-window correlation size of 240s for a representative isoflurane-anesthetized monkey (M2, scan 2). The top five rows represent a single windowed correlation between the times. The bottom row displays the average for the entire run. Column 1 shows the pairwise correlation matrix of “oculomotor” network seeds in the same fashion as the blue bounded box in Fig. 4.6. Column 2 and 3 display the flattened cortical views of the left and right hemisphere, respectively, overlaid with voxel-wise correlation maps for the left FEF seed normalized to the space of the F99 template (Van Essen, 2004). Column 4 displays the graph representation of the functional “oculomotor” network connectivity in which each seed represents a node and pair-wise correlation  $r < 0.4$  represented by an edge. The size of the node represents its

degree centrality. Reprinted with permission from Hutchison, Womelsdorf, Gati, Everling & Menon (2012). ..... 160

Figure 4.14. Network changes across time with a sliding-window correlation size of 60s for a representative awake human subject (S7). The top five rows represent a single windowed correlation between the times. The bottom row displays the average for the entire run. Column 1 shows the pairwise correlation matrix of “oculomotor” network seeds in the same fashion as the blue bounded box in Fig. 4.9. Column 2 and 3 display the flattened cortical views of the left and right hemisphere, respectively, overlaid with voxel-wise correlation maps for the left FEF seed normalized to the space of the PALS-B12 template (Van Essen, 2005). Column 4 displays the graph representation of the functional “oculomotor” network connectivity in which each seed represents a node and pair-wise correlation  $r < 0.4$  represented by an edge. The size of the node represents its degree centrality. Reprinted with permission from Hutchison, Womelsdorf, Gati, Everling & Menon (2012). ..... 162

Figure 4.15. Time-series and sliding-window correlation coefficients between the left frontal eye fields (FEF) and “oculomotor” network seeds (A) left intraparietal cortex (IP), (B) left middle superior temporal cortex (MST), (C) right FEF, and (D) left posterior cingulate cortex (PCC) shown for one representative isoflurane-anesthetized monkey (M2, scan 2). The top panel shows the BOLD time series of the left FEF seed (blue) and the comparative seed (red). The middle panel shows the sliding-window coefficients for 30s (cyan), 60s (pink), 120s (green), and 240s (orange) windows. For each of the correlation time courses the bottom panel shows the Fast-Fourier transform (right side) and the percentage of time of above and below 0. Reprinted with permission from Hutchison, Womelsdorf, Gati, Everling & Menon (2012). ..... 164

Figure 4.16. Confidence intervals for sliding-window correlation coefficients shown in Fig. 4.15 between the left frontal eye fields (FEF) and “oculomotor” network seeds (A) left intraparietal cortex (IP), (B) left middle superior temporal cortex (MST), (C) right FEF, and (D) left posterior cingulate cortex (PCC) shown for one

representative isoflurane-anesthetized monkey (M2, scan 2). Sliding-window coefficients are shown for 30s (cyan), 60s (pink), 120s (green), and 240s (orange) windows and shaded bars represent the lower and upper bounds for a 95% confidence interval for each coefficient. Reprinted with permission from Hutchison, Womelsdorf, Gati, Everling & Menon (2012). ..... 165

Figure 4.17. Time-series and sliding-window correlation coefficients between the left frontal eye fields (FEF) and “oculomotor” network seeds (A) left intraparietal cortex (IP), (B) left middle superior temporal cortex (MST), (C) right FEF, and (D) left posterior cingulate cortex (PCC) shown for one representative awake human subject (S7). The top panel shows the BOLD time series of the left FEF seed (blue) and the comparative seed (red). The middle panel shows the sliding-window coefficients for 30s (cyan), 60s (pink), 120s (green), and 240s (orange) windows. For each of the correlation time courses the bottom panel shows the Fast-Fourier transform (right side) and the percentage of time of above and below 0. Reprinted with permission from Hutchison, Womelsdorf, Gati, Everling & Menon (2012). ..... 167

Figure 4.18. Sliding-window pair-wise correlations of “oculomotor” network (OCM), ventral premotor network (vPM), and white matter (WM) seeds over time for a representative isoflurane-anesthetized macaques (M2, scan 2). Every vertical line of each image represents the unfolded pair-wise correlation matrix as seen in Fig 4.6 averaged across 30s (row 1), 60s (row 2), 120s (row 3), and 240s (row 4) windows for the entire scan. Plots for all monkeys and both scans are shown in Fig. 4.20. Reprinted with permission from Hutchison, Womelsdorf, Gati, Everling & Menon (2012). ..... 169

Figure 4.19. Sliding-window pair-wise correlations of “oculomotor” network (OCM), ventral premotor network (vPM), and white matter (WM) seeds over time for all monkeys (M1-M6) for both scans. Every vertical line of each image represents the unfolded pair-wise correlation matrix as seen in Fig. 4.6 averaged across 60s windows for the entire scan. Reprinted with permission from Hutchison, Womelsdorf, Gati, Everling & Menon (2012). ..... 170

- Figure 4.20. Average pairwise correlation values across all “oculomotor” network (OCM, red), ventral premotor network (vPM, blue), and white matter (WM, cyan) seeds over time for all monkeys (M1-M6, scan 2) with a sliding window of 60s. To the right of each plot shows the frequency distribution of the correlation coefficients for each of the three time series. For scan 1, see Fig. 4.21. Reprinted with permission from Hutchison, Womelsdorf, Gati, Everling & Menon (2012)..... 172
- Figure 4.21. Average pairwise correlation values across all “oculomotor” network (OCM, red), ventral premotor network (vPM, blue), and white matter (WM, cyan) seeds over time for all monkeys (M1-M6, scan 1) with a sliding window of 60s. To the right of each plot shows the frequency distribution of the correlation coefficients for each of the three time series. For scan 2, see Fig. 4.20. Reprinted with permission from Hutchison, Womelsdorf, Gati, Everling & Menon (2012)..... 173
- Figure 4.22. Sliding-window pair-wise correlations of “oculomotor” network seeds over time for a representative awake human subject (S7). Every vertical line of each image represents the unfolded pair-wise correlation matrix as seen in Fig. 4.09 averaged across 30s (row 1), 60s (row 2), 120s (row 3), and 240s (row 4) windows for the entire scan. Plots for all subjects are shown in Supplementary Fig. 4.23. Reprinted with permission from Hutchison, Womelsdorf, Gati, Everling & Menon (2012). ..... 175
- Figure 4.23. Sliding-window pair-wise correlations of “oculomotor” network (OCM) and white matter (WM) seeds over time for all human subjects (S1-S12). Every vertical line of each image represents the unfolded pair-wise correlation matrix as seen in Fig. 4.09 averaged across 60s windows for the entire scan. Reprinted with permission from Hutchison, Womelsdorf, Gati, Everling & Menon (2012)..... 176
- Figure 5.1. Simplified cladogram of mammals, indicating the divergence times of selected groups. Time scale in millions of years before the present. The encephalization quotient indicates the deviation of the brain size of a species from brain size expected on the basis of a ‘standard’ species of the same taxon, in this case of the cat. Modified with permission from Wise, 2008. The bottom panel displays the cortical surfaces of the highlighted species. .... 203

Figure 5.2. Brain weight, encephalization quotient and number of cortical neurons in selected mammals. Modified with permission from Roth & Dicke, 2005. Data calculated from Jerison, 1973; Russell, 1979; Haug, 1987. ....204

Figure 5.3. Resting-state networks of the awake (left column) and medetomidine-anesthetized (right column) rat. Both studies utilized ICA to show bilaterally homologous networks through cortical and subcortical structures. Reproduced with permission from Liang et al., 2011; Jonckers et al., 2011.....206

Figure 5.4. Sensory and motor resting-state networks of the macaque (left column) and human (right column) showing connectivity between bilateral homologues. Macaque networks reproduced with permission from Hutchison et al., 2011a. Human connectivity maps (N = 12) derived from ICA of Chapter 4 data. ....207

Figure 5.5. Segregation of the whole-brain network of the awake rat brain. a, The global functional network constructed based on significant intercomponent connections. Each colored box represents an ICA component labeled with its corresponding anatomy and the ICA number. Each line represents a significant connection between two components. Nodes within the same module are displayed in the same color (red, green, and yellow). Three modules were obtained by the spectral partitioning algorithm. B, Bilateral; L, left; R, right; AMG, amygdala; INS, insula; NAcc, nucleus accumbens; MO, motor cortex; HC, hippocampus; HY, hypothalamus; OB, olfactory bulb; Pir, piriform cortex; PTL, parietal cortex; S, septum; TE, temporal cortex; TH, thalamus; VIS, visual cortex. b– d, Community structures of the whole-brain network revealed by spectral partitioning. b, The first module is dominated by cortical ribbon. c, The second module is highlighted by the olfactory pathway and its interaction with PFC, and the integration of other sensory input, cognitive processing, and output in cortical and subcortical regions like thalamus and hippocampus. d, The third module includes regions important for emotional and autonomic functions such as amygdala, insular cortex, PFC, and hypothalamus. The same colors are used in b, c, and d as those in a. Distance to bregma (in millimeters) is labeled at the bottom of each image. Reprinted with permission from Liang et al., 2011.....209

Figure 5.6. Homologous higher-order resting-state networks of the macaque (left column) and human (right column). Putative functional roles of the networks are indicated on the left. Macaque networks modified with permission from Hutchison et al., 2011a. Human connectivity maps (N = 12) derived from ICA of Chapter 4 data. ....212

Figure 5.7. Bilateral functional connectivity of FEF seeds in humans (A,B) and macaque monkeys (C,D). Dorsal view of the left and right hemisphere in humans (N = 12) for left (A) and right (B) hemisphere seeds. Thresholded z-score maps normalized to the space of the PALS-B12 template (Van Essen 2005) are overlaid. Dorsal view of the left and right hemisphere in macaques (N =6) for left (C) and right (D) hemisphere seeds. Thresholded z-score maps normalized to the space of the F99 template (Van Essen 2004) are overlaid. Note that the thresholded z-scores differ between human and monkey maps. Black asterisks indicate the location of the FEF seeds. as, arcuate sulcus; cs, central sulcus; ifs, inferior frontal sulcus; ls, lunate sulcus; mfs, middle frontal sulcus; pos, parieto-occipital sulcus; pocs, posterior central sulcus; prcs, precentral sulcus; ps, principal sulcus.; sfs, superior frontal sulcus; sts, superior temporal sulcus.. Reprinted with permission from Hutchison et al., 2012b.....213

Figure 5.8. Registration of resting-state functional connectivity maps between macaques and humans. (A) Dorsal view of the macaque (left) and human (right) cortical surface. Superimposed are the thresholded z-score maps of macaques normalized to the F99 macaque brain (left) and transformed to the space of the human PALS-B12 template (right). (B) Dorsal view of the human (left) and macaque (right) cortical surface. Superimposed are the thresholded z-score maps of humans normalized to the PALS-B12 human template (left) and transformed to the space of the F99 macaque template (right). as, arcuate sulcus; cas, calcarine sulcus; cs, central sulcus; ifs, inferior frontal sulcus; lus, lunate sulcus; mfs, middle frontal sulcus; pos, parieto-occipital sulcus; pocs, posterior central sulcus; prcs, precentral sulcus; ps, principal sulcus; sfs, superior frontal sulcus; sts, superior temporal sulcus. Reprinted with permission from Hutchison et al., 2012b.....214

Figure 5.9. Potential default-mode network homologue in (A) awake and (B) anesthetized rats. Modified with permission from (A) Upadhyay et al., 2011; (B) Lu et al., 2011. ....	217
Figure 5.10. Potential default-mode network homologue of the macaque across multiple studies. See text for description. Modified with permission from (A) Vincent et al., 2007; (B) Margulies et al., 2009; (C) Vincent et al., 2010; (D) Teichert et al., 2010; (E) Hutchison et al., 2011; (F) Hutchison et al., 2011; (G,H) Mantini et al., 2011. Reproduced with permission from Hutchison & Everling, 2012. ....	221
Figure 5.11. Homologous functional subdivisions of the anterior cingulate cortex. Functional connectivity profiles of seed regions within the anterior cingulate cortex are shown for the human (left column) and macaque (right column). Seed locations are shown on the standard MNI and F99 brains for the humans and monkeys, respectively (top). Putative functional roles are labeled. Modified with permission from Margulies et al., 2007; Hutchison et al., 2011b. Reproduced with permission from Hutchison & Everling, 2012. ....	223
Figure 5.12. Summary of findings. ....	225
Figure 5.13. Overlap of functional and structural connectivity patterns in the macaque. Modified with permission from Vincent et al., 2007; Margulies et al., 2009. ...	227
Figure 5.14. Overlap of functional and structural connectivity. (A) The top panel displays the functional connectivity matrix of 82 cortical seed regions averaged across 6 subjects. The corresponding structural connectivity matrix derived from the CoCoMac database is shown below. Strong (white), moderate (light grey), weak (dark grey) and no (black) anatomical connections are indicated. (B) Cosine similarity values of right hemisphere regions as both sources and targets. Values of left hemisphere regions were similar (not shown). Avg cosine was ~0.32. Reprinted with permission from Shen et al., 2012. ....	229

## List of Appendices

Appendix A: Documentation of Ethics Approval. ....	248
Appendix B: Permissions from Publishers.....	249

## List of Abbreviations

**aPFC:** anterior prefrontal cortex  
**as:** arcuate sulcus  
**BOLD:** blood-oxygenation-level dependent  
**cas:** calcarine sulcus  
**cis:** cingulate sulcus  
**cm:** centimeter  
**CPu:** caudate-putamen  
**cs:** central sulcus  
**CSF:** cerebral spinal fluid  
**DSI:** diffusion spectrum imaging  
**DTI:** diffusion tensor imaging  
**EEG:** electroencephalography  
**EPI:** echo-planar image  
**FEF:** frontal eye fields  
**fMRI:** functional magnetic resonance imaging  
**FOV:** field of view  
**FSL:** FMRIB Software Library  
**FWHM:** full-width half maximum  
**g:** gram  
**h:** hour  
**Hp:** hippocampus  
**hs:** hippocampal sulcus  
**Ht:** hypothalamus  
**HWHM:** half-width half maximum  
**IP:** intraparietal area  
**ip:** intraperitoneal  
**ips:** intraparietal sulcus  
**Ket:** ketamine  
**Km:** kilometer  
**ICA:** independent component analysis  
**LFF:** low frequency fluctuations

**LFP:** local field potentials  
**los:** lateral orbital sulcus  
**ls:** lingual sulcus  
**MEG:** magnetoencephalography  
**MFC:** medial frontal cortex  
**mg:** milligram  
**MST:** middle superior temporal cortex  
**min:** minute  
**MI:** primary motor cortex  
**MII:** secondary motor cortex  
**ml:** milliliter  
**ots:** occipito-temporal sulcus  
**p:** probability  
**PCA:** principal component analysis  
**PCC:** posterior cingulate cortex  
pos, parieto-occipital sulcus  
**PGM:** precuneus  
**ps:** principal sulcus  
**r:** radius  
**RF:** radio frequency  
**RPCC:** regional pair-wise correlation coefficient  
**RS-fMRI:** resting-state functional magnetic resonance imaging  
**RSN:** resting-state networks  
**SC:** superior colliculus  
**SD:** standard deviation  
**SI:** primary somatosensory cortex  
**SII:** secondary somatosensory cortex  
**sf:** sylvian fissure  
**SMA:** supplementary motor area  
**sts:** superior temporal sulcus  
**TE:** echo-time  
**Th:** thalamus

**TR:** repetition time

**VI:** primary visual cortex

**VII:** secondary visual cortex

**V4:** visual area 4

**WM:** white matter

**Xy:** xylazine

## Chapter 1 <sup>1</sup>

### 1 General Introduction

#### 1.1 Preamble

##### 1.1.1 Why study the brain?

We often gaze into the vastness of the night sky believing outer space represents the final frontier for human discovery. However, as we contemplate the exploration of far off galaxies and distant planets, we are often unaware of the ongoing activity occurring several millimeters from your eyes that is making this thought possible. Indeed, the three-pound, organic computing-machine remains a black box to the very mind that is the manifestation of its complex interactions. The brain is responsible for behaviour, cognition, and all aspects of what it means to be human. Our understanding of its structure and function, though limited, has hinted at the potential for understanding consciousness, unlocking the cures for psychiatric and developmental diseases, and explaining human interactions. It has been said that if the brain were simple enough for us to understand it, we would be too simple to understand it<sup>2</sup>, but the progress of neuroscientists around the world would disagree. It is with small and thorough steps, increased computing power, comparative studies, cross discipline work, and multimodal approaches that will allow us to truly elucidate all that is human.

##### 1.1.2 Focus and scale

During my undergraduate studies, the focus of many neuroscience courses was primarily concerned with teaching fundamentals related to the activity of single neurons - mechanisms of action potentials, neurotransmitter release, and other topics of this sort. I always felt that there was a disconnection between these lessons and the complex

---

<sup>1</sup> Portions of this chapter have been published in Hutchison, R.M., & Everling, S. (2012). Monkey in the middle: Why non-human primates are needed to bridge the gap in resting-state investigations. *Frontiers in Neuroanatomy*. Under review.

<sup>2</sup> Ken Hill quoted by Buzsaki, 2006.

behaviours that were discussed in my cognitive psychology courses. Of course, to understand the functions of microcircuits in cortical columns or peripheral pain pathways, the role of individual neurons and their interconnections are invaluable. But how does the depolarization of a single neuron result in memories, language, or emotion? Something was missing and during my first year as a graduate student, I read a phrase that best encapsulated the problem. In a review article, Nikos Logothetis (2008) quoted the neuroanatomist Valentino Braitenberg who stated, “*it makes no sense to read a newspaper with a microscope.*” The issue was a matter of the appropriate focus of investigation. The human cerebral cortex contains approximately  $8.3 \times 10^9$  neurons coupled through  $6.7 \times 10^{13}$  connections that span between  $1 \times 10^5$  and  $1 \times 10^7$  km (Murre & Sturdy, 1995) forming an expansive and intricately connected system. So in the same way that examining individual letter features would fail to capture the message of a newspaper article, characterizing the behaviour of a single neuron cannot adequately explain the complex interactions of the brain. This phrase would inspire my research and shape my approach to neuroscience.

As I will discuss frequently throughout my thesis, the brain represents a network of interconnected components whose architecture supports the emergence of behavior and cognition. Due to the hierarchical nature of the brain’s organization, there are multiple levels of connectivity beyond the single cell that may be explored (Fig. 1.1) and a choice has to be made about the spatial scale at which the analysis is to be performed. I examine large-scale brain networks linking segregated functional subunits. It is important to note that this by no means underrates the contributions of smaller scale investigations. This meticulous work has provided a framework for all ongoing neuroscience experimentation. I contend however, that by examining brain activity on a larger scale, it will be possible to bridge the gap between electrical impulses and cognition, local field potentials and behaviour, or receptive fields and perception.

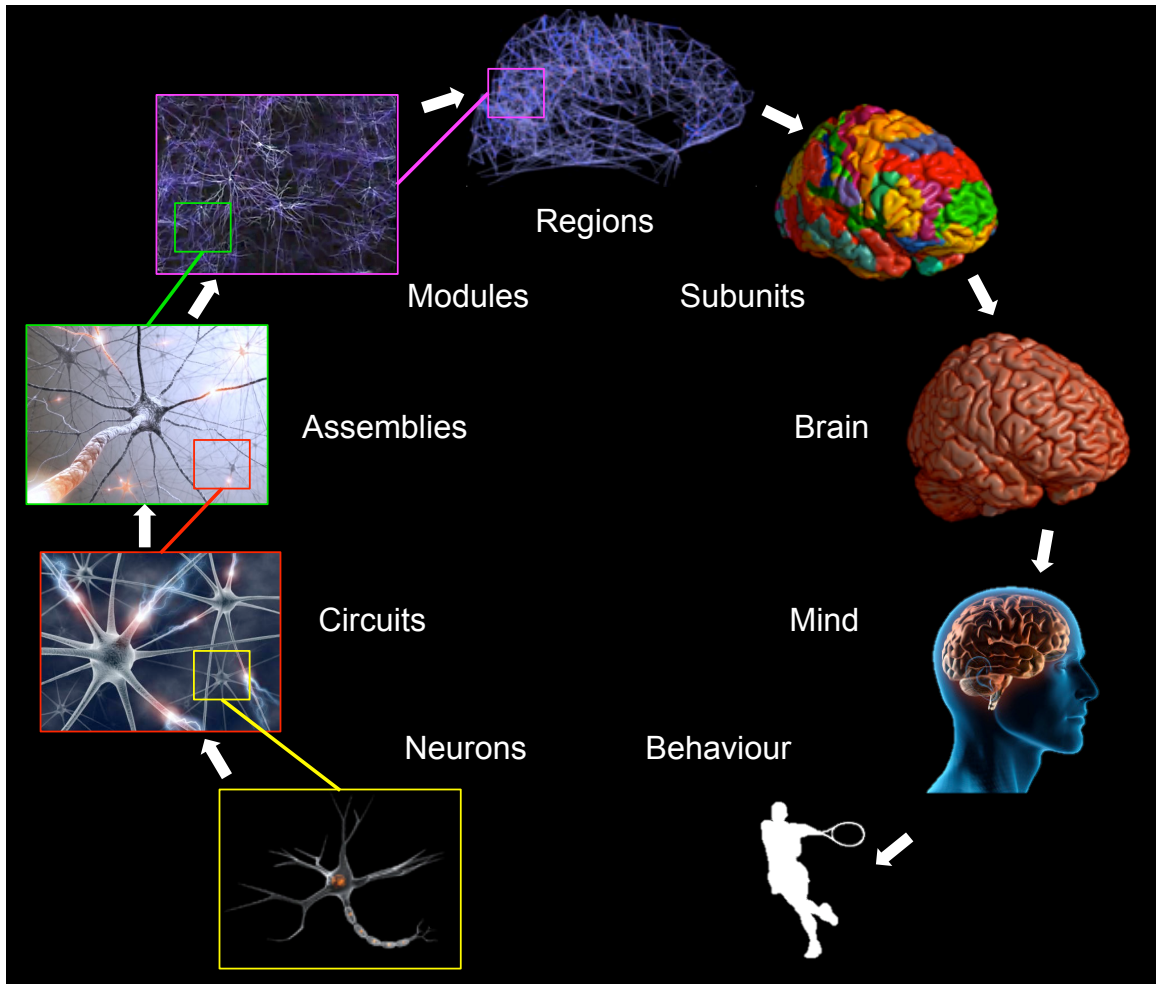


**Figure 1.1. The multiple levels of brain organization.**

## 1.2 Networks

A network represents a group or system of interconnected things, taking a variety of forms across multiple disciplines and scales (See Fig 1.2). Many biological, social, and technological systems can be represented as networks. For example, networks can characterize population interactions such as food webs (Cohen, Briand, & Newman, 1990; Williams & Martinez, 2000) or social relationships (Backstrom, Boldi, Rosa, Ugander, & Vigna, 2011), physiological systems including cellular and metabolic pathway interactions (Bhalla & Iyengar, 1999; Hartwell, Hopfield, Leibler, & Murray, 1999; Jeong, Tombor, Albert, Oltvai, & Barabási, 2000; Kohn, 1999) and brain organization (Achacoso & Yamamoto, 1992; Hagmann et al., 2008), utility architecture like electrical power grids (Watts & Strogatz, 1998), the World-Wide Web (Broder et al., 2000), and the Internet backbone (Faloutsos, Faloutsos, & Faloutsos, 1990), and even more abstract relationships such as co-authorship and citation networks of scientists (Newman, 2001). A network viewpoint shifts the focus from treating individual elements of the system as discrete units of analysis to examining the structure of connections, organization, and emergent properties of the elements interacting with each other. This is critical to the understanding of complex systems as their topology and dynamics are not evident at the element level and the network architecture can directly affect the functioning of the system (Strogatz, 2001).

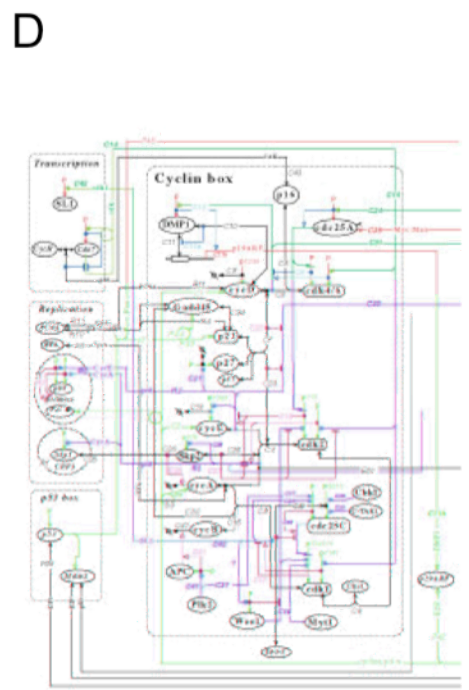
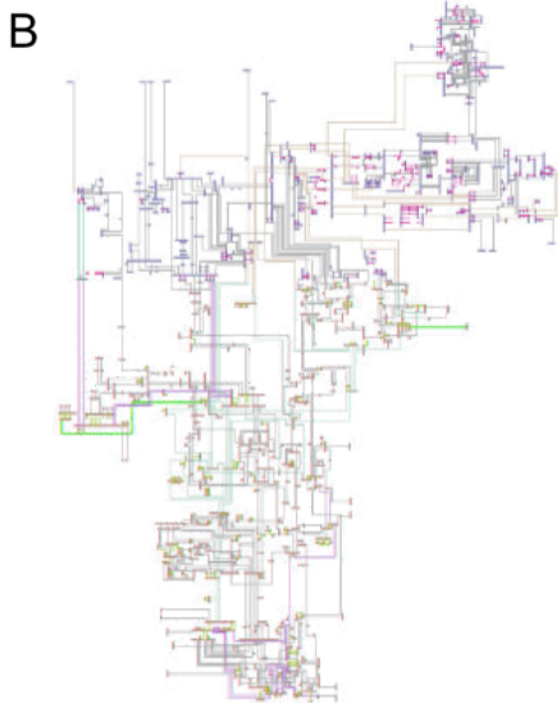
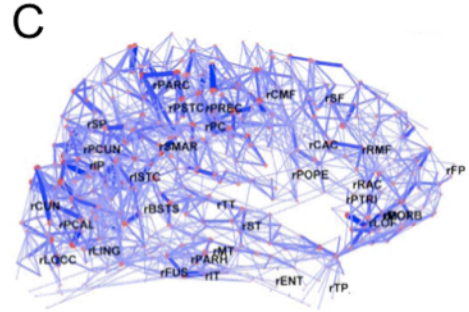
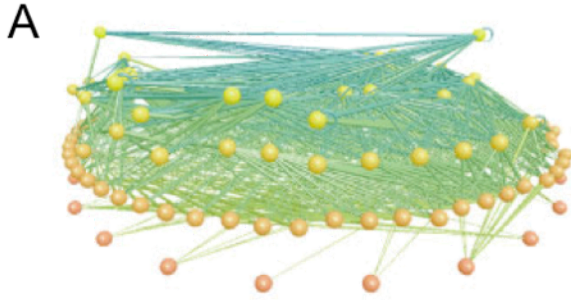


**Figure 1.2. Wiring diagrams for complex networks across multiple disciplines.** A. Food web of Little Rock Lake, Wisconsin, currently the largest food web in the primary literature. Nodes are functionally distinct ‘trophic species’ containing all taxa that share the same set of predators and prey. Height indicates trophic level with mostly phytoplankton at the bottom and fishes at the top. Cannibalism is shown with self-loops, and omnivory (feeding on more than one trophic level) is shown by different coloured links to consumers. B. New York State electric power grid. Generators and substations are shown as small blue bars. The lines connecting them are transmission lines and transformers. Line thickness and colour indicate the voltage level: red, 765 kV and 500 kV; brown, 345 kV; green, 230 kV; grey, 138 kV and below. Pink dashed lines are transformers. C. Connectivity backbone of human brain. Kamada-Kawai force-spring layout of the connectivity backbone. Labels indicating anatomical subregions are placed at their respective centers of mass. Nodes (individual ROIs) are coded according to strength and edges are coded according to connection weight. D. A portion of the molecular interaction map for the regulatory network that controls the mammalian cell cycle. Colours indicate different types of interactions: black, binding interactions and stoichiometric conversions; red, covalent modifications and gene expression; green, enzyme actions; blue, stimulations and inhibitions. Modified with permission from Kohn, 1999; Strogatz, 2001; Hagmann et al., 2008.

Research on complex networks can offer invaluable information in real world settings beyond simple academic interest. The topology of social networks affects the spread of both information and disease through the population; the topology of a power grid affects the robustness and stability of power transmission; and as I will discuss throughout the thesis, the topology of the brain affects our understanding of normal and abnormal brain function. Many complex systems — be they societies, power grids, or brains — possess the same characteristic network properties despite the considerable differences in the type of individual elements or their mechanisms of interaction. The shared topological features offer the possibility of quantifying systems of a very different nature within a single unifying mathematical framework.

### 1.2.1 Graph theory

Within the framework of graph theory, a graph (network) is a mathematical representation of a complex system. The graph is composed of nodes denoting the individual elements (people, computers, websites, neurons, etc.) that are connected by edges representing a pairwise connection or interaction (friendships, wires, hyper-links, synapses, etc.) between the elements. Edges can also be used to convey information concerning direction (a directed graph) or connection strength (a weighted graph). Essentially, the graph models the real system, providing a comprehensive and compact description about how the system's elements are linked or associated with each other. Fundamental organization characteristics of graphs can then be explored by quantitatively assessing their topology - the arrangement or configuration of the network elements – using various metrics (See Table 1 for a selection of metrics and Fig. 1.3 for illustrative example).

**Table 1.1. Network Measures.**

Measure	Definition
Assortativity	The correlation between the degrees of connected nodes. Positive assortativity indicates that high-degree nodes tend to connect to each other
Centrality	How many of the shortest paths between all other node pairs in the network pass through a node
Clustering coefficient	Quantifies the number of connections that exist between the nearest neighbours of a node as a proportion of the maximum number of possible connections (Watts & Strogatz, 1998)
Connection density/cost	The number of edges in the graph as a proportion of the total number of possible edges
Degree	The number of connections that link a node to the rest of the network
Degree distribution	The distribution of the degree values for all of the network's nodes (Amaral, Scala, Barthelemy, & Stanley, 2000)
Efficiency	Efficiency is inversely related to path length but is numerically easier to use to estimate topological distances between elements of disconnected graphs
Hub	Hubs are nodes with high degree, or high centrality.
Modularity	Nodes that are highly interconnected and that overlap in their external connection patterns. Modules may also be functionally defined on the basis of the pattern of functional or effective connections. A given network can be decomposed into a set of non-overlapping, overlapping, or hierarchical arranged modules (Sporns, 2010, p. 328)
Motifs	A small subset of network nodes and edges forming a subgraph (Sporns, 2010, p. 328). The distribution of different motif classes in a network provides information about the types of local interactions that the network can support (Sporns & Kötter, 2004)
Path length	The minimum number of edges that must be traversed to go from one node to another.
Robustness	Robustness refers either to the structural integrity of the network following deletion of nodes or edges or to the effects of perturbations on local or global network states.
Triangle	The number of triangles around a node.

Notes: Modified with permission from Bullmore & Sporns, 2009.

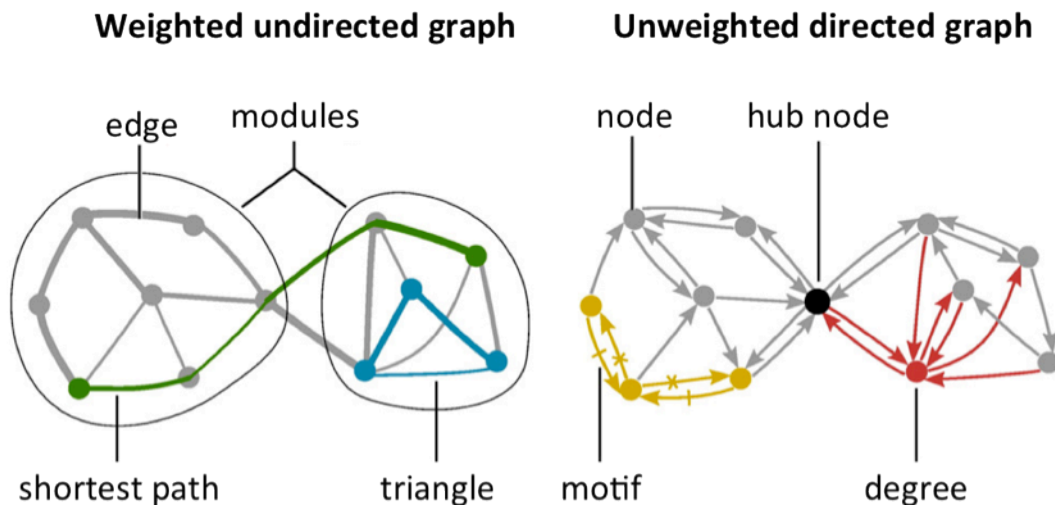


**Figure 1.3. Features of a graph upon which network topology is assessed.** Measures of integration are based on shortest path lengths (green), while measures of segregation are often based on triangle counts (blue) but also include more sophisticated decomposition into modules (ovals). Measures of centrality may be based on node degree (red) or on the length and number of shortest paths between nodes. Hub nodes (black) often lie on a high number of shortest paths and consequently often have high betweenness centrality. Patterns of local connectivity are quantified by network motifs (yellow). An example three-node and four-link anatomical motif contains six possible functional motifs, of which two are shown—one motif containing dashed links, and one motif containing crossed links. Modified with permission from Rubinov & Sporns, 2010.

### 1.2.2 Complex networks

Real-world network architectures tend to fall between two discrete classes of graphs, regular and random (Sporns, 2010, p. 23). The regular (or lattice) graph has an ordered pattern between nodes in which connected nodes tend to have the same neighbours resulting in high local clustering and long characteristic path lengths (Watts & Strogatz, 1998; Fig 1.4A left). Random graphs show the opposite pattern; all connections are equally probable resulting in a Gaussian and symmetrically centered degree distribution and few shared neighbours between nodes. The consequence of this organization is low local clustering and short characteristic path lengths (Watts & Strogatz, 1998; Fig 1.4A right). Both of these topologies are not ideal as both high clustering and short path length are essential for high local efficiency of information transfer and maintaining low cost, respectively. An eloquent balance between the two graphs was first described by Watts and Strogatz (1998). They showed that by increasing the rewiring probability (or randomness) of a regular graph, the clustering remained high, but the new random “long-range” connections significantly decreased the average path length (Fig 1.4B). This has now become known as small-world topology (Fig. 1.4A middle).

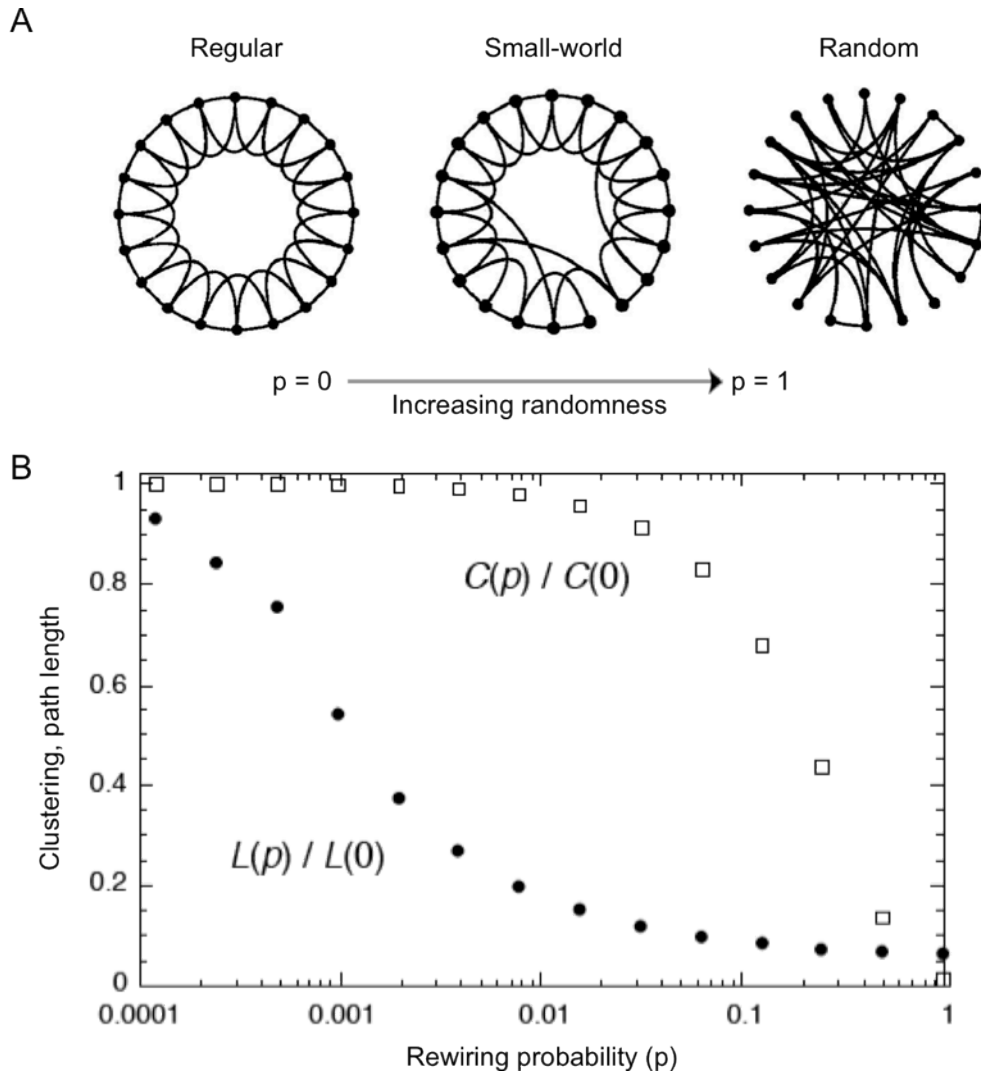


**Figure 1.4. The emergence of small world networks.** (A) A random rewiring procedure starts with a regular ring lattice with edges connecting node with probability  $p$ . As  $p$  increases, the graph becomes increasingly disordered until for  $p = 1$ , all edges are rewired randomly. For intermediate values of  $p$ , the graph is a small-world network: highly clustered like a regular graph, yet with small characteristic path length, like a random graph. (B) The characteristic path length  $L(p)$  and clustering coefficient  $C(p)$  for the family of randomly rewired graphs described in A. Note that a logarithmic horizontal scale has been used to resolve the rapid drop in  $L(p)$ , corresponding to the onset of the small-world phenomenon. During this drop,  $C(p)$  remains almost constant at its value for the regular lattice, indicating that the transition to a small world is almost undetectable at the local level. Modified with permission from Watts & Strogatz, 1998.

In addition to small-world properties, most complex networks have non-Gaussian degree distributions, often with a long tail towards high degrees that follow a power law (Barabasi & Albert, 1999). This implies that “the probability of finding a node with a degree that is twice as large as an arbitrary number decreases by a constant factor” and indicates a scale-free organization in which “zooming in on any segment of the distribution does not change its shape” (Sporns, 2010, p. 20). Nodes with a disproportionately high number of connections are referred to as hubs and serve to integrate diverse informational sources enabling globally efficient information flow (Sporns, Honey, & Kötter, 2007). Hubs also facilitate small-world network organization, minimizing wiring and metabolic costs by providing long-distance connections that integrate local networks (Bassett & Bullmore, 2006). Lastly, complex networks tend to exhibit modularity where the modules contain several densely interconnected nodes with relatively few connections between nodes in different modules (Meunier, Lambiotte, & Bullmore, 2010).

Discovering some of the overarching principles of complex networks is only the first step towards a comprehensive understanding of how these networks are structurally organized and generate complex dynamics. Extending beyond topological quantifications, research must focus on their development and evolution, linking network topology to network dynamics, and exploring network robustness and vulnerability — topics that are directly relevant in the study of brain organization.

### 1.3 Brain networks

Most early work in neuroscience emphasized the specialization of brain areas, parcellating grey matter into ever smaller functional subdivisions based on an assortment of experimental techniques (Finger, 1994). The assignment of mental faculties to distinct regions can be traced to the work of Joseph Gall in the early 19<sup>th</sup> century (Fig. 1.5A). Gall was the original proponent of phrenology, a premise that attributed bumps or indentations in a patient's skull to respective expansion or shrinkage of underlying brain areas that corresponded to psychological and personality traits. Although much of his work is now forsaken as pseudoscience, his ideas left a lasting impression in the field and shaped the thinking of neuroscientists for over a century. Investigations during the first half of the 20<sup>th</sup> century continued to segment the brain, albeit with scientifically valid and rigorous cytoarchitecture investigations (Zilles & Amunts, 2010) (Fig. 1.5B-D). The trend is still pervasive today, perpetuated by extensive human imaging investigations assigning functional labels to those brain areas eliciting “activation” in response to a specific task (van Eijsden, Hyder, Rothman, & Shulman, 2009).



Despite these ongoing modular investigations of brain function postulating the independent processing of specific cognitive functions, focus has been gradually shifting away from the notion of functional specialization towards one of functional integration (Breakspear & McIntosh, 2011; Bressler & Menon, 2010; Bullmore & Sporns, 2009; Sporns, 2002). Across multiple modalities and levels of investigation, evidence has suggested that specialization cannot account for the complex manifestations of brain function such as perception, cognition, and behaviour. Even the roles of primary sensory areas, typically viewed as the “pinnacles of modularity” (Bressler & Menon, 2010, p. 227), are being redefined by recent evidence of complex cross-modal and cross-module interactions (Ghazanfar & Schroeder, 2006). The new framework emphasizes instead the conjoint function of brain areas working together as large-scale networks. Both localized and distributed aspects of brain function can be incorporated under this network perspective when viewing the “local specialization as the result of patterned distributed interactions that confer different functional attributes to individual network elements” (Sporns, 2010, p. 72). Interest in the dynamics of large-scale neuronal populations has emerged in parallel, in which the examination of the temporal properties and network dependencies of brain regions extends and offers better predictive ability than traditional models (Buzsaki, 2006; Deco, Buehlmann, Masquelier, & Hugues, 2011; Engel, Fries, & Singer, 2001; Varela, Lachaux, Rodriguez, & Martinerie, 2001). In essence, the brain is being reconceptualized as a complex, distributed system (McIntosh, 2004), in which the organization and activity within this system underlies all human perception and cognition (Bressler & Menon, 2010; Bullmore & Sporns, 2009; Sporns, 2002; Sporns, 2010).

## 1.4 Brain Connectivity

Brain networks are not random, but form highly specific patterns that may be defined based on functional or structural (anatomical) connectivity. Functional connectivity refers to the “joint activity in different brain structures that is co-dependent under variation of a functional or behavioral parameter” (Bressler & Menon, 2010, p. 278). In practice, this is quantified through the evaluation of patterns of temporal correlations that exists between distinct neuronal units. The time-scale and classification of which are determined by the scale and type of investigation (Bressler & Menon, 2010; Bullmore & Sporns, 2009; Sporns, 2002; Sporns, 2010). Effective connectivity, a related measure, involves estimation of the direction and strength of connections between the regions (Büchel & Friston, 2001) and can facilitate the analysis of directed graphs.

Structural connectivity refers to the set of physical or structural connections linking neuronal units at a given time (Sporns, 2002). Structural networks often provide the architecture that promotes the dynamic interactions between nodes that give rise to the functional networks. As with functional connectivity, the properties are dependent upon the level of the spatial scale at which the analysis is being performed (Bressler & Menon, 2010; Bullmore & Sporns, 2009; Sporns, 2002; Sporns, 2010). At the local circuit level, the pattern of connections between individual neurons that occur via axons, dendrites, and gap junctions would be considered. Analyses of connections within a neural module (e.g., primary visual area) would model “connection bundles” that link the local neuronal populations (e.g., ocular columns). Representations of large-scale structural patterns focus on white matter tract connection pathways linking segregated brain areas. These tracts comprise- thousands or millions of individual axons that directly interconnect large groups of spatially separated regions. The structure of the large-scale pathways provides the framework that facilitates signaling along preferred pathways to achieve specific cognitive functions. While functional connectivity is the focus of the analyses in the current work, diffusion imaging techniques and tracing-studies have derived large-scale structural networks of the human (Gong et al., 2009; Hagmann et al., 2008; Iturria-Medina et al., 2007) and macaque (Hilgetag, Burns, O’Neill, Scannell, & Young, 2000; Modha & Singh, 2010) brains, respectively (Fig. 1.6).



**Figure 1.6. Structural connectivity of human (A) and monkey (B) brain.** A. Dorsal and lateral views of the human connectivity backbone. Labels indicating anatomical subregions are placed at their respective centers of mass. Nodes (individual ROIs) are coded according to strength and edges are coded according to connection weight. B. Macaque brain long-distance network in which each vertex of the network corresponds to a brain region in the hierarchical brainmap and each edge encodes the presence of long-distance connection between corresponding brain regions. A colorwheel is used for better discrimination amongst brain regions. Modified with permission from Hagmann et al., 2008 and Modha & Singh, 2010.

The brain's structural and functional networks both have features expected of complex networks including small-world topology, hierarchy, centrality, hubs, and modularity that enable efficient information integration and processing (for reviews see (Bressler & Menon, 2010; Bullmore & Sporns, 2009). The relationship between the connectivity types is both mutual and reciprocal; structural connectivity constrains the patterns of functional connectivity that can be generated and functional interactions can contribute to the shaping of the underlying anatomical structure through activity dependent modification. Therefore, investigation of both dimensions of brain connectivity and their interaction are essential for a complete understanding of brain organization and the complex network dynamics that emerge.

## 1.5 Network communication: Oscillations and synchrony

Functional communication of the collective behaviour of neurons in different brain areas occurs via coherent oscillatory activity (Buzsaki, 2006; Buzsáki & Draguhn, 2004). The oscillations provide a mechanism of synchronization between individual and groups of neurons that provide an energy-efficient physical mechanism for temporal coordination (Buzsáki & Draguhn, 2004). The occurrence of synchronized electrical activity across multiple bands (delta, theta, alpha, gamma, etc.) change as function of behavioural-state and task demands (Engel et al., 2001). These distributed oscillatory systems act as resonant communication networks through which large populations of neurons are synchronized, providing a temporal frame for the timing of discharges and the encoding of information (Buzsaki, 2006). Synchronization can enhance the salience of signals, bias input selection, facilitate signal propagation across sparsely connected networks, regulate synaptic plasticity, support temporal representations, as well as allow long-term consolidation of information (Buzsaki, 2006; Buzsáki & Draguhn, 2004). In addition, systematic phase shifts between the discharges of individual neurons and population oscillations appear to be exploited for cortical computations (Lisman & Buzsáki, 2008; Womelsdorf, Vinck, Leung, & Everling, 2010). High frequency-band oscillations are typically confined to a relatively small area, linking local populations of neurons, whereas distributed brain regions are recruited during slow oscillations to form

large-scale networks (Buzsáki & Draguhn, 2004; Csicsvari, Jamieson, Wise, & Buzsáki, 2003; Steriade, 2001). Importantly, the relationship between neural oscillations and the brain's anatomical architecture permit processing to be carried out independently or in parallel at multiple temporal and spatial scales (Buzsáki & Draguhn, 2004; Buzsáki, Geisler, Henze, & Wang, 2004).

## 1.6 Methodologies

There are a number of methodological techniques for exploring brain function (Fig. 1.7). Neuronal communication via oscillation is primarily examined with the use of electroencephalography (EEG) recorded at the scalp surface, electrocorticography (ECoG) recorded at the cortical surface, or depth electrodes recorded at specific locations within the brain. The techniques allow measurement of extracellular field potentials generated by a population of neurons referred to as local field potentials (LFP). LFPs reflect the weighted average of input signals of neurons and change with cognitive processing, allowing quantification of changes in endogenous brain states and events (Womelsdorf & Fries, 2006). Electrophysiological methodologies, however, have a number of disadvantages that prevent adequate exploration and understanding of the activity and functional connectivity of complex networks. EEG, despite its excellent temporal resolution (milliseconds), is unable to accurately discern or record all cortical and subcortical activity (Gloor, 1985). This is due to biophysical challenges related to convolution of the cortical surface, distortion from cerebral spinal fluid, neuron orientation, synchronization, skull conduction, and other sources of attenuation or loss (Ritter & Villringer, 2006). ECoG circumvents several of these limitations, but is extremely invasive. Source localization is limited in both of the techniques because of the inverse problem; there are an infinite number of possible locations and magnitudes of the intracranial current sources within the brain making a unique mathematical solution impossible (Niedermeyer & Lopes da Silva, 2004). Depth electrodes offer precise spatial localization, but only record activity in the immediate vicinity of the known electrode tip locations, thereby offering an incomplete view of brain activity. Further, they represent an invasive procedure only feasible in certain patient populations. Motivated by the

shortcoming of electrophysiological methods, various imaging methodologies have been developed.

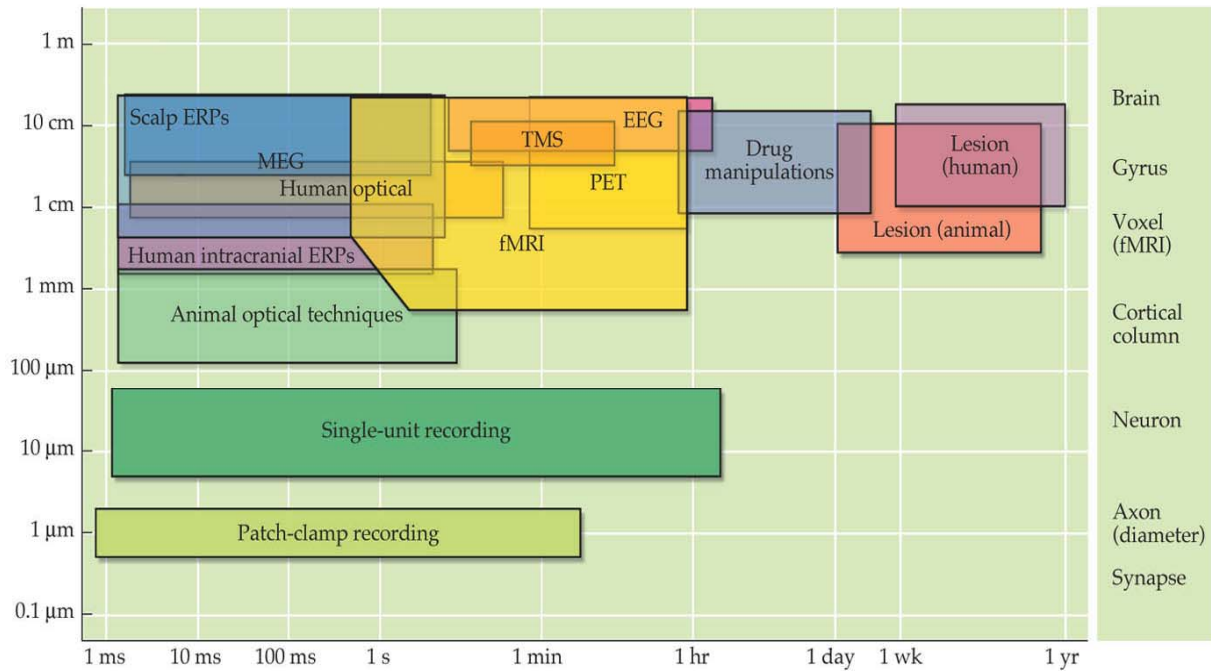


**Figure 1.7. Neuroscience techniques differ in their spatial and temporal resolution.** Functional MRI provides a good balance of spatial and temporal resolution and thus is appropriate for a wide range of experimental questions. Other approaches, including electrophysiology, lesion studies, and drug manipulations, can provide complementary information. Reprinted with permission from Huettel, Song, & McCarthy, 2004.

Neuroimaging techniques provide non-invasive methods capable of exploring the structural and functional connectivity of brain networks while providing precise spatial localization. The most widely used technique is blood-oxygenation-level-dependent (BOLD) fMRI. This technique exploits the paramagnetic properties of deoxygenated hemoglobin (dHb) that disrupt the local magnetic field to reveal changes in functional brain activity with high spatial resolution and whole brain coverage across multiple levels (Menon, Ogawa, Strupp, & Uğurbil, 1997; Ogawa et al., 1993). The BOLD response has been shown to reflect input and intracortical processing, in which LFPs are better predictors of the BOLD response than multiple-unit or single-unit spiking (Logothetis, Pauls, Augath, Trinath, & Oeltermann, 2001; Logothetis & Wandell, 2004).

Tracking the activity of an assembly of neurons responding to a stimulus, there is first an increase in the integration of and signaling of neurons. Excitatory and inhibitory post-synaptic potentials demand a great deal of energy resources for maintaining their electrochemical gradients and following the stimulus-induced activity these need to be restored. Neurons utilize available energy resources (oxygen, ATP, glucose) to accomplish this and in the process further deplete available energy supplies as well as increasing the concentration of metabolic by-products ( $\text{CO}_2$ ). Neurovascular coupling (potentially facilitated by astrocytes (Iadecola & Nedergaard, 2007)) allows the vasculature to respond to changes in energy demands leading to dilation of local arteriols and upstream vessels. The increase in vessel diameter decreases resistance and increases blood flow to the capillary bed. Increased blood flow brings an increase of oxygenated hemoglobin (HbO). HbO thereby reduces the deoxyHb concentration and causes an increase in the coherent spin of hydrogen atoms of diffusing water molecules mitigating the disruptive effects of dHb. The result is an increase of the local BOLD signal (Attwell & Iadecola, 2002). Therefore, although the fMRI BOLD signal arises from changes in blood flow and metabolism, it is intimately related to ongoing dendritic potentials within neurons. The technique has afforded unparalleled access in the exploration of the topology of brain systems and been used to explore changes in neuronal activity related to sensory, motor, cognitive, and integrative functions (Logothetis, 2008).

## 1.7 Resting-state fMRI (RS-fMRI)

Task-based paradigms are ubiquitous in the fMRI literature. Depending upon the hypothesis, these can take a variety of forms in which participants can perform overt or covert behaviours. The timing and modeling of the task can also vary considerably, but many follow a simple subtraction method in which participants alternate between the task (e.g. visual stimulation) and a baseline period (e.g. no stimulation) in a block design. The states are then subtracted and areas where modulation of the BOLD signal is observed (e.g. visual cortex) are attributed to the experimental paradigm, thereby allowing researchers to relate brain topography to function (Fig. 1.8). The technique has also revealed that neural processing relies on the dynamic integration of cortical and subcortical areas within large-scale and distributed brain networks (Guye, Bartolomei, & Ranjeva, 2008; Sporns, Tononi, & Kötter, 2005).

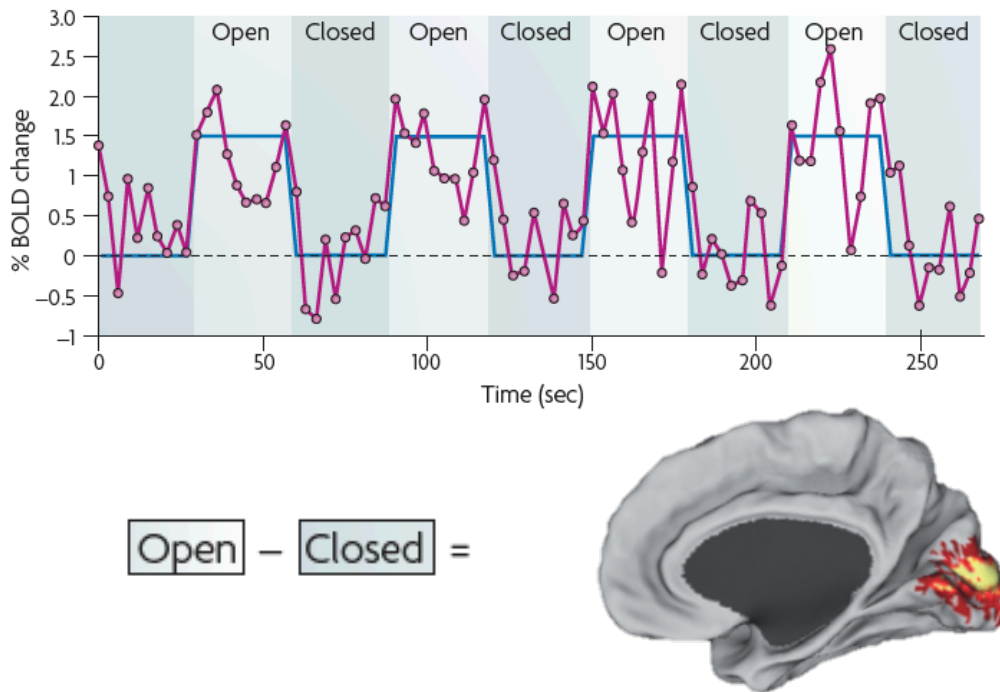


**Figure 1.8. Traditional fMRI analysis and BOLD noise.** Unaveraged blood oxygen level dependent (BOLD) time course (magenta) from a region in the primary visual cortex during a simple task paradigm that requires subjects to open and close their eyes. The paradigm is shown in blue (delayed to account for the hemodynamic response). Traditional functional magnetic resonance imaging (fMRI) analysis involves correlating BOLD data with a stimulation time-course across multiple blocks. This in effect averages across each condition and performs a subtraction, minimizing ‘noise’ in the BOLD signal and highlighting regions that are modulated by the task paradigm. In this case, subtraction of the eyes-closed condition from the eyes-open condition identifies a BOLD signal intensity difference in the primary visual cortex (shown below). Modified with permission from Fox & Raichle, 2007.

A block or event related paradigm of this type is problematic in several regards. When the brain is “at rest,” it consumes 20% of the body’s energy despite only representing 2% of the total body mass, dedicating the majority of this energy expenditure to support ongoing neuronal signaling (Raichle & Mintun, 2006; Shulman, Rothman, Behar, & Hyder, 2004). This large metabolic cost implies that the baseline periods do not actually reflect an absence of cognitive processing implicit in the theoretical design of the experiments (Raichle et al., 2001; Raichle, 2010; Stark & Squire, 2001). During the task portion of the paradigm, the reported neuronal metabolism measured using BOLD-fMRI typically only increases 1-2%, very rarely exceeding 5% in typical studies. The finding is not isolated to imaging studies and supported by an extensive number of electrophysiological studies also reporting spontaneous time-varying, network dynamics and ongoing brain activity over a wide range of temporal and spatial scales (for review see Raichle, 2010; Ringach, 2009; Sadaghiani, Hesselmann, Friston, & Kleinschmidt, 2010; Vogels, Rajan, & Abbott, 2005). The relatively small fraction of energy usage when compared to the large resting energy consumption suggests that task-related paradigms only study a minor component of total brain activity. The point is further highlighted when examining a timecourse of the BOLD signal from all brain areas, including those eliciting activation during the task (Fig. 1.8); depending on the task, large amplitude fluctuations can be observed during both task and rest conditions that have magnitudes matching task-evoked activity. The low frequency signal changes are not attributable to the experimental paradigm or any other explicit input or output. Ongoing brain activity changes in the absence of stimuli or behaviour of this type was historically characterized as background “noise” in both electrophysiological and imaging fields- believed to be a manifestation of cardiac, breathing, motion, and scanner artifacts. The contribution of these signals were then minimized through averaging.

A significant paradigm shift occurred following the discovery that spontaneous BOLD fluctuations measured in the left somatomotor cortex were correlated with the spontaneous fluctuations in the right somatomotor cortex as well as supplementary motor areas (Biswal, Yetkin, Haughton, & Hyde, 1995). The group of regions closely matched the task-evoked dorsal motor network, though in this case, the network was revealed from data acquired in the absence of any overt motor task (Fig. 1.9). The results indicated

that a component of the spontaneous BOLD activity is not solely random noise or a consequence of physiological or scanner artifact, but specifically organized in the resting human brain and thus could be mapped non-invasively without any task requirement. These findings were the catalyst for a new avenue of network research called resting-state fMRI (RS-fMRI)

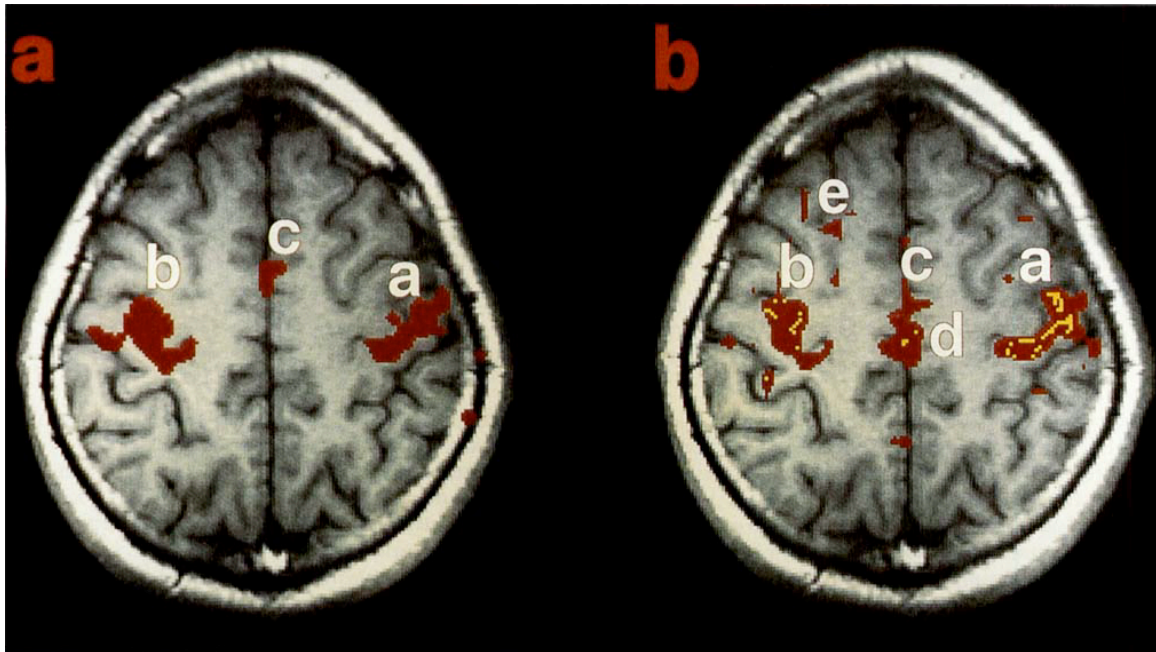


**Figure 1.9. The first comparison of task-based and resting-state functional maps.** A. fMRI task-activation response to bilateral left and right finger movement, superimposed on an anatomical image. B. Correlation map derived using a resting-state scan. Red is positive correlation, and yellow is negative. Reprinted with permission from Biswal, Yetkin, Haughton, & Hyde, 1995.

### 1.7.1 Resting-state signal

Spontaneous BOLD fluctuations follow a  $1/f$  distribution, meaning that there is increasing power at lower frequencies (Zarahn, Aguirre, & D'Esposito, 1997). When plotted on a log-log plot, the slope of the power spectral density function will be close to -1. This distinguishes the fluctuations from random (white) noise that would be characterized by a flat power spectral density function that contains equal power across all frequencies. A  $1/f$  distribution has also been observed across a range of other neuroscience methodologies examining spontaneous brain activity such as EEG (Linkenkaer-Hansen, Nikouline, Palva, & Ilmoniemi, 2001; Cornelis Jan Stam & de Bruin, 2004), magnetoencephalography (MEG) (Linkenkaer-Hansen et al., 2001), and LFP recordings (Leopold, Murayama, & Logothetis, 2003). Across this distribution, it has been shown that frequencies below 0.1 Hz primarily contribute to the regionally specific BOLD fluctuations (Cordes et al., 2001). Physiological signals relating to respiratory (0.1 - 0.5 Hz) and cardiovascular (0.6 - 1.2 Hz) factors are above this range (the values are higher in rats and monkeys) though aliasing is still a concern (Birn, Murphy, & Bandettini, 2008). Based on this finding, the majority of spontaneous BOLD studies low-pass filter data at a cut-off of 0.1 Hz and refer to the fluctuations as "low-frequency." It should be noted that due to the sluggishness of the hemodynamic response and low sampling rate used in fMRI acquisitions (on the order of seconds) analysis of higher frequency contributions is limited and contributions from broadband neural activity (possibly) underlying the hemodynamic dynamics cannot be excluded (Cole, Smith, & Beckmann, 2010). Other temporal properties of the hemodynamic fluctuations such as frequency profiles, magnitude, and transient events - attributes typically studied in other methodologies - require further examination though have been shown to possess valuable information (Baria, Baliki, Parrish, & Apkarian, 2011; Li et al., 2000). Greater emphasis has been placed on the spatial patterns of correlations.

### 1.7.1.1 Correlate

As mentioned earlier, the BOLD signal is not a direct measure of neural activity as would be recorded in electrophysiological experiments. Instead, it represents a surrogate signal reflecting local variations in deoxyhemoglobin concentration determined by a combination of blood flow, blood volume, and oxygen metabolism that are then partially coupled to the underlying neural activity (Raichle & Mintun, 2006). Task-evoked activity has been best linked to changes in LFPs (Logothetis et al., 2001), but the same correlation has not been confirmed for spontaneous hemodynamic fluctuations. A growing body of studies does support the notion that resting-state BOLD fluctuations of cortical and sub-cortical regions originate from the coupling of spontaneous neuronal activity to a hemodynamic response function. Early multi-modal evidence in anesthetized rats demonstrated tight coupling between spontaneous cerebrovascular fluctuations and bursts of electrocortical activity (Golanov, Yamamoto, & Reis, 1994). This has been expanded in future work attempting to more precisely determine the underlying electrophysiological correlate. Two related approaches have emerged, one attempting to determine the correlation of the two signals at a single site and a second focusing instead on overlapping spatial correlation patterns of each of the signals (discussed in Chapter 4).

A leading candidate for the neural correlate of spontaneous BOLD fluctuations is the slow fluctuation of power in the gamma frequency range. Electrical activity in the gamma frequency band fluctuates at 60-100 Hz, however, Leopold and colleagues (2003) showed in nonhuman primates that the power of gamma at a particular moment also fluctuates, albeit at a much slower rate ( $<0.1$  Hz). Besides sharing a similar frequency as the hemodynamic changes, the slow power fluctuations also exhibit  $1/f$  behaviour and are correlated across large regions of cortex (Leopold et al., 2003). Later, it was showed using simultaneous fMRI and LFP recordings that the power fluctuations are in fact correlated with spontaneous BOLD fluctuations (Shmuel & Leopold, 2008).

First proposed by Fox and Raichle, (2007), infraslow oscillations represent another potential candidate not completely independent of the gamma power changes. Using direct current-coupled EEG, which circumvents the limited recording bandwidth of most EEG systems ( $>0.5$  Hz), large-scale infraslow oscillations (0.02 - 0.2 Hz) can be

recorded across widespread regions in the human cortex (Vanhatalo et al., 2004). The oscillations are themselves correlated with changes in the power of higher frequency bands including gamma, leading to the notion of a causal role between the two processes in which infraslow oscillations modulate the power of higher frequency activity. In this model, the rapid fluctuations coordinate the neuronal activity at small spatial scales, whereas the much slower power fluctuations allow for long-range coordination. This is supported by empirical evidence (Buzsáki & Draguhn, 2004), however its relation to BOLD fluctuations remains to be determined.

Beyond the electrophysiological correlates, a number of other hemodynamic and metabolic variables have been put forth by Fox and Raichle (2007) and need to be considered. Oxygen availability, nicotinamide adenine dinucleotide levels, spontaneous neurotransmitter release, cytochrome oxidase activity, blood volume, and blood flow demonstrate spontaneous low-frequency fluctuations that can have  $1/f$  distributions and similar spatial patterns to those seen with BOLD (Fox & Raichle, 2007). Taken together, it is clear that further work is needed using invasive recordings to determine the origin of hemodynamic, metabolic, and electrophysiological fluctuations.

### 1.7.2 Methodology

Most studies utilizing RS-fMRI follow a similar experimental paradigm as was first proposed by Biswal and colleagues (1995). Efforts are made to minimize any changes in sensory input over time and subjects are required to refrain from making responses or performing specific cognitive tasks. The subject simply lies still in the scanner and refrains from falling asleep with their eyes closed or open and fixating. After data acquisition, there are two primary methods used to identify spatial patterns of spontaneous activity: hypothesis-dependent and hypothesis-independent analyses.

### 1.7.2.1 Seed-region analysis

Seed-based analysis for connectivity mapping is a widely used approach for RS-fMRI investigations and the most popular hypothesis-dependent method. It offers simplicity, sensitivity, and ease of interpretation, revealing the network of regions most strongly connected with the a priori defined seed-region (Cole et al., 2010; Fox & Raichle, 2007). The seed can be a voxel, cluster, or brain region – selected from previously published coordinates or functional activation maps from a localizer task. The average of all included voxels are calculated for each time point to create a timeseries to be used as a regressor in a linear correlation or multiple regression analysis across all other voxels. The result is a whole-brain, voxel-wise functional connectivity map of covariance with the specified seed-region. Seed-based approaches have been employed by many research groups and proven invaluable for revealing reliable connectivity properties of many seed areas (Shehzad et al., 2009) – providing a direct answer to a direct question.

The approach, however, suffers from several inherent limitations. The resulting maps are dependent upon an a priori defined seed size, shape, and location. Difficulties with the technique are also apparent when attempting to design a stimulation task to elicit robust and localized hemodynamic changes in specialized brain areas. Spatial smoothing and misalignment of functional areas during inter-subject registration can further compound the errors in seed selection. Multiple systems cannot be studied simultaneously and the extracted waveform may not be a true independent variable when assessing statistical significance. Owing to the constraints of seed-region analysis, exploratory techniques that do not require defining seed regions are now frequently applied to spontaneous BOLD data that circumvent some of these limitations.

### 1.7.2.2 Independent component analysis (ICA)

There are a variety of popular data-driven methods. These fall within two broad categories: decomposition through such techniques as principal component analysis (PCA) (Friston, Frith, Liddle, & Frackowiak, 1993), singular value decomposition, and

independent component analysis (ICA) (Beckmann, DeLuca, Devlin, & Smith, 2005) or clustering using such techniques as hierarchical (Dietmar Cordes, Haughton, Carew, Arfanakis, & Maravilla, 2002), fuzzy (Baumgartner et al., 2000), and normalized cut clustering (van den Heuvel, Mandl, & Hulshoff Pol, 2008). ICA represents the most prevalent of these approaches that have been successfully applied to resting-state data.

ICA is a statistical technique that uses a linear model to decompose independent, uncorrelated, and non-Gaussian datasets into distinct subparts that represent underlying “hidden” sources (Vigário, Särelä, Jousmäki, Hämäläinen, & Oja, 2000). The type of signals can vary and could for example represent audio recordings of microphones placed throughout a room during a party. ICA could then be used to decompose the mixed conversations into the individual voice patterns of people in the room. Within the field of neuroscience, the technique was first applied to EEG data (Onton, Westerfield, Townsend, & Makeig, 2006) and later to task-based fMRI investigations (McKeown et al., 1998). Its use in the analysis of resting-state data began in the early 2000s (Kiviniemi, Kantola, Jauhiainen, Hyvärinen, & Tervonen, 2003). In terms of examining the resting-state BOLD signal, ICA is able to identify signal fluctuations by virtue of their spatial and temporal profiles without the need to specify an explicit model or voxel. Multiple temporally coherent functional networks are extracted without constraining the temporal domain and are a priori independent (McKeown et al., 1998). It does this by first concatenating all voxel time points across the duration of the scan into a two-dimensional data matrix. By optimizing a measure of non-Gaussianity, the algorithm identifies sets of voxels whose activity both varies together over time and is maximally different from the activity in other sets. The voxels contributing to each component need not be contiguous and spatial overlap between components is possible. Apart from identifying networks of coherent voxels, ICA is able to reveal the integrative and dissociative relationships within and between networks capturing the functional hierarchy of the human brain (Abou-Elseoud et al., 2010; Kiviniemi et al., 2009; Smith et al., 2009). The approach is also less prone to artifactual sources from physiologic and scanner noise than seed-based analysis due to the ability of the method to account for the existence of such structured noise effects within additional components.

There are several limitations of ICA. When implementing the analysis, dimensionality reduction through PCA is typically performed and then an a priori prediction about the number of underlying sources in the data is required (the model order). Choices at both of these steps can be somewhat arbitrary, but result in dramatic changes in the resulting components. Most relevant to brain networks, increasing the model order fractures networks into smaller sub-networks. While this can underlie real hierarchical relationships within the network (Abou-Elseoud et al., 2010; Kiviniemi et al., 2009; Smith et al., 2009), it is then difficult to determine the best level of analysis and the point at which the “full” network is represented. Approaches have been developed to optimally select the number of independent components for a given dataset according to statistical criteria (Jafri, Pearlson, Stevens, & Calhoun, 2008; Li, Adali, & Calhoun, 2007) though their validity needs further testing (Zuo et al., 2010) – particularly across different groups and species. Interpretation of the resulting component maps, whereby biologically relevant components are distinguished from noise and artifacts, is also non-trivial. ICA does not rank or order components and the maps must be sorted manually, matched to predefined spatial or temporal templates, or characterized with various assessment algorithms (De Martino et al., 2007; Moritz, Rogers, & Meyerand, 2003; Zeng, Qiu, Chodkowski, & Pekar, 2009).

In summary, there are several approaches for identifying patterns of coherent activity from resting-state fMRI data, but the field is currently dominated by the use of seed-based analysis and ICA. Although the different techniques each have strengths and weaknesses, and differ in the types of questions they can answer, they converge on a similar finding: network architecture can be reliably and reproducibly detected at individual subject and group levels from spontaneous BOLD activity.

### 1.7.3 Resting-state networks (RSNs)

RS-fMRI can identify large-scale spatial patterns of coherent signals representing integrated networks of information processing and accordingly, has been shown to provide reliable connectivity maps in humans (Beckmann et al., 2005; Biswal et al.,

1995; Damoiseaux et al., 2006), nonhuman primates (Hutchison et al., 2011a; Hutchison et al., 2011b; Vincent et al., 2007), and rodents (Hutchison, Mirsattari, Jones, Gati, & Leung, 2010; Jonckers, Van Audekerke, De Visscher, Van der Linden, & Verhoye, 2011; Pawela et al., 2008). The anatomically separated, but functionally linked brain regions showing a high level of ongoing functional connectivity during rest are referred to as resting-state networks (RSNs). The most consistent and commonly reported human RSNs (Beckmann et al., 2005; Damoiseaux et al., 2006; De Luca, Beckmann, De Stefano, Matthews, & Smith, 2006; Smith et al., 2009) are shown in Fig. 1.10. These eight RSNs reflect functional systems supporting core perceptual and cognitive processes. They include: (A) a primary visual network encompassing primary visual cortex; (B) an extrastriate visual network; (C) a network encompassing auditory and other sensory association cortices; (D) a somatomotor network as was first shown by Biswal et al. (1995); (E) the “default-mode” network (DMN), deactivated during demanding cognitive tasks and involved in episodic memory processes and self-referential mental representations (Buckner & Vincent, 2007; Fox et al., 2005; Raichle & Snyder, 2007); (F) a frontal network implicated in executive control and salience processing; and (G, H) two right- and left-lateralized fronto-parietal networks spatially similar to the bilateral dorsal attention network and implicated in working memory and cognitive attentional processes (Maurizio Corbetta & Shulman, 2002). Note that the intra-network connectivity is not restricted to cortical areas and RSNs display functional connectivity patterns with specific thalamic (Dongyang Zhang, Snyder, Shimony, Fox, & Raichle, 2010) and cerebellar nuclei (Krienen & Buckner, 2009).

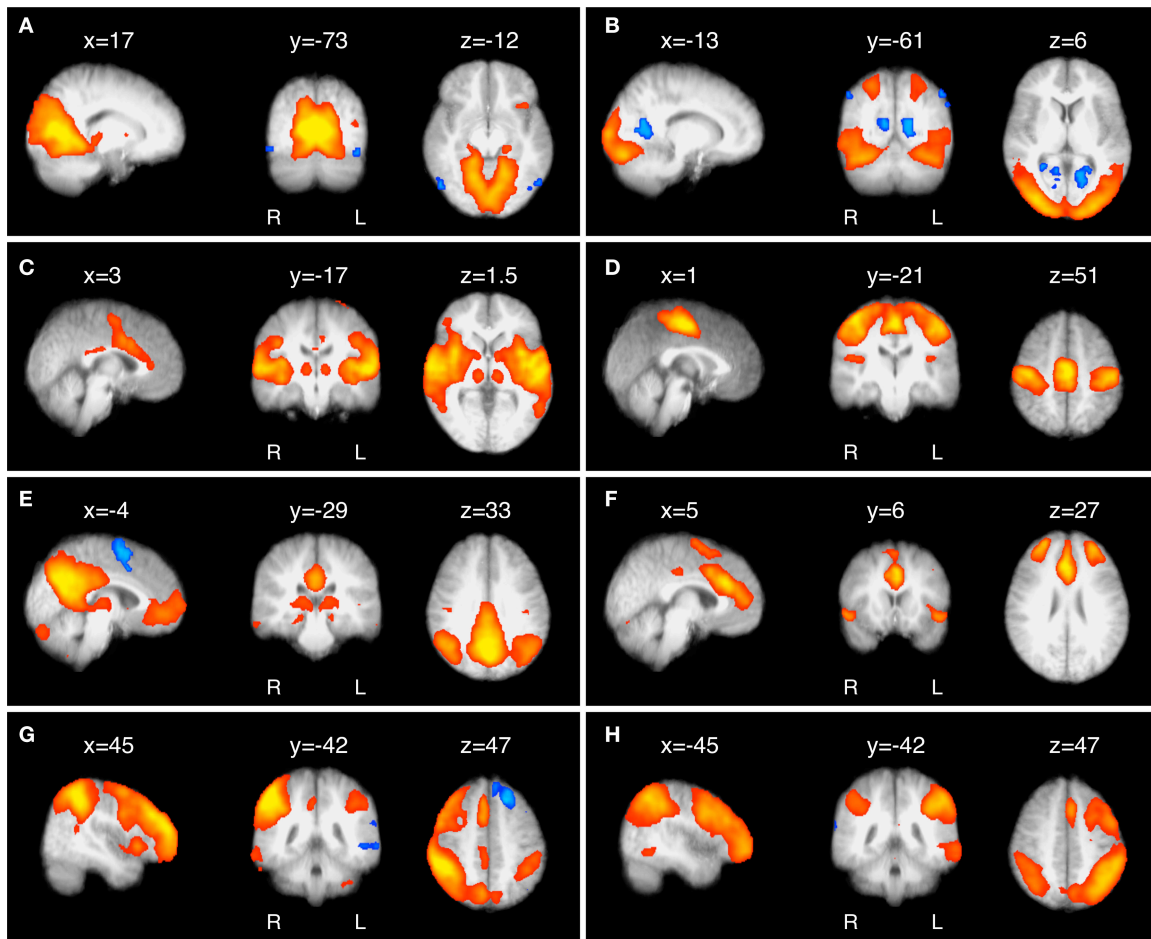


**Figure 1.10.** Eight of the most common and consistent RSNs identified by ICA. Sagittal, coronal, and axial views of different spatial maps associated with low-frequency resting patterns estimated from a group of 10 subjects. All images have been coregistered into the space of the MNI template. The coordinates refer to mm distances from the anterior commissure and images are shown in radiological convention. Reprinted with permission from Beckmann, DeLuca, Devlin, & Smith, 2005.

The aforementioned RSNs have been reported across subjects, studies, scanners, field strengths, and analysis techniques demonstrating characteristic systems of functional integration at rest (Cole et al., 2010; van den Heuvel & Hulshoff Pol, 2010). Resting-state networks manifest highly organized patterns of coherence across stages of cognitive development (Fair et al., 2007; Fransson et al., 2007), degrees of consciousness (Boly et al., 2008; Norton et al., 2012), under multiple types of general anesthesia (Boveroux et al., 2010; Deshpande, Kerssens, Sebel, & Hu, 2010; Greicius et al., 2008), and across mammalian species (see proceeding chapters). That is not to say, however, that the patterns are identical across all subjects or conditions. RSN activity and within-network connection properties have been previously demonstrated to be both state-dependent (Bianciardi et al., 2009; Horovitz et al., 2009, 2008), task-modulated (Esposito et al., 2006; Fransson, 2006; Smith et al., 2009; Sun, Miller, Rao, & D'Esposito, 2007), and indicative of individual variability (Fox, Snyder, Zacks, & Raichle, 2006; Kelly, Uddin, Biswal, Castellanos, & Milham, 2008). Further, RSNs are sensitive to pharmacological manipulations (Anand et al., 2005; Kelly et al., 2009), and as will be discussed in section 1.7.6, disease (Greicius, 2008).

The patterns of intrinsic functional connectivity are consistent with stimulus-evoked maps supporting their functional relevance, but also suggesting that the overlap may in fact be reflective of a common underlying system. Indeed, RSNs are activated or deactivated during specific cognitive and motor tasks (Calhoun et al., 2002; Jiang, He, Zang, & Weng, 2004; Moussa et al., 2011). Investigations have also continued to reveal new RSNs or sub-networks such as those related to memory, language, or self-referential systems (Li et al., 2011; Liao et al., 2009; Mantini, Perrucci, Del Gratta, Romani, & Corbetta, 2007; Vincent, Kahn, Van Essen, & Buckner, 2009) that link resting and task-state patterns. In this regard, it has been suggested that RSNs could be better classified as intrinsic connectivity networks (Seeley et al., 2007) to more accurately reflect the true nature of the networks - that despite being studied during “rest” the systems are actively involved in all aspects of cognition and behaviour and represent the functional topography of the mammalian brain.

#### 1.7.4 The relationship between function and structure

By definition, RSNs are composed of anatomically separated brain regions. These can include contralateral homologues or more distributed patterns within and between hemispheres. Given the growing evidence supporting a neural origin of resting-state fluctuations and their synchronization, many have hypothesized that the functional connectivity is supported by direct structural connections via white matter fiber tracts (Damoiseaux & Greicius, 2009). While direct evidence is limited in human subjects, there have been a number of studies that support this claim. Studies of functional connectivity in patients with agenesis (Quigley et al., 2003) or resection (Johnston et al., 2008) of the corpus callosum have shown significantly decreased functional connectivity between the neocortices. The reduced interhemispheric correlations do suggest that the commissure fibers are necessary for communication, though new evidence has questioned this claim (Tyszka, Kennedy, Adolphs, & Paul, 2011) leading to some ambiguity. The majority of other studies have examined the relationship between spontaneous BOLD correlations and anatomical connectivity using diffusion imaging techniques such as diffusion tensor imaging (DTI) and diffusion spectrum imaging (DSI). At a local level, Koch and coworkers found that regions on either side of a sulcus showing high functionally connectivity were also structurally connected by short-range fibers (Koch, Norris, & Hund-Georgiadis, 2002). This has since been shown at the whole brain level, in which regions with a higher level of structural connectivity showed higher levels of functional connectivity (Hagmann et al., 2008; Honey, Kötter, Breakspear, & Sporns, 2007; Honey et al., 2009). Indeed, almost all functionally linked regions of the most commonly reported RSNs appear to be constrained by known white matter tracts (Greicius, Supekar, Menon, & Dougherty, 2009; Honey et al., 2007; van den Heuvel, Mandl, Kahn, & Hulshoff Pol, 2009; Vincent et al., 2007).

The relationship between structural and functional connections is not, however, one-to-one and there are a number of discrepancies. Studies have reported areas that share no direct connections (Habas, 2009; Honey et al., 2009; Krienen & Buckner, 2009). For example, primary visual cortex has been found to be robustly connected to its contralateral homologue, though no direct connections exist (Van Essen, Newsome, &

Bixby, 1982). This implies that some of reported functional connectivity is driven by polysynaptic pathways. The opposite pattern has also been reported in which areas known to have structural connections do not show functional connectivity (Hutchison et al., 2011b). To summarize, the results point towards the existence of a general structural core of white matter connections supporting the functional connectivity observed between RSNs, but the precise relationship is unknown. The results are not necessarily surprising given that the structural brain network needs to facilitate a vast array of functional configurations to achieve different states (van den Heuvel & Hulshoff Pol, 2010). Further insight into the relationship between the two connectivity types is needed and will likely come from an experimental system in which anatomical connectivity can be more easily assessed and manipulated — that is, in an animal model.

### 1.7.5 Applying graph analysis to resting-state fMRI

As stated previously, the use of graph theory metrics allows for a theoretical framework conducive to the exploration of network topology. Graph theory can be applied directly to RS-fMRI data as it provides whole brain assessment of functional connectivity and therefore can reveal important information about the organization of functional brain networks. Though the application of established metrics to resting-state data is in its infancy, studies have supported findings from other methodologies (Bassett & Bullmore, 2006; Fallani et al., 2010; Micheloyannis et al., 2006; Stam, 2004) reporting efficient modular and small-world organization at rest when examining the regional brain area (Achard, Salvador, Whitcher, Suckling, & Bullmore, 2006; He et al., 2009; Y. Liu et al., 2008; Meunier et al., 2010; Salvador et al., 2005) or individual voxel (van den Heuvel, Stam, Boersma, & Hulshoff Pol, 2008) levels. The human brain was also shown to possess a core of highly connected hubs with an exponentially truncated power law degree distribution (Achard et al., 2006; Buckner et al., 2009; Liu et al., 2008; Salvador et al., 2005). These properties reflect a robust complex network organization that is resilient against random attacks or disruption (Bullmore & Sporns, 2009). Although, disruption of hub nodes can result in a catastrophic breakdown of connectivity (see below). Taken together, graph analysis of resting-state data has shown the human brain is

not just a random network, but one with an organization optimized towards a high level of local and global efficiency.

### 1.7.6 Resting-state networks and disease

In the summer of 2003, the tripping of a generation unit in Ohio led, through a cascading series of failures, to blackouts in eight US states and Ontario, leaving approximately 55 million people without power for up to 17 hours in the second worst blackout in history<sup>3</sup>. Networks emerge or are created across disciplines because they facilitate efficient information transfer and allow the emergence of properties not possible when the nodes are in isolation. These could include, for example, increased processing capabilities, stability, or resource sharing. However, alteration or breakdown of the network, especially of hub nodes, can create detrimental dynamics and catastrophic failure across the entire system as was observed in the breakdown of a single node in the complex northeastern power grid network resulting in 508 off-line units and near complete system failure. In a similar manner, the brain is sensitive to manipulations that alter its functional and structural organization.

A growing and promising avenue of research is exploring the use of RS-fMRI measures in assessing clinical disorders; the overarching hypothesis across many of these studies being that alteration of brain networks are the cause or consequence of the abnormal manifestations characteristic of the disease. The technique is particularly well suited for investigations of non-normal populations, such as subjects with severe cognitive or physical impairments compared to other methodologies, including task-based fMRI. This is because resting-state investigations require minimal task compliance and therefore allow for accurate comparisons of brain connectivity and dynamics. For example, a task requiring memory encoding can be of particular concern when evaluating patients suffering from neurodegenerative diseases.

---

<sup>3</sup> U.S.-Canada Power System Outage Task Force, August 14th Blackout: Causes and Recommendations

Although their meaning is not fully understood, changes in functional RSNs have been reported in multiple psychiatric and neurologic disorders including depression (Greicius et al., 2007; Kühn & Gallinat, 2011; Lui et al., 2011), attention deficit-hyperactivity disorder (Castellanos et al., 2008; Fair et al., 2010), schizophrenia (Bassett, Nelson, Mueller, Camchong, & Lim, 2011; Kühn & Gallinat, 2011; Whitfield-Gabrieli et al., 2009), Alzheimer's disease (Chen et al., 2011; Greicius, Srivastava, Reiss, & Menon, 2004), epilepsy (Waites, Briellmann, Saling, Abbott, & Jackson, 2006; Zhang et al., 2011), coma (Norton et al., 2012), multiple sclerosis (Lowe et al., 2008, 2002), and amyotrophic lateral sclerosis (Mohammadi et al., 2009) (for review see Greicius, 2008; van den Heuvel & Hulshoff Pol, 2010). Many early studies focused on the default-mode RSN, as the network seems particularly sensitive to disruption in disease states, but more recent work has now started to examine other networks as well as changes in the overall organization of functional brain network using graph analysis techniques (Jafri et al., 2008). For example, through graph analysis of resting-state data it was revealed that the locations of high concentrations of amyloid deposits in Alzheimer's disease patients were highly correlated with the location of highly connected hub-regions in the human brain suggesting that disruption of integrative hubs may result in the decreased functional brain efficiency in these patients (Buckner et al., 2009). Taken together, the extensive documentation of altered RSN topology suggests that brain diseases are targeting interconnected cortical networks, rather than a single region and may help explain some of the complex manifestations seen in these patient populations.

Given that the examination of spatiotemporal properties of RSNs studied with RS-fMRI can delineate abnormal neural functional architecture, the natural extension of the methodology would be using RSN-related metrics as potential screening devices for disease. However, many of the robust changes across the range of aforementioned disorders have been derived and significance-tested for “proof of concept” at the group level. These represent valuable contributions towards understanding abnormal brain activity and connectivity, but characterizing patterns of functional variability between normal and patient groups is far from providing clinical diagnostics at the single-subject level. The correlative results also present a directionality problem, in that the relationship between the disease and altered connectivity are unclear. The functional disruptions could

represent a consequence of the disease or be the underlying cause and this could vary across disease types. Despite these concerns, evidence is emerging to suggest that the obstacles can be overcome and changes can be robust enough to detect for the single subject (Fleisher et al., 2009). Given the extraordinary potential for RSNs as possible diagnostic or prognostic markers, it is crucial to understand the physiological mechanisms of fluctuation, regulation, and entrainment of LFFs and the RSNs that are revealed through their synchronization.

## 1.8 Resting-state investigations of animal models

Owing to the non-invasive nature of the technique, RS-fMRI is able to study the human brain and assess brain topology in both normal and disease subject groups. Consequently, the vast majority of studies on intrinsic brain activity and resting-state functional connectivity have been conducted on human subjects. There is, however, a requisite for the examination of the brain functional organization in other animals. At the most basic level, the study of other species can significantly enhance our understanding of mammalian brain organization and evolution through cross-species evaluation of homologies. RS-fMRI is particularly well suited for this task as the same methodology can be used across species. Animals also allow experimental manipulations to be carried out that are not practical in human subjects. Many of these species are used as research models across multiple branches of science to elucidate features of normal and abnormal human conditions; resting-state fMRI can provide valuable information on the altered brain changes that are occurring in these models. This is particularly useful in lesion and drug manipulation studies that cause widespread effects that cannot be captured using standard methodologies. Importantly, with the use of animal models it will be possible to investigate unanswered questions concerning RS-fMRI itself. Functional maps can be directly compared to structural connectivity maps derived from anatomical tracing studies (even in the same animal) to reveal what the correlations in the signals are reflecting. The origin and potential function of the resting-state signal and the synchronization across distributed areas can be directly assessed with depth recording, high-field studies, and pharmacological investigations. In the same vein, the relationship between disease and

alterations of connectivity can be assessed through experimental manipulations – revealing a causal role not possible in human work. Future work in animal RS-fMRI is a promising avenue, though in all of these applications it is critical to first assess the “baseline” or normal functional networks.

## 1.9 Summary and current projects

The human brain is a complex system composed of multiple levels organized into integrative network configurations. At a gross topological scale, spatially distributed, interconnected brain areas interact to perform circumscribed functions – communicating via oscillatory patterns of synchronization supported by long-range white matter fiber tracts. RS-fMRI has become an important tool for characterizing these functional brain networks in normal and disease states by analyzing the coherence in low-frequency fluctuations of the BOLD signal that are presumably overlying ongoing neural activity. Open questions regarding the origin, function, and direction of disease-related changes of the signal correlations, as well as knowledge concerning the homology and evolution of the networks are necessary for basic and applied applications. These highlight the need for animal investigations using RS-fMRI.

In Chapter 2 of this thesis, I examined the spatiotemporal characteristics of anesthetized rats at rest with two different anesthetic regimes (Hutchison et al., 2010). Previous reports using RS-fMRI were primarily limited to seed region analysis in the somatosensory cortex and caudate-putamen. Using ICA, I was able to probe the entire brain without the need for predefined regions or functional localizer tasks allowing a more complete understanding of the rat’s functional brain topology. I found independent, synchronous LFFs of BOLD signals existed in clustered, bilaterally symmetric regions of both cortical and subcortical structures. Similar independent network components were found under both types of anesthesia and showed homologous organization with previously reported patterns observed in anesthetized monkeys and awake humans. The results represent an essential step in the understanding of rat brain networks necessary for homology comparisons and framing changes induced by experimental manipulations.

In Chapter 3 of this thesis, I extend the methodology used in Chapter 2 to non-human primates and present a comprehensive assessment of macaque RSNs using group-ICA (Hutchison et al., 2011a). Nonhuman primates and in particular macaque monkeys have been used as surrogates for the study of human brain function for several decades and might therefore represent an ideal animal model for the study of RSNs. Similar to the investigation of RS-fMRI in the rat, previously published reports were limited by seed-region analysis of specific brain areas. In the present work, ICA revealed RSNs underlying multiple levels of sensory, motor, and cognitive processing. The results demonstrated that macaques share remarkable homologous network organization with humans, thereby providing strong support for their use as an animal model of human brain function.

Finally, in Chapter 4 of this thesis I investigated the assumption of network stationarity implicit in most RS-fMRI investigations by characterizing RSN dynamics of anesthetized macaques and awake human subjects using a sliding-window correlation analysis (Hutchison, Womelsdorf, Gati, Everling, & Menon, 2012a). I found that functional connectivity among nodes comprising RSNs strongly fluctuated over time during awake as well as anaesthetized states. For time dependent correlational analysis with short windows (<60s), periods of positive functional correlations alternated with prominent anti-correlations that were missed when assessed with longer time windows. Similarly, time varying analysis identified network nodes that transiently link to the core RSN that did not emerge in average RSN analysis. Furthermore, time-dependent analysis reliably revealed transient states of large-scale synchronization that spanned all seeds. The results illustrated that resting-state functional connectivity is not static and that RSNs can exhibit non-stationary, spontaneous relationships irrespective of conscious, cognitive processing. The findings imply that mechanistically important network information can be missed when using average functional connectivity as the single network measure and that ongoing RSN dynamics represent an evolutionarily preserved aspect of brain function.

Taken together, these experiments provide a more complete understanding of the network organization, homologies, and dynamics across three species: rats, monkeys, and

humans. The findings are essential for establishing the normal baseline condition for subsequent work examining experimental manipulations of all three species.

## 1.10 References

- Abou-Elseoud, A., Starck, T., Remes, J., Nikkinen, J., Tervonen, O., & Kiviniemi, V. (2010). The effect of model order selection in group PICA. *Hum Brain Map*, *31*, 1207–1216.
- Broder, A., Kumar, R., Maghoul, F., Raghavan, P., Rajagopalan, S., Stata, R., Tomkins, A., and Wiener, J. (2000), Graph structure in the web, *Comput Netw*, *33*, 309–320.
- Achacoso, T. B., & Yamamoto, W. S. (1992). *AY's neuroanatomy of C. elegans for computation*. CRC Press.
- Achard, S., Salvador, R., Whitcher, B., Suckling, J., & Bullmore, E. (2006). A resilient, low-frequency, small-world human brain functional network with highly connected association cortical hubs. *J Neurosci*, *26*, 63–72.
- Amaral, L. A., Scala, A., Barthelemy, M., & Stanley, H. E. (2000). Classes of small-world networks. *Proc Natl Acad Sci U S A*, *97*, 11149–11152.
- Anand, A., Li, Y., Wang, Y., Wu, J., Gao, S., Bukhari, L., Mathews, V. P., et al. (2005). Antidepressant effect on connectivity of the mood-regulating circuit: an FMRI study. *Neuropsychopharmacology*, *30*, 1334–1344.
- Attwell, D., & Iadecola, C. (2002). The neural basis of functional brain imaging signals. *Trends Neurosci*, *25*, 621–625.
- Backstrom, L., Boldi, P., Rosa, M., Ugander, J., & Vigna, S. (2011). Four Degrees of Separation. arXiv:1111.4570.
- Barabasi, & Albert. (1999). Emergence of scaling in random networks. *Science*, *286*, 509–512.
- Baria, A. T., Baliki, M. N., Parrish, T., & Apkarian, A. V. (2011). Anatomical and Functional Assemblies of Brain BOLD Oscillations. *J Neurosci*, *31*, 7910–7919.
- Bassett, D.S., & Bullmore, E. (2006). Small-world brain networks. *Neuroscientist*, *12*, 512–523.
- Bassett, Danielle S, Nelson, B. G., Mueller, B. A., Camchong, J., & Lim, K. O. (2011). Altered resting state complexity in schizophrenia. *NeuroImage*, *59*, 2196-207.

- Baumgartner, R., Ryner, L., Richter, W., Summers, R., Jarmasz, M., & Somorjai, R. (2000). Comparison of two exploratory data analysis methods for fMRI: fuzzy clustering vs. principal component analysis. *Magn Reson Imaging, 18*, 89–94.
- Beckmann, C. F., DeLuca, M., Devlin, J. T., & Smith, S. M. (2005). Investigations into resting-state connectivity using independent component analysis. *Philos Trans R Soc Lond B Biol Sci, 360*, 1001–1113.
- Bhalla, U. S., & Iyengar, R. (1999). Emergent properties of networks of biological signaling pathways. *Science, 283*, 381–387.
- Bianciardi, M., Fukunaga, M., van Gelderen, P., Horovitz, S. G., de Zwart, J. A., & Duyn, J. H. (2009). Modulation of spontaneous fMRI activity in human visual cortex by behavioral state. *NeuroImage, 45*, 160–168.
- Birn, R. M., Murphy, K., & Bandettini, P. A. (2008). The effect of respiration variations on independent component analysis results of resting state functional connectivity. *Hum Brain Mapp, 29*, 740–750.
- Biswal, B., Yetkin, F. Z., Haughton, V. M., & Hyde, J. S. (1995). Functional connectivity in the motor cortex of resting human brain using echo-planar MRI. *Magn Reson Med, 34*, 537–541.
- Boly, M., Phillips, C., Tshibanda, L., Vanhaudenhuyse, A., Schabus, M., Dang-Vu, T. T., Moonen, G., et al. (2008). Intrinsic brain activity in altered states of consciousness: how conscious is the default mode of brain function? *Ann N Y Acad Sci 1129*, 119–129.
- Boveroux, P., Vanhaudenhuyse, A., Bruno, M.-A., Noirhomme, Q., Lauwick, S., Luxen, A., Degueldre, C., et al. (2010). Breakdown of within- and between-network resting state functional magnetic resonance imaging connectivity during propofol-induced loss of consciousness. *Anesthesiology, 113*, 1038–1053.
- Breakspear, M., & McIntosh, A. R. (2011). Networks, noise and models: reconceptualizing the brain as a complex, distributed system. *NeuroImage, 58*, 293–295.
- Bressler, S. L., & Menon, V. (2010). Large-scale brain networks in cognition: emerging methods and principles. *Trends Cogn Sci, 14*, 277–290.
- Brodmann, K. in *Handbuch der Neurologie* (ed. Lewandowsky, M.) 206–307 (Springer, Berlin, 1910).
- Büchel, C., & Friston, K. (2001). Interactions among neuronal systems assessed with functional neuroimaging. *Revue Neurologique, 157*(8-9 Pt 1), 807–815.
- Buckner, R. L., & Vincent, J. L. (2007). Unrest at rest: default activity and spontaneous network correlations. *Neuroimage, 37*, 1091–1096.

- Buckner, Randy L, Sepulcre, J., Talukdar, T., Krienen, F. M., Liu, H., Hedden, T., Andrews-Hanna, J. R., et al. (2009). Cortical hubs revealed by intrinsic functional connectivity: mapping, assessment of stability, and relation to Alzheimer's disease. *J Neurosci*, *29*, 1860–1873.
- Bullmore, E., & Sporns, O. (2009). Complex brain networks: graph theoretical analysis of structural and functional systems. *Nat Rev Neurosci*, *10*, 186–198.
- Buzsáki, G. (2006). *Rhythms of the Brain* (1st ed.). Oxford University Press, USA.
- Buzsáki, G., & Draguhn, A. (2004). Neuronal oscillations in cortical networks. *Science* *304*, 1926–1929.
- Buzsáki, G., Geisler, C., Henze, D. A., & Wang, X.-J. (2004). Interneuron Diversity series: Circuit complexity and axon wiring economy of cortical interneurons. *Trend Neurosci*, *27*, 186–193.
- Calhoun, V. D., Pekar, J. J., McGinty, V. B., Adali, T., Watson, T. D., & Pearlson, G. D. (2002). Different activation dynamics in multiple neural systems during simulated driving. *Hum Brain Mapp*, *16*, 158–167.
- Castellanos, F. X., Margulies, D. S., Kelly, C., Uddin, L. Q., Ghaffari, M., Kirsch, A., Shaw, D., et al. (2008). Cingulate-precuneus interactions: a new locus of dysfunction in adult attention-deficit/hyperactivity disorder. *Biol Psychiatry*, *63*, 332–337.
- Chen, G., Ward, B. D., Xie, C., Li, W., Wu, Z., Jones, J. L., Franczak, M., et al. (2011). Classification of Alzheimer disease, mild cognitive impairment, and normal cognitive status with large-scale network analysis based on resting-state functional MR imaging. *Radiology*, *259*, 213–221.
- Cohen, J. E., Briand, F., & Newman, C. M. (1990). *Community Food Webs: Data and Theory*. Springer-Verlag.
- Cole, D. M., Smith, S. M., & Beckmann, C. F. (2010). Advances and pitfalls in the analysis and interpretation of resting-state FMRI data. *Front Syst Neurosci*, *4*, 8.
- Corbetta, M., & Shulman, G. L. (2002). Control of goal-directed and stimulus-driven attention in the brain. *Nat Rev Neurosci*, *3*, 201–215.
- Cordes, D, Haughton, V. M., Arfanakis, K., Carew, J. D., Turski, P. A., Moritz, C. H., Quigley, M. A., et al. (2001). Frequencies contributing to functional connectivity in the cerebral cortex in “resting-state” data. *AJNR*, *22*, 1326–1333.
- Cordes, Dietmar, Haughton, V., Carew, J. D., Arfanakis, K., & Maravilla, K. (2002). Hierarchical clustering to measure connectivity in fMRI resting-state data. *Magn Reson Imaging*, *20*, 305–317.

- Csicsvari, J., Jamieson, B., Wise, K. D., & Buzsáki, G. (2003). Mechanisms of gamma oscillations in the hippocampus of the behaving rat. *Neuron*, *37*, 311–322.
- Damoiseaux, J. S., Rombouts, S. A. R. B., Barkhof, F., Scheltens, P., Stam, C. J., Smith, S. M., & Beckmann, C. F. (2006). Consistent resting-state networks across healthy subjects. *Proc Natl Acad Sci U S A*, *103*, 13848–13853.
- Damoiseaux, Jessica S., & Greicius, M. D. (2009). Greater than the sum of its parts: a review of studies combining structural connectivity and resting-state functional connectivity. *Brain Struct Func*, *213*, 525–533.
- De Luca, M., Beckmann, C. F., De Stefano, N., Matthews, P. M., & Smith, S. M. (2006). fMRI resting state networks define distinct modes of long-distance interactions in the human brain. *NeuroImage*, *29*, 1359–1367.
- De Martino, F., Gentile, F., Esposito, F., Balsi, M., Di Salle, F., Goebel, R., & Formisano, E. (2007). Classification of fMRI independent components using IC-fingerprints and support vector machine classifiers. *NeuroImage*, *34*, 177–194.
- Deco, G., Buehlmann, A., Masquelier, T., & Hugues, E. (2011). The role of rhythmic neural synchronization in rest and task conditions. *Front Hum Neurosci*, *5*, 4.
- Deshpande, G., Kerssens, C., Sebel, P. S., & Hu, X. (2010). Altered local coherence in the default mode network due to sevoflurane anesthesia. *Brain Res*, *1318*, 110–121.
- Engel, A. K., Fries, P., & Singer, W. (2001). Dynamic predictions: oscillations and synchrony in top-down processing. *Nat Rev Neurosci*, *2*, 704–716.
- Esposito, F., Bertolino, A., Scarabino, T., Latorre, V., Blasi, G., Popolizio, T., Tedeschi, G., et al. (2006). Independent component model of the default-mode brain function: Assessing the impact of active thinking. *Brain Res Bull*, *70*, 263–269.
- Fair, D. A., Dosenbach, N. U. F., Church, J. A., Cohen, A. L., Brahmbhatt, S., Miezin, F. M., Barch, D. M., et al. (2007). Development of distinct control networks through segregation and integration. *Proc Natl Acad Sci U S A*, *104*, 13507–13512.
- Fair, D. A., Posner, J., Nagel, B. J., Bathula, D., Dias, T. G. C., Mills, K. L., Blythe, M. S., et al. (2010). Atypical default network connectivity in youth with attention-deficit/hyperactivity disorder. *Biol Psychiatry*, *68*, 1084–1091.
- Fallani, F. D. V., Costa, L. da F., Rodriguez, F. A., Astolfi, L., Vecchiato, G., Toppi, J., Borghini, G., et al. (2010). A graph-theoretical approach in brain functional networks. Possible implications in EEG studies. *Nonlinear Biomedl Phys*, *4*, Suppl 1:S8.
- Faloutsos, M., Faloutsos, P., & Faloutsos, C. (1999). On power-law relationships of the internet topology. *Comp Comm Rev* *29*, 251–262.

- Finger, S. (1994). *Origins of Neuroscience: A History of Explorations into Brain Function* (1st ed.). Oxford University Press, USA.
- Fleisher, A. S., Sherzai, A., Taylor, C., Langbaum, J. B. S., Chen, K., & Buxton, R. B. (2009). Resting-state BOLD networks versus task-associated functional MRI for distinguishing Alzheimer's disease risk groups. *NeuroImage*, *47*, 1678–1690.
- Fox, M. D., Snyder, A. Z., Vincent, J. L., Corbetta, M., Van Essen, D. C., & Raichle, M. E. (2005). The human brain is intrinsically organized into dynamic, anticorrelated functional networks. *Proc Natl Acad Sci U S A*, *102*, 9673–9678.
- Fox, M.D., & Raichle, M. E. (2007). Spontaneous fluctuations in brain activity observed with functional magnetic resonance imaging. *Nat Rev Neurosci*, *8*, 700–711.
- Fox, M.D., Snyder, A. Z., Zacks, J. M., & Raichle, M. E. (2006). Coherent spontaneous activity accounts for trial-to-trial variability in human evoked brain responses. *Nat Neurosci*, *9*, 23–25.
- Fransson, P., Skiöld, B., Horsch, S., Nordell, A., Blennow, M., Lagercrantz, H., & Aden, U. (2007). Resting-state networks in the infant brain. *Proc Natl Acad Sci U S A*, *104*, 15531.
- Fransson, P. (2006). How default is the default mode of brain function? Further evidence from intrinsic BOLD signal fluctuations. *Neuropsychologia*, *44*, 2836–2845.
- Friston, K. J., Frith, C. D., Liddle, P. F., & Frackowiak, R. S. (1993). Functional connectivity: the principal-component analysis of large (PET) data sets. *J Cereb Blood Metab*, *13*, 5–14.
- Ghazanfar, A. A., & Schroeder, C. E. (2006). Is neocortex essentially multisensory? *Trends Cogn Sci*, *10*, 278–285.
- Gloor, P. (1985). Neuronal generators and the problem of localization in electroencephalography: application of volume conductor theory to electroencephalography. *J Clin Neurophysiol*, *2*, 327–354.
- Golanov, E. V., Yamamoto, S., & Reis, D. J. (1994). Spontaneous waves of cerebral blood flow associated with a pattern of electrocortical activity. *Am J Physiol*, *266*, 204–214.
- Gong, G., He, Y., Concha, L., Lebel, C., Gross, D. W., Evans, A. C., & Beaulieu, C. (2009). Mapping anatomical connectivity patterns of human cerebral cortex using in vivo diffusion tensor imaging tractography. *Cereb Cortex*, *19*, 524–536.
- Greicius, M. (2008). Resting-state functional connectivity in neuropsychiatric disorders. *Curr Opin Neurol*, *21*, 424–430.

- Greicius, M. D, Supekar, K., Menon, V., & Dougherty, R. F. (2009). Resting-state functional connectivity reflects structural connectivity in the default mode network. *Cereb Cortex*, *19*, 72-78.
- Greicius, M.D., Kiviniemi, V., Tervonen, O., Vainionpää, V., Alahuhta, S., Reiss, A. L., & Menon, V. (2008). Persistent default-mode network connectivity during light sedation. *Hum Brain Mapp*, *29*, 839–847.
- Greicius, M.D, Flores, B. H., Menon, V., Glover, G. H., Solvason, H. B., Kenna, H., Reiss, A. L., et al. (2007). Resting-state functional connectivity in major depression: abnormally increased contributions from subgenual cingulate cortex and thalamus. *Biol Psychiatry*, *62*, 429–437.
- Greicius, M.D., Srivastava, G., Reiss, A. L., & Menon, V. (2004). Default-mode network activity distinguishes Alzheimer’s disease from healthy aging: evidence from functional MRI. *Proc Natl Acad Sci U S A*, *101*, 4637–4642.
- Guye, M., Bartolomei, F., & Ranjeva, J.-P. (2008). Imaging structural and functional connectivity: towards a unified definition of human brain organization? *Curr Opin Neurol*, *21*, 393–403.
- Habas, C. (2009). Functional connectivity of the human rostral and caudal cingulate motor areas in the brain resting state at 3T. *Neuroradiology*, *52*, 47–59.
- Hagmann, P., Cammoun, L., Gigandet, X., Meuli, R., Honey, C. J., Wedeen, V. J., & Sporns, O. (2008). Mapping the structural core of human cerebral cortex. *PLoS Biology*, *6*, e159.
- Hartwell, L. H., Hopfield, J. J., Leibler, S., & Murray, A. W. (1999). From molecular to modular cell biology. *Nature*, *402*, 47–52.
- He, Y., Wang, J., Wang, L., Chen, Z. J., Yan, C., Yang, H., Tang, H., et al. (2009). Uncovering intrinsic modular organization of spontaneous brain activity in humans. *PloS One*, *4*, e5226.
- Hilgetag, C. C., Burns, G. A., O’Neill, M. A., Scannell, J. W., & Young, M. P. (2000). Anatomical connectivity defines the organization of clusters of cortical areas in the macaque monkey and the cat. *Philos Trans R Soc Lond B Biol Sci*, *355*, 91–110.
- Honey, C. J., Kötter, R., Breakspear, M., & Sporns, O. (2007). Network structure of cerebral cortex shapes functional connectivity on multiple time scales. *Proc Natl Acad Sci U S A*, *104*, 10240-10245.
- Honey, C. J., Sporns, O., Cammoun, L., Gigandet, X., Thiran, J. P., Meuli, R., & Hagmann, P. (2009). Predicting human resting-state functional connectivity from structural connectivity. *Proc Natl Acad Sci U S A*, *106*, 2035-2040.

- Horovitz, S. G., Braun, A. R., Carr, W. S., Picchioni, D., Balkin, T. J., Fukunaga, M., & Duyn, J. H. (2009). Decoupling of the brain's default mode network during deep sleep. *Proc Natl Acad Sci U S A*, *106*, 11376–11381.
- Horovitz, S. G., Fukunaga, M., de Zwart, J. A., van Gelderen, P., Fulton, S. C., Balkin, T. J., & Duyn, J. H. (2008). Low frequency BOLD fluctuations during resting wakefulness and light sleep: a simultaneous EEG-fMRI study. *Hum Brain Mapp*, *29*, 671–682.
- Huettel, S. A., Song, A. W., & McCarthy, G. (2004). *Functional Magnetic Resonance Imaging*. Sinauer Associates.
- Hutchison, R. M., Mirsattari, S. M., Jones, C. K., Gati, J. S., & Leung, L. S. (2010). Functional Networks in the Anesthetized Rat Brain Revealed by Independent Component Analysis of Resting-State fMRI. *J Neurophys*, *103*, 3398–3406.
- Hutchison, R. M., Leung, L. S., Mirsattari, S. M., Gati, J. S., Menon, R. S., & Everling, S. (2011a). Resting-state networks in the macaque at 7 T. *NeuroImage*, *56*, 1546–1555.
- Hutchison, R. M., Womelsdorf, T., Gati, J. S., Leung, L. S., Menon, R. S., & Everling, S. (2011b). Resting-State Connectivity Identifies Distinct Functional Networks in Macaque Cingulate Cortex. *Cereb Cortex*.
- Hutchison RM, Womelsdorf T, Gati JS, Everling S, Menon RS. (2012a). Resting-state networks show dynamic functional connectivity in awake humans and anesthetized macaques. *Hum Brain Mapp*. *In press*.
- Iadecola, C., & Nedergaard, M. (2007). Glial regulation of the cerebral microvasculature. *Nat Neurosci*, *10*, 1369–1376.
- Iturria-Medina, Y., Canales-Rodríguez, E. J., Melie-García, L., Valdés-Hernández, P. A., Martínez-Montes, E., Alemán-Gómez, Y., & Sánchez-Bornot, J. M. (2007). Characterizing brain anatomical connections using diffusion weighted MRI and graph theory. *NeuroImage*, *36*, 645–660.
- Jafri, M. J., Pearlson, G. D., Stevens, M., & Calhoun, V. D. (2008). A method for functional network connectivity among spatially independent resting-state components in schizophrenia. *Neuroimage*, *39*, 1666–1681.
- Jeong, H., Tombor, B., Albert, R., Oltvai, Z. N., & Barabási, A. L. (2000). The large-scale organization of metabolic networks. *Nature*, *407*, 651–654.
- Jiang, T., He, Y., Zang, Y., & Weng, X. (2004). Modulation of functional connectivity during the resting state and the motor task. *Hum Brain Mapp*, *22*, 63–71.
- Johnston, J. M., Vaishnavi, S. N., Smyth, M. D., Zhang, D., He, B. J., Zempel, J. M., Shimony, J. S., et al. (2008). Loss of resting interhemispheric functional

- connectivity after complete section of the corpus callosum. *J Neurosci*, 28, 6453-6458.
- Jonckers, E., Van Audekerke, J., De Visscher, G., Van der Linden, A., & Verhoye, M. (2011). Functional Connectivity fMRI of the Rodent Brain: Comparison of Functional Connectivity Networks in Rat and Mouse. *PLoS ONE*, 6, e18876.
- Kelly, A. M. C., Uddin, L. Q., Biswal, B. B., Castellanos, F. X., & Milham, M. P. (2008). Competition between functional brain networks mediates behavioral variability. *NeuroImage*, 39, 527–537.
- Kelly, C., de Zubicaray, G., Di Martino, A., Copland, D. A., Reiss, P. T., Klein, D. F., Castellanos, F. X., et al. (2009). L-dopa modulates functional connectivity in striatal cognitive and motor networks: a double-blind placebo-controlled study. *J Neurosci*, 29, 7364–7378.
- Kiviniemi, V., Kantola, J.-H., Jauhiainen, J., Hyvärinen, A., & Tervonen, O. (2003). Independent component analysis of nondeterministic fMRI signal sources. *NeuroImage*, 19, 253–260.
- Kiviniemi, V., Starck, T., Remes, J., Long, X., Nikkinen, J., Haapea, M., Veijola, J., et al. (2009). Functional segmentation of the brain cortex using high model order group PICA. *Hum Brain Mapp*, 30, 3865–3886.
- Koch, M. A., Norris, D. G., & Hund-Georgiadis, M. (2002). An investigation of functional and anatomical connectivity using magnetic resonance imaging. *NeuroImage*, 16, 241–250.
- Kohn, K. W. (1999). Molecular interaction map of the mammalian cell cycle control and DNA repair systems. *Mol Biol Cell*, 10, 2703–2734.
- Krienen, F. M., & Buckner, R. L. (2009). Segregated fronto-cerebellar circuits revealed by intrinsic functional connectivity. *Cereb Cortex*, 19, 2485–2497.
- Kühn, S., & Gallinat, J. (2011). Resting-State Brain Activity in Schizophrenia and Major Depression: A Quantitative Meta-Analysis. *Schizophr Bull. In press*
- Leopold, D. A., Murayama, Y., & Logothetis, N. K. (2003). Very slow activity fluctuations in monkey visual cortex: implications for functional brain imaging. *Cereb Cortex*, 13, 422-433.
- Li, R., Chen, K., Fleisher, A. S., Reiman, E. M., Yao, L., & Wu, X. (2011). Large-scale directional connections among multi resting-state neural networks in human brain: a functional MRI and Bayesian network modeling study. *NeuroImage*, 56, 1035–1042.
- Li, S. J., Biswal, B., Li, Z., Risinger, R., Rainey, C., Cho, J. K., Salmeron, B. J., et al. (2000). Cocaine administration decreases functional connectivity in human

- primary visual and motor cortex as detected by functional MRI. *Magn Reson Med*, 43, 45–51.
- Li, Y.O., Adali, T., & Calhoun, V. D. (2007). Estimating the number of independent components for functional magnetic resonance imaging data. *Hum Brain Mapp*, 28, 1251–1266.
- Liao, W., Mantini, D., Zhang, Z., Pan, Z., Ding, J., Gong, Q., Yang, Y., et al. (2009). Evaluating the effective connectivity of resting state networks using conditional Granger causality. *Biol Cybern*, 102, 57–69.
- Linkenkaer-Hansen, K., Nikouline, V. V., Palva, J. M., & Ilmoniemi, R. J. (2001). Long-range temporal correlations and scaling behavior in human brain oscillations. *The J Neurosci*, 21, 1370–1377.
- Lisman, J., & Buzsáki, G. (2008). A neural coding scheme formed by the combined function of gamma and theta oscillations. *Schizophr Bull*, 34, 974–980.
- Liu, Y., Liang, M., Zhou, Y., He, Y., Hao, Y., Song, M., Yu, C., et al. (2008). Disrupted small-world networks in schizophrenia. *Brain*, 13, 945–961.
- Logothetis, N K, Pauls, J., Augath, M., Trinath, T., & Oeltermann, A. (2001). Neurophysiological investigation of the basis of the fMRI signal. *Nature*, 412, 150–157.
- Logothetis, Nikos K, & Wandell, B. A. (2004). Interpreting the BOLD signal. *Annual Review of Physiology*, 66, 735–769.
- Lowe, M. J., Beall, E. B., Sakaie, K. E., Koenig, K. A., Stone, L., Marrie, R. A., & Phillips, M. D. (2008). Resting state sensorimotor functional connectivity in multiple sclerosis inversely correlates with transcallosal motor pathway transverse diffusivity. *Hum Brain Mapp*, 29, 818–827.
- Lowe, M. J., Phillips, M. D., Lurito, J. T., Mattson, D., Dzemedzic, M., & Mathews, V. P. (2002). Multiple sclerosis: low-frequency temporal blood oxygen level-dependent fluctuations indicate reduced functional connectivity initial results. *Radiology*, 224, 184–192.
- Lui, S., Wu, Q., Qiu, L., Yang, X., Kuang, W., Chan, R. C. K., Huang, X., et al. (2011). Resting-state functional connectivity in treatment-resistant depression. *Am J Psychiatry*, 168, 642–648.
- Mantini, D., Perrucci, M. G., Del Gratta, C., Romani, G. L., & Corbetta, M. (2007). Electrophysiological signatures of resting state networks in the human brain. *Proc Natl Acad Sci U S A*, 104, 13170-13175.
- McIntosh, A. R. (2004). Contexts and catalysts: a resolution of the localization and integration of function in the brain. *Neuroinformatics*, 2, 175–182.

- McKeown, M. J., Makeig, S., Brown, G. G., Jung, T. P., Kindermann, S. S., Bell, A. J., & Sejnowski, T. J. (1998). Analysis of fMRI data by blind separation into independent spatial components. *Hum Brain Mapp*, *6*, 160–188.
- Menon, R. S., Ogawa, S., Strupp, J. P., & Uğurbil, K. (1997). Ocular dominance in human V1 demonstrated by functional magnetic resonance imaging. *J Neurophys*, *77*, 2780–2787.
- Meunier, D., Lambiotte, R., & Bullmore, E. T. (2010). Modular and Hierarchically Modular Organization of Brain Networks. *Front Neurosci*, *4*, 200.
- Micheloyannis, S., Pachou, E., Stam, C. J., Vourkas, M., Erimaki, S., & Tsirka, V. (2006). Using graph theoretical analysis of multi channel EEG to evaluate the neural efficiency hypothesis. *Neurosci Lett*, *402*, 273–277.
- Milgram, S. The small world problem. *Psychol. Today* *2*, 60–67 (1967).
- Modha, D. S., & Singh, R. (2010). Network architecture of the long-distance pathways in the macaque brain. *Proc Natl Acad Sci U S A*, *107*, 13485–13490.
- Mohammadi, B., Kollwe, K., Samii, A., Krampfl, K., Dengler, R., & Münte, T. F. (2009). Changes of resting state brain networks in amyotrophic lateral sclerosis. *Exp Neurol*, *217*, 147–153.
- Moritz, C. H., Rogers, B. P., & Meyerand, M. E. (2003). Power spectrum ranked independent component analysis of a periodic fMRI complex motor paradigm. *Hum Brain Mapp*, *18*, 111–122.
- Moussa, M. N., Vechlekar, C. D., Burdette, J. H., Steen, M. R., Hugenschmidt, C. E., & Laurienti, P. J. (2011). Changes in cognitive state alter human functional brain networks. *Front Hum Neurosci*, *5*, 83.
- Murre, J. M., & Sturdy, D. P. (1995). The connectivity of the brain: multi-level quantitative analysis. *Biol Cybern*, *73*, 529–545.
- Newman, M. E. (2001). The structure of scientific collaboration networks. *Proc Natl Acad Sci U S A*, *98*, 404–409.
- Niedermeyer, E., & Silva, F. L. da. (2004). *Electroencephalography: Basic Principles, Clinical Applications, and Related Fields (Fifth.)*. Lippincott Williams & Wilkins.
- Norton, L., Hutchison, R. M., Young, G. B., Lee, D. H., Sharpe, M. D., & Mirsattari, S. M. (2012). Disruptions of functional connectivity in the default mode network of comatose patients. *Neurology*, *78*, 175–181.
- Ogawa, S., Menon, R. S., Tank, D. W., Kim, S. G., Merkle, H., Ellermann, J. M., & Ugurbil, K. (1993). Functional brain mapping by blood oxygenation level-

dependent contrast magnetic resonance imaging. A comparison of signal characteristics with a biophysical model. *Biophys J*, 64, 803–812.

- Onton, J., Westerfield, M., Townsend, J., & Makeig, S. (2006). Imaging human EEG dynamics using independent component analysis. *Neurosci Biobehav Rev*, 30, 808–822.
- Pawela, C. P., Biswal, B. B., Cho, Y. R., Kao, D. S., Li, R., Jones, S. R., Schulte, M. L., et al. (2008). Resting-state functional connectivity of the rat brain. *Magn Reson Med*, 59, 1021–1029.
- Quigley, M., Cordes, D., Turski, P., Moritz, C., Haughton, V., Seth, R., & Meyerand, M. E. (2003). Role of the corpus callosum in functional connectivity. *AJNR Am J Neuroradiol*, 24, 208-212.
- Raichle, M E, MacLeod, A. M., Snyder, A. Z., Powers, W. J., Gusnard, D. A., & Shulman, G. L. (2001). A default mode of brain function. *Proc Natl Acad Sci U S A*, 98, 676–682.
- Raichle, M. E., & Mintun, M. A. (2006). Brain work and brain imaging. *An Rev Neurosci*, 29, 449–476.
- Raichle, M. E. (2010). Two views of brain function. *Trends Cogn Sci*, 14, 180–190.
- Raichle, Marcus E, & Snyder, A. Z. (2007). A default mode of brain function: a brief history of an evolving idea. *NeuroImage*, 37, 1083–1090.
- Ringach, D. L. (2009). Spontaneous and driven cortical activity: implications for computation. *Curr Opin Neurobiol*, 19, 439–444.
- Ritter, P., & Villringer, A. (2006). Simultaneous EEG-fMRI. *Neurosci Biobehav Rev*, 30, 823–838.
- Rubinov, M., & Sporns, O. (2010). Complex network measures of brain connectivity: uses and interpretations. *Neuroimage*, 52, 1059-1069.
- Sadaghiani, S., Hesselmann, G., Friston, K. J., & Kleinschmidt, A. (2010). The relation of ongoing brain activity, evoked neural responses, and cognition. *Front Syst Neurosci*, 4, 20.
- Salvador, R., Suckling, J., Coleman, M. R., Pickard, J. D., Menon, D., & Bullmore, E. (2005). Neurophysiological architecture of functional magnetic resonance images of human brain. *Cereb Cortex*, 15, 1332–1342.
- Sarkisov, S. A., Filimonoff, I. N. & Preobrashenskaya, N. S. (1949). Cytoarchitecture of the Human Cortex Cerebri. Medgiz, Moscow.

- Seeley, W. W., Menon, V., Schatzberg, A. F., Keller, J., Glover, G. H., Kenna, H., Reiss, A. L., et al. (2007). Dissociable intrinsic connectivity networks for salience processing and executive control. *J Neurosci*, *27*, 2349–2356.
- Shehzad, Z., Kelly, A. M. C., Reiss, P. T., Gee, D. G., Gotimer, K., Uddin, L. Q., Lee, S. H., et al. (2009). The resting brain: unconstrained yet reliable. *Cereb Cortex*, *19*, 2209–2229.
- Shmuel, A., & Leopold, D. A. (2008). Neuronal correlates of spontaneous fluctuations in fMRI signals in monkey visual cortex: Implications for functional connectivity at rest. *Hum Brain Mapp*, *29*, 751–761.
- Shulman, R. G., Rothman, D. L., Behar, K. L., & Hyder, F. (2004). Energetic basis of brain activity: implications for neuroimaging. *Trends Neurosci*, *27*, 489–495.
- Smith, S. M., Fox, P. T., Miller, K. L., Glahn, D. C., Fox, P. M., Mackay, C. E., Filippini, N., et al. (2009). Correspondence of the brain's functional architecture during activation and rest. *Proc Natl Acad Sci U S A*, *106*, 13040–13045.
- Sporns, O. (2002). Network analysis, complexity, and brain function. *Complexity*, *8*, 56–60.
- Sporns, O. (2010). *Networks of the Brain* (1st ed.). The MIT Press.
- Sporns, O., & Kötter, R. (2004). Motifs in brain networks. *PLoS Biol*, *2*, e369.
- Sporns, O., Tononi, G., & Kötter, R. (2005). The human connectome: A structural description of the human brain. *PLoS Comput Biol*, *1*, e42.
- Stam, C. J. (2004). Functional connectivity patterns of human magnetoencephalographic recordings: a “small-world” network? *Neurosci Lett*, *355*, 25–28.
- Stam, Cornelis J., & de Bruin, E. A. (2004). Scale-free dynamics of global functional connectivity in the human brain. *Hum Brain Mapp*, *22*, 97–109.
- Stark, C. E., & Squire, L. R. (2001). When zero is not zero: the problem of ambiguous baseline conditions in fMRI. *Proc Natl Acad Sci U S A*, *98*, 12760–12766.
- Steriade, M. (2001). Impact of network activities on neuronal properties in corticothalamic systems. *J Neurophys*, *86*, 1–39.
- Strogatz, S. H. (2001). Exploring complex networks. *Nature*, *410*, 268–276.
- Sun, F. T., Miller, L. M., Rao, A. A., & D'Esposito, M. (2007). Functional connectivity of cortical networks involved in bimanual motor sequence learning. *Cereb Cortex*, *17*, 1227–1234.

- Tyszka, J. M., Kennedy, D. P., Adolphs, R., & Paul, L. K. (2011). Intact bilateral resting-state networks in the absence of the corpus callosum. *J Neurosci*, *31*, 15154–15162.
- van den Heuvel, M P, Stam, C. J., Boersma, M., & Hulshoff Pol, H. E. (2008). Small-world and scale-free organization of voxel-based resting-state functional connectivity in the human brain. *NeuroImage*, *43*, 528–539.
- van den Heuvel, M., Mandl, R., & Hulshoff Pol, H. (2008). Normalized cut group clustering of resting-state fMRI data. *PloS One*, *3*, e2001.
- van den Heuvel, Martijn P, & Hulshoff Pol, H. E. (2010). Exploring the brain network: a review on resting-state fMRI functional connectivity. *Eur Neuropsychopharmacol*, *20*, 519–534.
- van den Heuvel, Martijn P, Mandl, R. C. W., Kahn, R. S., & Hulshoff Pol, H. E. (2009). Functionally linked resting-state networks reflect the underlying structural connectivity architecture of the human brain. *Hum Brain Mapp*, *30*, 3127–3141.
- von Economo, C. & Koskinas, G. N. (1925). *Die Cytoarchitektonik der Hirnrinde des erwachsenen Menschen*. Springer, Berlin.
- van Eijsden, P., Hyder, F., Rothman, D. L., & Shulman, R. G. (2009). Neurophysiology of functional imaging. *NeuroImage*, *45*, 1047–1054.
- Van Essen, D. C., Newsome, W. T., & Bixby, J. L. (1982). The pattern of interhemispheric connections and its relationship to extrastriate visual areas in the macaque monkey. *J Neurosci*, *2*, 265–283.
- Vanhatalo, S., Palva, J. M., Holmes, M. D., Miller, J. W., Voipio, J., & Kaila, K. (2004). Infralow oscillations modulate excitability and interictal epileptic activity in the human cortex during sleep. *Proc Natl Acad Sci U S A*, *101*, 5053-5057.
- Varela, F., Lachaux, J. P., Rodriguez, E., & Martinerie, J. (2001). The brainweb: phase synchronization and large-scale integration. *Nat Rev Neurosci*, *2*, 229–239.
- Vigário, R., Särelä, J., Jousmäki, V., Hämäläinen, M., & Oja, E. (2000). Independent component approach to the analysis of EEG and MEG recordings. *IEEE Trans on BioMed Eng*, *47*, 589–593.
- Vincent, J. L., Kahn, I., Van Essen, D. C., & Buckner, R. L. (2010). Functional Connectivity of the Macaque Posterior Parahippocampal Cortex. *Journal of Neurophysiology*, *103*(2), 793–800. doi:10.1152/jn.00546.2009
- Vincent, J. L., Patel, G. H., Fox, M. D., Snyder, A. Z., Baker, J. T., Van Essen, D. C., Zempel, J. M., et al. (2007). Intrinsic functional architecture in the anaesthetized monkey brain. *Nature*, *447*, 83–86.

- Vogels, T. P., Rajan, K., & Abbott, L. F. (2005). Neural network dynamics. *Annual Review of Neuroscience*, 28, 357–376.  
doi:10.1146/annurev.neuro.28.061604.135637
- Waites, A. B., Briellmann, R. S., Saling, M. M., Abbott, D. F., & Jackson, G. D. (2006). Functional connectivity networks are disrupted in left temporal lobe epilepsy. *Annals of Neurology*, 59, 335–343.
- Watts, D. J., & Strogatz, S. H. (1998). Collective dynamics of “small-world” networks. *Nature*, 393, 440–442.
- Whitfield-Gabrieli, S., Thermenos, H. W., Milanovic, S., Tsuang, M. T., Faraone, S. V., McCarley, R. W., Shenton, M. E., et al. (2009). Hyperactivity and hyperconnectivity of the default network in schizophrenia and in first-degree relatives of persons with schizophrenia. *Proc Natl Acad Sci U S A*, 106, 1279–1284.
- Williams, R. J., & Martinez, N. D. (2000). Simple rules yield complex food webs. *Nature*, 404(6774), 180–183. doi:10.1038/35004572
- Womelsdorf, T., & Fries, P. (2006). Neuronal coherence during selective attentional processing and sensory-motor integration. *J Phys*, 100, 182–193.
- Womelsdorf, T., Vinck, M., Leung, L. S., & Everling, S. (2010). Selective theta-synchronization of choice-relevant information subserves goal-directed behavior. *Front Hum Neurosci*, 4, 210.
- Zarahn, E., Aguirre, G. K., & D’Esposito, M. (1997). Empirical analyses of BOLD fMRI statistics. I. Spatially unsmoothed data collected under null-hypothesis conditions. *NeuroImage*, 5, 179–197.
- Zeng, W., Qiu, A., Chodkowski, B., & Pekar, J. J. (2009). Spatial and temporal reproducibility-based ranking of the independent components of BOLD fMRI data. *NeuroImage*, 46, 1041–1054.
- Zhang, D., Snyder, A. Z., Shimony, J. S., Fox, M. D., & Raichle, M. E. (2010). Noninvasive functional and structural connectivity mapping of the human thalamocortical system. *Cereb Cortex*, 20, 1187–1194.
- Zhang, Z., Liao, W., Chen, H., Mantini, D., Ding, J.-R., Xu, Q., Wang, Z., et al. (2011). Altered functional-structural coupling of large-scale brain networks in idiopathic generalized epilepsy. *Brain*, 134, 2912–2928.
- Zilles, K., & Amunts, K. (2010). Centenary of Brodmann’s map—conception and fate. *Nat Rev Neurosci*, 11, 139–145.

Zuo, X.-N., Kelly, C., Adelstein, J. S., Klein, D. F., Castellanos, F. X., & Milham, M. P. (2010). Reliable intrinsic connectivity networks: test-retest evaluation using ICA and dual regression approach. *NeuroImage*, *49*, 2163–2177.

## Chapter 2

# 2 Functional Networks in the Anesthetized Rat Brain Revealed by Independent Component Analysis of Resting-State fMRI<sup>4</sup>

## 2.1 Introduction

Resting-state functional magnetic resonance imaging (fMRI) examines temporal correlations in the blood-oxygen-level-dependent (BOLD) signal in the absence of a specific task. It is believed that the coherence in low-frequency baseline fluctuations (LFFs; 0.01–0.1 Hz) arises from neurovascular mechanisms regulating blood flow and is presumed to reflect intrinsic functional connectivity of the brain (Biswal, Yetkin, Haughton, & Hyde, 1995). The widely separated brain regions identified with resting-state analysis have also been shown to reveal structural connectivity (Greicius, Supekar, Menon, & Dougherty, 2009). Distinct networks serving vision, motor, auditory, language, cognitive, and default-mode functions (Beckmann, DeLuca, Devlin, & Smith, 2005; Hampson, Peterson, Skudlarski, Gatenby, & Gore, 2002; Raichle et al. 2001) have been identified in humans. The networks manifest highly organized patterns of coherence across mammalian species (Pawela et al. 2008; Vincent et al. 2006, 2007) and persist regardless of the depth or type of general anesthetic (Kannurpatti, Biswal, Kim, & Rosen, 2008; Lu et al. 2007; Vincent et al. 2007; Zhao, Zhao, Zhou, Wu, & Hu, 2008).

Although the precise physiological origin and mechanism of regulation of LFFs have not been fully explained, studies have demonstrated changes in functional networks in a variety of human disease states including Alzheimer's disease (Greicius, Srivastava, Reiss, & Menon, 2004), autism (Cherkassky, Kana, Keller, & Just, 2006), depression (Greicius et al. 2007), epilepsy (Waites, Briellmann, Saling, Abbott, & Jackson, 2006), multiple sclerosis (Lowe, Phillips, Lurito, Mattson, Dziedzic, & Mathews, 2002), and

---

<sup>4</sup> A version of this chapter has been published. Hutchison, R.M., Mirsattari, S.M., Jones, C.K., Gati, J.S., & Leung, L.S. (2010). Functional networks in the anesthetized rat brain revealed by independent component analysis of resting-state fMRI. *J Neurophys*, 103, 3398-3406.

schizophrenia (Bluhm et al. 2007). As disruptions in functional connectivity have been suggested as possible causes or consequences of pathological states, there is increased interest to extend the study of resting-state networks to animal models. Genetic, physical, and chemical models exist for a variety of disease states and afford experimental manipulations not possible in humans. Through this avenue, we will gain a better understanding of the physiological mechanisms of entrainment, regulation, and fluctuation of the synchronous hemodynamic signals.

Initial examinations of physiological fluctuations in BOLD signals of rats have revealed substantial inter-hemispheric synchrony across multiple brain areas with reproducible, independent, homologous networks observed for the primary somatosensory cortex, primary visual cortex, and caudate-putamen (Kannurpatti, Biswal, Kim, & Rosen, 2008; Lu et al. 2007; Pawela et al. 2008, 2010; Zhao, Zhao, Zhou, Wu, & Hu, 2008). This is in accordance with network connectivity patterns seen in human (Cordes et al. 2001) and monkey (Vincent et al. 2007) studies that demonstrated bilateral motor, auditory, and visual networks. In humans, these networks have been shown to be present at birth (Fransson et al. 2009; Lin et al. 2008). Higher order resting-state networks also exhibit high degrees of synchronization between cortical and subcortical inter-hemispheric homologues (Beckmann, DeLuca, Devlin, & Smith, 2005).

Spatial functional connectivity maps of the rat are typically inferred by a cross-correlation analysis of the voxel-wise fMRI recordings against a reference time course. The seed voxel or region is typically chosen from an area found to be active during a stimulation paradigm and believed to be of functional relevance (Beckmann, DeLuca, Devlin, & Smith, 2005). The technique fundamentally tests a specific hypothesis and the functional connectivity map greatly depends on the choice of the seed region and on the correlational value used to threshold each map (Cole, Smith, Beckmann, 2010). Difficulties with the technique are also apparent when attempting to design a stimulation task to elicit robust and localized hemodynamic changes in specialized brain areas. The matter is further complicated by the use of anesthesia, typical of most fMRI experiments with rodents, which may prevent the necessary motor, visual, or auditory responses. It is for these reasons that most investigations have primarily focused on the connectivity of

the somatosensory cortices because the latter could be easily identified by the BOLD signal increase following electrical paw stimulation in the rat (Zhao, Zhao, Zhou, Wu, & Hu, 2008).

To avoid the constraints of these analytical techniques in the estimation of LFFs, hypothesis-independent, exploratory techniques such as ICA have been applied to functional data sets (Beckmann, DeLuca, Devlin, & Smith, 2005; Correa, Adali, & Calhoun, 2007; Greicius Srivastava, Reiss, & Menon, 2004). ICA is a statistical technique that uses a linear model to decompose independent, uncorrelated, and non-Gaussian datasets into distinct subparts (Vigário, Särelä, Jousmäki, Hämäläinen, & Oja, 2000). In terms of examining the BOLD signal, ICA is able to identify signal fluctuations by virtue of their spatial and temporal profiles without the need to specify an explicit model or voxel. The nonoverlapping, temporally coherent functional networks are extracted without constraining the temporal domain and are a priori independent (McKeown et al. 1998). In the present study, we used ICA to examine the spatiotemporal characteristics of the LFFs of anesthetized rats at rest with two different anesthetic regimes. Similar to network patterns observed in monkeys and humans, it is hypothesized that multiple independent, bilaterally synchronous resting-state networks exist in cortical and subcortical areas of the rat brain.

## 2.2 Methods

### 2.2.1 Animal usage and preparation

A total of 20 male Long-Evans rats (250–350 g body weight) were used. Animals were provided with normal food and water ad libitum and subjected to a 12:12 h light/dark cycle. All experiments were carried out in accordance with the guidelines established by the Canadian Council on Animal Care and approved by the Animal Use Committee of the University of Western Ontario.

In isoflurane animals ( $n = 10$ ), general anesthesia was induced with 5% isoflurane mixed with oxygen, using a calibrated vaporizer (Harvard Apparatus, Holliston, MA). Isoflurane

was then maintained at 2% while the animal was being prepared in the stereotaxic frame and then lowered to 1% following insertion into the magnet for image acquisition. At least 30 min was allowed for the isoflurane level and global hemodynamics to stabilize at the 1% concentration, during which shimming and image localization were performed. The gaseous mixture was delivered to a nosecone for spontaneous respiration throughout the experiment. Ketamine/xylazine animals ( $n = 10$ ) were initially anesthetized with a dose of 80 mg/kg ip ketamine and 10 mg/kg ip xylazine and then maintained with a continuous infusion of ketamine ( $50 \text{ mg} \cdot \text{kg}^{-1} \cdot \text{h}^{-1}$  ip) xylazine ( $6 \text{ mg} \cdot \text{kg}^{-1} \cdot \text{h}^{-1}$  ip), and saline ( $0.8 \text{ ml} \cdot \text{kg}^{-1} \cdot \text{h}^{-1}$  ip) using a syringe pump (PHD2000, Harvard Apparatus, Holliston, MA). Once anesthetized, the rats were secured in a custom-built nylon stereotaxic frame (Mirsattari et al. 2005) using ear and bite bars to prevent head motion. The rectal temperature was measured with a fiber-optic probe and maintained at  $\sim 37^\circ\text{C}$  via a feedback-controlled warm air system (MR compatible small animal monitoring and gating system, SA Instruments, Stoney Brook, NY) along with a heated feedback-controlled, water-circulated heating pad (TP500, Gaymar Industries, Orchard Park, NY). Respiration was monitored using a pneumatic pillow (SA Instruments) taped to the chest wall of the rat. Heart rate and blood oxygen saturation were measured using an MR compatible pulse oximeter (8600V, Nonin Medical, Plymouth, MN) positioned on the hindpaw. Physiological parameters were in the normal range (temperature:  $36.5\text{--}37^\circ\text{C}$ , heart rate:  $250\text{--}370$  beat/min, breathing:  $60\text{--}90$  breath/min, oxygen saturation:  $>95\%$ ) throughout the duration of the experiment.

### 2.2.2 MRI acquisition

All experiments were performed using a Varian DirectDrive imaging console (Palo Alto, CA) with a Magnex 31 cm actively shielded 9.4 T horizontal bore magnet equipped with an actively shielded gradient set (12 cm ID,  $\text{SR} = 3,000 \text{ mT} \cdot \text{m}^{-1} \cdot \text{s}^{-1}$ ; Yarnton, UK). An optimized home-built  $1.5 \times 2.0$  cm linear transmit-receive surface coil was positioned proximally to the anterior aspect of the rat's head for imaging. An automated shimming algorithm was used to optimize the magnetic field over our imaging

volume of interest using RASTAMAP (Klassen & Menon, 2004). Ten or 13 1-mm-thick coronal or horizontal slices covering the brain were selected. A fast spin echo (FSE) anatomical (effective echo train (TE) = 40 ms, reception time (TR) = 5 s, echo train length (ETL) = 4) was acquired with a  $256 \times 256$  matrix and a field of view (FOV) of  $25.6 \times 25.6$  mm. Functional images were acquired using an echo planar imaging sequence (TE = 15 ms, volume acquisition (Vol Acq) time = 1,000 ms, flip angle =  $40^\circ$ ), with a  $64 \times 64$  matrix, and a FOV of  $25.6 \times 25.6$  mm, corresponding to an in-plane spatial resolution of  $400 \times 400 \mu\text{m}^2$ . For each fMRI run, 300 (1 isoflurane anesthetized rat, 3 ketamine/xylazine anesthetized rats) or 600 (9 isoflurane anesthetized rats, 7 ketamine/xylazine anesthetized rats) images were acquired over 5 or 10 min, respectively, while the rat was resting in the scanner.

### 2.2.3 Image analysis

Preprocessing steps were carried out in BrainVoyager QX ([www.BrainVoyager.com](http://www.BrainVoyager.com)). Trilinear three-dimensional (3D) motion correction and spatial smoothing using a Gaussian filter (full-width at half-maximum = 1.2 mm) was applied to each data set. An eighth-order Butterworth low-pass filter with a cutoff at 0.1 Hz was implemented in MATLAB (Mathworks, Natick, MA) and applied to all voxel time courses on a voxel by voxel basis covering the entire brain (Hampson, Peterson, Skudlarski, Gatenby, & Gore, 2002). Following data reduction using principal component analysis (PCA) in which >99.5% of the variability in the data were retained, the images were subjected to spatial independent component analysis (ICA) using the infomax algorithm (Bell & Sejnowski 1995) implemented in the GIFT software package (GIFT, 2008). Currently, there are no established criteria to guide the selection of an optimal number of components for a given data set. Using a similar strategy employed by Calhoun et al. (2001), 40 components were chosen for each rat as this preserves most of the variance in the data and gives a manageable number of components. The independent components were then scaled to empirically derived z-scores by dividing by the SD of the original time sequence. The z-scores approximate the temporal correlation between each voxel and the associated component where the magnitude of the z-score specifies the

strength of the linear relationship (Mannell, Franco, Calhoun, Cañive, Thoma, & Mayer, 2009). A z-score value of 1 was used as the lower limit threshold of functional connectivity. The ICA derived components of each rat were then visually inspected and labeled based on the spatial patterns in reference to known anatomical and functional locations (Paxinos & Watson, 1986). Components were not regressed against a previously defined template, a common technique performed in human ICA investigations (Greicius, Srivastava, Reiss, & Menon, 2004). There are currently no standardized rat templates available and the creation of the template would require the acquisition of a separate dataset that would then have to be manually labeled, negating the benefit of the template.

Functional connectivity was also examined using seed-region analysis in four rats (2 from each anesthetic group) to demonstrate that ICA results corroborated traditional analysis strategies. Data were preprocessed in the same manner used for ICA. Spherical seed regions (0.5 mm radius) were selected in the right medial frontal cortex, parietal cortex, hippocampus, caudate-putamen, thalamus, and hypothalamus using a rat atlas (Paxinos & Watson 1986) without the use of a functional localizer as no functional paradigms were performed. The extracted BOLD time course of each seed region was averaged and then cross-correlated with all voxels within the brain to derive a corresponding connectivity map, displayed using different thresholds. The analysis was implemented using the resting-state fMRI data analysis toolkit (Rest, 2007).

## 2.3 Results

Without a priori defined templates or constrained modeling, clearly identifiable regions were apparent from visual inspection alone. ICA was able to extract bilateral synchronous activity of multiple brain structures in all 20 rats of which 10 rats anesthetized with isoflurane and the remaining 10 rats with ketamine/xylazine (methods). The neocortex was separated into eight components corresponding to functional brain areas. These were the medial and lateral frontal cortex (primary and secondary motor areas), parietal cortex (primary somatosensory area), temporoparietal cortex (secondary

somatosensory area), medial (visual area) and lateral occipital (auditory) cortex, and the posterior and anterior cingulate cortex (Fig. 2.1). The most clearly identifiable subcortical areas were the caudate-putamen, hippocampus, thalamus, and hypothalamus (Fig. 2.1). The thalamus and hypothalamus were not separated into individual nuclei as the resolution, smoothing, and lowered signal-to-noise ratio distal to the position of the surface coil prevented accurate identification. Five rats also showed a distinctive cerebellar component; however, in 15 rats, the field of view did not encompass a large enough proportion of the cerebellum to allow objective comparison or grouping.

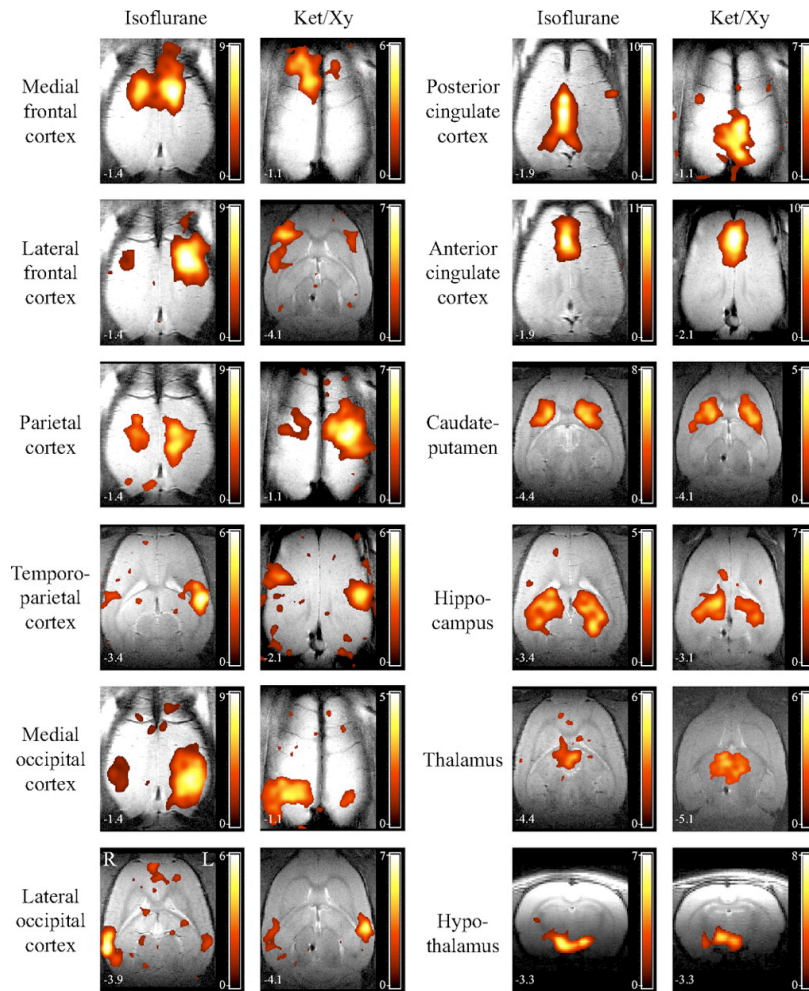


**Figure 2.1. Homologous resting-state networks of representative isoflurane and ketamine/xylazine (Ket/Xy) anesthetized rats derived using independent component analysis (ICA) of blood-oxygen-level-dependent (BOLD) functional time courses overlaid on the respective anatomical images (Paxinos and Watson 1986).** Except for the hypothalamus, horizontal slices were obtained from 1 rat, anesthetized with isoflurane or Ket/Xy, with distance (mm) ventral to bregma shown in the left lower corner. The hypothalamus component map was derived from a different rat for each anesthetic, and is displayed in a coronal orientation referenced posterior to bregma (mm), to allow better anatomical localization. Reprinted with permission from Hutchison, Mirsattari, Jones, Gati, & Leung (2010).

**Table 2.1. Number of rats in isoflurane and ketamine/xylazine anesthesia groups that had independent spatial components corresponding to anatomical locations (Paxinos & Watson, 1986) in both hemispheres (bilaterally synchronous), or in the left or right hemisphere.**

Anatomical brain area (Functional representation)	Isoflurane (N=10)			Ketamine/xylazine (N=10)		
	Bilat.	Left	Right	Bilat.	Left	Right
Medial frontal cortex (primary motor area)	10	3	4	10	1	3
Lateral frontal cortex (secondary motor area)	7	3	8	10	3	2
Parietal cortex (primary somatosensory area)	9	9	8	10	6	5
Temporoparietal cortex (secondary somatosensory area)	3	7	9	7	3	3
Medial occipital cortex (primary visual area)	10	8	6	10	5	4
Lateral occipital cortex (primary auditory area)	6	3	4	6	4	4
Posterior cingulate cortex	10	-	-	10	-	-
Anterior cingulate cortex	9	-	-	10	-	-
Caudate-Putamen	7	2	2	10	2	2
Hippocampus	10	4	2	10	2	2
Thalamus	8	-	-	7	-	-
Hypothalamus	5	-	-	6	-	-

Notes: A single rat may have both bilateral and unilateral components corresponding to a functional area. See Table 2 for distribution of components. The posterior cingulate cortex, anterior cingulate cortex, thalamus, and hypothalamus were not grouped into left and right hemisphere components due to restrictions imposed by the resolution

**Table 2.2. Distribution of rats (N=20, combining 10 rats under isoflurane and 10 under ketamine/xylazine anesthetic) that had unilateral and bilateral components corresponding to anatomical locations (Paxinos & Watson, 1986).**

Anatomical brain area (Functional representation)	Bilateral and no unilateral components	Bilateral and one unilateral component	Bilateral and two unilateral components	Two unilateral components	One unilateral component	No component
Medial frontal cortex (primary motor area)	12 (60%)	5 (25%)	3 (15%)	0 (0%)	0 (0%)	0 (0%)
Lateral frontal cortex (secondary motor area)	7 (35%)	7 (35%)	3 (15%)	1 (5%)	2 (10%)	0 (0%)
Parietal cortex (primary somatosensory area)	1 (5%)	10 (50%)	8 (40%)	1 (5%)	0 (0%)	0 (0%)
Temporoparietal cortex (secondary somatosensory area)	4 (20%)	4 (20%)	2 (10%)	3 (15%)	7 (35%)	0 (0%)
Medial occipital cortex (primary visual area)	6 (30%)	5 (25%)	9 (45%)	0 (0%)	0 (0%)	0 (0%)
Lateral occipital cortex (primary auditory area)	5 (25%)	6 (30%)	1 (5%)	4 (20%)	1 (5%)	3 (15%)
Caudate-Putamen	13 (65%)	2 (10%)	2 (10%)	1 (5%)	1 (5%)	1 (5%)
Hippocampus	11 (55%)	7 (35%)	2 (10%)	0 (0%)	0 (0%)	0 (0%)

Notes: n = 20, combining 10 rats under isoflurane and 10 under Ketamine/xylazine anesthetic. Data are from Paxinos & Watson (1986). Values in parentheses are percentages.

As presented in Table 2.1, the majority of rats were found to have a corresponding bilateral component for each of the identified brain areas. It was also found that some rats had one or two separate components for the analogous structure in addition to or in the place of the bilateral component (Table 2.2). Network connectivity was present regardless of the type of anesthetic and a  $\chi^2$  test for independence showed there was no significant difference between the two groups in terms of the number of rats demonstrating each particular anatomically relevant bilateral component [ $\chi^2(11) = 2.21$ ,  $P = 0.998$ ].

Frequency analysis of the BOLD time courses of components of individual rats (Fig. 2.2B) showed power at low frequencies of  $<0.1$  Hz. Time-spectral analysis showed frequency peaks and distribution that varied over time (Fig. 2.2C). While the power spectrum (and corresponding time function) of each ICA component was distinct in each individual rat, averaging the ICA components of the same structure across rats did not reveal consistent frequency peaks. The latter may be expected because ICA does not separate components based on the frequency of the time course.

Seed-region analysis revealed synchronized LFFs of the BOLD signal between the seed-region and analogous area in the contralateral hemisphere for both cortical and subcortical areas in all four rats examined. Functional connectivity maps of the two representative rats from each anesthetic group are shown in Fig. 2.3 in which a spherical seed was placed in the right medial frontal cortex (MFC; primary motor cortex; Fig. 2.3A), parietal cortex (primary somatosensory area; SSI; B), hippocampus (Hp; C), caudate-putamen (CPu; D), thalamus (Th; E), or hypothalamus (Ht; F). LFF synchronization was apparent under ketamine/xylazine (Fig. 2.3, rats 1 and 2) and isoflurane (Fig. 2.3, rats 3 and 4) anesthesia. The functional maps showed a variable degree of synchronization with other structures and different thresholds were needed to display the bilateral hemispheric connectivity. One rat did not have a prominent network in the caudate-putamen (Fig. 2.3D, rat 4).

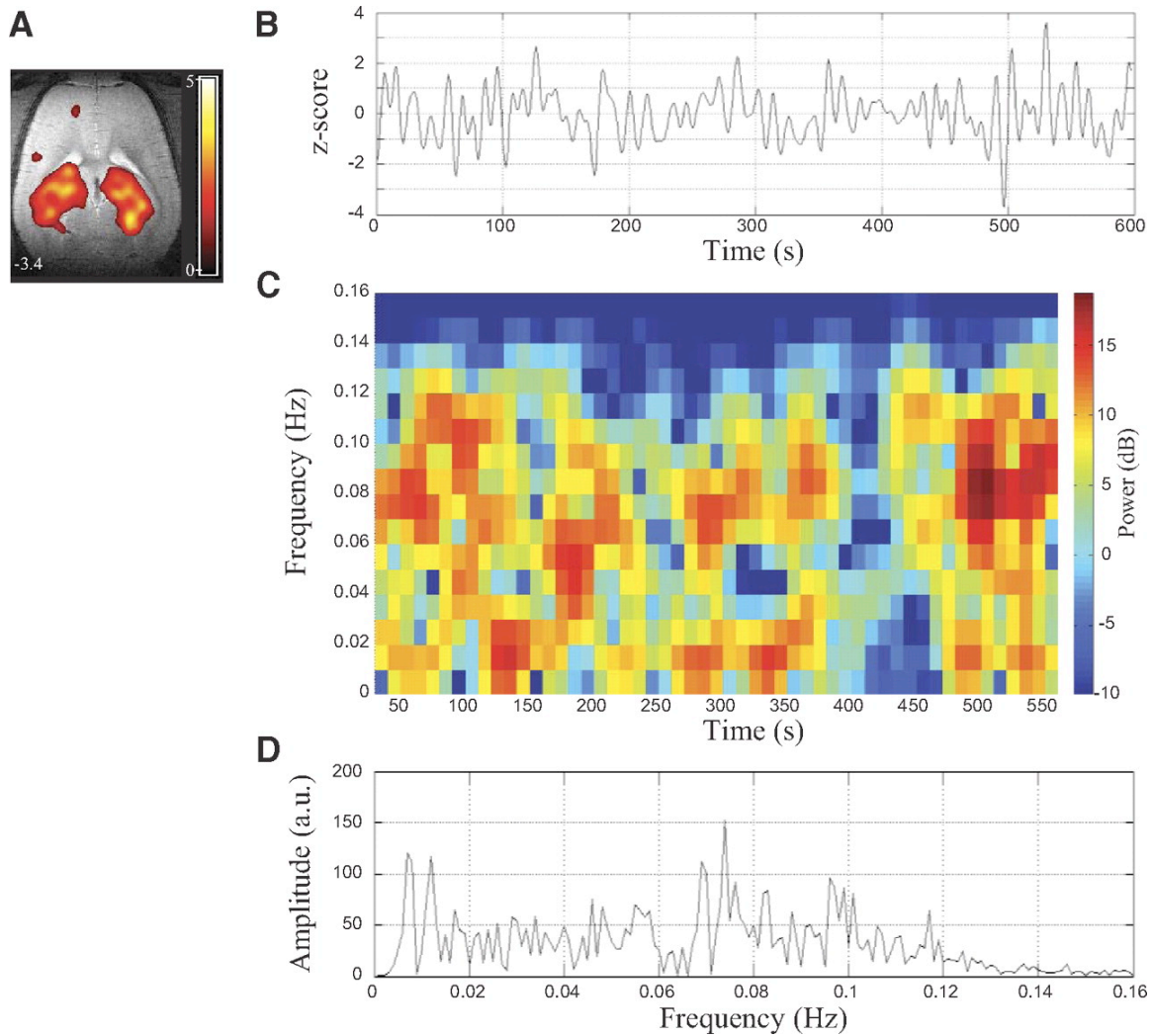


**Figure 2.2. Frequency analysis of the hippocampus component isolated by independent component analysis in a representative rat under isoflurane anesthesia, showing spatial connectivity map (A), time course (B), time-frequency analysis of the time course (C), and amplitude spectrum in arbitrary units (a.u.) of the entire time course (D).** Reprinted with permission from Hutchison, Mirsattari, Jones, Gati, & Leung (2010).

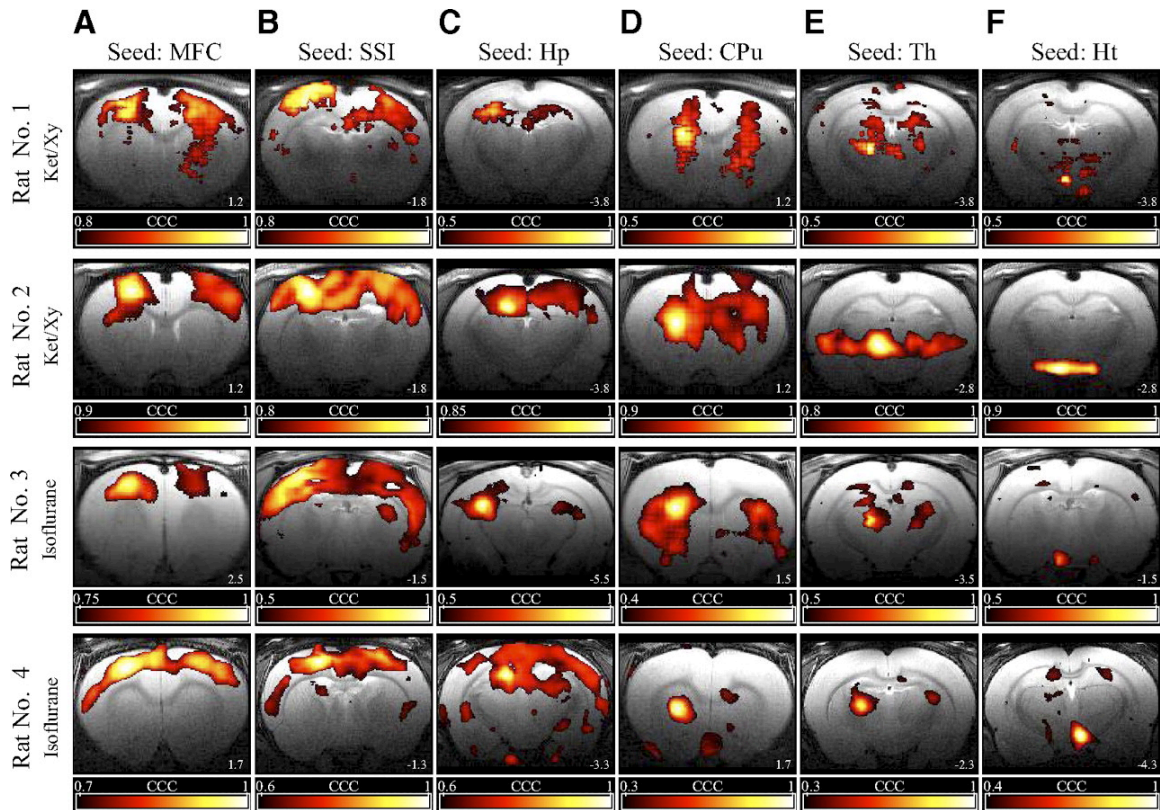


**Figure 2.3. Resting-state connectivity of representative ketamine/xylazine (Ket/Xy; rats 1 and 2) and isoflurane (rats 3 and 4) anesthetized rats derived using seed-region analysis.** Cross-correlation coefficient (CCC) maps were calculated by correlating the time course of all voxels with the average time course of a spherical seed region (0.5 mm radius) in the medial frontal cortex (MFC; A), primary somatosensory cortex (SSI; B), hippocampus (Hp; C), caudate-putamen (CPu; D), thalamus (Th; E), or hypothalamus (Ht; F). Different CCC thresholds were used for each image, as indicated by the color bar below each image. Coronal images are displayed and distance (mm) from bregma is shown at the right lower corner of each image (positive anterior, negative posterior to bregma). Reprinted with permission from Hutchison, Mirsattari, Jones, Gati, & Leung (2010).

## 2.4 Discussion

Functional resting-state networks in the rodent brain have been inferred based on synchronous fluctuations of the hemodynamic signals investigated using ICA. With this technique, the entire brain was probed for functional network connectivity without requiring seed regions or the stimulus tasks necessary to activate brain areas. Spontaneous BOLD resting-state fluctuations were found to be bilaterally synchronous across multiple brain structures including the hippocampus, hypothalamus, thalamus, cingulate cortices, auditory cortices, and sensorimotor cortical areas. Such a large number of independent networks ( $\leq 12$  coexisting in a particular animal) have not been reported before, and in particular, specific, homologous functional networks have not been reported for the auditory cortices, secondary somatosensory and motor cortices, posterior and anterior cortices, hippocampus, thalamus and hypothalamus, as shown in a summary of the literature (Table 2.3). Connectivity between some of these areas has been observed in more diffuse, possibly higher-order visual and sensorimotor networks (Pawela et al. 2008) although these do not represent independent networks.

**Table 2.3. Previously identified resting-state networks of the rat corresponding to anatomical locations (Paxinos & Watson, 1986).**

Reference	Anesthesia	Seed-region selection	Identified networks	Other findings
Kannurpatti et al., 2008	Isoflurane 1.2%	Stereotaxic atlas	bilateral SI (sparse)	Blood extraction ↑ bilateral connectivity in cortex and Th
Zhao et al., 2007	Medetomidine 0.1 mg/kg/h	Paw stimulation	bilateral SI bilateral CPu	Magnitude of LFFs similar to humans
Lu et al., 2007	α-chloralose 30, 70, 100 mg/kg/h	Paw stimulation	bilateral SI	↓ bilateral connectivity with ↑ dose
Pawela et al., 2008	Medetomidine 0.1 mg/kg/h	Nerve stimulation Light stimulation	bilateral MI/MII, SI/SII, & Th bilateral VI/VII, SC, & Th	RPCC matrices show high correlations between many sensory/motor areas
Majeed et al., 2009	α-chloralose 27 mg/kg/h	Paw stimulation	bilateral SI/SII bilateral CPu	2 frequency peaks Dynamic LFFs
Pawela et al., 2010	Medetomidine 0.1 mg/kg/h	Nerve stimulation Light stimulation	bilateral MI/MII, SI/SII, & Th bilateral VI/VII, SC, & Th	Network changes following limb deafferentation

Notes: Individual thalamic nuclei have been grouped into the term thalamus as there is diffuse functional connectivity between these regions. CPu, caudate-putamen; LFFs, Low frequency fluctuations; MI, Primary motor cortex; MII, Secondary motor cortex; RPCC, Regional pair-wise correlation coefficient; SC, Superior colliculus; SI, Primary Somatosensory cortex; SII, Secondary somatosensory cortex; Th, Thalamus; VI, Primary visual cortex; VII, Secondary visual cortex.

The functional connectivity revealed by ICA could also be shown using seed-region analysis. However, the size and placement of the seed within a brain structure was subjective, and the resulting functional connectivity maps were much more diffuse despite the use of variable thresholds. ICA was better able to identify bilateral networks among the noise without the assumption of seed regions or functional paradigms.

### 2.4.1 Connectivity patterns

The brain relies on constant inter-hemispheric communication for coherent integration of cognition and behavior (Compton, 2002). It has been shown that hemispheric interaction is critical for a unified representation of world (Houzel, Carvalho, & Lent, 2002), coordinating movement (Gerloff & Andres, 2002), attentional processing (Banich, 1998), pooling processing resources (Liederman, 1998), and parallel processing (Compton, 2002) among others. Bilaterally synchronous BOLD fluctuations have been previously observed in the motor cortex (Cordes et al. 2000), visual cortex, thalamus, and hippocampus of humans (Stein, Moritz, Quigley, Cordes, Haughton, & Meyerand, 2000) and in the oculomotor and somatomotor areas of monkeys (Vincent et al. 2007). We report that the analogous brain areas of the rat also show bilaterally synchronous hemodynamic fluctuations. This suggests that interhemispheric synchronization of LFFs is phylogenetically preserved across all mammalian species and may underlie rudimentary brain functioning.

The observed bilateral synchrony of cortical and subcortical BOLD signals suggests inter-hemispheric neuronal connections. In the neocortex, the corpus callosum serves to interconnect most areas, while the smaller anterior commissure serves to connect the temporal neocortex. Studies of functional connectivity in patients with agenesis (Quigley et al. 2003) or resection (Johnston et al. 2008) of the corpus callosum have shown significantly decreased functional connectivity between the neocortices. It is therefore plausible that the observed bilateral synchrony of BOLD signals is a result of commissural connections between the two brain regions, but it remains to be confirmed

for subcortical structures with weak commissural connections (e.g., caudate-putamen, hypothalamus).

Bilateral as well as unilateral components for the same functional area were observed in a number of rats from both anesthesia groups (Table 2). Using a model order of 40 components could have overestimated the number of networks in some rats, dividing the bilateral network of a functional area into two unilateral components. Previous human studies using ICA have also reported that functionally connected regions can split into separate components at high model order dimensionalities (Abou-Elseoud, Starck, Remes, Nikkinen, Tervonen, Kiviniemi, 2010; Smith et al. 2009; van de Ven, Formisano, Prvulovic, Roeder, Linden, 2004). It has been proposed that the stable components represent less connected nodes, while branching ones function as network connector hubs (Abou-Elseoud, Starck, Remes, Nikkinen, Tervonen, Kiviniemi, 2010) though there is currently little quantitative evidence to support this.

The typical result in the present study was the presence of both bi- and unilateral components in the same animal. We believe that unilateral components represent the local connectivity, which is both independent and concurrent with the interhemispheric connectivity of each functional area. The ability of homologous brain areas to operate both uni- and bilaterally has been documented in behavioral and electrophysiological literature (Banich & Belger 1990; MacDonald, Brett, & Barth, 1996; Nikouline, Linkenkaer-Hansen, Huttunen, & Ilmoniemi, 2001). As an example, the left paw of the rat can operate independently of the right; however, both paws may also act in unison during a coordinated movement. Interestingly, Pawela and colleagues (2010) have shown significant disruption of sensorimotor inter-hemispheric LFFs following limb deafferentation while unilateral (intra-hemispheric) connectivity was preserved. Unilateral components may not be observed in animals with only a bilateral network component as a result of ICA underestimation or a high degree of temporal pattern similarity between local and inter-hemispheric networks. ICA would then be extracting a composite of both underlying processes within the same network component (Seifritz et al. 2002).

Most networks for both groups were spatially symmetric as seen in Fig. 2.1. There are, however, networks in which the spatial extent of the clusters can be larger in one hemisphere (Fig. 2.1, lateral occipital cortex, isoflurane anesthesia). The “dominant” (increased ipsilateral cluster size) hemisphere varied within anesthesia groups and within the same rat for different networks (see Fig 2.4.). This is commonly reported in seed-region investigations of humans, monkeys, and rats (Cordes et al. 2001; Lu et al. 2007; Vincent et al. 2007) in which placement of the seed predicts the larger cluster in that hemisphere. Previous investigations of resting-state networks using single-subject ICA have also extracted asymmetric functional networks (Fransson et al. 2009). This effect may not be as apparent in human studies using group ICA as individual hemispheric differences may be averaged out. Currently, the functional significance of this property is unknown but may reflect hemispheric dominance.

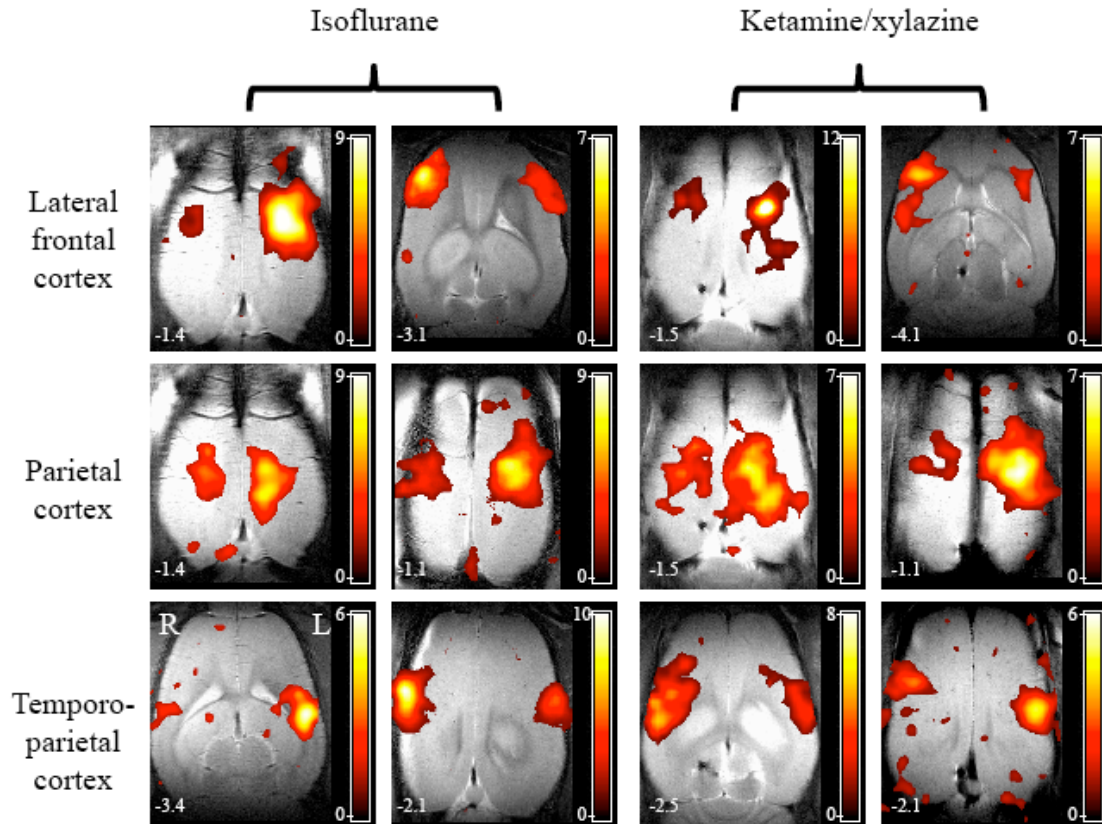


**Figure 2.4. Spatially asymmetrical cortical resting-state networks derived using independent component analysis of BOLD functional time courses overlaid on the respective anatomical images (Paxinos and Watson, 1986).** Left or right network dominance (defined as the hemisphere with the greater voxel spatial extent) in four rats is shown to vary within animals (columns), within networks (rows), and within anesthesia groups (isoflurane anesthetized animal in the two left columns; ketamine/xylazine anesthetized animals in the two right columns). The distance of the slice (mm) ventral to bregma is shown in the left lower corner. Reprinted with permission from Hutchison, Mirsattari, Jones, Gati, & Leung (2010).

## 2.4.2 Anesthesia

The present study represents the first report of LFFs and resting-state network connectivity in the rat under ketamine/xylazine anesthesia. Ketamine, a noncompetitive N-methyl-d-aspartate (NMDA) receptor antagonist (Duncan, Miyamoto, Leipzig, & Lieberman, 1999) and xylazine, an  $\alpha$ -2-adrenergic receptor agonist (Greene & Thurmon, 1998), are commonly used for animal anesthesia and have been increasingly used for imaging experiments (Hildebrandt, Su, & Weber, 2008; Wood, Klide, Pickup, & Kundel, 2001). Use of this anesthetic regime in BOLD-fMRI has been limited to the study of nociceptive stimuli (Shih et al. 2008), electrically induced partial limbic seizures (Englot Modi, Mishra, DeSalvo, Hyder, & Blumenfeld, 2009), and spinal cord investigations of the cat (Cohen-Adad et al. 2009). The present study confirms that the ketamine/xylazine combination is useful for the study of resting networks as substantial inter-hemispheric communication persisted over extended periods of time (e.g., during the 10-min scan). Its usefulness in task-elicited BOLD responses remains to be evaluated.

Isoflurane is a vasodilator (Farber, Harkin, Niedfeldt, Hudetz, Kampine, & Schmeling, 1997) that can alter cerebrovascular activity and has been shown to have dose-dependent effects on task-elicited BOLD responses in the rat cortex (Masamoto, Fukuda, Vazquez, & Kim, 2009). However, Vincent et al. (2007) reported that task-independent, coherent spontaneous BOLD fluctuations persisted in the monkey under increasing levels of isoflurane anesthesia though connectivity was decreased. A similar observation was also made in rats under  $\alpha$ -chloralose (Lu et al. 2007). Using an isoflurane dose (1%) that approached the minimum required for maintaining immobility (Masamoto, Fukuda, Vazquez, & Kim, 2009), the present study revealed more robust network activity than a previous report on isoflurane-anesthetized rats (Kannurpatti, Biswal, Kim, & Rosen, 2008). However, there was no apparent difference in the resting-state LFFs under ketamine/xylazine and isoflurane anesthesia. Thus we extend the notion that resting-state LFFs persist under general anesthetics with different mechanisms of action, such as medetomidine (Pawela et al. 2008; Zhao, Zhao, Zhou, Wu, & Hu, 2008),  $\alpha$ -chloralose (Lu et al. 2007; Majeed, Magnuson, & Keilholz, 2009), isoflurane

(Kannurpatti, Biswal, Kim, & Rosen, 2008), and now ketamine/xylazine. Taken together, we believe that resting hemodynamic fluctuations represent a ubiquitous intrinsic property of functional brain organization.

### 2.4.3 Physiological fluctuations

Physiological fluctuations due to respiration and cardiac movements can alias into the low-frequency range, which is used for connectivity mapping (Biswal et al. 1996; Fukunaga et al. 2006). Our BOLD signal sampling rate of 1 Hz could allow aliasing of the rat breathing ( $\sim 1$  Hz) and heart (4–6 Hz) rate. A higher sampling rate could prevent aliasing, but it would greatly reduce image resolution and the number of slices acquired. The result that ICA components were found in localized areas, or selectively in homologous areas of both hemispheres, cannot be attributed to physiological fluctuations. The temporal patterns and power spectra of the different network components were distinct and not indicative of a common source. In addition, signals that share a single source, such as respiration will be isolated following the ICA processing. As shown by De Luca and colleagues (2006) in human studies and argued by Zhao et al. (2008) for rats, a substantial contribution of autoregulation of the cerebral vasculature to the observed network connectivity is unlikely.

## 2.5 Conclusions

Using ICA of the BOLD signals, we inferred that the rat brain is composed of multiple, independent functional networks that involve cortical and subcortical structures. The functional connectivity among multiple structures was revealed in a single scanning session without the use of a motor task or a sensory stimulus. This will facilitate future studies of the mechanisms and function of the resting-state under physiological and pathological conditions.

## 2.6 References

- Abou-Elseoud, A., Starck, T., Remes, J., Nikkinen, J., Tervonen, O., & Kiviniemi, V. (2010). The effect of model order selection in group PICA. *Hum Brain Mapp*, *31*, 1207-1216.
- Banich, M.T., & Belger, A. (1990). Interhemispheric interaction: how do the hemispheres divide and conquer a task? *Cortex*, *26*, 77-94.
- Banich, M.T. (1998) The missing link: the role of interhemispheric interaction in attentional processing. *Brain Cogn*, *36*, 128-157.
- Beckmann, C.F., DeLuca, M., Devlin, J.T., & Smith, S.M. (2005). Investigations into resting-state connectivity using independent component analysis. *Philos Trans R Soc Lond B Biol Sci*, *360*, 1001-1013.
- Bell, A.J., & Sejnowski, T.J. (1995). An information-maximization approach to blind separation and blind deconvolution. *Neural Comput*, *7*, 1129-1159.
- Biswal, B., DeYoe, E.A., & Hyde, J.S. (1996). Reduction of physiological fluctuations in fMRI using digital filters. *Magn Reson Med*, *35*, 117-123.
- Biswal, B., Yetkin, F.Z., Haughton, V.M., Hyde, J.S. (1995). Functional connectivity in the motor cortex of resting human brain using echo-planar MRI. *Magn Reson Med*, *34*, 537-541.
- Bluhm, R.L., Miller, J., Lanius, R.A., Osuch, E.A., Boksman, K., Neufeld, R.W., Théberge, J., Schaefer, B., & Williamson, P. (2007). Spontaneous low-frequency fluctuations in the BOLD signal in schizophrenic patients: anomalies in the default network. *Schizophr Bull*, *33*, 1004-1012.
- Calhoun, V.D., Adali, T., McGinty, V.B., Pekar, J.J., Watson, T.D., & Pearlson, G.D. (2001) fMRI activation in a visual-perception task: network of areas detected using the general linear model and independent components analysis. *Neuroimage*, *14*, 1080-1088.
- Cherkassky, V.L., Kana, R.K., Keller, T.A., & Just, M.A. (2006). Functional connectivity in a baseline resting-state network in autism. *Neuroreport*, *17*, 1687-1690.
- Cohen-Adad, J., Hoge, R.D., Leblond, H., Xie, G., Beaudoin, G., Song, A.W., Krueger, G., Doyon, J., Benali, H., & Rossignol, S. (2009) Investigations on spinal cord fMRI of cats under ketamine. *Neuroimage*, *44*, 328-339.
- Cole, D.M., Smith, S.M., & Beckmann, C.F. (2010). Advances and pitfalls in the analysis and interpretation of resting-state FMRI data. *Front Syst Neurosci*, *4*, 8.
- Compton, R.J. (2002). Inter-hemispheric interaction facilitates face processing. *Neuropsychologia*, *40*, 2409-2419.

- Cordes, D., Haughton, V.M., Arfanakis, K., Carew, J.D., Turski, P.A., Moritz, C.H., Quigley, M.A., & Meyerand, M.E. (2001). Frequencies contributing to functional connectivity in the cerebral cortex in “resting-state” data. *Am J Neuroradiol*, *22*, 1326-1333.
- Cordes, D., Haughton, V.M., Arfanakis, K., Wendt, G.J., Turski, P.A., Moritz, C.H., Quigley, M.A., & Meyerand, M.E. (2000). Mapping functionally related regions of brain with functional connectivity MRI. *Am J Neuroradiol*, *21*, 1636-1644..
- Correa, N., Adali, T., & Calhoun, V.D. (2007). Performance of blind source separation algorithms for fMRI analysis using a group ICA method. *Magn Reson Imaging*, *25*, 684-694.
- De Luca, M., Beckmann, C.F., De Stefano, N., Matthews, P.M., & Smith, S.M. (2006) fMRI resting state networks define distinct modes of long-distance interactions in the human brain. *Neuroimage*, *29*, 1359-1367.
- Duncan, G.E., Miyamoto, S., Leipzig, J.N., & Lieberman, J.A. (1999). Comparison of brain metabolic activity patterns induced by ketamine, MK-801 and amphetamine in rats: support for NMDA receptor involvement in responses to subanesthetic dose of ketamine. *Brain Res*, *843*, 171-183.
- Englot, D.J., Modi, B., Mishra, A.M., DeSalvo, M., Hyder, F., & Blumenfeld, H. (2009). Cortical deactivation induced by subcortical network dysfunction in limbic seizures. *J Neurosci*, *29*, 13006-13018.
- Farber, N.E., Harkin, C.P., Niedfeldt, J., Hudetz, A.G., Kampine, J.P., & Schmeling, W.T. (1997). Region-specific and agent-specific dilation of intracerebral microvessels by volatile anesthetics in rat brain slices. *Anesthesiology*, *87*, 1191-1198.
- Fransson, P., Skiöld, B., Engström, M., Hallberg, B., Mosskin, M., Aden, U., Lagercrantz, H., & Blennow, M. (2009). Spontaneous brain activity in the newborn brain during natural sleep—an fMRI study in infants born at full term. *Pediatr Res*, *66*, 301-305.
- Fukunaga, M., Horovitz, S.G., van Gelderen, P., de Zwart, J.A., Jansma, J.M., Ikonomidou, V.N., Chu, R., Deckers, R.H.R., Leopold, D.A., & Duyn, J.H. (2006). Large amplitude, spatially correlated fluctuations in BOLD fMRI signals during extended rest and early sleep stages. *Magn Reson Imaging*, *24*, 979-992.
- Gerloff, C., & Andres, F.G. (2002). Bimanual coordination and interhemispheric interaction. *Acta Psychol*, *110*, 161-186.
- GIFT. (2008). Group ICA of fMRI Toolbox (GIFT). <http://icatb.sourceforge.net>.
- Greene, S.A., & Thurmon, J.C. (1998). Xylazine—a review of its pharmacology and use in veterinary medicine. *J Vet Pharmacol Ther*, *11*, 295-313.

- Greicius, M.D., Flores, B.H., Menon, V., Glover, G.H., Solvason, H.B., Kenna, H., Reiss, A.L., & Schlaggar, B.L. (2007). Resting-state functional connectivity in major depression: abnormally increased contributions from subgenual cingulate cortex and thalamus. *Biol Psychiatry*, *62*, 429-437.
- Greicius, M.D., Srivastava, G., Reiss, A.L., Menon, V. (2004). Default-mode network activity distinguishes Alzheimer's disease from healthy aging: evidence from functional MRI. *Proc Natl Acad Sci U S A*, *101*, 4637-4642.
- Greicius, M.D., Supekar, K., Menon, V., & Dougherty, R.F. (2009). Resting-state functional connectivity reflects structural connectivity in the default mode network. *Cereb Cortex*, *19*: 72-78.
- Hampson, M., Peterson, B.S., Skudlarski, P., Gatenby, J.C., & Gore, J.C. (2002). Detection of functional connectivity using temporal correlations in MR images. *Hum Brain Mapp*, *15*, 247-262.
- Hildebrandt, I.J., Su, H., & Weber, W.A. (2008). Anesthesia and other considerations for in vivo imaging of small animals. *ILAR J*, *49*, 17-26.
- Houzel, J.C., Carvalho, M.L., & Lent, R. (2002). Interhemispheric connections between primary visual areas: beyond the midline rule. *Braz J Med Biol Res*, *35*, 1441-1453.
- Johnston, J.M., Vaishnavi, S.N., Smyth, M.D., Zhang, D., He, B.J., Zempel, J.M., Shimony, J.S., Snyder, A.Z., & Raichle, M.E. (2008). Loss of resting interhemispheric functional connectivity after complete section of the corpus callosum. *JNeurosci*, *28*, 6453-6458.
- Kannurpatti, S.S., Biswal, B.B., Kim, Y.R., & Rosen, B.R. (2008). Spatio-temporal characteristics of low-frequency BOLD signal fluctuations in isoflurane-anesthetized rat brain. *Neuroimage* *40*, 1738-1747.
- Klassen, L.M., & Menon, R.S. (2004). Robust automated shimming technique using arbitrary mapping acquisition parameters (RASTAMAP). *Magn Reson Med*, *51*: 881-887.
- Laufs, H., Krakow, K., Sterzer, P., Eger, E., Beyerle, A., & Salek-Haddadi, A., Kleinschmidt, A. (2003). Electroencephalographic signatures of attentional and cognitive default modes in spontaneous brain activity fluctuations at rest. *Proc Natl Acad Sci U S A*, *100*, 11053-11058.
- Liederman, J. (1998). The dynamics of interhemispheric collaboration and hemispheric control. *Brain Cogn*, *36*, 193-208.
- Lin, W., Zhu, Q., Gao, W., Chen, Y., Toh, C.H., Styner, M., Gerig, G., Smith, J.K., Biswal, B., & Gilmore, J.H. (2008). Functional connectivity MR imaging reveals

- cortical functional connectivity in the developing brain. *Am J Neuroradiol*, 29, 1883-1889.
- Lowe, M.J., Phillips, M.D., Lurito, J.T., Mattson, D., Dzemidzic, M., & Mathews, V.P. (2002). Multiple sclerosis: Low-frequency temporal blood oxygen level-dependent fluctuations indicate reduced functional connectivity initial results. *Radiology*, 224, 184-192.
- Lu, H., Zuo, Y., Gu, H., Waltz, J.A., Zhan, W., Scholl, C.A., Rea, W., Yang, Y., Stein, E.A. (2007). Synchronized delta oscillations correlate with the resting-state functional MRI signal. *Proc Natl Acad Sci U S A*, 104, 18265-18269.
- MacDonald, K.D., Brett, B., & Barth, D.S. (1996). Inter- and intra-hemispheric spatiotemporal organization of spontaneous electrocortical oscillations. *J Neurophysiol*, 76, 423-437.
- Majeed, W., Magnuson, M., & Keilholz, S.D. (2009). Spatiotemporal dynamics of low frequency fluctuations in BOLD fMRI of the rat. *J Magn Reson Imaging*, 30, 384-393.
- Mannell, M.V., Franco, A.R., Calhoun, V.D., Cañive, J.M., Thoma, R.J., & Mayer, A.R. (2010). Resting state and task-induced deactivation: a methodological comparison in patients with schizophrenia and healthy controls. *Hum Brain Mapp*, 31, 424-437.
- Masamoto, K., Fukuda, M., Vazquez, A., & Kim, S.G. (2009). Dose-dependent effect of isoflurane on neurovascular coupling in rat cerebral cortex. *Eur J Neurosci*, 30, 242-250.
- McKeown, M.J., Makeig, S., Brown, G.G., Jung, T.P., Kindermann, S.S., Bell, A.J., & Sejnowski, T.J. (1998). Analysis of fMRI data by blind separation into independent spatial components. *Hum Brain Mapp* 6, 160-188, 1998.
- Mirsattari, S.M., Bihari, F., Leung, L.S., Menon, R.S., Wang, Z., Ives, J.R., & Bartha, R. (2005). Physiological monitoring of small animals during magnetic resonance imaging. *J Neurosci Methods*, 144, 207-213.
- Morcom, A.M., & Fletcher, P.C. (2007). Does the brain have a baseline? Why we should be resisting a rest. *Neuroimage*, 37, 1073-1082.
- Nikouline, V.V., Linkenkaer-Hansen, K., Huttunen, J., & Ilmoniemi, R.J. (2001). Interhemispheric phase synchrony and amplitude correlation of spontaneous beta oscillations in human subjects: a magnetoencephalographic study. *Neuroreport*, 12, 2487-2491.
- Pawela, C.P., Biswal, B.B., Cho, Y.R., Kao, D.S., Li, R., Jones, S.R., Schulte, M.L., Matloub, H.S., Hudetz, A.G., & Hyde, J.S. (2008). Resting-state functional connectivity of the rat brain. *Magn Reson Med*, 59, 1021-1029.

- Pawela, C.P., Biswal, B.B., Hudetz, A.G., Li, R., Jones, S.R., Cho, Y.R., Matloub, H.S., & Hyde, J.S. (2010). Interhemispheric neuroplasticity following limb deafferentation detected by resting-state functional connectivity magnetic resonance imaging (fcMRI) and functional magnetic resonance imaging (fMRI). *Neuroimage*, *49*, 2467-2478.
- Paxinos, G., & Watson, C. (1986). *The Rat Brain in Stereotaxic Coordinates*. New York: Academic Press.
- Quigley, M., Cordes, D., Turski, P., Moritz, C., Haughton, V., Seth, R., & Meyerand, M.E. (2003). Role of the corpus callosum in functional connectivity. *Am J Neuroradiol*, *24*, 208-212.
- Raichle, M.E., MacLeod, A.M., Snyder, A.Z., Powers, W.J., Gusnard, D.A., & Shulman, G.L. (2001). A default mode of brain function. *Proc Natl Acad Sci U S A*, *98*, 676-682.
- Rest. (2007). Resting-State fMRI Data Analysis Toolkit (REST). Song, X., Yan, C., Dong, Z. (<http://www.restfmri.net>).
- Seifritz, E., Esposito, F., Hennel, F., Mustovic, H., Neuhoﬀ, J.G., Bilecen, D., Tedeschi, G., Scheﬄer, K., & Di Salle, F. (2002). Spatiotemporal pattern of neural processing in the human auditory cortex. *Science*, *297*, 1706-1708.
- Shih, Y.Y., Chang, C., Chen, J.C., & Jaw, F.S. (2008). BOLD fMRI mapping of brain responses to nociceptive stimuli in rats under ketamine anesthesia. *Med Eng Phys*, *30*, 953-958.
- Smith, S.M., Fox, P.T., Miller, K.L., Glahn, D.C., Fox, P.M., Mackay, C.E., Filippini, N., Watkins, K.E., Toro, R., Laird, A.R., & Beckmann, C.F. (2009). Correspondence of the brain's functional architecture during activation and rest. *Proc Natl Acad Sci U S A*, *106*, 13040-13045.
- Stein, T., Moritz, C., Quigley, M., Cordes, D., Haughton, V., Meyerand, M. (2000). Functional connectivity in the thalamus and hippocampus studied with fMRI. *Am J Neuroradiol*, *21*, 1397-1401.
- van de Ven, V.G., Formisano, E., Prvulovic, D., Roeder, C.H., & Linden, D.E. (2004). Functional connectivity as revealed by spatial independent component analysis of fMRI measurements during rest. *Hum Brain Mapp*, *22*, 165-178.
- Vanhatalo, S., Palva, J.M., Holmes, M.D., Miller, J.W., Voipio, J., & Kaila, K. (2004). Infralow oscillations modulate excitability and interictal epileptic activity in the human cortex during sleep. *Proc Natl Acad Sci USA*, *101*, 5053-5057.
- Vigário, R., Särelä, J., Jousmäki, V., Hämäläinen, M., Oja, E. (2000). Independent component approach to the analysis of EEG and MEG recordings. *IEEE Trans Biomed Eng*, *47*, 589-593.

- Vincent, J.L., Patel, G.H., Fox, M.D., Snyder, A.Z., Baker, J.T., Van Essen, D.C., Zempel, J.M., Snyder, L.H., Corbetta, M., & Raichle, M.E. (2007). Intrinsic functional architecture in the anaesthetized monkey brain, *Nature* 447, 83-86.
- Vincent, J.L., Snyder, A.Z., Fox, M.D., Shannon, B.J., Andrews, J.R., Raichle, M.E., & Buckner, R.L. (2006). Coherent spontaneous activity identifies a hippocampal-parietal memory network. *J Neurophysiol*, 96, 3517-3531.
- Waites, A.B., Briellmann, R.S., Saling, M.M., Abbott, D.F., & Jackson, G.D. (2006). Functional connectivity networks are disrupted in left temporal lobe epilepsy. *Ann Neurol*, 59: 335–343, 2006.
- Wood, A.K., Klide, A.M., Pickup, S., Kundel, H.L. (2001). Prolonged general anesthesia in MR studies of rats. *Acad Radiol*, 8, 1136-1140.
- Zhao, F., Zhao, T., Zhou, L., Wu, Q., Hu, X. (2008). BOLD study of stimulation-induced neural activity and resting-state connectivity in medetomidine-sedated rat. *Neuroimage*, 39, 248-260.

## Chapter 3

### 3 Resting-state networks in the macaque at 7 T<sup>5</sup>

#### 3.1 Introduction

The mammalian brain is composed of functional networks operating at different spatial and temporal scales — characterized by patterns of interconnections linking sensory, motor, and cognitive systems (Felleman & Van Essen, 1991; Young, 1993; Friston, 2002). Neuroimaging has afforded unparalleled access in the exploration of the topology of these systems, and has revealed that neural processing relies on the dynamic integration of cortical and subcortical areas within large-scale and distributed brain networks (Sporns, Tononi, & Kötter, 2005; Guye, Bartolomei, & Ranjeva, 2008). Network activity is typically assessed using functional connectivity measures. This is an examination of temporal correlations that exist between distinct brain areas (Friston, 1994) connected directly or indirectly by long-range cortical and subcortical polysynaptic pathways (Hagmann et al., 2008). Using this definition, functional connectivity has been derived using spontaneous blood oxygenation-level-dependent (BOLD) fluctuations measured by functional magnetic resonance imaging (fMRI; Biswal, Yetkin, Haughton, & Hyde, 1995). Correlation of low frequency fluctuations (LFFs; 0.01–0.1 Hz) of the BOLD signal acquired in the absence of a task has been shown to reflect anatomical connectivity (Vincent et al., 2007; Honey et al., 2009; Greicius, Supekar, Menon, & Dougherty, 2009) and presumed to be a hemodynamic manifestation of functional connectivity between slow fluctuations in neuronal activity (Fox & Raichle, 2007; Shmuel & Leopold, 2008).

Investigations of functional connectivity through the evaluation of LFF synchrony during rest have demonstrated that the human brain is spatially organized into coherent patterns characterized as networks. These robust and reproducible resting-state networks

---

<sup>5</sup> A version of this chapter has been published. Hutchison, R.M., Leung, L.S., Mirsattari, S.M., Gati, J.S., Menon, R.S., & Everling S. (2011a). Resting-state networks in the macaque at 7 T. *NeuroImage* 56, 1546-1555.

(RSNs) have been reported for visual, motor, auditory, language, memory, executive, and attention systems, as well as the default-mode network (Cordes et al., 2000; Raichle, MacLeod, Snyder, Powers, Gusnard, & Shulman; Hampson, Peterson, Skudlarski, Gatenby, & Gore, 2002; Beckmann, DeLuca, Devlin, & Smith, 2005; Damoiseaux et al., 2006). RSNs parallel previously identified task-based networks and spatio-temporal network synchronization is preserved during sedation and anesthesia in humans, monkeys, and rats (Kiviniemi et al., 2005; Vincent et al., 2007; Hutchison, Mirsattari, Jones, Gati, & Leung, 2010). RSNs can be identified through a seed-region analysis in which spatial functional connectivity maps are inferred by a cross-correlation analysis of the voxel-wise fMRI recordings against a reference time-course. The shortcoming of this technique is that it tests a specific hypothesis and is limited to those areas that are selected as seed-regions (Cole, Smith, & Beckmann, 2010). Owing to the constraints of seed-region analysis, exploratory techniques such as independent component analysis (ICA) are now frequently applied to human functional data sets, where they have revealed RSNs that had not been previously shown with seed-region techniques (Beckmann, DeLuca, Devlin, & Smith, 2005; Smith et al., 2009).

Although their meaning is not fully understood, changes in functional RSNs have been recently reported in several psychiatric and developmental disorders including depression, attention deficit-hyperactivity disorder, schizophrenia, Alzheimer's disease, epilepsy, and multiple sclerosis (Auer, 2008; Greicius, 2008). Given the extraordinary potential for RSNs as possible diagnostic or prognostic markers, it is crucial to understand the physiological mechanisms of fluctuation, regulation, and entrainment of LFFs and the RSNs that are revealed through their synchronization.

Nonhuman primates and in particular macaque monkeys have been used as surrogates for the study of human brain function for several decades and might therefore represent an ideal animal model for the study of RSNs. Although macaque and human brains share a high degree of similarity in terms of cytoarchitecture (Petrides & Pandya; Petrides & Pandya, 2002a; Ongür, Ferry, & Price, 2003), functional organization (Rees, Friston, & Koch, 2000; Koyama, Hasegawa, Osada, Adachi, Nakahara, & Miyashita, 2004; Petrides, Cadoret, & Mackey, 2005; Nakahara, Adachi, Osada, & Miyashita,

2007), and anatomical connections (Crosson et al., 2005; Kelly et al., 2010), there also exist structural (Preuss, 2000; Rilling, 2006), morphological (Buxhoeveden, Switala, Roy, Litaker, & Casanova, 2001), and functional (Orban, Van Essen, & Vanduffel, 2004; Preuss, 2004) differences between the brains of these two primate species (Passingham, 2009).

While a few recent studies have revealed homologous RSNs between human and nonhuman primates, these studies either utilized seed-region analysis (Vincent et al., 2007; Vincent, Kahn, Van Essen, & Buckner, 2010; Margulies et al., 2009) or ICA in only two animals (Moeller, Nallasamy, Tsao, & Freiwald, 2009). Here, we present a comprehensive evaluation of macaque RSNs at 7 T using group ICA and an analysis methodology that is very similar to what has been used in humans. The results show striking similarity of macaque RSNs to previously described human RSNs.

## 3.2 Methods

### 3.2.1 Animal preparation

Data was obtained from 6 macaque monkeys (*Macaca fascicularis*; 2 male, 4 female) whose weights ranged from 3.6 kg to 5.3 kg (mean  $\pm$  SD = 4.58  $\pm$  1.4 kg). Surgical and experimental procedures were carried out in accordance with the Canadian Council of Animal Care policy on the use of laboratory animals and approved by the Animal Use Subcommittee of the University of Western Ontario Council on Animal Care.

Animals were initially prepared for imaging by undergoing a surgical procedure to place an MRI-compatible, custom-built acrylic head post that served to restrain the head during image acquisition. The post was anchored to the skull with 6 mm ceramic bone screws (Thomas Recording, Giessen, Germany) and dental acrylic.

On the day of scanning, anesthesia was first induced by intramuscular injections of atropine (0.4 mg/kg), ipratropium (0.025 mg/kg), and ketamine hydrochloride (7.5

mg/kg). Animals were then administered 3 ml of propofol (10 mg/ml) intravenously via the saphenous vein. Following oral intubation with an endotracheal tube, anesthesia was maintained using 1.5% isoflurane mixed with oxygen. Animals were spontaneously breathing throughout the duration of the experiment. The animal was placed in a custom-built primate chair containing fixation for head immobilization and an integrated custom RF coil, and inserted into the bore for image acquisition. The isoflurane level was then lowered to 1% for imaging experiments. Rectal temperature via a fiber-optic temperature probe (FISO, Quebec City, QC), respiration via bellows (Siemens Corp., Union, NJ), and end-tidal CO<sub>2</sub> via capnometer (Covidien-Nellcor, Boulder, CO) were continuously monitored. Physiological parameters were in the normal range (temperature: 36.5 °C; breathing: 25–30 breaths/min; end-tidal CO<sub>2</sub>: 24–28 mm Hg) throughout the duration of the experiment. Warmth was maintained using a heating disk (Snugglesafe, Littlehampton, West Sussex, UK) and thermal insulation.

Anesthesia was utilized in this study to eliminate motion effects, physiological stress, and training requirements. Although isoflurane has been shown to have vasodilator properties (Farber, Harkin, Niedfeldt, Hudetz, Kampine, & Schmeling, 1997) altering cerebrovascular activity in a dose-dependent manner (Vincent et al., 2007), synchronous spontaneous BOLD fluctuations have been previously reported using an isoflurane regime in both monkeys (Vincent et al., 2007) and rats (Hutchison, Mirsattari, Jones, Gati, & Leung, 2010). However, it is still likely that anesthesia can affect RSNs.

### 3.2.2 Data acquisition

All data were acquired on an actively shielded 7 Tesla 68 cm horizontal bore human head scanner with a DirectDrive console (Varian, Yarnton, UK; Walnut Creek, CA) and a Siemens AC84 gradient sub-system (Erlangen, Germany) operating at a slew rate of 350 mT/m/s. An in-house designed and manufactured conformal 5 channel transceive primate head RF coil was used for all experiments. Magnetic field optimization (B<sub>0</sub> shimming) was performed using an automated, three-dimensional mapping procedure over the specific imaging volume of interest. For each monkey, 2

runs of 300 continuous EPI functional volumes (TR = 2000 ms; TE = 16 ms; flip angle = 70°, slices = 30, matrix = 72 × 72; FOV = 96 × 96 mm; acquisition voxel size = 1.3 × 1.3 × 1.5 mm) were acquired. The total acquisition time of each scan was 10 min. EPI images were acquired with GRAPPA at an acceleration factor of 2. Every image was corrected for physiological fluctuations using navigator-echo-correction. A high-resolution T2-weighted anatomical reference volume was acquired along the same orientation as the functional images using a fast spin echo acquisition scheme (TR = 5000 ms; TE = 38.6 ms; echo train length = 5, effective echo = 3, slices = 30, matrix = 256 × 250; FOV = 96 × 96 mm; acquisition voxel size = 375 μm × 384 μm × 1.5 mm). T2 imaging using fast spin echo, as compared to gradient echo based imaging such as T1-weighted MP-RAGE, reduced the amount of image distortion caused by skull implants such as the ceramic bone screws and plastic head post.

### 3.2.3 Image preprocessing

All preprocessing was implemented using the FSL software package (<http://www.fmrib.ox.ac.uk>) and included motion correction (six parameter affine transformation), brain extraction, spatial smoothing (FWHM = 3 mm), high-pass temporal filtering (Gaussian-weighted least-squares straight line fitting with sigma = 100 s), low-pass temporal filtering (HWHM = 2.8 s, Gaussian filter), and normalization (12 DOF linear affine transformation implemented in FLIRT) to the F99 atlas template (Van Essen, 2004; see <http://sumsdb.wustl.edu.proxy1.lib.uwo.ca:2048/sums/macaque.more.do>).

### 3.2.4 Group independent component analysis

Group ICA, unlike single-subject ICA, allows inferences to be made at the group level. When examining subjects individually, it is difficult to compare components since they are not ordered and different components may be revealed in each subject. Entering all subjects into an ICA analysis and estimating one set of components has the advantage

of ordering the components of different subjects in the same way. This produces a single set of “group” components that can then be interpreted. Additionally, weak sources with different characteristics across subjects (i.e., noise) will be suppressed allowing a more accurate reflection of population dynamics.

Group ICA was conducted using the GIFT software package (Calhoun, Adali, Pearlson, Pekar, 2001; <http://icatb.sourceforge.net>). Data from both runs of all animals were concatenated, and the temporal dimension of this aggregated data set was reduced by means of principal component analysis (PCA). This was followed by spatial component estimation using the Infomax algorithm. Component time-courses and spatial maps for each animal were then back-reconstructed, using the aggregated components and the results from the data reduction step (Jafri, Pearlson, Stevens, & Calhoun, 2008; Calhoun, Adali, Pearlson, Pekar, 2001). Because ICA is a stochastic estimation process, the final component maps can vary depending on the initial algorithm conditions. To quantify the reliability of the decomposition, ICA was reiterated 20 times using the ICASSO toolbox (Himberg, Hyvarinen, Esposito, 2004). ICASSO represents each of the estimated components for each iteration as a point in the signal space. It then returns a stability index of the estimate cluster computed as the difference between the average intra- and inter-cluster similarities. In the ideal case, the repeated estimates are concentrated in compact and close-to-orthogonal clusters resulting in an index of all estimate-clusters that approaches one.

There are currently no well-established criteria to guide the selection of an optimal number of independent components (ICs) for a given data set (Cole, Smith, & Beckmann, 2010). The model order or dimension estimate defines the number of components that the algorithm will extract and in that regard represents a prediction about the number of underlying sources in the data. If the model order is increased, a greater number of networks will be found accounting for the data in a more detailed way, albeit causing networks to branch into smaller sub-networks (Smith et al., 2009; Abou-Elseoud, Starck, Remes, Nikkinen, Tervonen, & Kiviniemi, 2010). One proposed method uses the minimum description length criterion for dimension estimation (Jafri, Pearlson, Stevens, & Calhoun, 2008; Li, Adali, & Calhoun, 2007); however when applied to our

data set, this technique resulted in an estimation of 253 ICs. Instead, 20 components were chosen, as this gave a manageable number of components and approximated model orders commonly used in human studies large-scale brain networks (Smith et al., 2009; Abou-Elseoud, Starck, Remes, Nikkinen, Tervonen, & Kiviniemi, 2010; Calhoun, Adali, Pearlson, & Pekar, 2001; Demirci et al., 2009).

The mean group ICs were then scaled to empirically derived z-scores by dividing by the standard deviation of the original time-course. The z-scores approximate the temporal correlation between each voxel and the associated component where the magnitude of the z-score specifies the strength of the linear relationship. A negative z-score indicates voxels in which the BOLD signals are modulated opposite to that of the IC time-course. A z-score value of  $\pm 1$  was used as the lower limit threshold of functional connectivity.

### 3.2.5 RSN identification and visualization

The ICA derived components were visually inspected and labeled based on the activation patterns in reference to known anatomical and functional locations. Classification of the components in terms of RSNs was performed by comparison with known macaque functional networks and previously identified RSNs from ICA studies in humans (Beckmann, DeLuca, Devlin, & Smith, 2005; Damoiseaux et al., 2006; Smith et al., 2009). In addition to identifying spatially independent networks, ICA is able to parse out noise due to physiological fluctuations, motion, and hardware artifacts from the original source data (Thomas, Harshman, & Menon, 2002; Liao, McKeown, & Krolak, 2006; Perlberg, Bellec, Anton, Péligrini-Issac, Doyon, & Benali, 2007). Components with high spatial correspondence to cerebrospinal spinal fluid (see Fig. 3.1) or with low correlation to gray matter, were discarded.

Group data were projected from volume data to the F99 cortical surface using the CARET (<http://www.nitrc.org/projects/caret>) enclosed-voxel method.

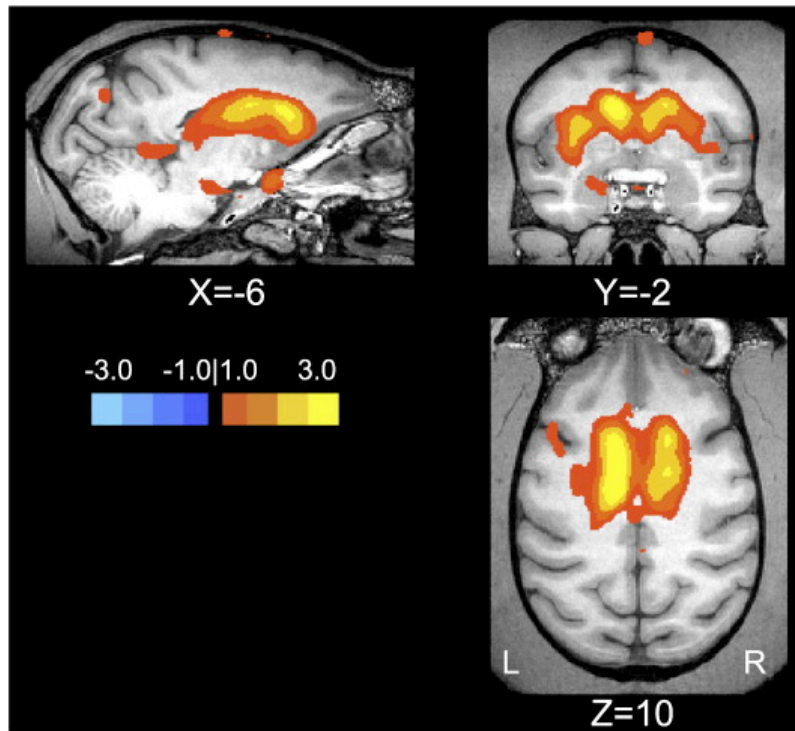


**Figure 3.1. Cerebrospinal fluid related artifact decomposed from resting-state functional data using independent component analysis.** Overlaid color maps represent thresholded z-scores displayed on the MR image of the F99 atlas (Van Essen, 2004; see <http://sumsdb.wustl.edu.proxy1.lib.uwo.ca:2048/sums/macquemore.do>). Numerical values indicate the distance (mm) from the anterior commissure. Reprinted with permission from Hutchison, Leung, Mirsattari, Gati, Menon, & Everling (2011).

### 3.2.6 Single-subject ICA

Single-subject ICA is better suited to reveal individual features of resting-state connectivity as subtle differences between subjects may get lost in an ICA of a group data set. To examine individual subject maps and allow comparison with a previously published report (Moeller, Nallasamy, Tsao, & Freiwald, 2009), single subject-ICA was conducted using the same parameters as the group-ICA. The unthresholded group-ICA derived networks were then used as templates to order the component maps from the individual ICA by calculating the spatial correlation coefficient of the unthresholded individual maps.

### 3.2.7 Functional network connectivity

Spatial ICA maximizes the statistical independence in the spatial domain, though the components are not temporally constrained and ICs can exhibit considerable temporal correlations (Calhoun, Adali, Pekar, & Pearlson, 2003). The temporal dependencies are significant, albeit not as high as those between regions within an IC (Jafri et al., 2008). Functional network connectivity (FNC) analysis examines these temporal dependencies among ICs to establish the functional connectivity among the large-scale networks and has been shown to provide additional information regarding macroscopic brain organization (Jafri, Pearlson, Stevens, & Calhoun, 2008; Demirci et al., 2009) FNC analysis was conducted using the FNC software package (<http://mialab.mrn.org/software/>) using analysis steps described previously (Jafri et al., 2008). One-sample Student's t-tests were used to test statistically significant maximal lagged correlation ( $\pm 3$  s) combinations from the 55 possible combinations ( $p < 0.05$ , corrected for multiple comparisons).

## 3.3 Results

### 3.3.1 Resting-state networks

Group-ICA successfully decomposed the resting-state functional data of 6 monkeys into 20 independent components. ICASSO returned a stability index for each estimate-cluster that approached 1 (mean  $\pm$  SD = 0.980  $\pm$  0.006), indicating that the components are concentrated in compact and close-to-orthogonal clusters and highly consistent across multiple ICA runs. Eleven components were found to have a high correspondence with gray matter as well as showing network characteristics (i.e. spatial maps containing more than one functional area) and were thereby deemed to be physiologically relevant. The spatial maps of the RSNs obtained with ICA analysis are illustrated in Fig. 3.2 (for RSN maps displayed on a flattened cortex see Fig. 3.3). The components accounted for 59.81% of the data's variance. The degree of cortical coverage is illustrated in Fig. 3.4. Despite inclusion of the entire brain, components were primarily restricted to cortical areas. Therefore we focus on cortical connectivity in this study. On the basis of our classification results, the 11 RSNs can be described as follows:

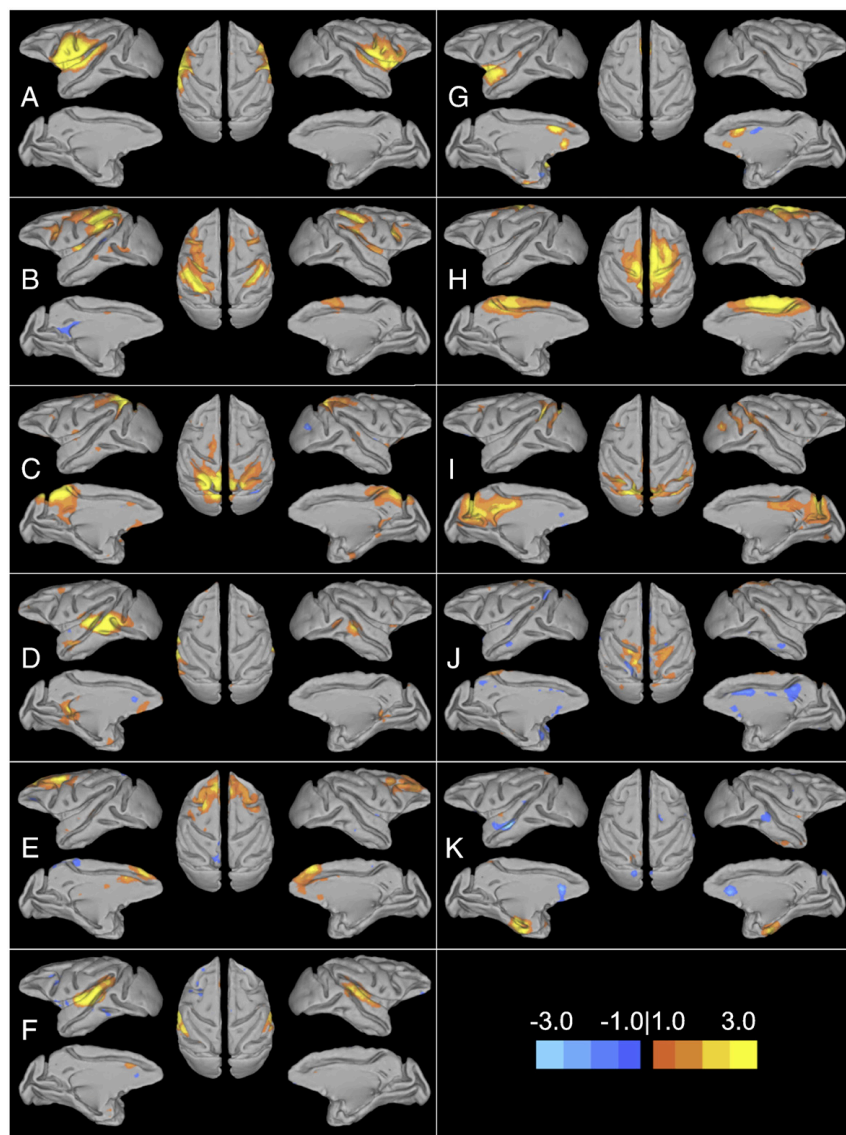


**Figure 3.2. Cortical representation of eleven resting-state networks (RSNs) identified by independent component analysis of fMRI data acquired from isoflurane-anesthetized macaque monkeys (N=6).** Overlaid color maps represent thresholded z-scores. All images have been normalized to the space of the F99 template (Van Essen, 2004; see <http://sumsdb.wustl.edu/sums/macquemore.do>). For each RSN, the left images depict lateral and medial views of left hemisphere, the center images depict the dorsal view of both hemispheres, and the right images depict the lateral and medial views of right hemisphere. Potential functional roles of each network are discussed in the text. Reprinted with permission from Hutchison, Leung, Mirsattari, Gati, Menon, & Everling (2011).

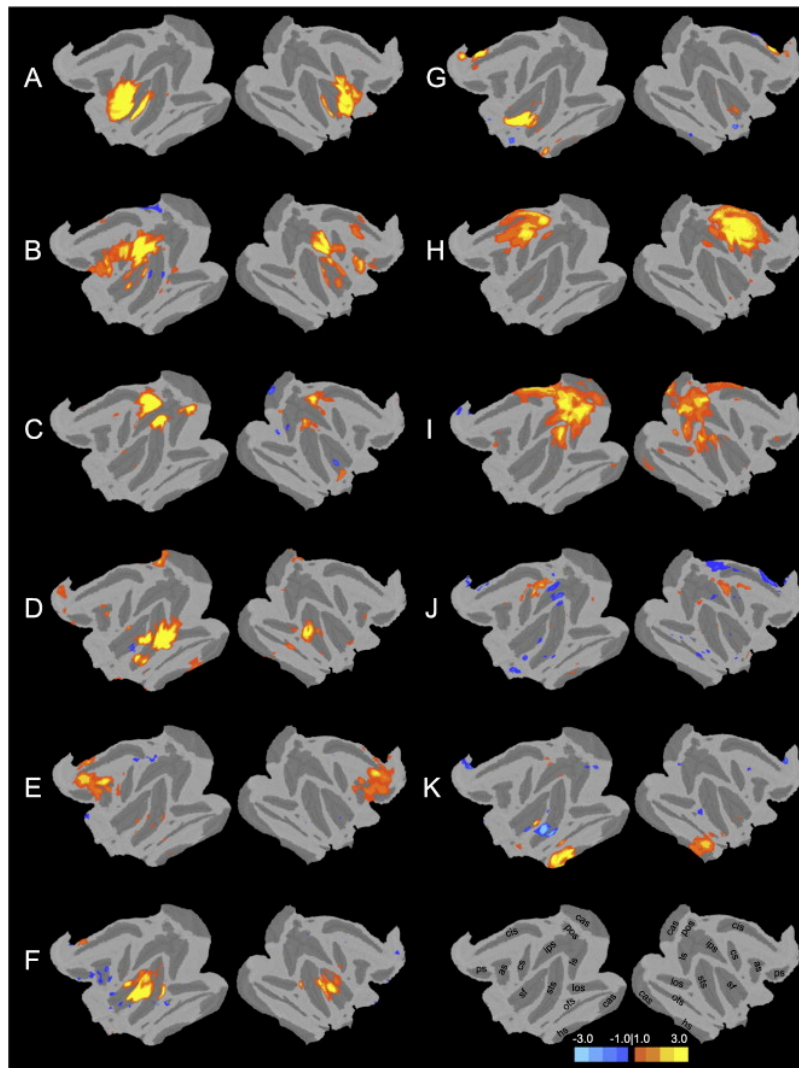


**Figure 3.3.** The eleven resting-state networks (RSNs) presented in Fig. 3.2 projected onto a flattened brain. RSNs were identified by group independent component analysis of fMRI data from six isoflurane-anesthetized macaque monkeys. Overlaid color maps represent thresholded z-scores. All images have been normalized to the space of the F99 template (Van Essen, 2004; see <http://sumsdb.wustl.edu.proxy1.lib.uwo.ca:2048/sums/macquemore.do>). The left and right images correspond to the left and right hemispheres, respectively. Sulci and color bar are shown in the bottom right quadrant. as, arcuate sulcus; cas, calcarine sulcus; cis, cingulate sulcus; cs, central sulcus; hs, hippocampal sulcus; ips, intraparietal sulcus; los, lateral orbital sulcus; ls, lingual sulcus; ots, occipito-temporal sulcus; sf, sylvian fissure; sts, superior temporal sulcus; pos, parieto-occipital sulcus; ps, principal sulcus. Reprinted with permission from Hutchison, Leung, Mirsattari, Gati, Menon, & Everling (2011).

- RSN A (precentral–temporal): The RSN included extended bilateral areas of the ventral precentral gyrus, corresponding to ventral premotor areas F4 and F5, activation in the inferior ramus of the arcuate sulcus, the precentral opercular cortex, primary and secondary somatosensory cortex, and insular cortex. In addition, connectivity was observed with the auditory cortex. The network included areas that correspond to the ventral motor system thought to play an important role in understanding action and visuomotor control of grasping and also included areas underlying the control of mouth and tongue ([Nelissen et al., 2005], [Joly et al., 2009] and [Phillips and Porter, 1977]).

- RSN B (fronto-parietal): Bilateral connectivity was found in the anterior bank, fundus, and posterior bank of the inferior arm of the arcuate sulcus. The anterior extent of this region corresponds to the location of the frontal eye fields (Bruce and Goldberg, 1985). Connectivity was found in the ventral prefrontal cortex and dorsal premotor cortex. Further network connectivity was found in area 3B in the dorsal central sulcus fundus and in both banks of the intraparietal sulcus. In addition, the right hemisphere showed positive correlation of area 6, corresponding to the supplementary motor area or possibly the supplementary eye fields (Schlag and Schlag-Rey, 1987). The network includes brain areas associated with the oculomotor system (also referred to as the dorsal attention network) responsible for goal-oriented saccadic eye movements (Johnston and Everling, 2008) and mediating goal-directed top-down processing (Noudoost et al., 2010). The functional network has been previously reported in eye movement tasks ([Baker et al., 2006] and Ford et al., 2009) and resting-state analysis (Vincent et al., 2007) of the macaque.

- RSN C (posterior-parietal): The network encompassed the posterior cingulate/precuneus cortex, bilateral areas PG and PE of the parietal cortex, and visual areas V2 and V3. In addition, this network contained connectivity patterns in the dorsolateral prefrontal cortex and in the dorsal premotor cortex in the left hemisphere. The brain areas include areas found in the default-mode network (DMN) areas that are deactivated during attention-

demanding cognitive tasks and in humans has been suggested to support higher-order mental faculties (Raichle et al., 2001).

- RSN D (occipito-temporal): Network areas included bilateral area TO, V4, TEO, and the arcuate sulcus. Bilateral area 29 and Brodmann area 10 (left hemisphere) were also functionally connected. Previous studies have shown these temporal lobe areas are critical for higher-order visual processing (Tsao et al., 2003).

- RSN E (frontal): This RSN encompassed bilateral regions in several prefrontal areas, including the anterior bank of the arcuate sulcus, corresponding to the frontal eye fields, the upper ramus of the arcuate sulcus, the posterior portion of the principal sulcus, as well as the dorsal bank of the principal sulcus. In addition, LFF synchronization was also found in area 9, the premotor cortex and the anterior cingulate cortex. These frontal/prefrontal areas have been shown to be components of the executive system suggested to provide bias signals to other areas of the brain in order to implement cognitive control (Miller and Cohen, 2001).

- RSN F (superior-temporal): A network encompassing the auditory belt, parabelt, and bilateral area 22 on the superior temporal gyrus. Anti-correlated areas were found in the left principal sulcus and in the left arcuate sulcus. The network pattern resembles the mean functional activity resulting from the presentation of multiple sounds categories in a previous task-based fMRI study of the awake monkey (Petkov et al., 2008) and is likely responsible for acoustic processing and interpretation (Rauschecker and Scott, 2009).

- RSN G (cingulo-insular): A network of areas including bilateral regions in the insular cortex, the anterior cingulate cortex area 24a/b, and the orbitofrontal cortex, area 14.

These areas have been associated with the reward system involved in the regulation and control of behavior (Kringelbach, 2005).

- RSN H (paracentral): A network reflective of the dorsal motor system involved in the control of limb movements (Dum and Strick, 2002). Network connectivity included bilateral primary motor cortex dorsally and also in the central sulcus, area F2, and the dorsal bank of the superior ramus of the arcuate sulcus. In addition, widespread connectivity was found in the medial wall, including the cingulate motor area, supplementary motor area, and medial parietal cortex. The network pattern closely resembles the “somatomotor” network previously described in the anesthetized macaque using a seed-region based approach (Vincent et al., 2007).
- RSN I (parieto-occipital): A network consisting of regions involved in visual processing including bilateral areas V1, V2, V2, V3, area PO, and area MT/MST. Connectivity was also observed unilaterally in area 8A (left hemisphere) and 46d (right hemisphere). Similar network patterns have been observed in the macaque in both resting-state (Vincent et al., 2007) and awake fMRI studies (Stefanacci et al., 1998).
- RSN J (postcentral): A network including the postcentral and precentral gyrus, areas dedicated to somatosensory processing (Kaas, 1993). Opposite modulation was found to occur in area PO and in the anterior cingulate cortex area 24 a/b.
- RSN K (hippocampal): A medial temporal network corresponding to areas associated with the macaque declarative memory system (Squire and Zola-Morgan, 1991). The RSN bilaterally encompassed the hippocampus, entorhinal, perirhinal, and parahippocampal cortical areas. Anti-correlated bilateral connectivity of anterior cingulate cortex area 25 was also observed. The network, although partially explored in several previous

electrophysiological studies (e.g. [Rolls et al., 1993] and [Wirth et al., 2003]) has not been shown with monkey fMRI possibly due to the difficult task demands required of the animals in order to elicit activations in these areas.

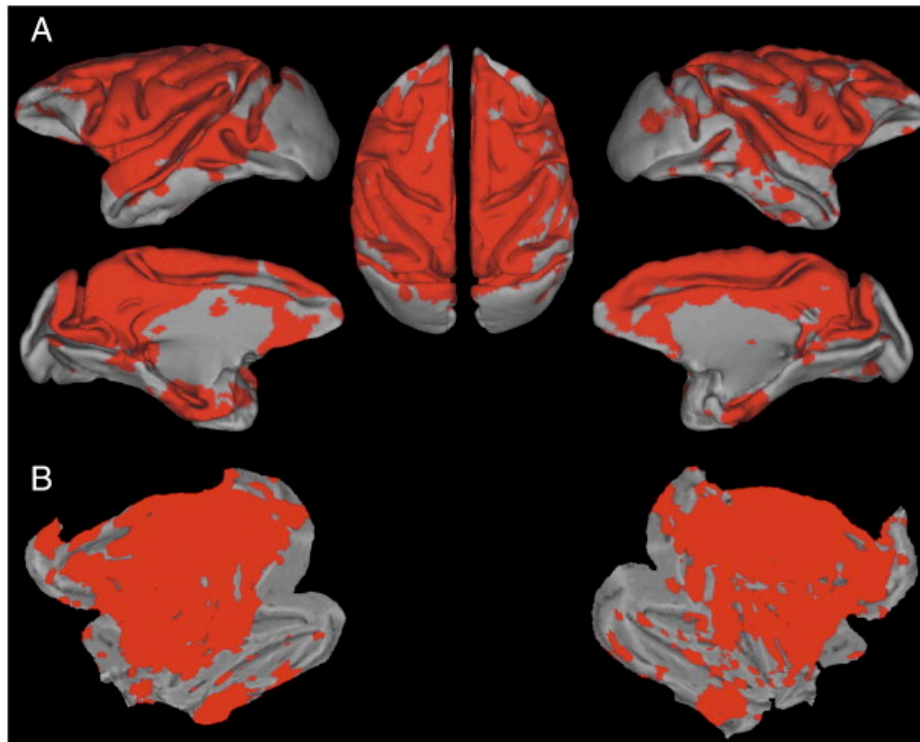


**Figure 3.4. Cortical coverage of eleven resting-state networks (RSNs) identified by group independent component analysis of fMRI data from six isoflurane-anesthetized macaque monkeys.** All images have been normalized to the space of the F99 template (Van Essen, 2004; see <http://sumsdb.wustl.edu.proxy1.lib.uwo.ca:2048/sums/macaquemore.do>). (A) The left images depict lateral and medial views of left hemisphere, the center images depict the dorsal view of both hemispheres, and the right images depict the lateral and medial views of right hemisphere. (B) Cortical coverage of (A) projected onto a flattened brain. Reprinted with permission from Hutchison, Leung, Mirsattari, Gati, Menon, & Everling (2011).

### 3.3.2 Single subject ICA

To compare single subject ICA with group ICA components, we spatially correlated unthresholded single subject IC maps with the unthresholded group IC maps. The correlation coefficients for all maps and all animals was significant ( $p < 10^{-20}$ ,  $p$  value corrected for multiple comparisons using Bonferroni correction). Table 1 shows the mean correlation coefficients between the single-subject ICA components and the group-ICA networks. Mean correlation values were found to be significantly different from 0 (one sample t-test,  $p < 0.01$ ). A representative network (RSN B — fronto-parietal) is shown for all monkeys in Fig. 3.5. Networks for all animals are shown in Figs 3.6-3.11. In some animals, the same single subject component was best correlated to two or more of the group ICA networks (for example, Fig. 3.7: components corresponding to networks D and I are the same).

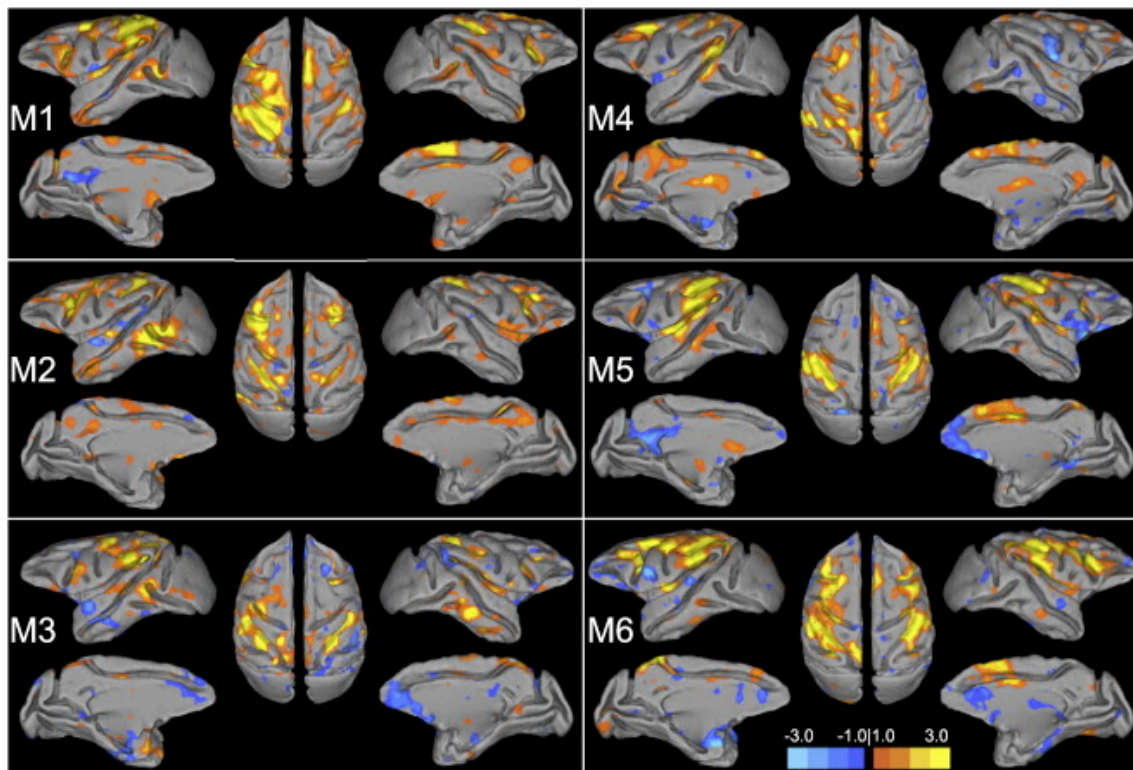


**Figure 3.5. Resting-state networks (RSN) of all monkeys (M1–M6) following single-subject independent component analysis (ICA) that were most spatially correlated to group-ICA identified RSN B (fronto-parietal).** Overlaid color maps represent thresholded z-scores. All images have been normalized to the space of the F99 template (Van Essen, 2004; see <http://sumsdb.wustl.edu/sums/macaquemore.do>). For each RSN, the left images depict lateral and medial views of left hemisphere, the center images depict the dorsal view of both hemispheres, and the right images depict the lateral and medial views of right hemisphere. Reprinted with permission from Hutchison, Leung, Mirsattari, Gati, Menon, & Everling (2011).

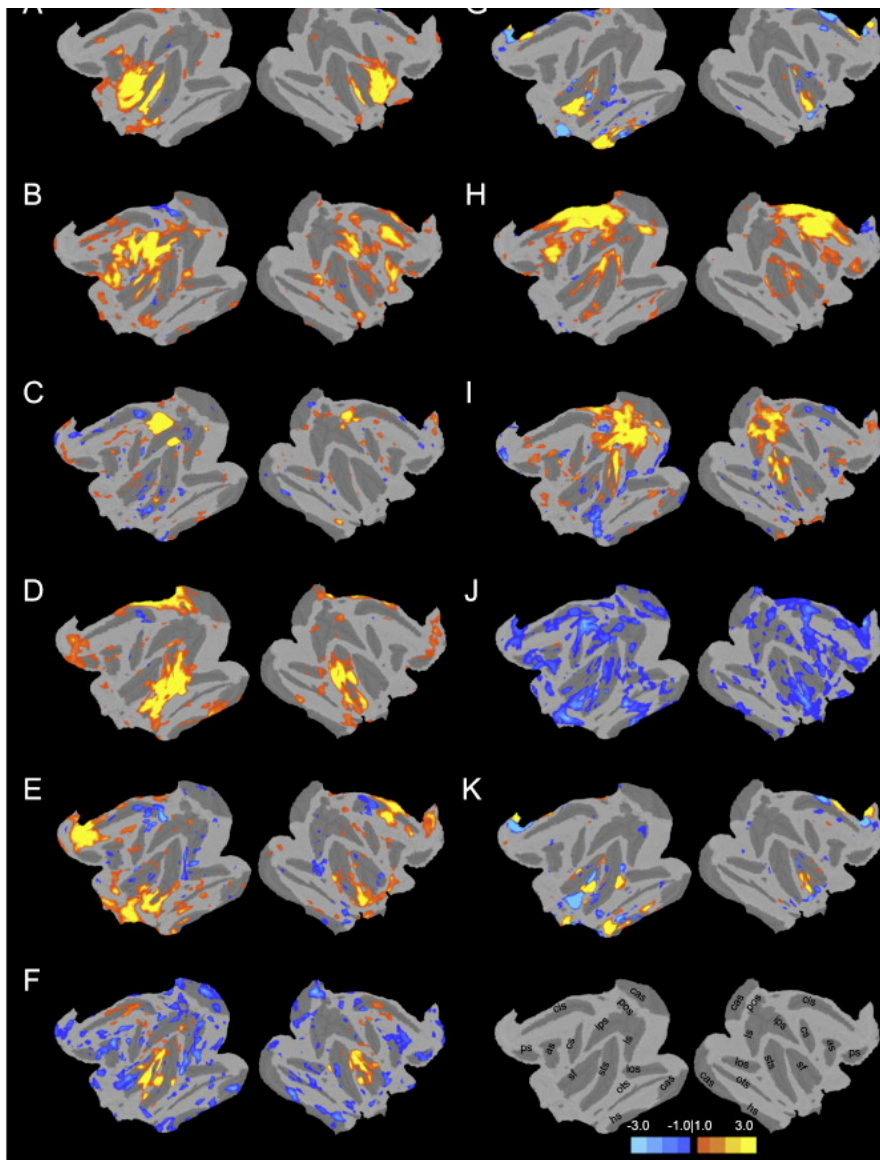


**Figure 3.6. Resting-state networks (RSN) of monkey M1 identified by single-subject independent component analysis (ICA) that were most spatially correlated to group-ICA identified networks seen in Fig. 3.2 and Fig. 3.3.** The networks are projected onto a flattened brain. Overlaid color maps represent thresholded z-scores. All images have been normalized to the space of the F99 template (Van Essen, 2004; see <http://sumsdb.wustl.edu.proxy1.lib.uwo.ca:2048/sums/macaqueuore.do>). The left and right images correspond to the left and right hemispheres, respectively. Sulci and color bar are shown in the bottom right quadrant; as, arcuate sulcus; cas, calcarine sulcus; cis, cingulate sulcus; cs, central sulcus; hs, hippocampal sulcus; ips, intraparietal sulcus; los, lateral orbital sulcus; ls, lingual sulcus; ots, occipito-temporal sulcus; sf, sylvian fissure; sts, superior temporal sulcus; pos, parieto-occipital sulcus; ps, principal sulcus. Reprinted with permission from Hutchison, Leung, Mirsattari, Gati, Menon, & Everling (2011).

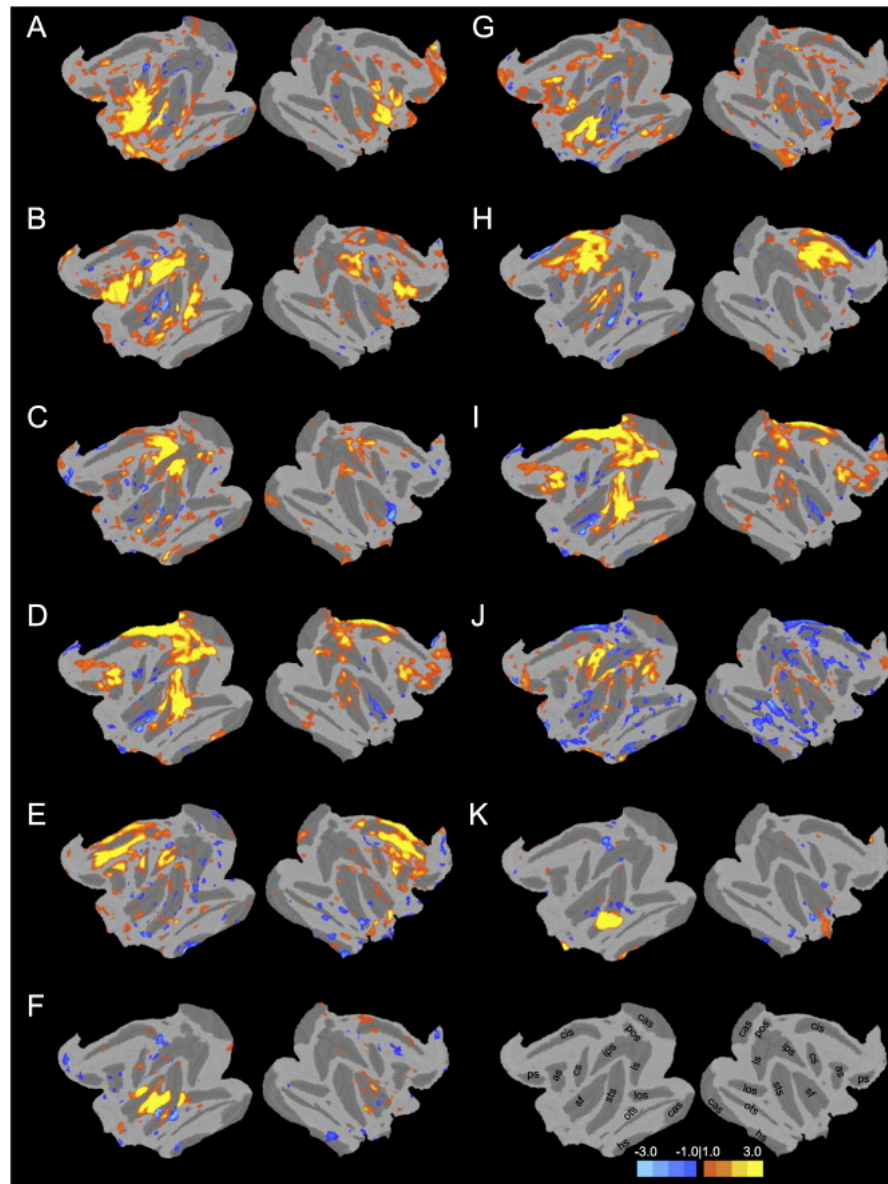


**Figure 3.7. Resting-state networks (RSN) of monkey M2 identified by single-subject independent component analysis (ICA) that were most spatially correlated to group-ICA identified networks seen in Fig. 3.2 and Fig. 3.3.** The networks are projected onto a flattened brain. Overlaid color maps represent thresholded z-scores. All images have been normalized to the space of the F99 template (Van Essen, 2004; see <http://sumsdb.wustl.edu.proxy1.lib.uwo.ca:2048/sums/macacuemore.do>). The left and right images correspond to the left and right hemispheres, respectively. Sulci and color bar are shown in the bottom right quadrant; as, arcuate sulcus; cas, calcarine sulcus; cis, cingulate sulcus; cs, central sulcus; hs, hippocampal sulcus; ips, intraparietal sulcus; los, lateral orbital sulcus; ls, lingual sulcus; ots, occipito-temporal sulcus; sf, sylvian fissure; sts, superior temporal sulcus; pos, parieto-occipital sulcus; ps, principal sulcus. Reprinted with permission from Hutchison, Leung, Mirsattari, Gati, Menon, & Everling (2011).

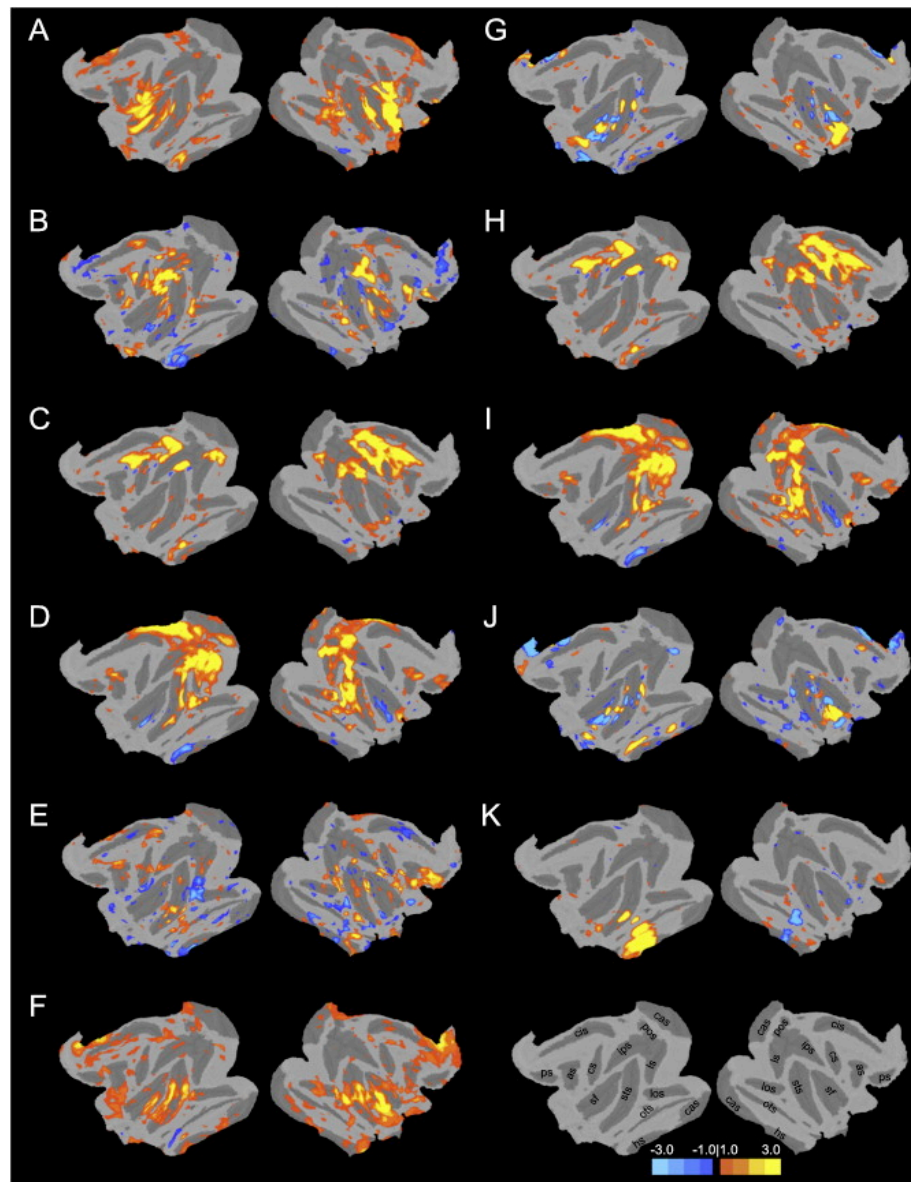


**Figure 3.8. Resting-state networks (RSN) of monkey M3 identified by single-subject independent component analysis (ICA) that were most spatially correlated to group-ICA identified networks seen in Fig. 3.2 and Fig. 3.3.** The networks are projected onto a flattened brain. Overlaid color maps represent thresholded z-scores. All images have been normalized to the space of the F99 template (Van Essen, 2004; see <http://sumsdb.wustl.edu.proxy1.lib.uwo.ca:2048/sums/macaqueuore.do>). The left and right images correspond to the left and right hemispheres, respectively. Sulci and color bar are shown in the bottom right quadrant; as, arcuate sulcus; cas, calcarine sulcus; cis, cingulate sulcus; cs, central sulcus; hs, hippocampal sulcus; ips, intraparietal sulcus; los, lateral orbital sulcus; ls, lingual sulcus; ots, occipito-temporal sulcus; sf, sylvian fissure; sts, superior temporal sulcus; pos, parieto-occipital sulcus; ps, principal sulcus. Reprinted with permission from Hutchison, Leung, Mirsattari, Gati, Menon, & Everling (2011).

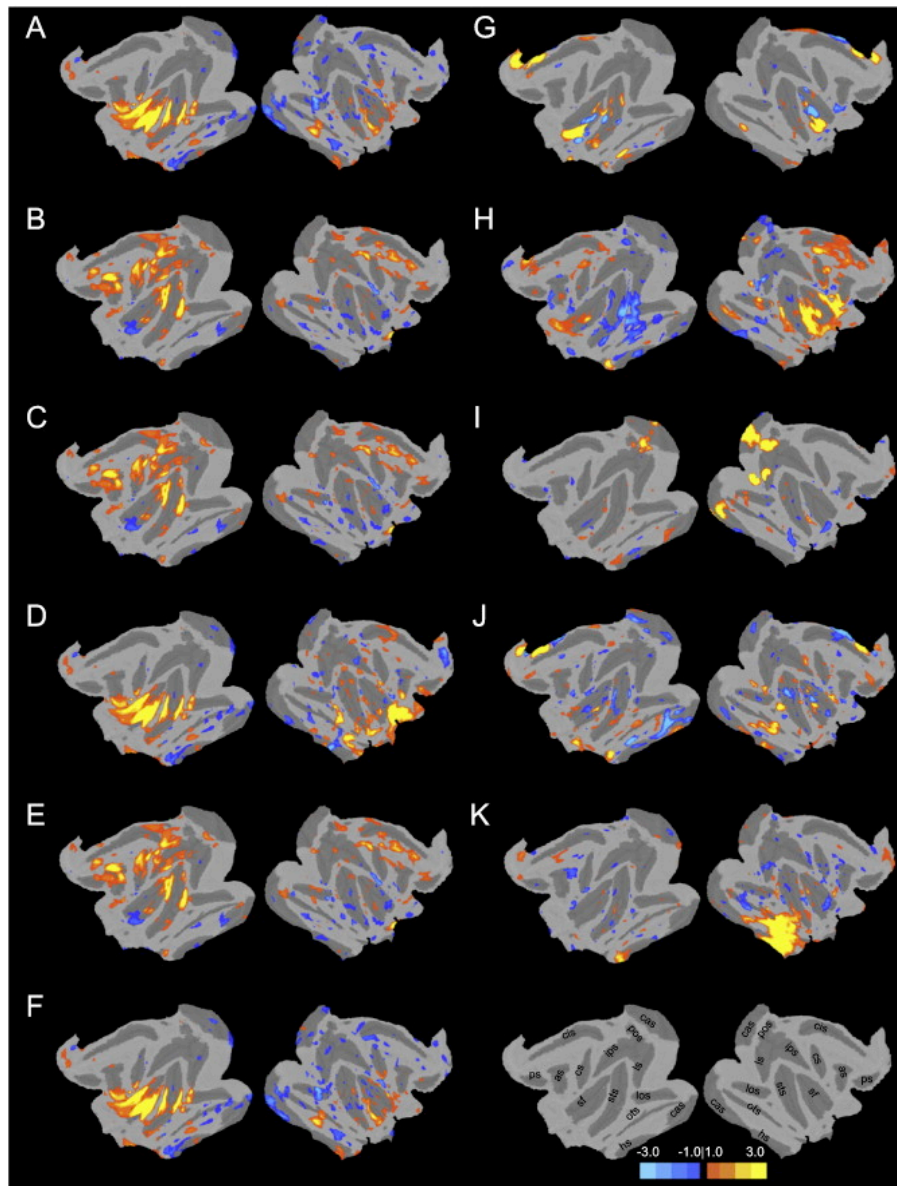


**Figure 3.9. Resting-state networks (RSN) of monkey M4 identified by single-subject independent component analysis (ICA) that were most spatially correlated to group-ICA identified networks seen in Fig. 3.2 and Fig. 3.3.** The networks are projected onto a flattened brain. Overlaid color maps represent thresholded z-scores. All images have been normalized to the space of the F99 template (Van Essen, 2004; see <http://sumsdb.wustl.edu.proxy1.lib.uwo.ca:2048/sums/macquemore.do>). The left and right images correspond to the left and right hemispheres, respectively. Sulci and color bar are shown in the bottom right quadrant; as, arcuate sulcus; cas, calcarine sulcus; cis, cingulate sulcus; cs, central sulcus; hs, hippocampal sulcus; ips, intraparietal sulcus; los, lateral orbital sulcus; ls, lingual sulcus; ots, occipito-temporal sulcus; sf, sylvian fissure; sts, superior temporal sulcus; pos, parieto-occipital sulcus; ps, principal sulcus. Reprinted with permission from Hutchison, Leung, Mirsattari, Gati, Menon, & Everling (2011).

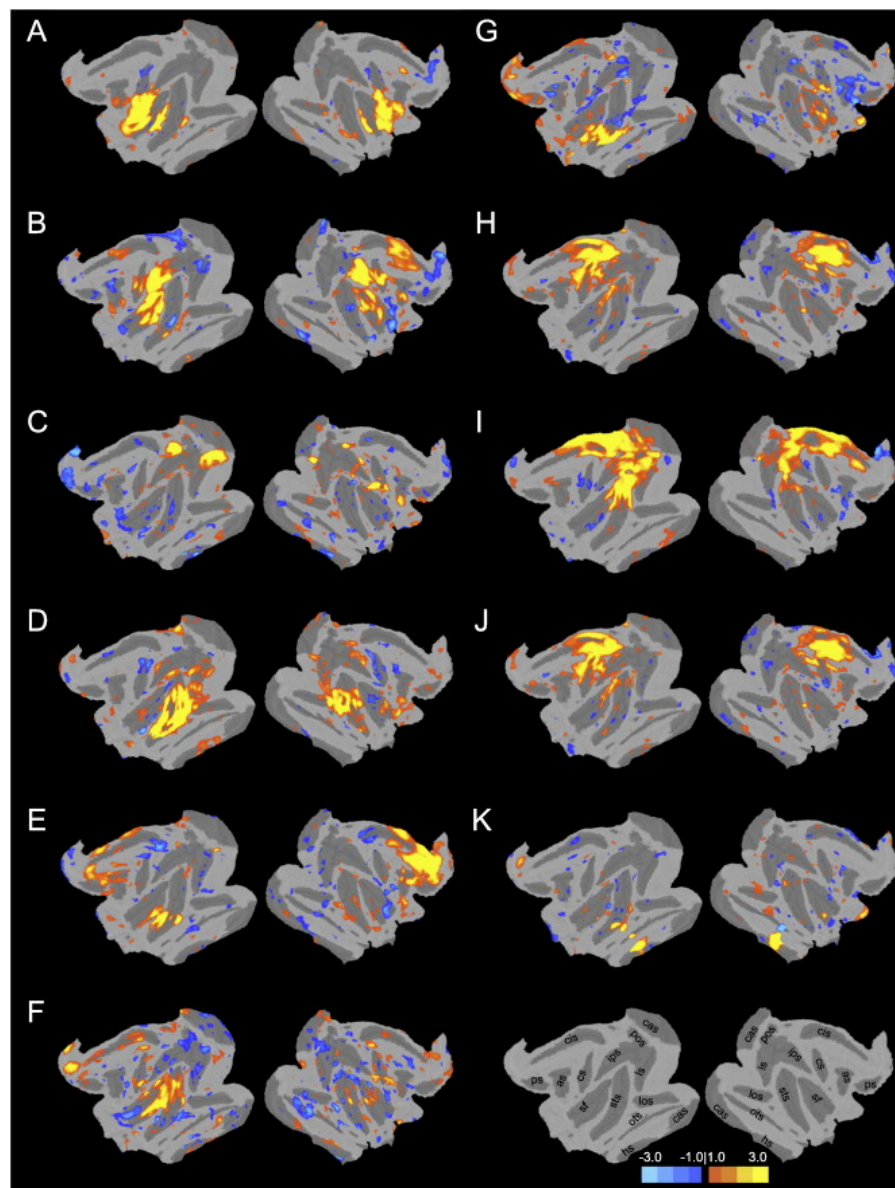


**Figure 3.10. Resting-state networks (RSN) of monkey M5 identified by single-subject independent component analysis (ICA) that were most spatially correlated to group-ICA identified networks seen in Fig. 3.2 and Fig. 3.3.** The networks are projected onto a flattened brain. Overlaid color maps represent thresholded z-scores. All images have been normalized to the space of the F99 template (Van Essen, 2004; see <http://sumsdb.wustl.edu.proxy1.lib.uwo.ca:2048/sums/macacuemore.do>). The left and right images correspond to the left and right hemispheres, respectively. Sulci and color bar are shown in the bottom right quadrant; as, arcuate sulcus; cas, calcarine sulcus; cis, cingulate sulcus; cs, central sulcus; hs, hippocampal sulcus; ips, intraparietal sulcus; los, lateral orbital sulcus; ls, lingual sulcus; ots, occipito-temporal sulcus; sf, sylvian fissure; sts, superior temporal sulcus; pos, parieto-occipital sulcus; ps, principal sulcus. Reprinted with permission from Hutchison, Leung, Mirsattari, Gati, Menon, & Everling (2011).

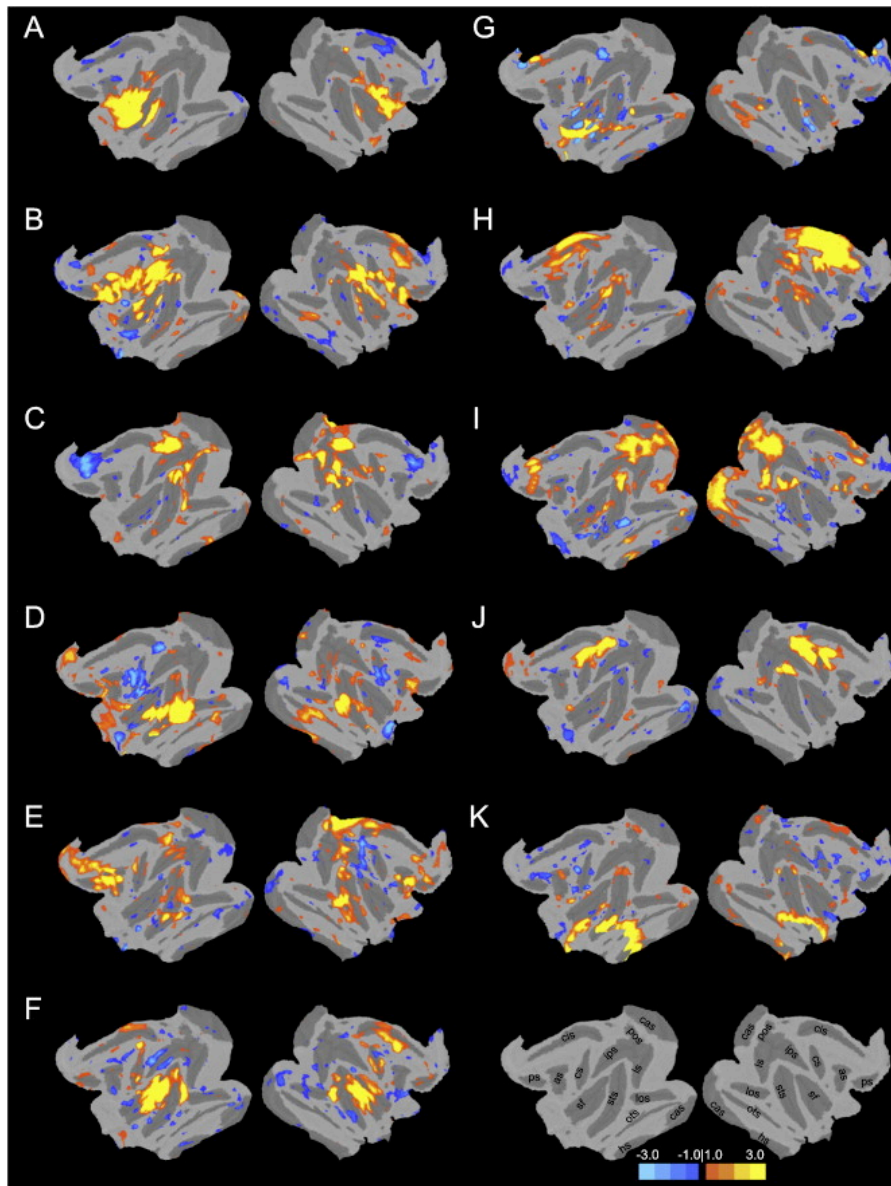


**Figure 3.11. Resting-state networks (RSN) of monkey M6 identified by single-subject independent component analysis (ICA) that were most spatially correlated to group-ICA identified networks seen in Fig. 3.2 and Fig. 3.3.** The networks are projected onto a flattened brain. Overlaid color maps represent thresholded z-scores. All images have been normalized to the space of the F99 template (Van Essen, 2004; see <http://sumsdb.wustl.edu.proxy1.lib.uwo.ca:2048/sums/macaqueuore.do>). The left and right images correspond to the left and right hemispheres, respectively. Sulci and color bar are shown in the bottom right quadrant; as, arcuate sulcus; cas, calcarine sulcus; cis, cingulate sulcus; cs, central sulcus; hs, hippocampal sulcus; ips, intraparietal sulcus; los, lateral orbital sulcus; ls, lingual sulcus; ots, occipito-temporal sulcus; sf, sylvian fissure; sts, superior temporal sulcus; pos, parieto-occipital sulcus; ps, principal sulcus. Reprinted with permission from Hutchison, Leung, Mirsattari, Gati, Menon, & Everling (2011).

**Table 3.1. Spatial correlations of single subject ICA derived networks to group-ICA derived networks**

<b>Network</b>	<b>Mean</b>	<b>STD ERR</b>	<b>Range</b>
A	0.691	0.068	0.383 - 0.841
B	0.560	0.082	0.176 - 0.750
C	0.463	0.062	0.227 - 0.649
D	0.501	0.078	0.215 - 0.743
E	0.373	0.046	0.275 - 0.584
F	0.459	0.073	0.184 - 0.623
G	0.372	0.060	0.200 - 0.586
H	0.559	0.059	0.272 - 0.661
I	0.501	0.065	0.199 - 0.655
J	0.375	0.045	0.207 - 0.546
K	0.264	0.017	0.186 - 0.302

*Note: Mean correlation values are significantly different from 0 (one sample t-test,  $p < 0.01$ ).*

### 3.3.3 Functional network connectivity

Fig. 3.12 shows a FNC diagram for the 11 identified RSNs. RSNs are represented by circular nodes and significantly correlated RSNs are represented by connecting lines. For example, a line connects networks I and J, representing significant functional connectivity between those two networks. RSN C (posterior-parietal) and RSN I (parieto-occipital) represent the most connected nodes. RSN D (occipito-temporal) and RSN E (frontal) also show a high degree of FNC. The other sensory networks show little or no connectivity with other RSNs.

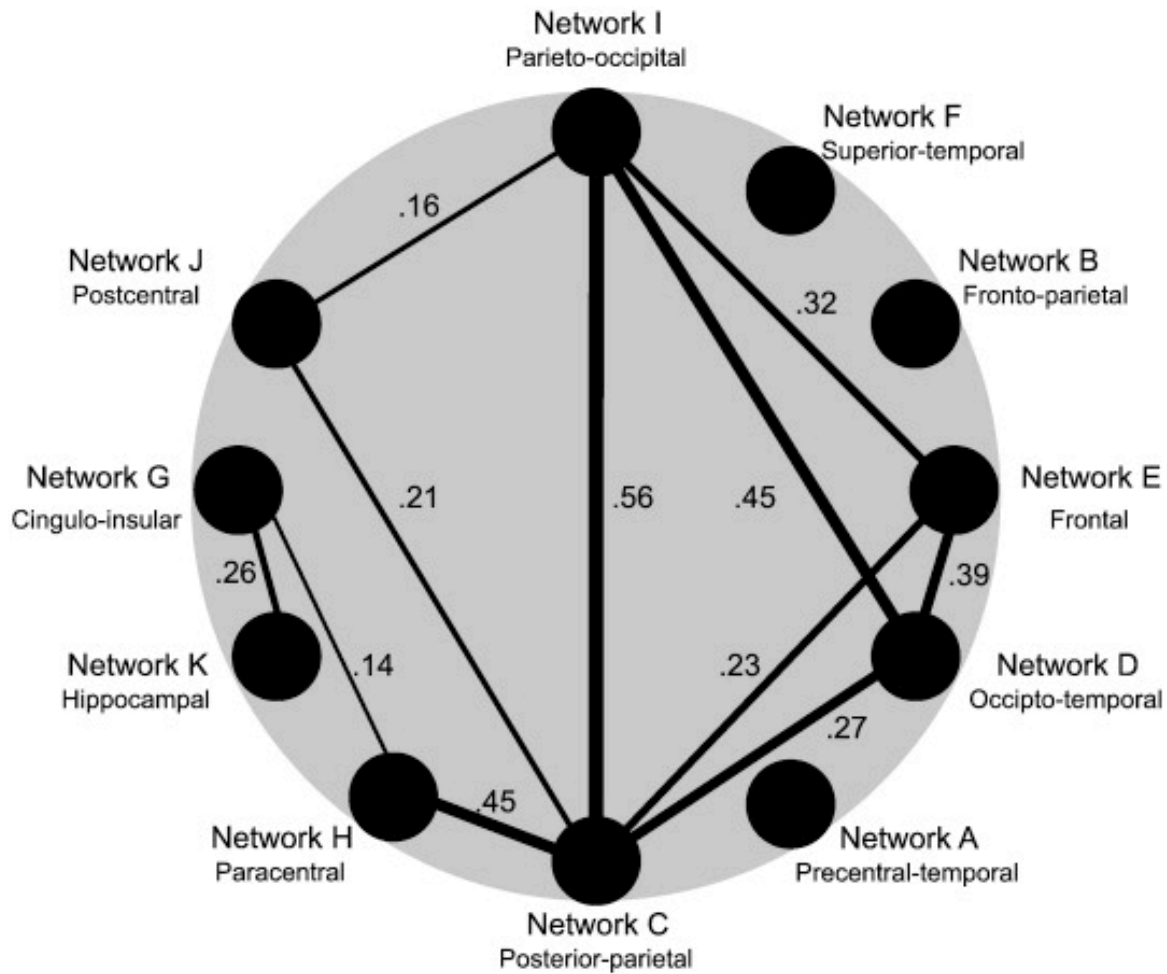


**Figure 3.12.** Average functional network connectivity of macaque resting-state networks (RSNs). Lines and numerical values indicate functional connectivity between two RSNs in which there was a significant temporal correlation of their respective time-courses (one-sample Student t-test,  $p < 0.05$ , corrected for multiple comparisons between 55 pairs, with a time lead/lag of  $\pm 3$  s). Network letters refer to spatial representations shown in Fig. 1. Reprinted with permission from Hutchison, Leung, Mirsattari, Gati, Menon, & Everling (2011).

### 3.4 Discussion

Alterations in functional connectivity recorded using spontaneous BOLD fluctuations have been suggested as the origin or product of multiple disease states (Auer, 2008; Greicius, 2008). Assessing their electrophysiological correlate(s) and establishing the relationship between large-scale functional network connectivity and disease require a suitable animal model. Here, to the best of our knowledge, we report the first comprehensive application of group independent component analysis (ICA) to monkey fMRI data and the first resting-state examination of the macaque at 7 T. ICA successfully identified 11 prominent macaque RSNs representing multiple levels of neural processing. Networks encompassing sensory and motor areas, including the visual, auditory, motor, and somato-sensory regions, can be considered to be lower-order in a cognitive processing hierarchy. The RSNs comprising areas known to be involved in executive control, attention, reward evaluation, and default-mode activity may represent higher-order processing, with temporal networks putatively responsible for visual processing and memory providing intermediate processing. In cases where the system has been explored with fMRI, the patterns of intrinsic functional connectivity are consistent with stimulus-evoked patterns found in task-based studies (see Results). The functional RSNs reported in the current study revealed highly similar, possibly homologous macroscopic brain organization between macaques and humans. RSNs B (fronto-parietal), C (posterior-parietal), D (occipito-temporal), E (frontal), F (superior-temporal), H (paracentral), and I (parieto-occipital) have been commonly reported following ICA of human resting-state data (Beckmann, DeLuca, Devlin, & Smith, 2005; Jafri, Pearlson, Stevens, & Calhoun, 2008; Smith et al., 2009). These have been labeled oculomotor/dorsal attention (see Figs. 6g, h of Beckmann, DeLuca, Devlin, & Smith, 2005), default-mode (see Fig. 6e of Beckmann, DeLuca, Devlin, & Smith, 2005), higher-order visual (see Fig. 6b of Beckmann, DeLuca, Devlin, & Smith, 2005), executive (see Fig. 6f of Beckmann, DeLuca, Devlin, & Smith, 2005), auditory (see Fig. 6c of Beckmann, DeLuca, Devlin, & Smith, 2005), somatomotor (see Fig. 6d of Beckmann, DeLuca, Devlin, & Smith, 2005), and primary visual (see Fig. 6a of Beckmann, DeLuca, Devlin, & Smith, 2005) networks respectively. Further, RSNs G (cingulo-insular), J (postcentral), and K (hippocampal) though not consistently reported in studies utilizing ICA, have homologous networks that

can be found when comparing task-based or seed-region analysis of human fMRI data (Kringelbach, 2005, Blatow, Nennig, Durst, Sartor, & Stippich, 2007; Burton, Dixit, Litkowski, & Wingert, 2009; Vincent et al., 2006).

Two recent studies have examined resting-state connectivity with hypotheses derived from experimental anterograde tracer studies of the macaque monkey (Margulies et al., 2009; Kelly et al., 2010). Kelly et al. (2010) examined the connectivity of ventrolateral frontal areas with parietal and temporal cortex in the human cortex. They found that the human brain maintains the same basic patterns observed in nonhuman primates (Petrides & Pandya, 2009). In the same way, Margulies et al. (2009) found functional subdivisions of the precuneus to be preserved between both species and also consistent with tracer studies (Pandya & Seltzer, 1982). These findings suggest that resting-state functional connectivity reflects the underlying structural anatomy (discussed below) and taken together with our current results, support the role of the macaque as a suitable animal model in the study of human brain organization and cross-species comparisons of functional neuroanatomy.

Despite the strong similarities in many of the macaque RSNs to human RSNs, our study also revealed a number of notable differences in RSNs between the two species. There was an absence of two commonly reported, lateralized fronto-parietal RSNs implicated in cognitive attentional processes as well as memory and language functions (Beckmann, DeLuca, Devlin, & Smith, 2005; Jafri, Pearlson, Stevens, & Calhoun, 2008; Smith et al., 2009). The homologous macaque network, RSN B (frontoparietal), though encompassing the same brain regions as the human networks, was relatively symmetrical and did not suggest lateralization of function. Given that the macaque brain appears to be less lateralized than the human brain (Kagan, Iyer, Lindner, & Andersenet, 2010), it is possible that the network represents the evolutionary predecessor to the lateralized human networks. Another functional connectivity difference was the lack of the dorsal medial prefrontal cortical (dmPFC) component of the DMN (Raichle, MacLeod, Snyder, Powers, Gusnard, & Shulman, 2001). A relatively weak network connection has been previously reported (Vincent, Kahn, Van Essen, Buckner, 2010), though it was absent in two other studies (Vincent et al., 2007; Teichert, Grinband, Hirsch, & Ferrera, 2010). It is difficult

to determine whether the dmPFC represents a less connected/weakly synchronized area of the DMN in the macaque, a brain area more vulnerable to BOLD fMRI artifactual sources (possibly due to the proximity to the eyes), an area highly sensitive to anesthesia level, or physiological variability in connectivity between animals. Finally, RSN K (hippocampal) shares a similar network pattern to the human memory RSN, however, there is an absence of parietal connectivity within the network that is found in the human brain (Vincent et al., 2006). RSN A (precentral–temporal) has not been reported as a separate network in resting-state or task-based studies of humans though the brain areas are implicated in more diffuse network patterns (Peeters et al., 2009). The ventral motor areas are critical for goal directed movements – particularly of the hand – in both species (Joly, Vanduffel, Orban, 2009; Callaert et al., in press]). In humans, however, there is a lateralization of motor function in which there is increased involvement of left motor areas resulting in functional asymmetries (Callaert et al., 2007). Monkeys show a weaker motor dominance than humans (Leca, Gunst, & Huffman, 2010) and the interhemispheric connectivity of the ventral motor system is supported by strong callosal connections between the homotopic functional areas. These factors could explain why a bilateral ventral motor RSN may not be found in the human at lower ICA model orders (20–40 ICs) as the synchronization between the systems might not be as tightly coupled.

RSNs are inferred from endogenous neural activity and their organization is likely shaped by structural connections (Sporns, 2010). There is increasing evidence to suggest that patterns of synchronous LFFs track underlying anatomical connectivity (Vincent et al., 2007; Hagmann et al., 2008; Skudlarski, Jagannathan, Calhoun, Hampson, Skudlarska, Pearlson, 2008; Honey et al., 2009; Margulies et al., 2009; Kelly et al., 2010). Anatomical connectivity may underlie some of the RSNs that we identified in the present study. In some cases, the observed RSNs are in good agreement with the known major bundles of fibers that connect sensory association areas of posterior cortex to frontal cortex. RSN B (fronto-parietal) contains areas in frontal and parietal cortex that are connected by subcomponents II and III of the superior longitudinal fasciculus and RSN C (posterior-parietal) is comprised of areas that are connected by the fronto-occipital fasciculus (Petrides & Pandya, 2002b). Structural connectivity via the uncinate fasciculus may underlie RSN G (cingulo-insular) (Petrides & Pandya, 2002b). At least

some of the areas in RSN D (occipito-temporal) are anatomically connected though the inferior longitudinal fasciculus (Petrides & Pandya, 2002b). Some of the other RSNs may reflect known connectivity by intrinsic connections (RSN E (Barbas & Pandya, 1989), RSN F (Pandya, 1995), RSN H (Vogt & Pandya, 1978)).

We also observed the opposite pattern in which little to no functional connectivity between hippocampal and parietal areas was observed whereas tracer methodology has revealed substantial connectivity between parietal and parahippocampal regions (Rockland & Van Hoesen, 1999). Similarly, RSN F (auditory) did not contain any prefrontal areas, despite the known connections of this area with ventral and dorsal areas through the extreme capsule (Petrides & Pandya, 2002b). It is important to note, however, the limitations of the data analysis when discussing the possible conclusions that are being drawn in terms of lateralization, connectivity, and absent homologous networks. Despite the link to structural organization, resting-state connectivity is not anatomical connectivity. The patterns of functional networks have been shown to capture polysynaptic connections (Vincent et al., 2007; O'Reilly, Beckmann, Tomassini, Ramnani, & Johansen-Berg, 2009) and functional connections have been shown where no direct structural connections exist (Uddin et al., 2008; Vincent, Kahn, Snyder, Raichle, & Buckner, 2008; Honey et al., 2009). The discrepancies further highlight the need for an animal model as a method to constrain and interpret the false presence and absence of known connectivity in the human brain found using diffusion tensor imaging and resting-state methods. Only tracer studies can address direct connections and these are not typically feasible in human investigations.

A previous report examining changes in functional connectivity of the macaque during various visual stimulus contexts also examined two monkeys at rest under ketamine anesthesia using single-subject ICA (Moeller, Nallasamy, Tsao, & Freiwald, 2009). Similar to the present study, networks encompassing primary sensory areas including auditory and visual systems were identified. These and other networks were typically bilateral, only comprising hemispheric functional homologous, a property also shown in rats (Hutchison, Mirsattari, Jones, Gati, & Leung, 2010). Our group data more closely resemble RSN organization of humans in which multiple subdivisions of a system

are functionally connected. Functionally connected regions can split into separate components at higher model orders (Abou-Elseoud, Starck, Remes, Nikkinen, Tervonen, & Kiviniemi, 2010), a property that reflects the hierarchical functional organization of the brain (Cole, Smith, & Beckmann, 2010). Moeller and colleagues (2009) used a model order of 300–1000 ICs whereas in the current study we used a model order of 20. The relatively large estimate could overestimate the number of networks and the use of an automated sorting algorithm specifying bilateralism could bias the results towards those reported in the study.

To delineate the effects of single-subject ICA and model order, single-subject ICA was conducted on our same data set using a model order of 20. The individual component maps varied in their spatial correlation to the group RSNs within and between animals. The differences could reflect individual differences in morphology, structural connectivity, or functional connectivity as well as an exacerbation of weaker spatial dependencies causing the ICA to decompose the data differently. Variability could also arise from noise sources unique to each animal that were not extracted as a unique component using group-ICA. The results also highlighted intersubject variability in regards to network decomposition as often single subject networks comprised areas encompassed by two (or more) group RSNs. Overall, the individual networks had more diffuse functionally connectivity patterns than group-ICA and considerably more connectivity than the small-scale networks previously identified (Moeller, Nallasamy, Tsao, & Freiwald, 2009). Therefore, the differences between our study and the work of Moeller et al. (2009) are more likely the result of a lower model order than group-level analysis. It is important to note however, that given the methodological differences including model order and anesthetic regime, a direct comparison between these studies is not possible.

Various network analysis strategies examining human and non-human primate brain connectivity have revealed that the cortex contains a small number of nodes having a disproportionately high number of connections (Sporns, Honey, & Kötter, 2007;

Hagmann et al., 2008; Buckner et al., 2009). These highly connected nodes are referred to as hubs and serve to integrate diverse informational sources enabling globally efficient information flow (Sporns, Honey, & Kötter, 2007). Hubs also facilitate small-world network organization, minimizing wiring and metabolic costs by providing long-distance connections that integrate local networks (Bassett & Bullmore, 2006). The locations of high functional centrality have a close correspondence with structural hubs (Honey et al., 2007; Hagmann et al., 2008; Buckner et al., 2009). The present study revealed substantial inter-network functional connectivity with RSN C (posterior-parietal) and RSN I (parieto-occipital). The precuneus/posterior cingulate cortex areas encompassed by RSN C have been previously shown to possess both structural and functional hub properties in the human brain (Hagmann et al., 2008; Buckner et al., 2009) and could play a substantial role in integrating or regulating activity of other RSNs particularly at rest (Greicius, Krasnow, Reiss, & Menon, 2003). A detailed analysis of the structural connectivity of the macaque cortex based on tracer studies suggested several structural hubs including frontal area 46 and visual area V4 (Honey et al., 2007; Sporns, Honey, Kötter, 2007) — areas encompassed by RSN I. These areas have been classified as association or integrative areas again reflecting their hub like properties. Thus, the results of the functional network connectivity analysis fit the current framework of known functional organization and further support the use of resting-state data in the evaluation of large-scale network dynamics and the use of FNC measures. It is important to note that like other functional connections, hubs have been shown to engage and disengage across time — dynamically altering their centrality (Honey et al., 2007). Evaluation of resting-state functional connectivity could provide an appropriate method to characterize the process by which the topology of functional networks changes over time.

### 3.5 Conclusions

In summary, our results demonstrate that ICA can identify RSNs in macaque monkeys that are likely homologous to those found in humans, thereby strongly supporting the use of monkeys as an ideal animal model for human brain function

(Passingham, 2009) while also reinforcing the use of resting-state functional connectivity in delineating complex neural circuits in vivo.

### 3.6 References

- Abou-Elseoud, A., Starck, T., Remes, J., Nikkinen, J., Tervonen, O., & Kiviniemi, V. (2010). The effect of model order selection in group PICA. *Hum Brain Mapp*, *31*, 1207–1216.
- Auer, D.P. (2008). Spontaneous low-frequency blood oxygenation level-dependent fluctuations and functional connectivity analysis of the ‘resting’ brain. *Magn Reson. Imaging*, *26*, 1055–1064.
- Baker, J.T., Patel, G.H., Corbetta, M., & Snyder, L.H. (2006). Distribution of activity across the monkey cerebral cortical surface, thalamus and midbrain during rapid, visually guided saccades. *Cereb Cortex*, *16*, 447–459.
- Barbas, H., & Pandya, D.N. (1989). Architecture and intrinsic connections of the prefrontal cortex in the rhesus monkey. *J Comp Neurol*, *286*, 353–375.
- Bassett, D.S., & Bullmore, E. (2006). Small-world brain networks. *Neuroscientist*, *12*, 512–523.
- Beckmann, C.F., DeLuca, M., Devlin, J.T., & Smith, S.M. (2005). Investigations into restingstate connectivity using independent component analysis. *Philos Trans R Soc Lond B Biol Sci*, *360*, 1001–1013.
- Biswal, B., Yetkin, F.Z., Haughton, V.M., & Hyde, J.S. (1995). Functional connectivity in the motor cortex of resting human brain using echo-planar MRI. *Magn Reson. Med*, *34*, 537–541.
- Blatow, M., Nennig, E., Durst, A., Sartor, K., & Stippich, C. (2007). fMRI reflects functional connectivity of human somatosensory cortex. *Neuroimage*, *37*, 927–936.
- Bruce, C.J., & Goldberg, M.E. (1985). Primate frontal eye fields. I. Single neurons discharging before saccades. *J Neurophysiol*, *53*, 603–635.
- Buckner, R.L., Sepulcre, J., Talukdar, T., Krienen, F.M., Liu, H., Hedden, T., Andrews-Hanna, J.R., Sperling, R.A., & Johnson, K.A. (2009). Cortical hubs revealed by intrinsic functional connectivity: mapping, assessment of stability, and relation to Alzheimer's disease. *J Neurosci*, *29*, 1860–1873.

- Burton, H., Dixit, S., Litkowski, P., & Wingert, J.R. (2009) Functional connectivity for somatosensory and motor cortex in spastic diplegia. *Somatosens. Mot Res*, *26*, 90–104.
- Buxhoeveden, D.P., Switala, A.E., Roy, E., Litaker, M., & Casanova, M.F. (2001). Morphological differences between minicolumns in human and nonhuman primate cortex. *Am J Phys Anthropol*, *115*, 361–371.
- Calhoun, V.D., Adali, T., Pearlson, G.D., & Pekar, J.J. (2001). A method for making group inferences from functional MRI data using independent component analysis. *Hum Brain Mapp*, *14*, 140–151.
- Calhoun, V.D., Adali, T., Pekar, J.J., & Pearlson, G.D. (2003). Latency (in) sensitive ICA: group independent component analysis of fMRI data in the temporal frequency domain. *Neuroimage*, *20*, 1661–1669.
- Callaert, D.V., Vercauteren, K., Peeters, R., Tam, F., Graham, S., Swinnen, S.P., Sunaert, S., & Wenderoth, N. (2011). Hemispheric asymmetries of motor versus nonmotor processes during (visuo) motor control. *Hum Brain Mapp*, *32*, 1311–29.
- Cole, D.M., Smith, S.M., & Beckmann, C.F. (2010). Advances and pitfalls in the analysis and interpretation of resting-state FMRI data. *Front Syst Neurosci*, *4*, 8.
- Cordes, D., Haughton, V.M., Arfanakis, K., Wendt, G.J., Turski, P.A., Moritz, C.H., Quigley, M.A., & Meyerand, M.E. (2000). Mapping functionally related regions of brain with functional connectivity MR imaging. *Am J Neuroradiol.*, *21*, 1636–1644.
- Croxson, P.L., Johansen-Berg, H., Behrens, T.E., Robson, M.D., Pinski, M.A., Gross, C.G., Richter, W., Richter, M.C., Kastner, S., & Rushworth, M.F. (2005). Quantitative investigation of connections of the prefrontal cortex in the human and macaque using probabilistic diffusion tractography. *J Neurosci*, *25*, 8854–8866.
- Damoiseaux, J.S., Rombouts, S.A., Barkhof, F., Scheltens, P., Stam, C.J., Smith, S.M., & Beckmann, C.F. (2006). Consistent resting-state networks across healthy subjects. *Proc Natl Acad Sci U.S.A.*, *103*, 13848–13853.
- Demirci, O., Stevens, M.C., Andreasen, N.C., Michael, A., Liu, J., White, T., Pearlson, G.D., Clark, V.P., & Calhoun, V.D. (2009). Investigation of relationships between fMRI brain networks in the spectral domain using ICA and Granger causality reveals distinct differences between schizophrenia patients and healthy controls. *Neuroimage*, *46*, 419–431.
- Dum, R.P., & Strick, P.L., 2002. Motor areas in the frontal lobe of the primate. *Physiol Behav*, *77*, 677–682.

- Farber, N.E., Harkin, C.P., Niedfeldt, J., Hudetz, A.G., Kampine, J.P., & Schmeling, W.T. (1997). Region-specific and agent-specific dilation of intracerebral microvessels by volatile anesthetics in rat brain slices. *Anesthesiology*, *87*, 1191–1198.
- Felleman, D.J., & Van Essen, D.C. (1991). Distributed hierarchical processing in the primate cerebral cortex. *Cereb Cortex*, *1*, 1–47.
- Ford, K.A., Gati, J.S., Menon, R.S., & Everling, S. (2009). BOLD fMRI activation for antisaccades in nonhuman primates. *Neuroimage*, *45*, 470–476.
- Fox, M.D., & Raichle, M.E. (2007). Spontaneous fluctuations in brain activity observed with functional magnetic resonance imaging. *Nat Rev Neurosci*, *8*, 700–711.
- Friston, K.J. (1994). Functional and effective connectivity in neuroimaging: a synthesis. *Hum Brain Mapp*, *2*, 56–78.
- Friston, K.J. (2002). Beyond phrenology: what can neuroimaging tell us about distributed circuitry. *Annu Rev Neurosci*, *25*, 221–250.
- Greicius, M. (2008). Resting-state functional connectivity in neuropsychiatric disorders. *Curr Opin Neurol*, *21*, 424–430.
- Greicius, M.D., Krasnow, B., Reiss, A.L., Menon, V., 2003. Functional connectivity in the resting brain: a network analysis of the default mode hypothesis. *Proc Natl Acad Sci U.S.A.*, *100*, 253–258.
- Greicius, M.D., Supekar, K., Menon, V., & Dougherty, R.F. (2009). Resting-state functional connectivity reflects structural connectivity in the default mode network. *Cereb.Cortex*, *19*, 72–78.
- Guye, M., Bartolomei, F., & Ranjeva, J.P. (2008). Imaging structural and functional connectivity: towards a unified definition of human brain organization? *Curr Opin Neurol*, *21*, 393–403.
- Hagmann, P., Cammoun, L., Gigandet, X., Meuli, R., Honey, C.J., Wedeen, V.J., & Sporns, O. (2008). Mapping the structural core of human cerebral cortex. *PLoS Biol*, *6*, e159.
- Hampson, M., Peterson, B.S., Skudlarski, P., Gatenby, J.C., & Gore, J.C. (2002). Detection of functional connectivity using temporal correlations in MR images. *Hum Brain Mapp*, *15*, 247–262.
- Himberg, J., Hyvarinen, A., & Esposito, F. (2004). Validating the independent components of neuroimaging time series via clustering and visualization. *Neuroimage*, *22*, 1214–1222.

- Honey, C.J., Kötter, R., Breakspear, M., & Sporns, O. (2007). Network structure of cerebral cortex shapes functional connectivity on multiple time scales. *Proc Natl Acad Sci U.S.A.*, *104*, 10240–10245.
- Honey, C.J., Sporns, O., Cammoun, L., Gigandet, X., Thiran, J.P., Meuli, R., & Hagmann, P. (2009). Predicting human resting-state functional connectivity from structural connectivity. *Proc Natl Acad Sci U.S.A.*, *106*, 2035–2040.
- Hutchison, R.M., Mirsattari, S.M., Jones, C.K., Gati, J.S., & Leung, L.S. (2010). Functional networks in the anesthetized rat brain revealed by independent component analysis of resting-state fMRI. *J Neurophysiol*, *103*, 3398–3406.
- Jafri, M.J., Pearlson, G.D., Stevens, M., & Calhoun, V.D. (2008). A method for functional network connectivity among spatially independent resting-state components in schizophrenia. *Neuroimage*, *39*, 1666–1681.
- Johnston, K., & Everling, S. (2008). Neurophysiology and neuroanatomy of reflexive and voluntary saccades in non-human primates. *Brain Cogn*, *68*, 271–283.
- Joly, O., Vanduffel, W., & Orban, G.A. (2009). The monkey ventral premotor cortex processes 3D shape from disparity. *Neuroimage*, *47*, 262–272.
- Kaas, J.H. (1993). The functional organization of somatosensory cortex in primates. *Ann Anat*, *175*, 509–518.
- Kagan, I., & Iyer, A., Lindner, A., Andersen, R.A., 2010. Space representation for eye movements is more contralateral in monkeys than in humans. *Proc Natl Acad Sci U.S.A.*, *107*, 7933–7938.
- Kelly, C., Uddin, L.Q., Shehzad, Z., Margulies, D.S., Castellanos, F.X., Milham, M.P., & Petrides, M., 2010. Broca's region: linking human brain functional connectivity data and non-human primate tracing anatomy studies. *Eur J Neurosci*, *32*, 383–398.
- Kiviniemi, V.J., Haanpää, H., Kantola, J.H., Jauhiainen, J., Vainionpää, V., Alahuhta, S., & Tervonen, O. & 2005. Midazolam sedation increases fluctuation and synchrony of the resting brain BOLD signal. *Magn Reson Imaging*, *23*, 531–537.
- Koyama, M., Hasegawa, I., Osada, T., Adachi, Y., Nakahara, K., & Miyashita, Y. (2004). Functional magnetic resonance imaging of macaque monkeys performing visually guided saccade tasks: comparison of cortical eye fields with humans. *Neuron*, *41*, 795–807.
- Kringelbach, M.L. (2005). The human orbitofrontal cortex: linking reward to hedonic experience. *Nat Rev Neurosci*, *6*, 691–702.

- Leca, J.B., Gunst, N., & Huffman, M.A. (2010). Principles and levels of laterality in unimanual and bimanual stone handling patterns by Japanese macaques. *J Hum Evol*, *58*, 155–165.
- Li, Y.O., Adali, T., & Calhoun, V.D. (2007). Estimating the number of independent components for functional magnetic resonance imaging data. *Hum Brain Mapp*, *28*, 1251–1266.
- Liao, R., McKeown, M.J., & Krolak, J.L. (2006). Isolation and minimization of head motion-induced signal variations in fMRI data using independent component analysis. *Magn Reson Med*, *55*, 1396–1413.
- Margulies, D.S., Vincent, J.L., Kelly, C., Lohmann, G., Uddin, L.Q., Biswal, B.B., Villringer, A., Castellanos, F.X., Milham, M.P., & Petrides, M. (2009). Precuneus shares intrinsic functional architecture in humans and monkeys. *Proc Natl Acad Sci U.S.A.*, *106*, 20069–20074.
- Miller, E.K., & Cohen, J.D. (2001). An integrative theory of prefrontal cortex function. *Annu Rev Neurosci*, *24*, 167–202.
- Moeller, S., Nallasamy, N., Tsao, D.Y., & Freiwald, W.A. (2009). Functional connectivity of the macaque brain across stimulus and arousal states. *J Neurosci*, *29*, 5897–5909.
- Nakahara, K., Adachi, Y., Osada, T., & Miyashita, Y. (2007). Exploring the neural basis of cognition: multi-modal links between human fMRI and macaque neurophysiology. *Trends Cogn Sci*, *11*, 84–92.
- Nelissen, K., Luppino, G., Vanduffel, W., Rizzolatti, G., & Orban, G.A. (2005). Observing others: multiple action representation in the frontal lobe. *Science*, *310*, 332–336.
- Noudoost, B., Chang, M.H., Steinmetz, N.A., & Moore, T. (2010). Top-down control of visual attention. *Curr Opin Neurobiol*, *20*, 183–190.
- O'Reilly, J.X., Beckmann, C.F., Tomassini, V., Ramnani, N., & Johansen-Berg, H. (2009). Distinct and overlapping functional zones in the cerebellum defined by resting state functional connectivity. *Cereb Cortex*, *20*, 953–965.
- Ongür, D., Ferry, A.T., & Price, J.L. (2003). Architectonic subdivision of the human orbital and medial prefrontal cortex. *J Comp Neurol*, *460*, 425–449.
- Orban, G.A., Van Essen, D., & Vanduffel, W. (2004). Comparative mapping of higher visual areas in monkeys and humans. *Trends Cogn, Sci*, *8*, 315–324.
- Pandya, D.N. (1995). Anatomy of the auditory cortex. *Rev Neurol (Paris)*, *151*, 486–494.

- Pandya, D.N., & Seltzer, B. (1982). Intrinsic connections and architectonics of posterior parietal cortex in the rhesus monkey. *J Comp Neurol*, *204*, 196–210.
- Passingham, R. (2009). How good is the macaque monkey model of the human brain? *Curr Opin Neurobiol*, *19*, 6–11.
- Peeters, R., Simone, L., Nelissen, K., Fabbri-Destro, M., Vanduffel, W., Rizzolatti, G., & Orban, G.A. (2009). The representation of tool use in humans and monkeys: common and uniquely human features. *J Neurosci*, *29*, 11523–11539.
- Perlberg, V., Bellec, P., Anton, J.L., Pélégrini-Issac, M., Doyon, J., & Benali, H. (2007). CORSICA: correction of structured noise in fMRI by automatic identification of ICA components. *Magn Reson Imaging*, *25*, 35–46.
- Petkov, C.I., Kayser, C., Steudel, T., Whittingstall, K., Augath, M., & Logothetis, N.K. (2008). A voice region in the monkey brain. *Nat Neurosci*, *11*, 367–374.
- Petrides, M. & Pandya, D.N. (1999). Dorsolateral prefrontal cortex: comparative cytoarchitectonic analysis in the human and the macaque brain and corticocortical connection patterns. *Eur J Neurosci*, *11*, 1011–1036.
- Petrides, M., & Pandya, D.N. (2002a). Comparative cytoarchitectonic analysis of the human and the macaque ventrolateral prefrontal cortex and corticocortical connection patterns in the monkey. *Eur J Neurosci*, *16*, 291–310.
- Petrides, M. & Pandya, D.N. (2002b). Association pathways of the prefrontal cortex and functional observations. In: Stuss, D.T., Knight, R.T. (Eds.), *Principles of Frontal Lobe Function*. Oxford University Press, New York, NY, pp. 31–84.
- Petrides, M. & Pandya, D.N. (2009). Distinct parietal and temporal pathways to the homologues of Broca's area in the monkey. *PLoS Biol*, *7*, e1000170.
- Petrides, M. & Cadoret, G., Mackey, S. (2005). Orofacial somatomotor responses in the macaque monkey homologue of Broca's area. *Nature*, *435*, 1235–1238.
- Phillips, C.G. & Porter, R. (1977). *Corticospinal Neurons*. Academic Press, London.
- Preuss, T.M., 2000. Taking the measure of diversity: comparative alternatives to the model-animal paradigm in cortical neuroscience. *Brain Behav Evol*, *55*, 287–329.
- Preuss, T.M. (2004). Specializations of the human visual system: the monkey model meets human reality. In: Kaas, J.H., Collins, C.E. (Eds.), *The Primate Visual System*. CRC Press, pp. 231–259.
- Raichle, M.E., MacLeod, A.M., Snyder, A.Z., Powers, W.J., Gusnard, D.A., Shulman, G.L. (2001). A default mode of brain function. *Proc Natl Acad Sci U.S.A.*, *98*, 676–682.

- Rauschecker, J.P. & Scott, S.K. (2009). Maps and streams in the auditory cortex: nonhuman primates illustrate human speech processing. *Nat Neurosci*, *12*, 718–724.
- Rees, G., Friston, K., & Koch, C. (2000). A direct quantitative relationship between the functional properties of human and macaque V5. *Nat Neurosci*, *3*, 716–723.
- Rilling, J. (2006). Human and nonhuman primate brains: are they allometrically scaled versions of the same design? *Evol Anthropol*, *15*, 65–77.
- Rockland, K.S., & Van Hoesen, G.W. (1999). Some temporal and parietal cortical connections converge in CA1 of the primate hippocampus. *Cereb Cortex*, *9*, 232–237.
- Rolls, E.T., Cahusac, P.M., Feigenbaum, J.D., & Miyashita, Y. (1993). Responses of single neurons in the hippocampus of the macaque related to recognition memory. *Exp Brain Res*, *93*, 299–306.
- Schlag, J., & Schlag-Rey, M. (1987). Evidence for a supplementary eye field. *J Neurophysiol*, *57*, 179–200.
- Shmuel, A. & Leopold, D.A. (2008). Neuronal correlates of spontaneous fluctuations in fMRI signals in monkey visual cortex: implications for functional connectivity at rest. *Hum Brain Mapp*, *29*, 751–761.
- Skudlarski, P., Jagannathan, K., Calhoun, V.D., Hampson, M., Skudlarska, B.A., & Pearlson, G. (2008). Measuring brain connectivity: diffusion tensor imaging validates resting state temporal correlations. *Neuroimage*, *43*, 554–561.
- Smith, S.M., Fox, P.T., Miller, K.L., Glahn, D.C., Fox, P.M., Mackay, C.E., Filippini, N., Watkins, K.E., Toro, R., Laird, A.R., & Beckmann, C.F. (2009). Correspondence of the brain's functional architecture during activation and rest. *Proc Natl Acad Sci U.S.A.*, *106*, 13040–13045.
- Sporns, O. (2010). *Networks of the Brain*. MIT Press, Cambridge.
- Sporns, O., Tononi, G., & Kötter, R. (2005). The human connectome: a structural description of the human brain. *PLoS Comput Biol*, *1*, 245–251.
- Sporns, O., Honey, C.J., & Kötter, R. (2007). Identification and classification of hubs in brain networks. *PLoS ONE*, *2*, e1049.
- Squire, L.R., & Zola-Morgan, S. (1991). The medial temporal lobe memory system. *Science*, *253*, 1380–1386.
- Stefanacci, L., Reber, P., Constanza, J., Wong, E., Buxton, R., Zola, S., Squire, L., & Albright, T. (1998). fMRI of monkey visual cortex. *Neuron*, *20*, 1051–1057.

- Teichert, T., Grinband, J., Hirsch, J., & Ferrera, V.P. (2010). Effects of heartbeat and respiration on macaque fMRI: implications for functional connectivity. *Neuropsychologia*, *48*, 1886–1894.
- Thomas, C.G., Harshman, R.A., & Menon, R.S. (2002). Noise reduction in BOLD-based fMRI using component analysis. *Neuroimage*, *17*, 1521–1537.
- Tsao, D.Y., Freiwald, W.A., Knutsen, T.A., Mandeville, J.B., & Tootell, R.B. (2003). Faces and objects in macaque cerebral cortex. *Nat Neurosci*, *6*, 989–995.
- Uddin, L.Q., Mooshagian, E., Zaidel, E., Scheres, A., Margulies, D.S., Kelly, A.M., Shehzad, Z., Adelstein, J.S., Castellanos, F.X., Biswal, B.B., Milham, M.P. (2008). Residual functional connectivity in the split-brain revealed with resting-state functional MRI. *NeuroReport*, *19*, 703–709.
- Van Essen, D.C. (2004). Surface-based approaches to spatial localization and registration in primate cerebral cortex. *Neuroimage*, *23* (Suppl 1), S97–S107.
- Vincent, J.L., Snyder, A.Z., Fox, M.D., Shannon, B.J., Andrews, J.R., Raichle, M.E., & Buckner, R.L. (2006). Coherent spontaneous activity identifies a hippocampal–parietal memory network. *J Neurophysiol*, *96*, 3517–3531.
- Vincent, J.L., Patel, G.H., Fox, M.D., Snyder, A.Z., Baker, J.T., Van Essen, D.C., Zempel, J.M., Snyder, L.H., Corbetta, M., Raichle, M.E. (2007). Intrinsic functional architecture in the anaesthetized monkey brain. *Nature*, *447*, 83–86.
- Vincent, J.L., Kahn, I., Snyder, A.Z., Raichle, M.E., Buckner, R.L. (2008). Evidence for a frontoparietal control system revealed by intrinsic functional connectivity. *J Neurophysiol*, *100*, 3328–3342.
- Vincent, J.L., Kahn, I., Van Essen, D.C., Buckner, R.L. (2010). Functional connectivity of the macaque posterior parahippocampal cortex. *J Neurophysiol*, *103*, 793–800.
- Vogt, B.A. & Pandya, D.N. (1978). Cortico-cortical connections of somatic sensory cortex (areas 3, 1, and 2) in the rhesus monkey. *J Comp Neurol*, *177*, 179–192.
- Wirth, S., Yanike, M., Frank, L.M., Smith, A.C., Brown, E.N., Suzuki, W.A. (2003). Single neurons in the monkey hippocampus and learning of new associations. *Science*, *300*, 1578–1581.
- Young, M.P. (1993). The organization of neural systems in the primate cerebral cortex. *Proc R Soc Lond, B* *252*, 13–18.

## Chapter 4

### 4 Resting-state networks show dynamic functional connectivity in awake humans and anesthetized macaques<sup>6</sup>

#### 4.1 Introduction

Since the first observation that task-independent fluctuations of the blood-oxygenation-level-dependent (BOLD) time series between different areas was correlated (Ogawa et al., 1993) and the demonstration of the first maps based on these spatio-temporal coherences (Biswal, Yetkin, Haughton, & Hyde, 1995), resting-state functional magnetic resonance imaging (RS-fMRI) has become an important tool for characterizing functional brain networks. These analyses have shown that the hemodynamic signals recorded from cortical and subcortical areas are synchronized, forming characteristic resting-state networks (RSN) in the absence of external input or stimulus-evoked cognitive processing (Beckmann, DeLuca, Devlin, & Smith, 2005; Damoiseaux et al., 2006). RSNs are shaped by structural connectivity (Vincent et al., 2007; Greicius, Supekar, Menon, & Dougherty, 2009; Honey et al., 2009; Margulies et al., 2009; Kelly et al., 2010), closely resemble task-based activation networks (Biswal, Yetkin, Haughton, & Hyde, 1995; Fox, Corbetta, Snyder, Vincent JL, & Raichle, 2006a; Vincent et al., 2007; Smith et al., 2009), and are believed to be of neuronal origin (Mantini, Perrucci, Del Gratta, Romani, & Corbetta, 2007; Laufs, 2008; Shmuel & Leopold, 2008; Nir et al., 2008; Britz, Van De Ville, Michel, 2010; Musso, Brinkmeyer, Mobascher, Warbrick, & Winterer, 2010), though their physiological origin remains uncertain (Buckner & Vincent, 2007; Fox & Raichle, 2007). Coherence of the slow hemodynamic fluctuations have been shown in all mammals studied to date including both awake and anesthetized states in mice, rats, monkeys, and humans (Kiviniemi et al., 2005; Vincent et al., 2007; Greicius et al., 2008; Hutchison, Mirsattari, Jones, Gati, Leung, 2010; Hutchison,

---

<sup>6</sup> A version of this chapter has been published. Hutchison, R.M., Womelsdorf, T, Gati, J.S., Everling, S., Menon, R.S. (2012a) Resting-state networks show dynamic functional connectivity in awake humans and anesthetized macaques. *Hum. Brain Mapp*, *in press*.

Mirsattari, Gati, Menon, & Everling, 2011a; Jonckers et al., 2011). The conservation of this phenomenon across species suggests that it is a fundamental mammalian brain property.

RSN activity and within-network connection properties have been previously demonstrated to be both state-dependent (Greicius et al., 2008; Horovitz et al., 2009; Bianciardi, Fukunaga, van Gelderen, Horovitz, de Zwart, & Duyn, 2009) and task-modulated (Fransson, 2006; Esposito et al., 2006; Sun, Miller, Rao, & D'Esposito, 2007). Recent work has now drawn into question the stability of RSNs in the absence of altered cognitive states or overt behavioral shifts (Sato et al., 2006; Majeed et al., 2009; Chang and Glover, 2010; Britz et al., 2010; Musso et al., 2010). Notably, Chang and Glover (2010) demonstrated that the coherence, phase, and strength of functional connections between the posterior cingulate cortex and other areas of the default-mode network in awake human subjects varied on the scale of seconds to minutes over the duration of a standard resting-state scan. Resting-state simulation (Honey et al., 2007; Sporns, 2010 p.174) and magnetoencephalography (MEG) investigations have also shown time-varying RSN topology. The later revealing transient formation of more complete and characteristic RSNs when taking into account the nonstationarity of the MEG signal correlations (de Pasquale et al., 2010). Taken together, these results cast doubt on the underlying assumptions of temporal stationarity implicit in common RSN analyses.

An extensive number of electrophysiological studies have reported spontaneous (stimulus-independent) time-varying, network dynamics and ongoing brain activity over a wide range of temporal and spatial scales (for review see Vogels, Rajan, & Abbott, 2005; Ringach, 2009; Sadaghiani, Hesselmann, Friston, & Kleinschmidt, 2010; Raichle, 2010). These electrophysiological signatures are possibly related to the aforementioned dynamic variations of RSN connectivity. To identify possible links, it is necessary to quantify and characterize the ongoing dynamic shifts in functional network architecture as they become apparent in RS-fMRI. One limitation in the characterization of the dynamics of RS-fMRI that has been pointed out by Chang and Glover (2010) and others (Sato et al., 2006; Mantini et al., 2007; Britz et al., 2010; Musso et al., 2010), is the inability to ensure an absence of conscious processes during image acquisition. When

given unconstrained cognitive periods, awake human subjects engage in a diverse range of mental activities that can alter the brain's functional organization (Shirer, Ryali, Rykhlevskaia, Menon, & Greicius, 2012). These can include a spectrum of stimulus-independent activities such as mind wandering (Mason et al., 2007; Christoff, Gordon, Smallwood, Smith, & Schooler, 2009) or more active, stimulus-oriented processing such as monitoring the internal or external environment (Gilbert, Dumontheil, Simons, Frith, & Burgess, 2007). Over periods of several minutes, there are also changes related to vigilance, attention, and arousal (Paus et al., 1997), in addition to memory formation (Squire & Zola-Morgan, 1991). Recent evidence has also shown that sub-millimeter head motion during scanning can have significant effects on RS-fMRI network measures (Van Dijk, Sabuncu, Buckner, 2012). These can occur even when preprocessing corrects for motion, because correction algorithms account for gross voxel shifting, not for the disruptions of the field homogeneity.

To examine the role of these issues in the determination of RSN connectivity maps, the present study examined the resting-state dynamics of the nonhuman primate (*Macaca fascicularis*) under anesthesia and compared them to the same networks in awake human subjects. Isoflurane anesthesia induces a controlled state of central nervous system suppression characterized by a loss of consciousness, amnesia, analgesia, ablation of autonomic reflexes, as well as a suppression of motor responses (Veselis, 2001; Brown, Lydic, & Schiff, 2010). Therefore, anesthesia eliminates conscious processes as a complicating factor. The use of anesthesia, together with head-post immobilization, also allows for the elimination of active subject motion as a confound. Seed regions were selected throughout the previously identified macaque (Vincent et al., 2007; Hutchison et al., 2011a, 2011b) and human (Beckmann et al., 2005; Damoiseaux et al., 2006) fronto-parietal RSNs. The potentially homologous networks (Hutchison et al., 2012) are putatively responsible for attention and oculomotor functions, encompassing many of the well-known saccade-related brain areas in both species (Paus, 1996; Luna et al. 1998; Desouza, Menon, & Everling, 2003; Koyama et al., 2004; Baker, Patel, Corbetta, & Snyder, 2006; Brown, Vilis, & Everling, 2007; Johnston & Everling, 2008; Ford, Gati, Menon, & Everling, 2009). As such, it is herein referred to as the oculomotor (OCM) network. The default-mode network, which was examined by Chang and Glover (2010),

was not chosen because network homologies between the species are not currently well established and there are known brain state dependencies (Greicius et al., 2008; Horowitz et al., 2008, 2009). Instead, the OCM RSN represents a distributed and well-studied network of both species and is supported by extensive electrophysiological and histological mapping (Johnston & Everling, 2008; Wurtz & Goldberg, 1989). In addition, it will allow us to investigate the generalizability of the dynamic network characteristics.

A sliding-window correlation procedure was employed to verify the following hypotheses: 1) that RSN connectivity is not static and that the spatial pattern of functional connectivity depends upon the temporal scale that is being examined; 2) that ongoing RSN dynamics represent an evolutionarily preserved aspect of brain function, and therefore should be exhibited in the brain networks of other mammalian species; and 3) that the fluctuating relationships between brain areas represent an intrinsic and spontaneous phenomenon, independent of conscious processes, and therefore should transcend levels of consciousness.

## 4.2 Methods

### 4.2.1 Macaque monkeys

All surgical and experimental procedures were carried out in accordance with the Canadian Council of Animal Care policy on the use of laboratory animals and approved by the Animal Use Subcommittee of the University of Western Ontario Council on Animal Care. Data was collected from six macaque monkeys (*Macaca fascicularis*; 4 females) whose weights ranged from 3.6 to 5.3 kg (mean  $\pm$  standard deviation =  $4.58 \pm 1.4$  kg). Prior to the imaging experiments, an MRI-compatible custom-built acrylic head post was anchored to the skull with 6-mm ceramic bone screws (Thomas Recording, Giessen, Germany) and dental acrylic that served to restrain the head during image acquisition and eliminate motion. In preparation for image acquisition, each monkey was injected with intramuscular injections of atropine (0.4 mg/kg), ipratropium (0.025 mg/kg), and ketamine hydrochloride (7.5 mg/kg), followed by intravenous administration of 3 mL propofol (10 mg/mL) via the saphenous vein. Anesthesia was then maintained

using 1.5% isoflurane mixed with oxygen following oral intubation with an endotracheal tube. Animals were spontaneously ventilating throughout the duration of scanning and the eyes were closed. The monkey was then placed in a custom-built monkey chair with its head immobilized using the head post and inserted into the magnet bore, at which time the isoflurane level was lowered to 1%. Physiological parameters were continuously monitored throughout the duration of scanning (rectal temperature via a fiber-optic temperature probe [FISO, Quebec City, QC] = 36.5 °C; respiration via bellows [Siemens Corp., Union, NJ] = 25-30 breaths/min; end-tidal CO<sub>2</sub> via capnometer [Covidien-Nellcor, Boulder, CO] = 24-28 mm Hg). Animal body temperature was maintained using a heating disk (Snugglesafe, Littlehampton, West Sussex, UK) and thermal insulation.

#### 4.2.1.1 Data acquisition and preprocessing of monkey scans

Data was acquired on an actively shielded 7-T 68-cm horizontal bore scanner with a DirectDrive console (Agilent, Santa Clara, California) with a Siemens AC84 gradient subsystem (Erlangen, Germany) operating at a slew rate of 350 mT/m/s. An in-house designed and manufactured conformal 5-channel transceive primate-head RF coil was used. Magnetic field optimization ( $B_0$  shimming) was performed using an automated 3D mapping procedure (Klassen and Menon, 2004) over the specific imaging volume of interest. For each monkey, 2 runs of 300 continuous EPI functional volumes (TR = 2000 ms; TE = 16 ms; flip angle = 70°; slices = 30; matrix = 72 x 72; FOV = 96 x 96 mm; acquisition voxel size = 1.3 mm x 1.3 mm x 1.5 mm) were acquired. Acquisition time of each scan was 10 min. EPI images were acquired with GRAPPA at an acceleration factor of 2. Every image was corrected for physiological fluctuations using navigator echo correction. A high-resolution T2-weighted anatomical reference volume was acquired along the same orientation as the functional images using a turbo spin echo acquisition scheme (TR = 5000 ms; TE = 38.6 ms; echo train length = 5, effective echo = 3, slices = 30, matrix = 256 x 250; FOV = 96 x 96 mm; acquisition voxel size = 375  $\mu$ m x 384  $\mu$ m x 1.5 mm).

All preprocessing was implemented using the FMRIB Software Library toolbox (FSL; <http://www.fmrib.ox.ac.uk>.) and included motion correction (six parameter affine transformation), brain extraction, spatial smoothing (Gaussian kernel of full-width at half-maximum [FWHM] 3 mm applied to each volume separately), high-pass temporal filtering (Gaussian-weighted least-squares straight line fitting with  $\sigma = 100$  s), low-pass temporal filtering (half-width at half-maximum [HWHM] = 2.8 s, Gaussian filter), and normalization (12 degrees-of-freedom [DOF] linear affine transformation) to the F99 atlas template (van Essen, 2004; see <http://sumsdb.wustl.edu/sums/macacuemore.do>). No lag correction for the interleaved slice order was used, as the full width at half maximum of the autocorrelation function for a time series was  $\sim 12$  s suggesting that errors in lags brought about by slice order differences in the 2 s TR period are minimal.

#### 4.2.1.2 Oculomotor network identification in monkeys

A spherical seed (radius = 1.5 mm, volume = 14.14 mm<sup>3</sup>) was placed in the anterior bank of the arcuate sulcus of the left hemisphere in F99 atlas space (Van Essen, 2004; Fig. 4.1), an area corresponding to the frontal eye fields (FEF; Area 8a, Bruce & Goldberg, 1985). The seed location has been previously shown to reveal the resting-state OCM network of the anesthetized macaque (Hutchison et al., 2011b). A voxel-wise correlation analysis was then conducted using a three-level analysis procedure. The mean time-course over all voxels within the FEF seed region was extracted for each animal and each scanning session and then correlated (with zero lag) with every brain voxel at the individual subject-level for each corresponding scanning session. The results were then averaged across sessions after a Fisher z-transform, and then averaged across monkeys before being converted back to correlation values. The group correlation values were projected from volume data to the F99 cortical surface using the CARET enclosed-voxel method (Van Essen et al., 2001). Group pair-wise correlations were also calculated in the same manner between all seed pair combinations to derive the group connectivity matrix.

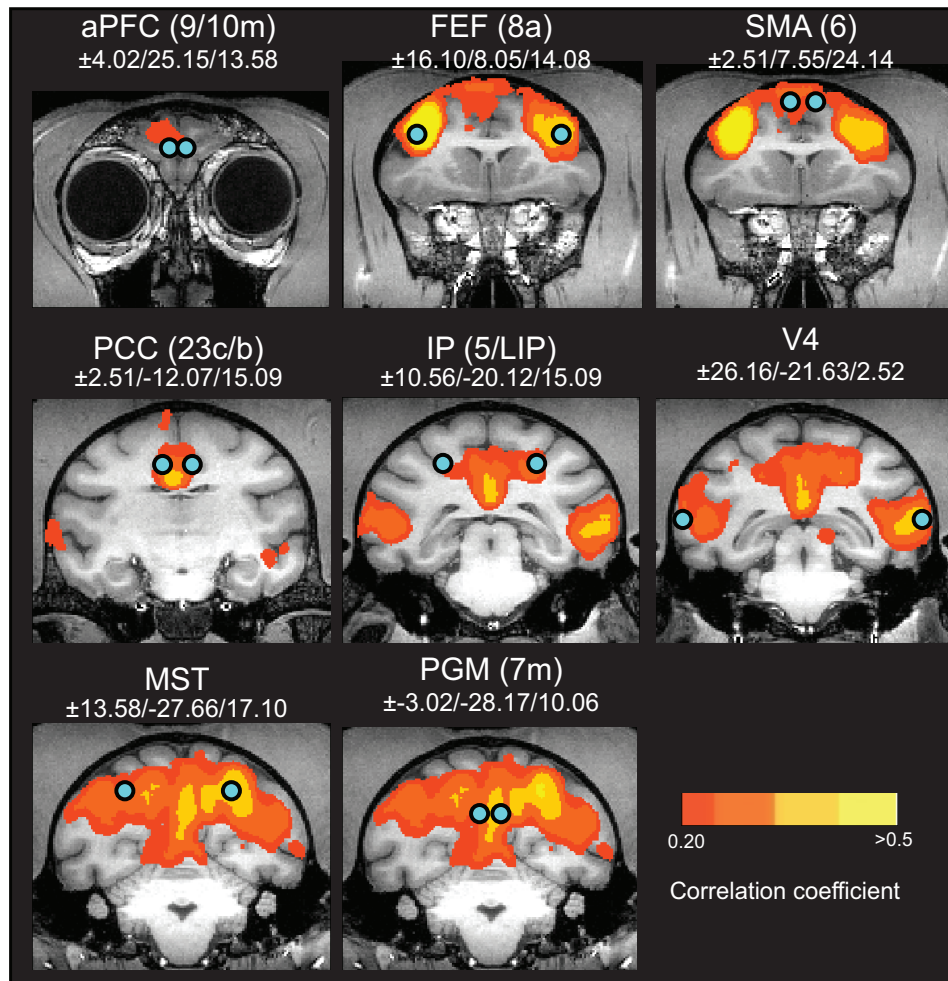


**Figure 4.1. Monkey Seed locations.** Spherical seeds ( $r = 1.5$  mm) are displayed to scale on coronal slices of the F99 atlas (Van Essen, 2004) overlaid with the group-averaged "oculomotor" network. Coordinates in F99 atlas space are indicated above below the brain area label. Abbreviations are indicated in the text. Reprinted with permission from Hutchison, Womelsdorf, Gati, Everling & Menon (2012).

In addition to the left hemisphere FEF seed, a corresponding contralateral FEF seed in the right hemisphere was selected. Seven other seeds of the same size as the left FEF seed (radius = 1.5 mm) were placed in each hemisphere to encompass bilaterally symmetric regions having voxels with the highest correlation from the group-averaged correlation map (Fig. 1.4). These 14 additional seeds included the anterior prefrontal cortex (aPFC) in area 9/10m, the supplementary motor area (SMA) in area 6, the posterior cingulate cortex (PCC) in area 23c/b, the intraparietal area (IP) in area 5/lateral intraparietal area, visual area 4 (V4), middle superior temporal cortex (MST), and the precuneus (PGM) in area 7. To serve as non-grey matter controls, 4 seeds (radius = 1.5 mm) were placed bilaterally (8 total) throughout the white matter (WM).

#### 4.2.1.3 Ventral premotor network identification in monkeys

To assess whether network dynamics are generalizable to other RSNs, the previously identified, bilaterally homologous “ventral premotor” (vPM) RSN, (Hutchison et al., 2011a) was also identified through the same correlational analysis approach used for the OCM RSN with a seed (radius = 1.5 mm) placed in the left primary ventral motor area (area 1/F1). The homologous right hemisphere seed and four additional bilateral sets of seeds (10 total seed regions) were selected from the group correlation map to encompass bilaterally symmetric regions having voxels with the highest correlation and corresponding to previously identified anatomical areas. These included seeds in the somatosensory cortex (areas 2/1), the para-auditory cortex, the lateral secondary somatosensory cortex (S2E), and the ventral-caudal subdivision of the arm, neck, and face/mouth area (area 6/F4) (Paxinos, Huang, & Toga, 1999).

#### 4.2.2 Human participants

Data was obtained from twelve right-handed volunteers (mean age = 26.2 years; 4 females) who were recruited from The University of Western Ontario (London, ON,

Canada). Signed informed consent was obtained in accordance with procedures approved by the University of Western Ontario Health Sciences Research Ethics Board.

#### 4.2.2.1 Data acquisition and preprocessing of human scans

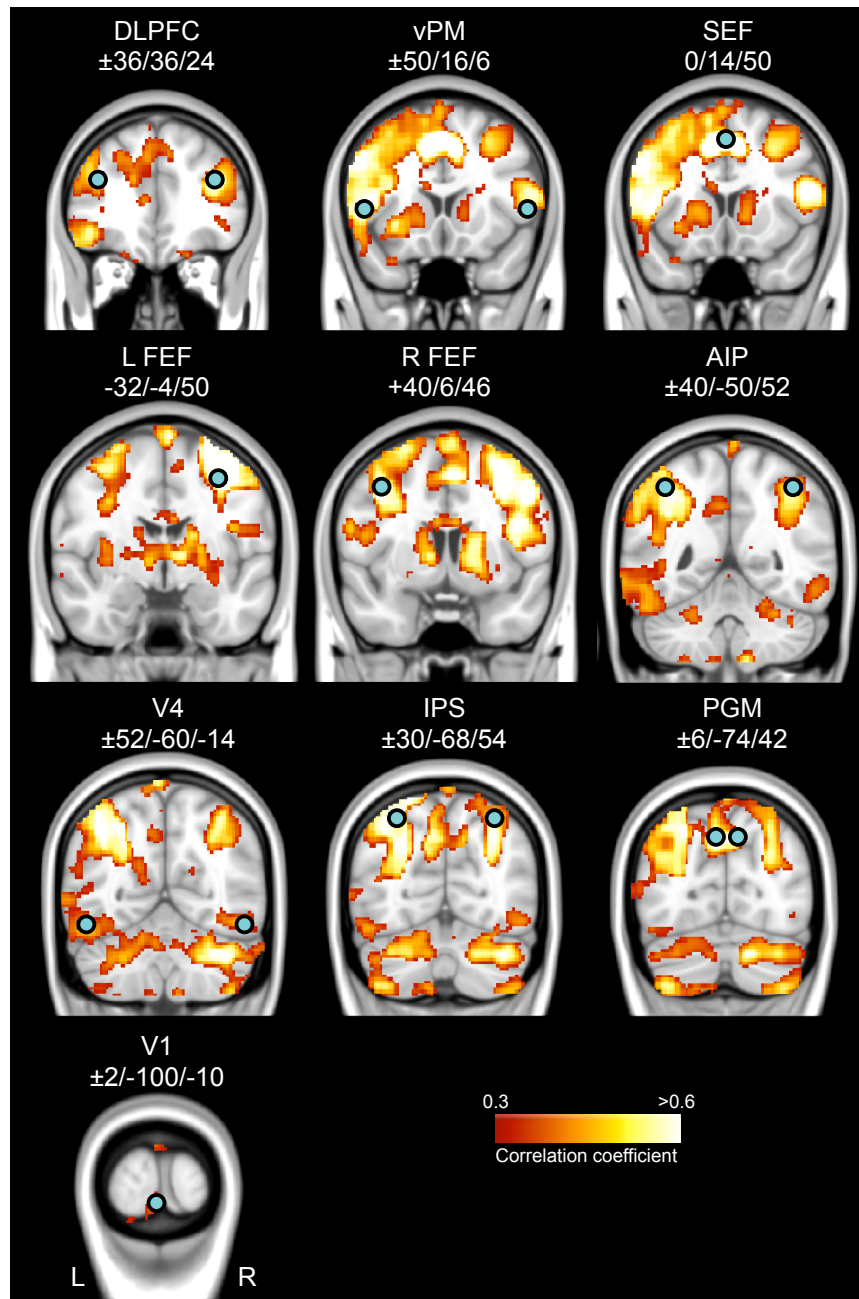
Imaging was performed on a 3 T Siemens TIM MAGNETOM Trio MRI scanner. For each participant, 1 run of 360 continuous functional volumes was collected using a T2\*-weighted single-shot gradient-echo echo-planar imaging (EPI) acquisition sequence with interleaved slice order (repetition time [TR] = 2000 ms; slice thickness = 3.5 mm; in-plane resolution = 3 mm x 3 mm; echo time [TE] = 30 ms; field of view [FOV] = 240 mm x 240 mm; matrix size = 80 x 80; flip angle = 90°) with a 32-channel receive-only head coil. Each volume was comprised of 34 contiguous (no gap) axial-oblique slices acquired at a ~30° caudal tilt with respect to the plane of the anterior and posterior commissure (AC-PC), providing near whole brain coverage. Acquisition time of each scan was 12 min. Subjects were instructed to rest with eyes open while fixating at a central location. A T1-weighted anatomical image was collected using an MPRAGE sequence (TR = 2300 ms; TE = 2.98 ms; FOV = 192 mm × 240 mm × 256 mm; matrix size = 192 × 240 × 256; flip angle = 9°; acquisition voxel size = 1 x 1 x 1 mm).

Image preprocessing was implemented in a similar fashion as carried out with the monkey data using the FSL toolbox. This consisted of slice time correction for interleaved acquisitions (using Fourier-space time-series phase shifting), motion correction (6-parameter affine transformation), brain extraction, spatial smoothing (spatial smoothing using a Gaussian kernel of FWHM 6 mm applied to each volume separately), high-pass temporal filtering (Gaussian-weighted least-squares straight line fitting with sigma = 100 s), low-pass temporal filtering (HWHM = 2.8 s, Gaussian filter), and normalization (12 DOF linear affine transformation) to the standard 152-brain MNI template (voxel size = 2 × 2 × 2 mm).

#### 4.2.2.2 Oculomotor network identification in humans

To allow localization of the frontal eye fields in humans, a saccade task was performed during a separate imaging session with the same subjects (data not shown). Participants looked towards one of two object locations following a vision and planning phase. Using the group-averaged task-based map as a reference, a spherical seed (radius = 5 mm, volume = 524 mm<sup>3</sup>) was placed at the junction of the superior frontal sulcus and the anterior bank of the precentral sulcus of the left hemisphere in MNI atlas space (Paus, 1996; Luna et al., 1998; Brown et al., 2004; Ford et al., 2005; Amiez et al., 2006). A voxel-wise correlation analysis was then conducted in a similar manner used for the monkeys. The mean time-course over all voxels within the FEF seed region was extracted for each subject and then correlated (with zero lag) with every brain voxel at the individual subject-level. After a Fisher z-transform, the results were averaged across subjects and then converted back to correlation values. The group correlation values were projected from volume data to the PALS-B12 cortical surface (Van Essen, 2005) using the CARET (<http://www.nitrc.org/projects/caret>) enclosed-voxel method (Van Essen et al., 2001). Group pair-wise correlations were also calculated in the same manner between all seed pair combinations to derive the group connectivity matrix.

In addition to the left hemisphere FEF seed, a corresponding contralateral FEF seed in the right hemisphere was selected. Eight other seeds of the same size as the left FEF seed (radius = 5 mm) were placed based on the generated group correlation map including seeds in the left and right hemisphere corresponding to the dorsal lateral prefrontal cortex (DLPFC), ventral premotor area (vPM), the intraparietal sulcus (IPS), anterior intraparietal cortex (AIP), visual area 4 (V4), and the precuneus (PGM) and two midline seeds in the supplementary eye fields (SEF) and primary visual area (V1) (see Fig. 4.2). To examine non-grey matter areas, 8 seeds were placed bilaterally throughout the white matter (WM).



**Figure 4.2. Human Seed locations.** Spherical seeds ( $r = 5$  mm) are displayed to scale on coronal slices of the MNI template atlas overlaid with the group-averaged "oculomotor" network. Coordinates in MNI atlas space are indicated above below the brain area label. Abbreviations are indicated in the text. Reprinted with permission from Hutchison, Womelsdorf, Gati, Everling & Menon (2012).

### 4.2.3 Sliding window correlation analysis

To explore the effects of possible time-varying dynamics, the correlational analysis of seed regions were repeated with truncated versions of the time series. The correlation between the time series derived from the left FEF seed (monkeys and humans) and left vPMs seeds (monkeys) and all brain voxels was calculated for truncation window sizes of 240s (120 volumes), 120s (60 volumes), 60s (30 volumes), and 30s (15 volumes). These window sizes were selected as it has been previously demonstrated that the average correlation values within and between RSNs stabilize at approximately 240s (Van Dijk et al., 2009). The remaining window sizes were then selected by decreasing the original window length by a factor of two. A 15s window and smaller was not used because the limited number of data points (volumes) did not result in significant correlations.

The window was advanced in increments of one time point along the entire time series and the correlation recalculated. This was repeated for all possible shifts of the window within the 300 and 360 images of a run for the monkey and human data, respectively. The voxel-wise sliding window correlation between the left FEF seed and all individual brain voxels was calculated at the single subject, single scan level. The pair-wise sliding window correlations between each of the 16 seed regions were also calculated for all animals and all scans.

### 4.2.4 Graph analysis

To graphically represent the OCM RSN at different time points, a Kamada-Kawai algorithm (Kamada & Kawai, 1989) was used. The process arranges the network nodes such that correlated nodes are closer together and weakly correlated nodes are further apart. The distance was calculated based on the absolute values of correlation coefficients. The graphs' edges were then thresholded at  $r \geq |0.4|$ . Degree centrality, the

number of edges of a node that connect it to other nodes, was also calculated (Hagmann et al., 2008).

## 4.3 Results

### 4.3.1 Monkey OCM and vPM network identification

Voxel-wise correlation with the time series from the left FEF seed at the group level revealed strong positive functional connectivity with multiple brain areas (Fig. 4.3) that were in agreement with previous results of task-based (Koyama et al., 2004; Baker et al., 2006; Vincent et al., 2007; Ford et al., 2009) and resting-state (Vincent et al., 2007; Hutchison et al., 2011a, 2011b) OCM network investigations of the macaque brain. There were no negative correlations with  $r$  values  $< -0.2$ . The strongest positive correlations were found in the ipsilateral and contralateral aPFC, FEF, SMA, PCC, IP, V4, MST, and PGM (see Fig. 4.4 for individual connectivity maps). To explore the dynamics of the OCM RSN, sixteen cortical seeds within this network (as described in the Methods) were chosen for further analysis (Fig. 4.1).

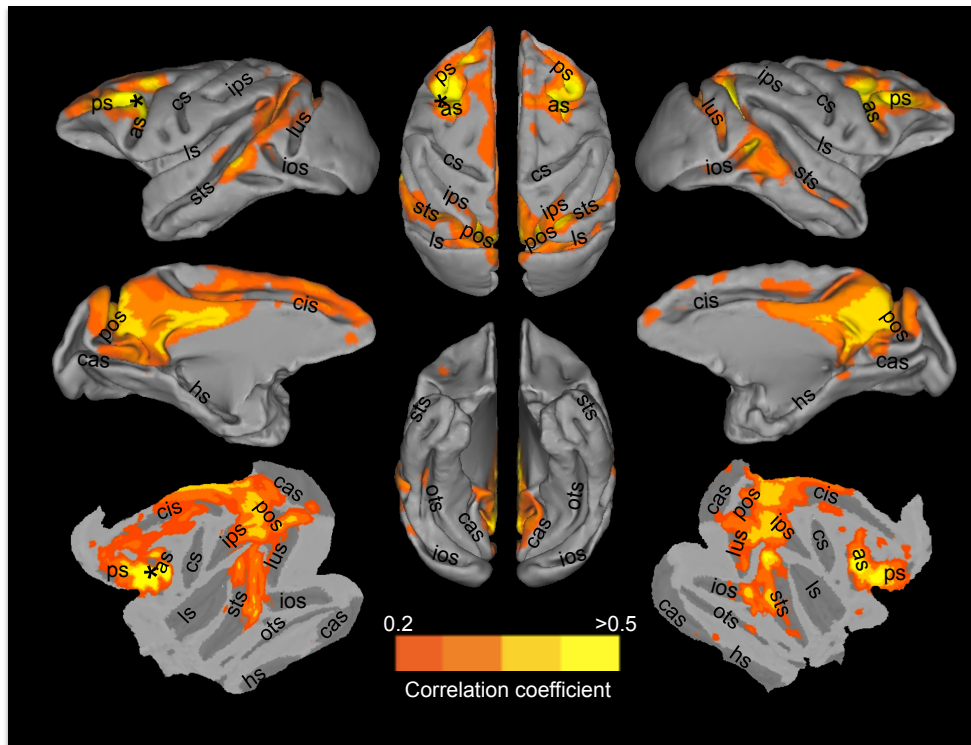


**Figure 4.3. Group-averaged “oculomotor” network following correlation analysis of isoflurane-anesthetized macaques (N = 6) with a seed placed in the anterior bank of the arcuate sulcus corresponding to the left frontal eye fields (FEF; black asterisks).** The lateral, medial, and flattened cortical views of the left (column 1) and right (column 3) hemisphere in addition to the dorsal and ventral views (column 2) are overlaid with thresholded correlation maps normalized to the space of the F99 template (Van Essen, 2004). No negative correlations were present at  $r < -0.2$ . Labels indicate prominent sulci. as, arcuate sulcus; cas, calcarine sulcus; cis, cingulate sulcus; cs, central sulcus; hs, hippocampal sulcus; ios, inferior occipital sulcus; ips, intraparietal sulcus; ls, lateral sulcus, lus, lunate sulcus; ots, occipito-temporal sulcus; sf, sylvian fissure; sts, superior temporal sulcus; pos, parieto-occipital sulcus; ps, principal sulcus. Reprinted with permission from Hutchison, Womelsdorf, Gati, Everling & Menon (2012).

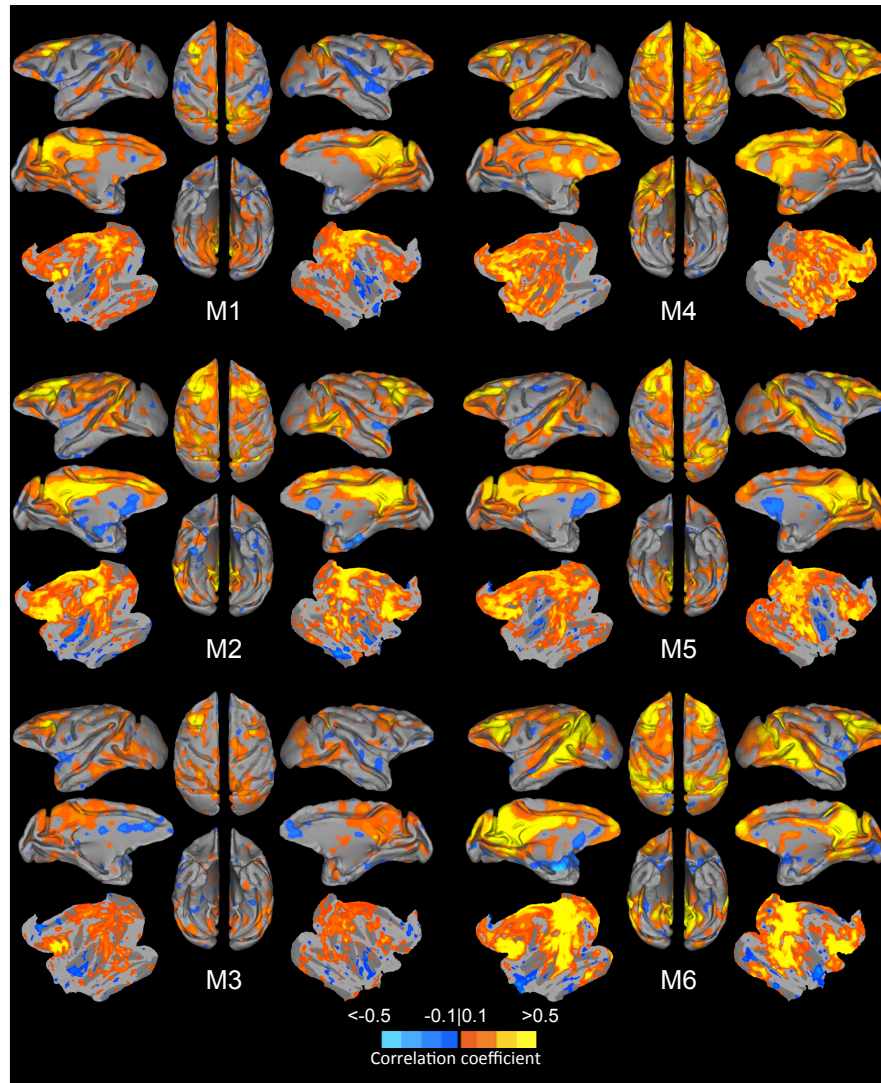


**Figure 4.4. Single-subject (averaged across both scans) “oculomotor” networks of all isoflurane-anesthetized macaques (M1-M6).** The lateral medial, and flattened cortical views of the left (column 1) and right (column 3) hemisphere in addition to the dorsal and ventral views (column 2) are overlaid with thresholded correlation maps normalized to the space of the F99 template (Van Essen, 2004). Reprinted with permission from Hutchison, Womelsdorf, Gati, Everling & Menon (2012).

Voxel-wise correlation with the time series from the left ventral motor area (area 1/F1) seed at the group level revealed strong positive functional connectivity with homologous structures in both hemispheres (Fig. 4.5) that closely matched the vPM RSN revealed by independent component analysis of the same data set (Hutchison et al., 2011a). The strongest positive correlations were found across somatosensory cortex (areas 2/1), the para-auditory cortex, the lateral secondary somatosensory cortex (S2E), and the ventral-caudal subdivision of the arm, neck, and face/mouth area (area 6/F4) (Paxinos, Huang, & Toga, 1999). Similar to the OCM network, there were no negative correlations present with  $r$  values  $< -0.2$ .

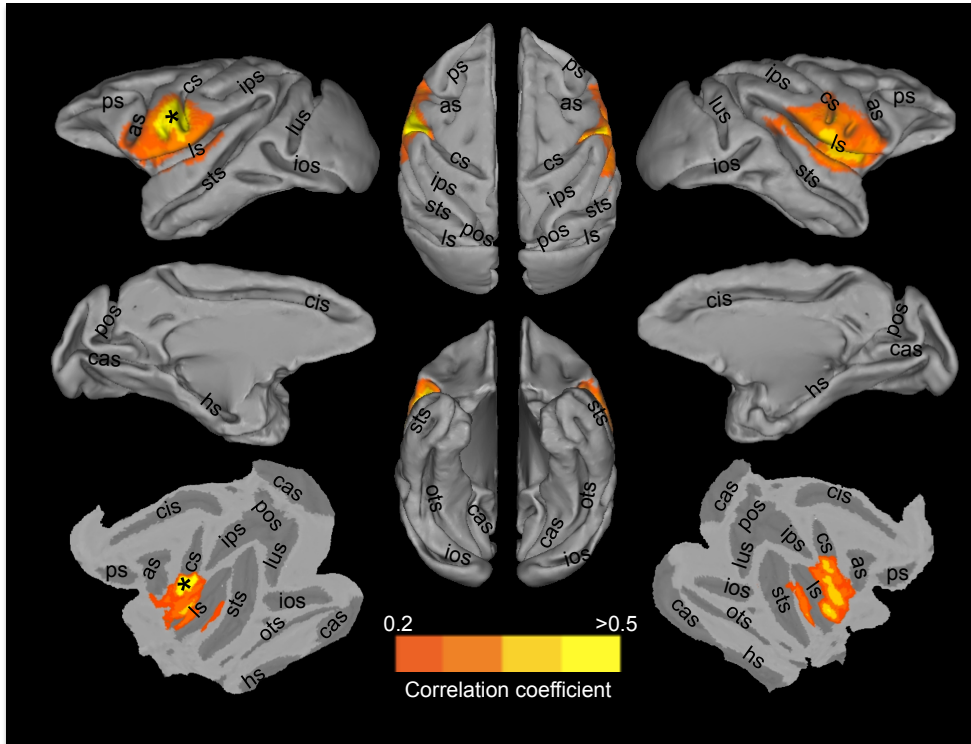


**Figure 4.5. Group-averaged ventral premotor network following correlation analysis of isoflurane-anesthetized macaques (N = 6) with a seed placed in the ventral motor area (area 1/F1; black asterisks).** The lateral medial, and flattened cortical views of the left (column 1) and right (column 3) hemisphere in addition to the dorsal and ventral views (column 2) are overlaid with thresholded correlation maps normalized to the space of the F99 template (Van Essen, 2004). No negative correlations were present at  $r < -0.2$ . Labels indicate prominent sulci. as, arcuate sulcus; cas, calcarine sulcus; cis, cingulate sulcus; cs, central sulcus; hs, hippocampal sulcus; ios, inferior occipital sulcus; ips, intraparietal sulcus; ls, lateral sulcus; lus, lunate sulcus; ots, occipito-temporal sulcus; sf, sylvian fissure; sts, superior temporal sulcus; pos, parieto-occipital sulcus; ps, principal sulcus. Reprinted with permission from Hutchison, Womelsdorf, Gati, Everling & Menon (2012).

Group pair-wise cross correlation of all seeds revealed strong intra-network connectivity of both the OCM and vPM networks (Fig. 4.6). The networks were independent of one another and seeds of both networks were not correlated with WM control seeds. All seed time courses were found to be stationary and not possess a unit root (Dickey-Fuller test,  $p > 0.05$ ) suggesting a stable mean and variance over time.

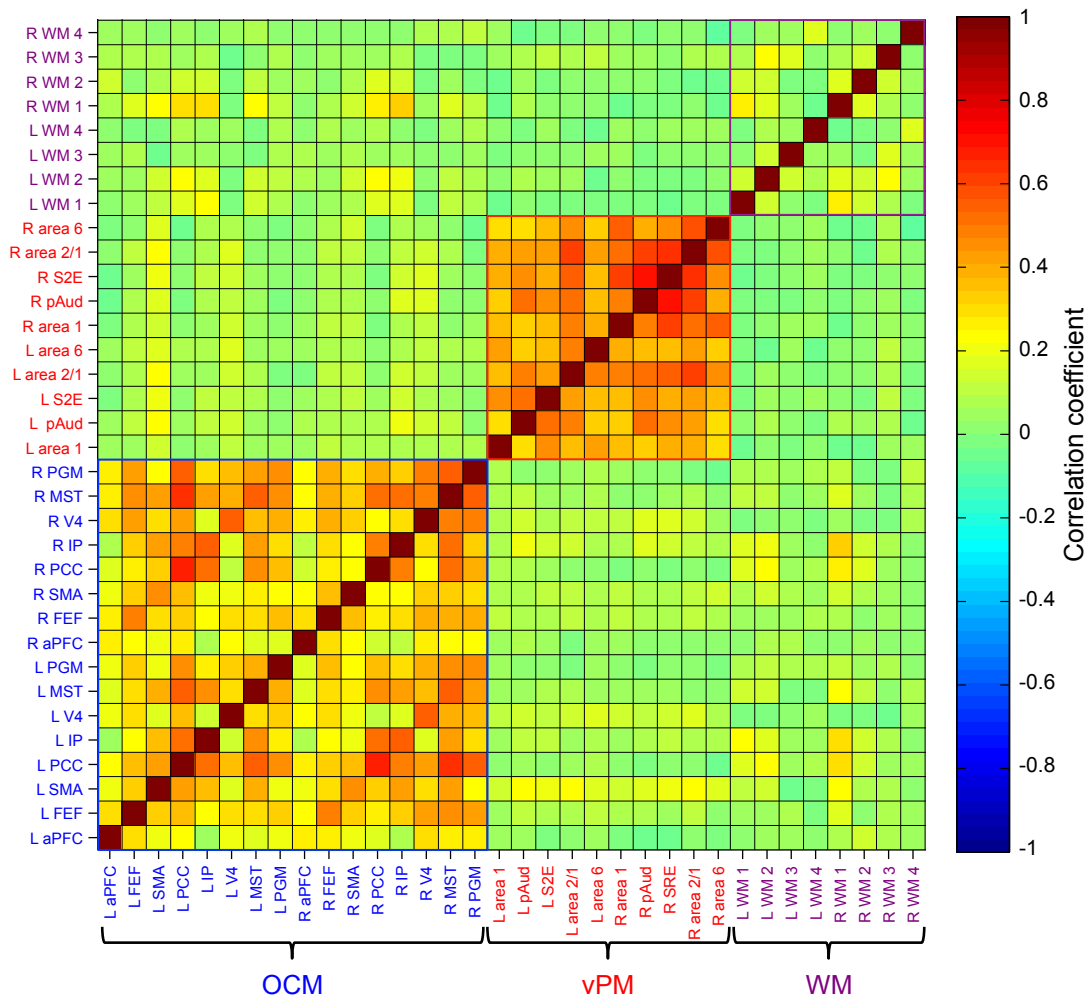


**Figure 4.6.** Average pair-wise correlation matrix of resting-state BOLD time-courses from 16 “oculomotor” (OCM) network, 10 ventral premotor (vPM) network, and 8 white matter (WM) seeds for isoflurane-anesthetized macaques (N = 6). Abbreviations are indicated in the text. Reprinted with permission from Hutchison, Womelsdorf, Gati, Everling & Menon (2012).

### 4.3.2 Human OCM network identification

To validate the methodology, test inter-species similarities, and rule out anesthesia as the cause of the observed results, we investigated the OCM RSN in the awake human brain. Voxel-wise correlation with the time series from the left FEF seed at the group level revealed strong positive functional connectivity with multiple distributed brain areas (Fig. 4.7). The RSN encompassed multiple areas that have been shown to be modulated during oculomotor tasks (Luna et al., 1998; DeSouza et al., 2003; Brown et al., 2004, 2007) and closely resembled the previously identified oculomotor/dorsal attention network in resting-state investigations (Beckmann et al., 2005; Damoiseaux et al., 2006). The strongest positive correlations were found in the ipsilateral and contralateral DLPFC, vPM, FEF, SEF, IPS, AIP, PGM, V4, and V1. There were no negative correlations with  $r$  values  $< -0.3$  (see Fig. 4.8 for individual human connectivity maps). Similar to the analysis of the monkey scans, 16 seeds were selected from the group map (Fig. 4.2; see Material and Methods section for details). Group pair-wise cross correlation of all seeds revealed strong intra-network connectivity of the OCM (Fig. 4.9) with none to weak connectivity with WM control seeds.

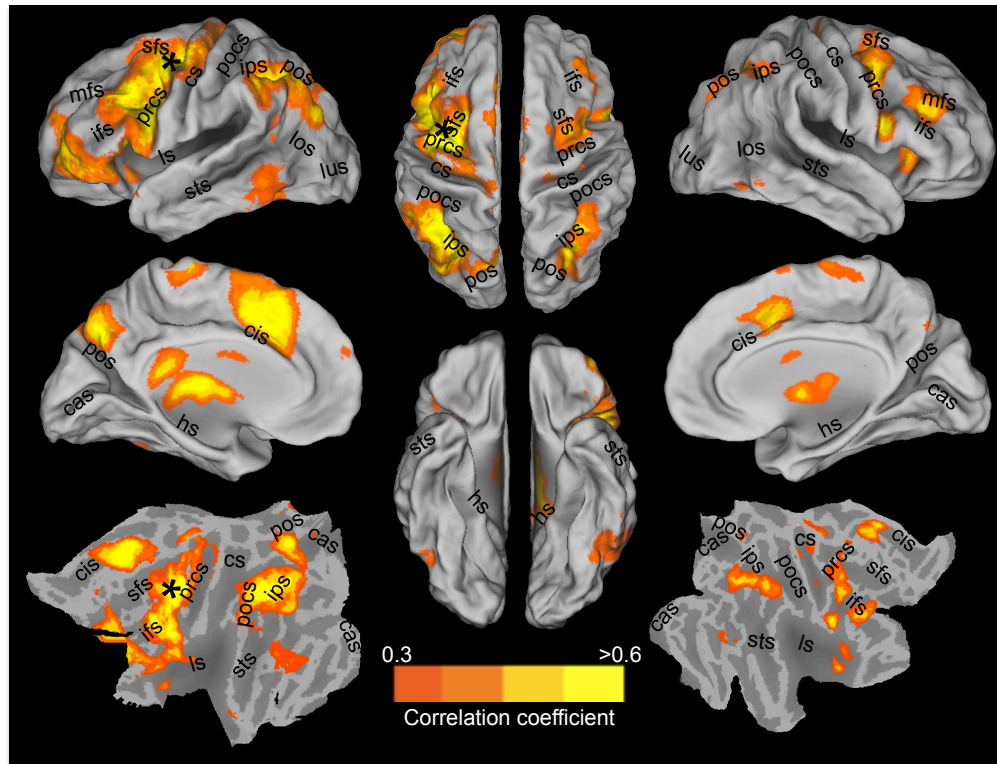


**Figure 4.7. Group-averaged “oculomotor” network following correlation analysis of awake human subjects (N = 12) with a seed placed in the left frontal eye fields (black asterisks).** The lateral, medial, and flattened cortical views of the left (column 1) and right (column 3) hemisphere in addition to the dorsal and ventral views (column 2) are overlaid with thresholded correlation maps normalized to the space of the PALS-B12 template (Van Essen, 2005). No negative correlations were present at  $r < -0.3$ . Labels indicate prominent sulci. Note that the correlation threshold differs between human and monkey maps shown in Fig 4.3. cas, calcarine sulcus; cis, cingulate sulcus; cs, central sulcus; ifs, inferior frontal sulcus; ls, lateral sulcus; lus, lunate sulcus; mfs, middle frontal sulcus; pos, parieto-occipital sulcus; pocs, posterior central sulcus; prcs, precentral sulcus; sfs, superior frontal sulcus; sts, superior temporal sulcus. Reprinted with permission from Hutchison, Womelsdorf, Gati, Everling & Menon (2012).

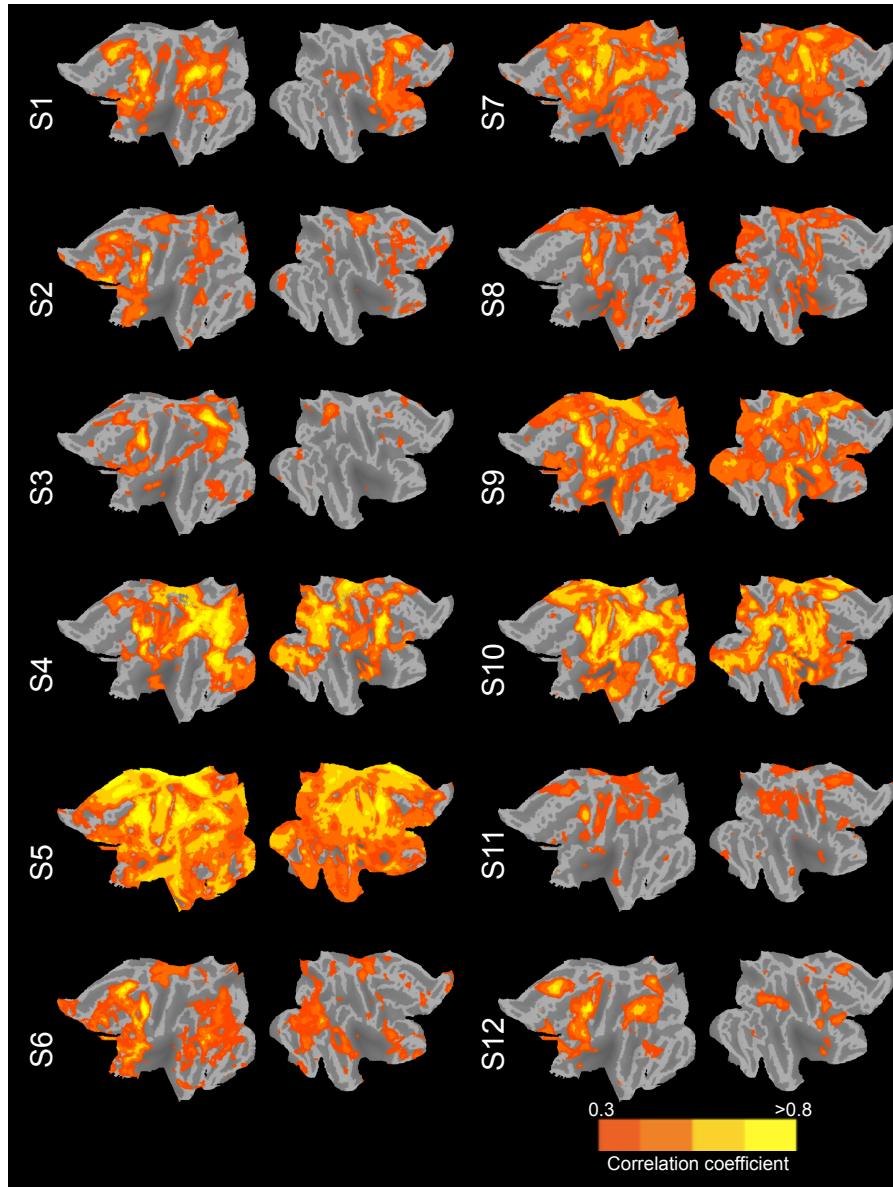


**Figure 4.8. Single-subject “oculomotor” networks of all awake human subjects (S-S12).** The flattened cortical views of the both hemispheres are overlaid with thresholded correlation maps normalized to the space of the PALS-B12 template (Van Essen, 2005). Reprinted with permission from Hutchison, Womelsdorf, Gati, Everling & Menon (2012).

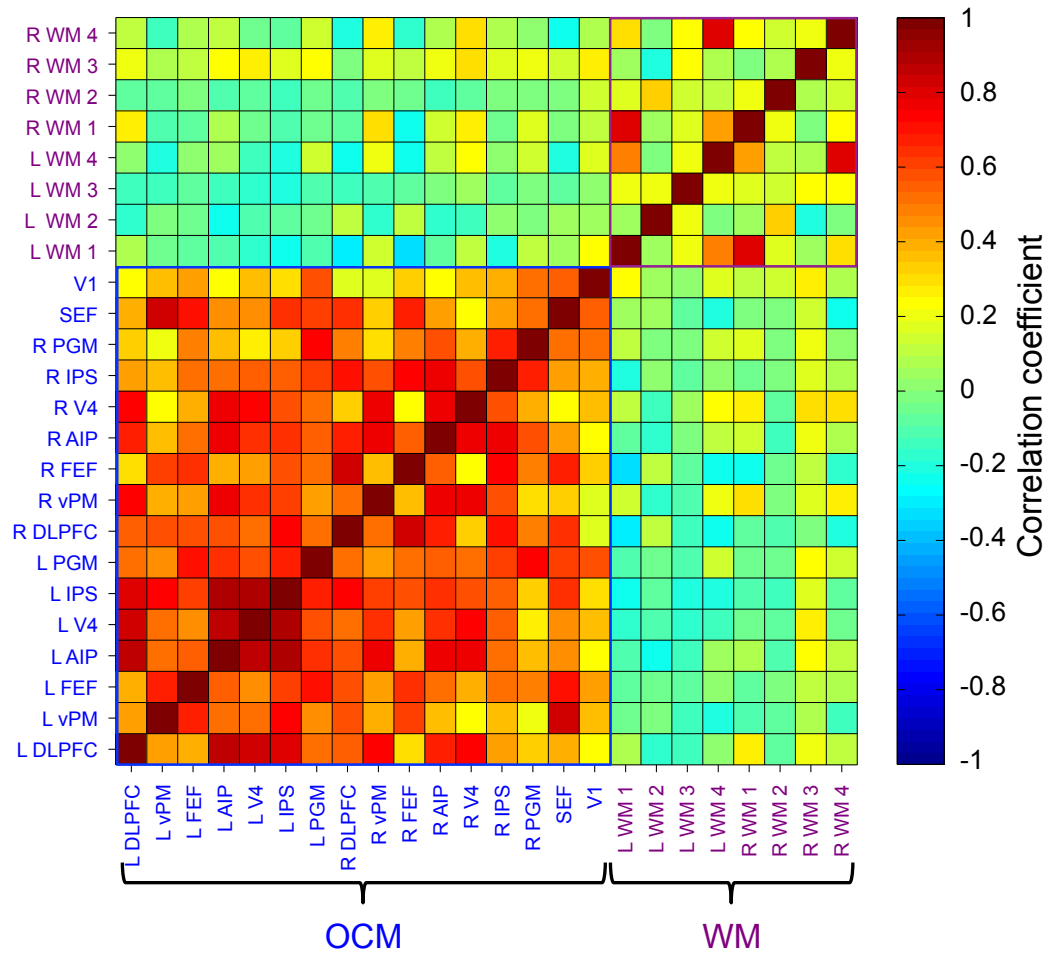


**Figure 4.9. Average pair-wise correlation matrix of resting-state BOLD time-courses from 16 “oculomotor” (OCM) network and 8 white matter (WM) seeds for awake human subjects (N = 12).** Abbreviations are indicated in the text. Reprinted with permission from Hutchison, Womelsdorf, Gati, Everling & Menon (2012).

### 4.3.3 Transient network states

To assess the stability of the OCM RSN's spatial architecture, five time-points were selected across the duration of the scan and analyzed. For a window size of 60s (Fig. 4.10; for window sizes of 30s, 120s, and 240s, see Figs. 4.11, 4.12, and 4.13, respectively), comparison of the cross-correlation matrices (column 1), voxel-wise FEF correlation maps (column 2 and 3), and graph representations (column 4, thresholded at  $r \geq 0.4$ ) demonstrated large, apparent differences in connectivity profiles within a single scan (M2, scan 2) not captured in the single-subject average (bottom row). The pairwise correlation matrix revealed periods of strong synchronization (50-110s) and at other times, an almost complete breakdown of the network (268-328s). Changing network architecture can also be observed in the graph representation (column 4) of the OCM RSN. Node arrangement, network inclusion, and degree centrality all vary at the different time points. Beyond the seeds defined by the group averaged FEF correlation map, the voxel-wise plots showed strongly (both negatively and positively) correlated cortical areas with the left FEF that were not captured when using the average time-course (Fig. 5). During the first selected time window, the entire anterior cingulate cortex and PFC are synchronized with the left FEF. Primary visual areas are also transiently correlated at multiple time points. Negatively correlated regions that approach  $r = -1$  occur throughout the scan between nodes of the OCM network and also distributed throughout the cortex. The unique spatial profiles do not emerge in the average or at longer time windows. Spontaneous changes in network connectivity are particularly evident when visualizing all successive sliding window increments. We visualize these dynamics in Supplementary Movies 1 and 2, which show pairwise seed correlations and voxel-wise left FEF seed correlations, respectively, for all window sizes across time. Changes in network states, including strong synchronization (26-86s), network breakdown (102-162s), and transient anti-correlated regions (280-340s) can also be seen in awake human subjects (Fig. 4.14; Subject 7).

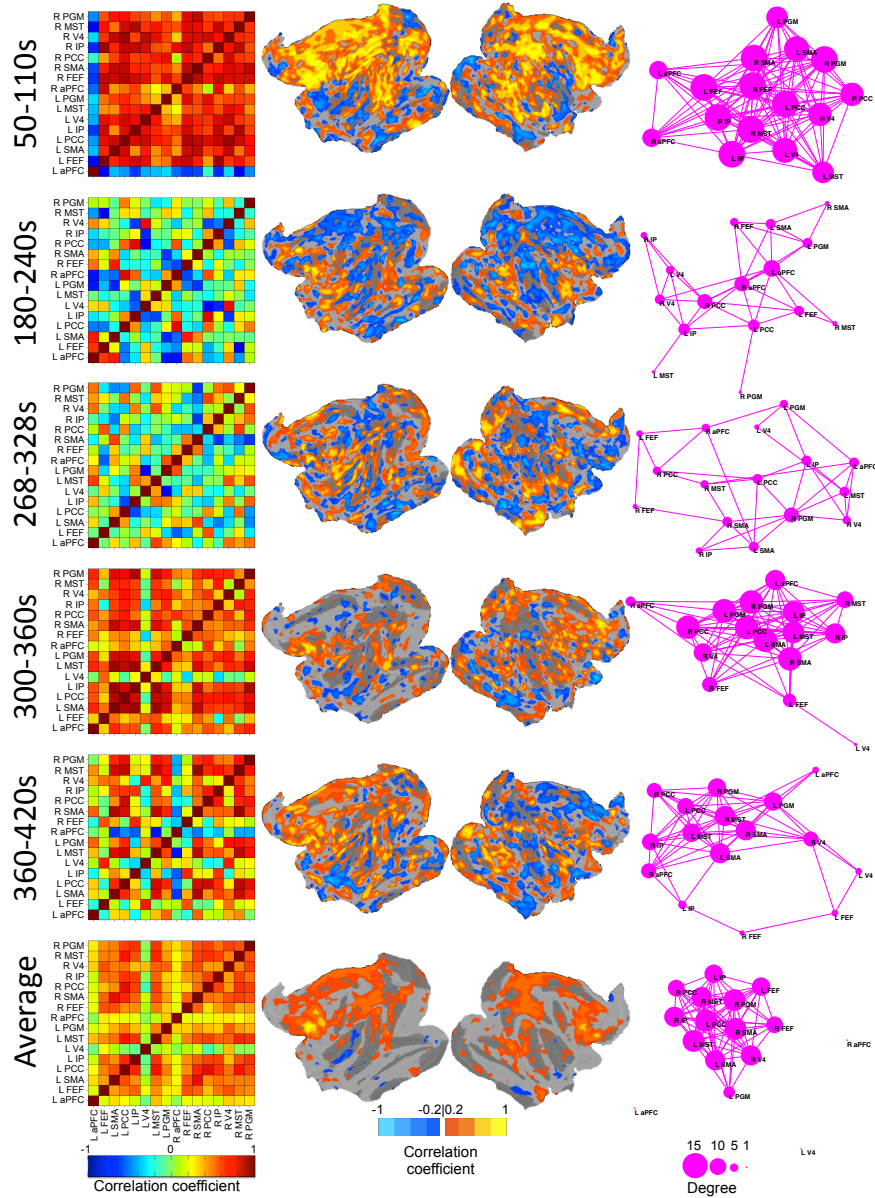


**Figure 4.10. Network changes across time with a sliding-window correlation size of 60s for a representative isoflurane-anesthetized monkey (M2, scan 2).** The top five rows represent a single windowed correlation between the times. The bottom row displays the average for the entire run. Column 1 shows the pairwise correlation matrix of “oculomotor” network seeds in the same fashion as the blue bounded box in Fig. 4.6. Column 2 and 3 display the flattened cortical views of the left and right hemisphere, respectively, overlaid with voxel-wise correlation maps for the left FEF seed normalized to the space of the F99 template (Van Essen, 2004). Column 4 displays the graph representation of the functional “oculomotor” network connectivity in which each seed represents a node and pair-wise correlation  $r < 0.4$  represented by an edge. The size of the node represents its degree centrality. For window sizes of 30, 120, and 240, see Supplementary Figs. 4.11, 4.12, and 4.13 respectively. For all time points of pair-wise correlations, see Supplementary Movie 1. For all time points of voxel-wise left FEF correlation see Supplementary Movie 2. Reprinted with permission from Hutchison, Womelsdorf, Gati, Everling & Menon (2012).

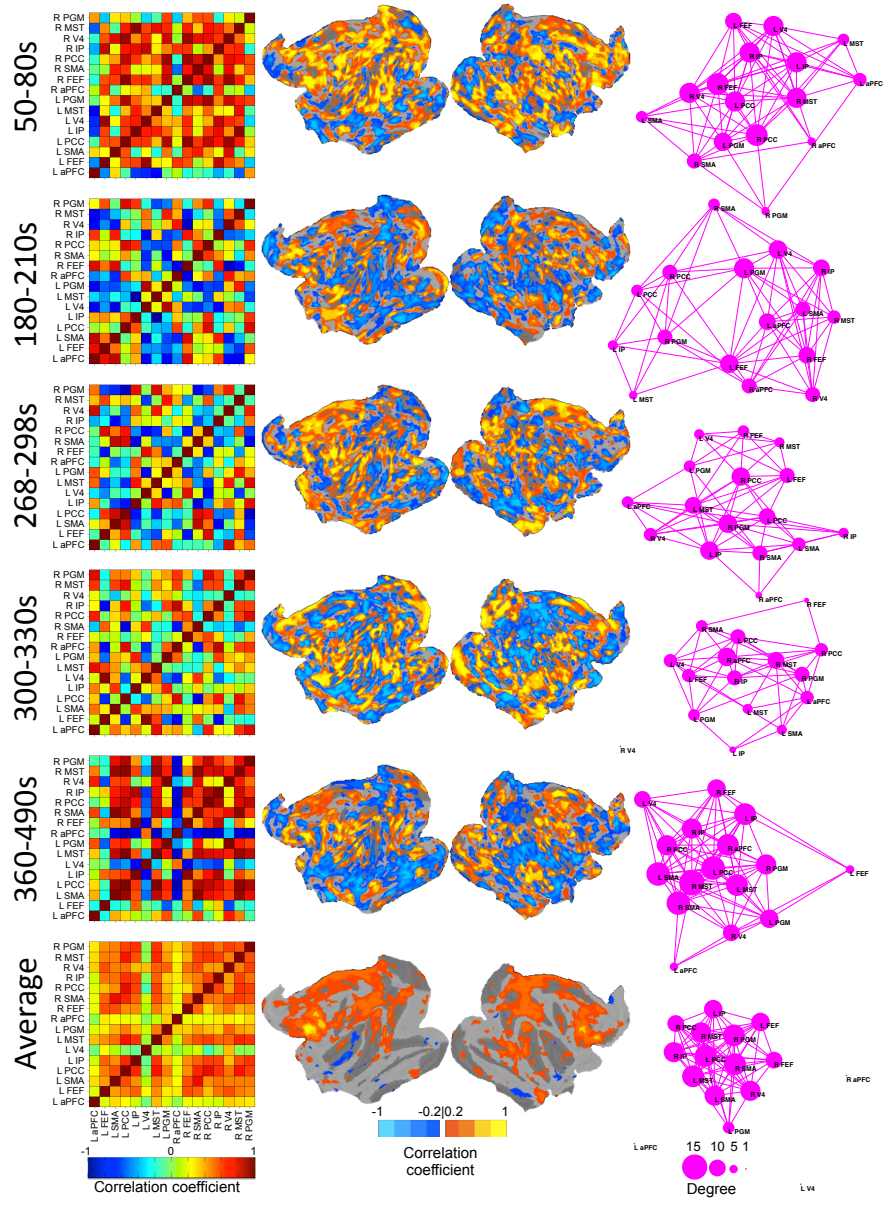


**Figure 4.11. Network changes across time with a sliding-window correlation size of 30s for a representative isoflurane-anesthetized monkey (M2, scan 2).** The top five rows represent a single windowed correlation between the times. The bottom row displays the average for the entire run. Column 1 shows the pairwise correlation matrix of “oculomotor” network seeds in the same fashion as the blue bounded box in Fig. 4.6. Column 2 and 3 display the flattened cortical views of the left and right hemisphere, respectively, overlaid with voxel-wise correlation maps for the left FEF seed normalized to the space of the F99 template (Van Essen, 2004). Column 4 displays the graph representation of the functional “oculomotor” network connectivity in which each seed represents a node and pair-wise correlation  $r < 0.4$  represented by an edge. The size of the node represents its degree centrality. Reprinted with permission from Hutchison, Womelsdorf, Gati, Everling & Menon (2012).

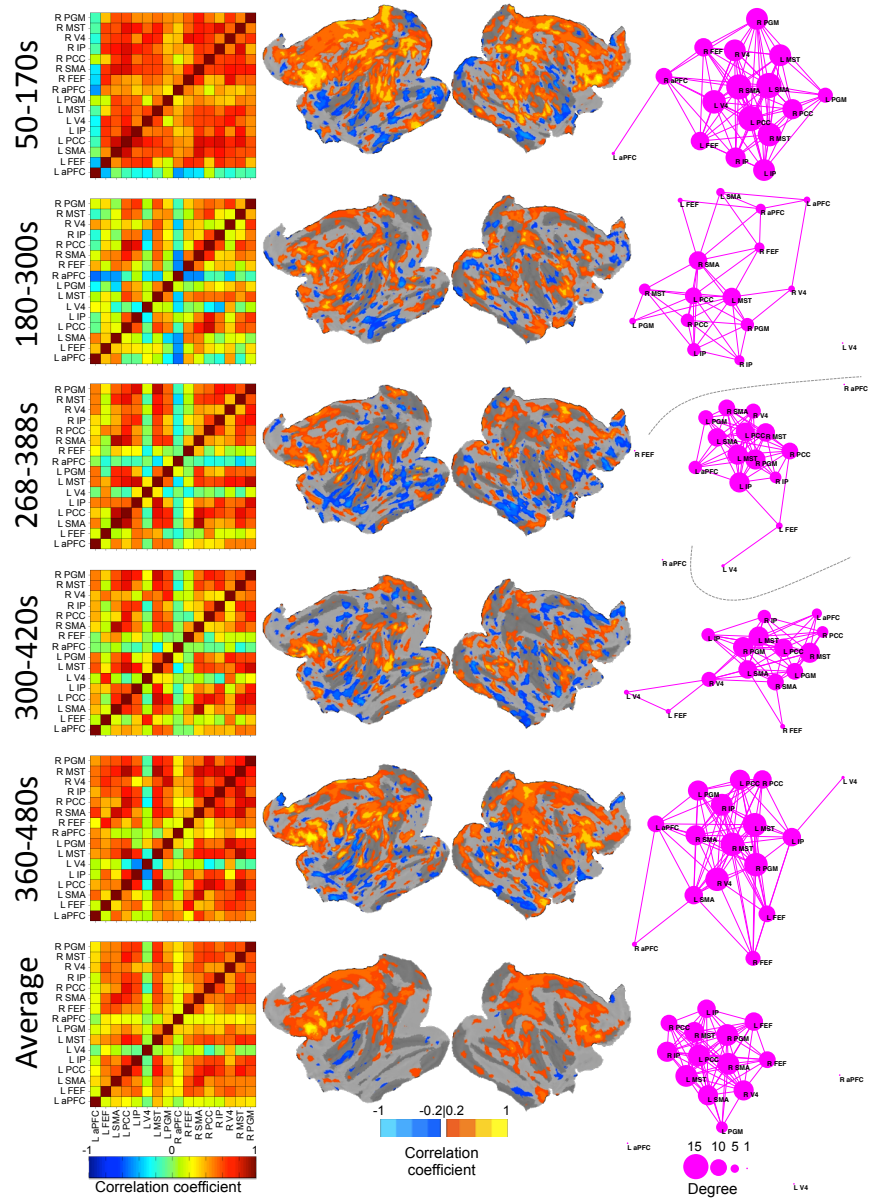


**Figure 4.12. Network changes across time with a sliding-window correlation size of 120s for a representative isoflurane-anesthetized monkey (M2, scan 2).** The top five rows represent a single windowed correlation between the times. The bottom row displays the average for the entire run. Column 1 shows the pairwise correlation matrix of “oculomotor” network seeds in the same fashion as the blue bounded box in Fig. 4.6. Column 2 and 3 display the flattened cortical views of the left and right hemisphere, respectively, overlaid with voxel-wise correlation maps for the left FEF seed normalized to the space of the F99 template (Van Essen, 2004). Column 4 displays the graph representation of the functional “oculomotor” network connectivity in which each seed represents a node and pair-wise correlation  $r < 0.4$  represented by an edge. The size of the node represents its degree centrality. Reprinted with permission from Hutchison, Womelsdorf, Gati, Everling & Menon (2012).

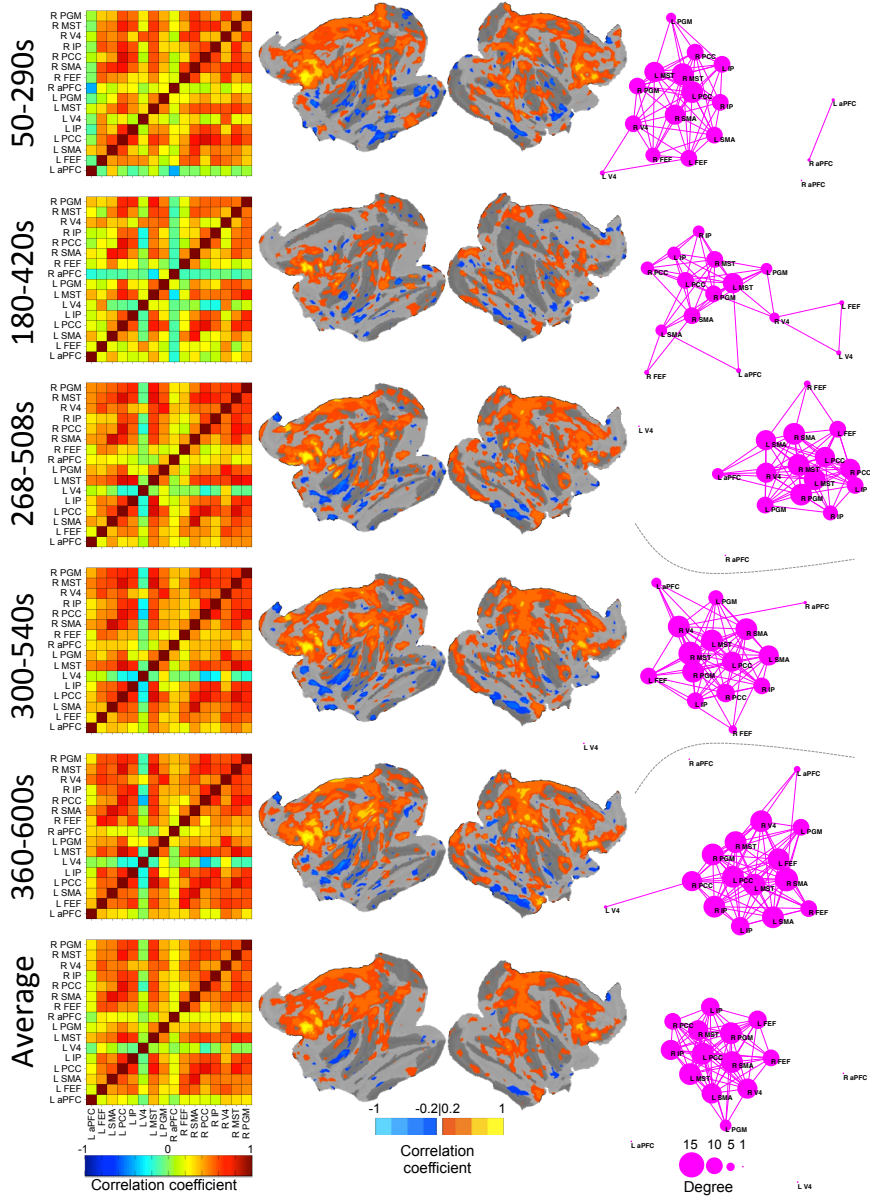


**Figure 4.13. Network changes across time with a sliding-window correlation size of 240s for a representative isoflurane-anesthetized monkey (M2, scan 2).** The top five rows represent a single windowed correlation between the times. The bottom row displays the average for the entire run. Column 1 shows the pairwise correlation matrix of “oculomotor” network seeds in the same fashion as the blue bounded box in Fig. 4.6. Column 2 and 3 display the flattened cortical views of the left and right hemisphere, respectively, overlaid with voxel-wise correlation maps for the left FEF seed normalized to the space of the F99 template (Van Essen, 2004). Column 4 displays the graph representation of the functional “oculomotor” network connectivity in which each seed represents a node and pair-wise correlation  $r < 0.4$  represented by an edge. The size of the node represents its degree centrality. Reprinted with permission from Hutchison, Womelsdorf, Gati, Everling & Menon (2012).

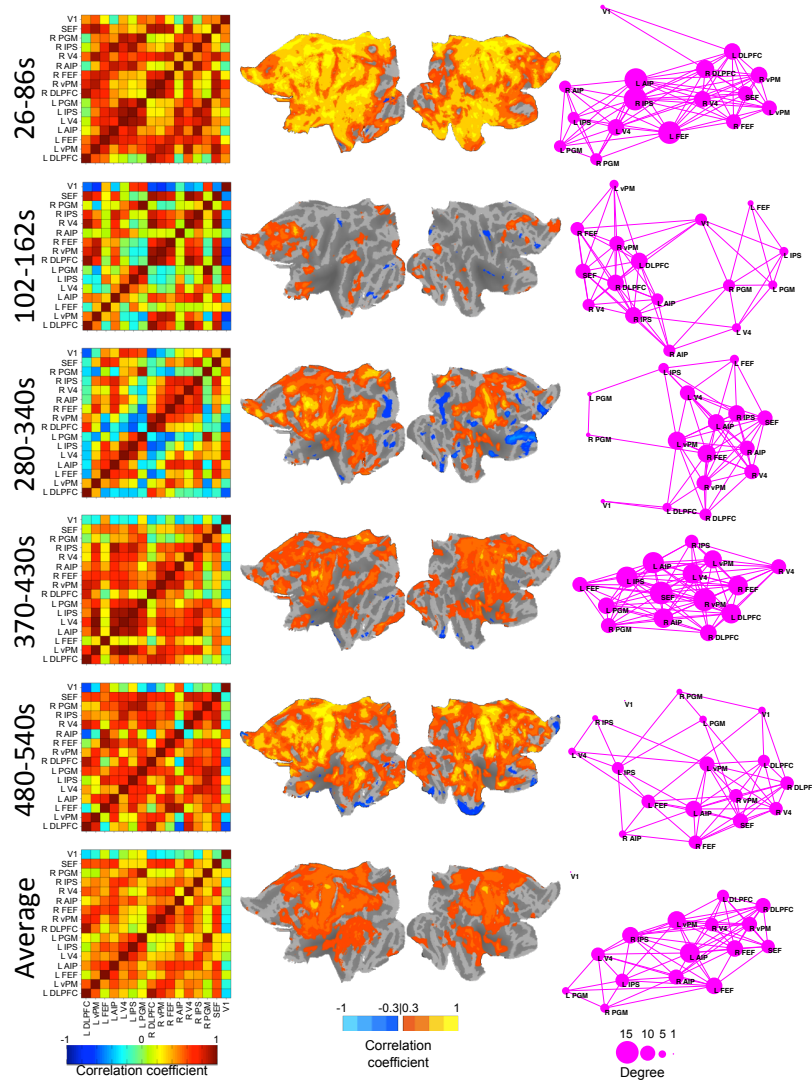


**Figure 4.14. Network changes across time with a sliding-window correlation size of 60s for a representative awake human subject (S7).** The top five rows represent a single windowed correlation between the times. The bottom row displays the average for the entire run. Column 1 shows the pairwise correlation matrix of “oculomotor” network seeds in the same fashion as the blue bounded box in Fig. 4.9. Column 2 and 3 display the flattened cortical views of the left and right hemisphere, respectively, overlaid with voxel-wise correlation maps for the left FEF seed normalized to the space of the PALS-B12 template (Van Essen, 2005). Column 4 displays the graph representation of the functional “oculomotor” network connectivity in which each seed represents a node and pair-wise correlation  $r < 0.4$  represented by an edge. The size of the node represents its degree centrality. Reprinted with permission from Hutchison, Womelsdorf, Gati, Everling & Menon (2012).

#### 4.3.4 Fluctuating connectivity dynamics during awake and anaesthetized states

The supplementary movies demonstrate ongoing changes in the spatial connectivity profiles over time. To further assess and quantify these changes we examined the temporal correlation strength between seeds over time. We calculated the time series of the left FEF seed and of the left IP (A), left MST (B), right FEF (C), left PCC (D), as illustrated for a representative monkey in Fig. 4.15 (M2, scan 2). Below the time series plots, the sliding window correlation values for all window lengths are shown. Considerable time resolved variations of functional correlations are apparent when compared to the whole scan average correlation value shown as a dashed line. All OCM RSN nodes show slow fluctuations of connectivity strength that dissipate at longer window sizes. To quantify the change in the frequency profiles of the correlation waveforms across the different time windows we calculated fast-Fourier transforms (FFTs) (Fig. 4.15, third row of each frame). Bar graphs (bottom right of each frame) represent the percentage of data points that showed positive correlations (+, red), and anti-correlations (-, blue). Consistent with Glover and Chang (2010) anti-correlations decreased as a function of increasing window size and failed to be apparent at larger window sizes. But at smaller window sizes, negative correlations accounted for > 30% of the observed data points. The larger variance of the pair-wise correlations at short time windows could be influenced by noise or random variability that may increase with fewer points in the short truncation windows. To test for this possibility, we quantified the variability and plot the confidence values for the correlation coefficients for the four areas presented in Fig. 4.15 and the left FEF (Fig. 4.16). The highest variances are found for near-zero correlation values, regardless of window size. The confidence values for the large positive and negative excursions stay similar across different window sizes.

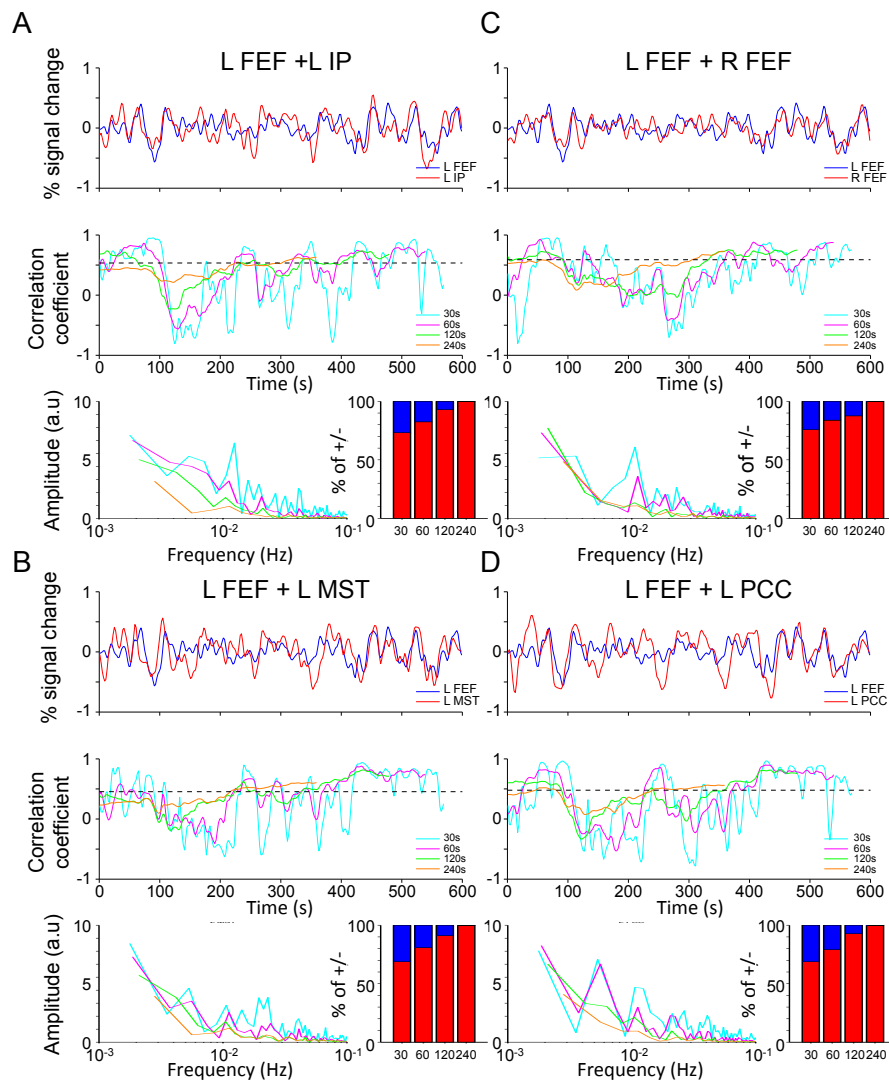


**Figure 4.15. Time-series and sliding-window correlation coefficients between the left frontal eye fields (FEF) and “oculomotor” network seeds (A) left intraparietal cortex (IP), (B) left middle superior temporal cortex (MST), (C) right FEF, and (D) left posterior cingulate cortex (PCC) shown for one representative isoflurane-anesthetized monkey (M2, scan 2).** The top panel shows the BOLD time series of the left FEF seed (blue) and the comparative seed (red). The middle panel shows the sliding-window coefficients for 30s (cyan), 60s (pink), 120s (green), and 240s (orange) windows. For each of the correlation time courses the bottom panel shows the Fast-Fourier transform (right side) and the percentage of time of above and below 0. Reprinted with permission from Hutchison, Womelsdorf, Gati, Everling & Menon (2012).

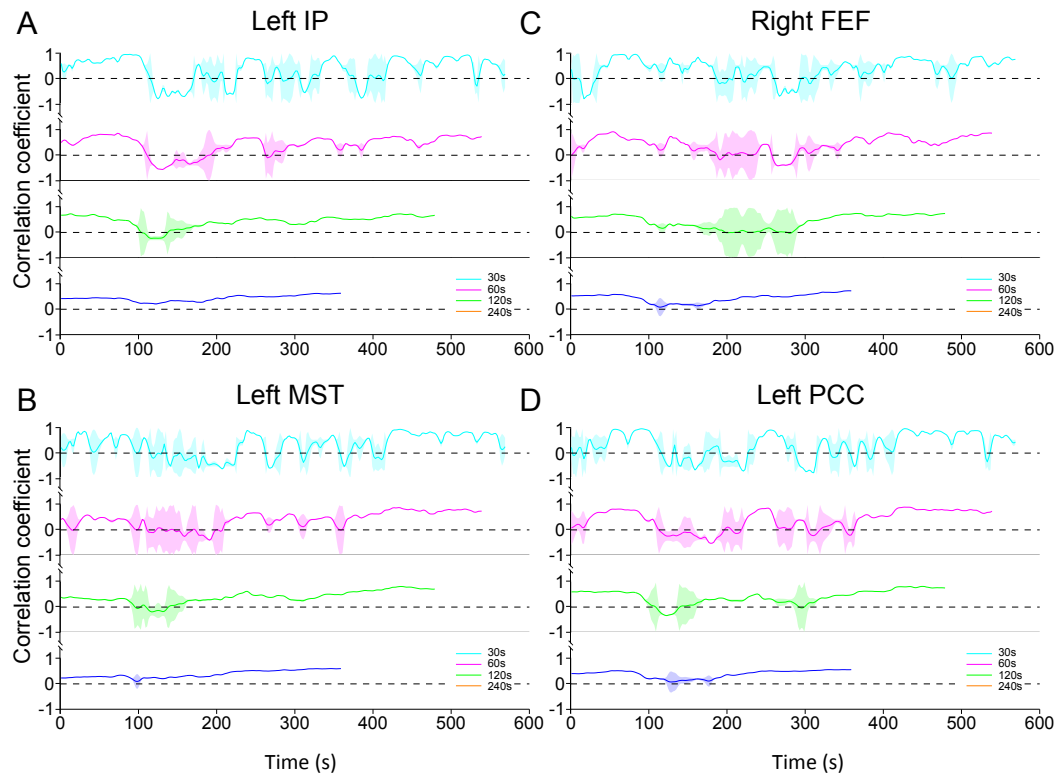


**Figure 4.16. Confidence intervals for sliding-window correlation coefficients shown in Fig. 4.15 between the left frontal eye fields (FEF) and “oculomotor” network seeds (A) left intraparietal cortex (IP), (B) left middle superior temporal cortex (MST), (C) right FEF, and (D) left posterior cingulate cortex (PCC) shown for one representative isoflurane-anesthetized monkey (M2, scan 2).** Sliding-window coefficients are shown for 30s (cyan), 60s (pink), 120s (green), and 240s (orange) windows and shaded bars represent the lower and upper bounds for a 95% confidence interval for each coefficient. Reprinted with permission from Hutchison, Womelsdorf, Gati, Everling & Menon (2012).

Similar temporal dynamics were observed for the human data across all nodes (Fig. 4.17; Subject 7). The results illustrate that like the anesthetized monkey, the correlation time courses are nonstationary and for time dependent analysis with windows of less than 60s periods, positive functional correlations alternated with prominent anti-correlations that were entirely missed when assessed with longer time windows.

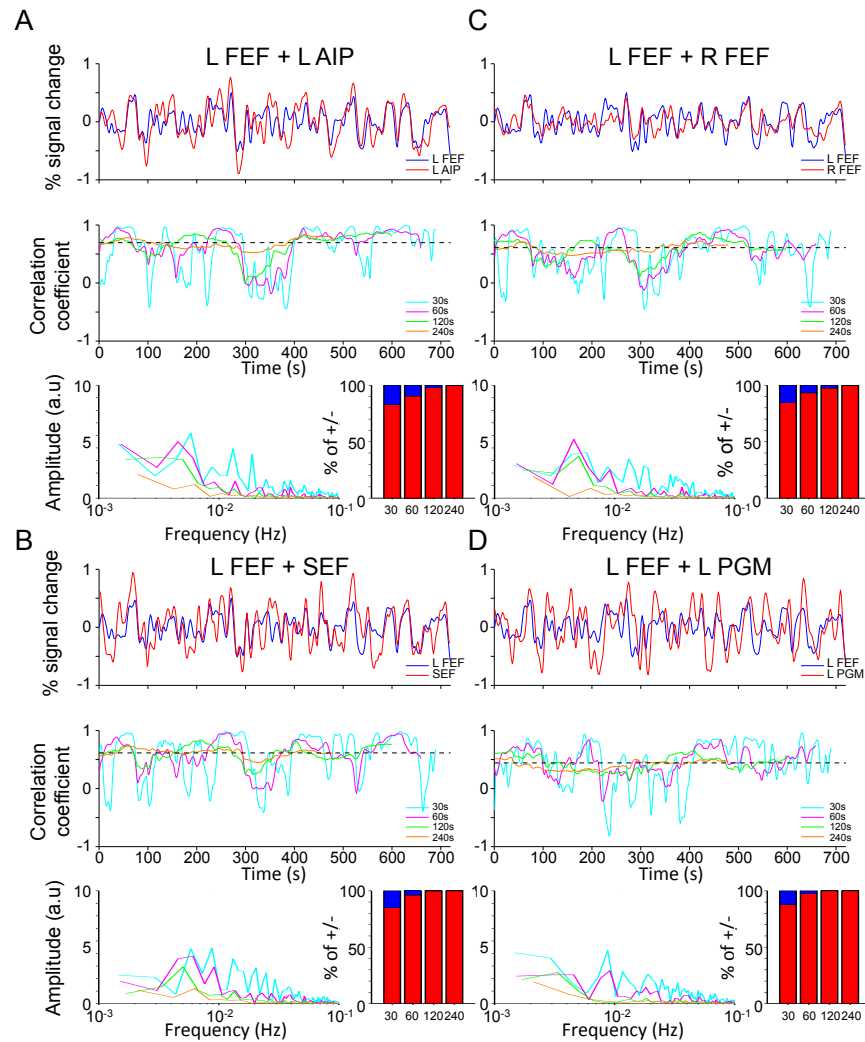


**Figure 4.17. Time-series and sliding-window correlation coefficients between the left frontal eye fields (FEF) and “oculomotor” network seeds (A) left intraparietal cortex (IP), (B) left middle superior temporal cortex (MST), (C) right FEF, and (D) left posterior cingulate cortex (PCC) shown for one representative awake human subject (S7).** The top panel shows the BOLD time series of the left FEF seed (blue) and the comparative seed (red). The middle panel shows the sliding-window coefficients for 30s (cyan), 60s (pink), 120s (green), and 240s (orange) windows. For each of the correlation time courses the bottom panel shows the Fast-Fourier transform (right side) and the percentage of time of above and below 0. Reprinted with permission from Hutchison, Womelsdorf, Gati, Everling & Menon (2012).

### 4.3.5 Hyper-synchronization

To further illustrate the fluctuating values of the correlations, Fig. 4.18 displays for the four sliding window lengths the pair-wise correlations of the OCM network seeds across all possible shifts of the truncation windows for the second scan of the same representative monkey (for all monkeys and scan 1, see Supplementary Fig. 4.19). Each of the 16 seed regions was correlated with the 15 other seed regions. The lines where each seed was correlated with itself are removed, resulting in 120 lines  $[(16 \times 15) / 2]$  in each subplot of Fig. 4.18. These plots reveal substantial changes in the correlation strength over time. In particular, there are periods of enhanced coherence between seed regions that we have tentatively labelled “hyper-synchronization” (see below) alternating with incoherent periods. These fluctuations are not observed at longer time windows.

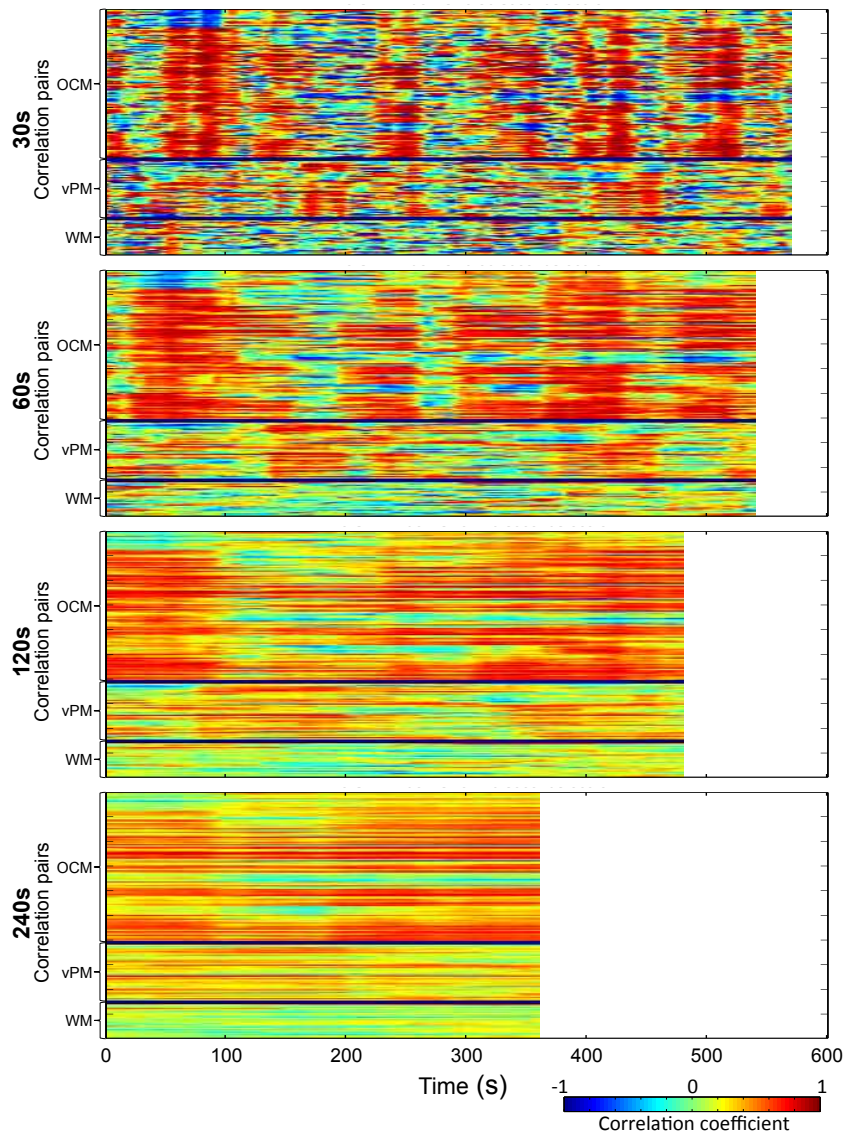


**Figure 4.18. Sliding-window pair-wise correlations of “oculomotor” network (OCM), ventral premotor network (vPM), and white matter (WM) seeds over time for a representative isoflurane-anesthetized macaques (M2, scan 2).** Every vertical line of each image represents the unfolded pair-wise correlation matrix as seen in Fig 4.6 averaged across 30s (row 1), 60s (row 2), 120s (row 3), and 240s (row 4) windows for the entire scan. Plots for all monkeys and both scans are shown in Fig. 4.20. Reprinted with permission from Hutchison, Womelsdorf, Gati, Everling & Menon (2012).

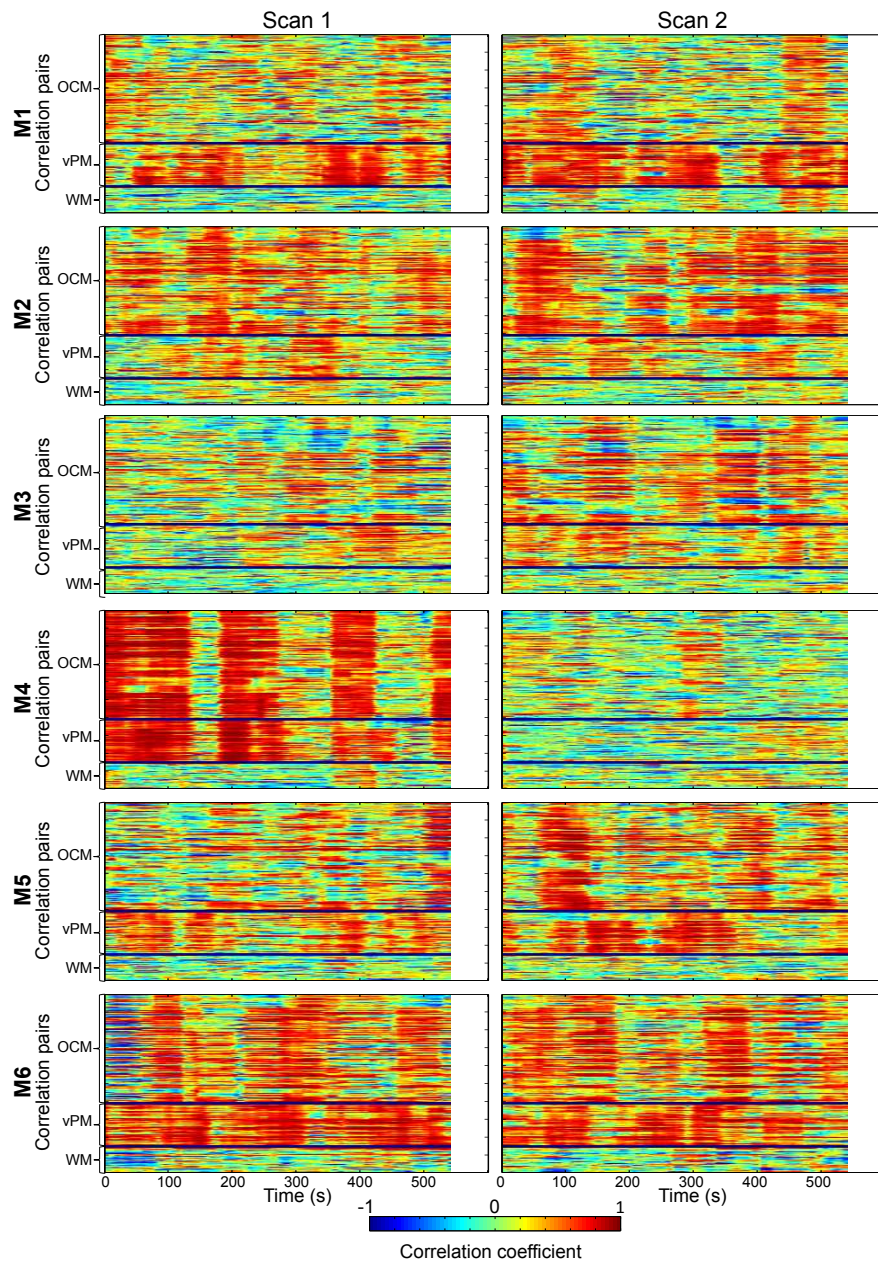


**Figure 4.19. Sliding-window pair-wise correlations of “oculomotor” network (OCM), ventral premotor network (vPM), and white matter (WM) seeds over time for all monkeys (M1-M6) for both scans.** Every vertical line of each image represents the unfolded pair-wise correlation matrix as seen in Fig. 4.6 averaged across 60s windows for the entire scan. Reprinted with permission from Hutchison, Womelsdorf, Gati, Everling & Menon (2012).

Hyper-synchronization was quantified for the OCM, vPM, and WM areas by calculating the average pairwise correlation values across all seeds within each network for all monkeys (Fig. 4.20; 60s sliding window; for scan 1, see Fig. 4.21). For the RSNs, periods of hyper-synchrony had average correlation values greater than + 0.6 whereas incoherent periods approached 0. The average network connectivity time courses were not significantly correlated, showing different correlation peaks and hyper-synchrony durations. Histograms display the amount of time in seconds spent at binned correlational values. WM values typically centered around 0 whereas vPM and OCM networks had mean correlation values that were moderate to strong. Within-network seeds display strong negative correlations, however the mean connectivity typically does not drop below 0 even with a 30s window. Hyper-synchronization was observed for most animals with the exception of M4 (scan 2), however, scan 1 of the same monkey showed the greatest synchronization across seeds encompassing both OCM and vPM nodes (though not WM).

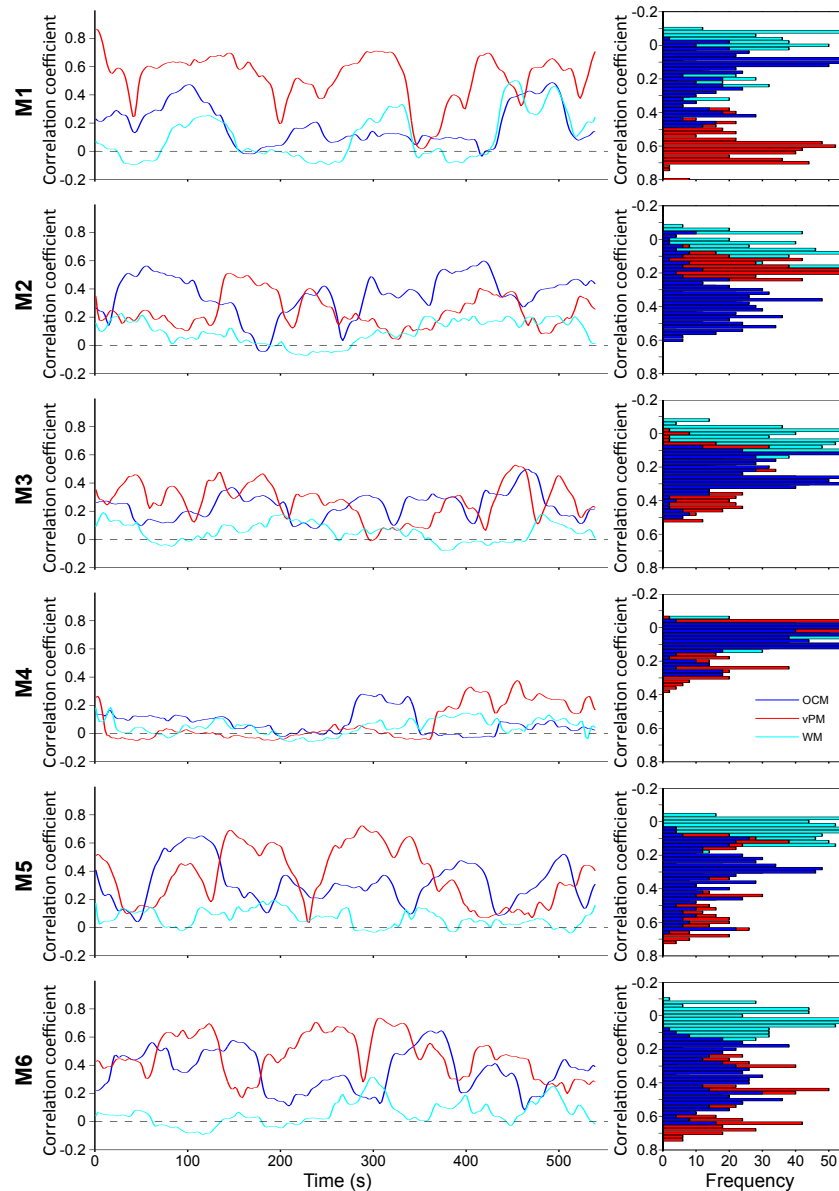


**Figure 4.20.** Average pairwise correlation values across all “oculomotor” network (OCM, red), ventral premotor network (vPM, blue), and white matter (WM, cyan) seeds over time for all monkeys (M1-M6, scan 2) with a sliding window of 60s. To the right of each plot shows the frequency distribution of the correlation coefficients for each of the three time series. For scan 1, see Fig. 4.21. Reprinted with permission from Hutchison, Womelsdorf, Gati, Everling & Menon (2012).

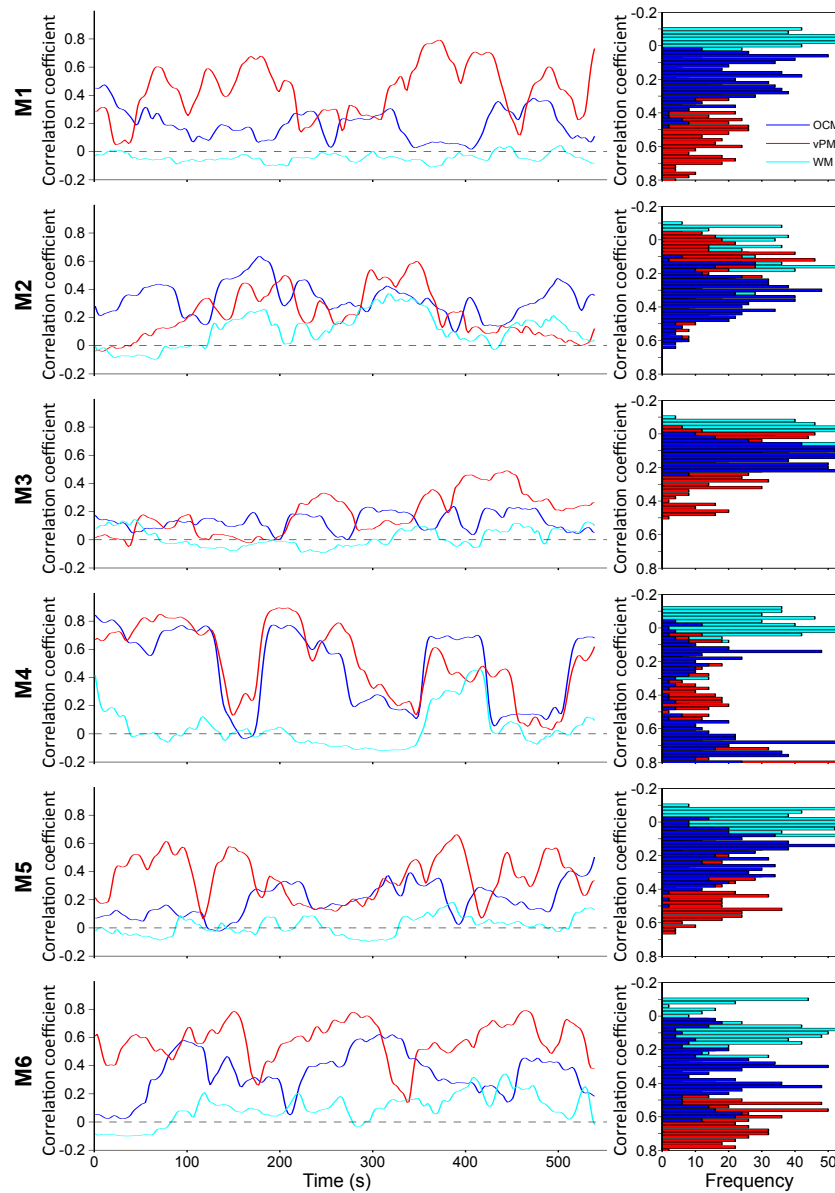


**Figure 4.21.** Average pairwise correlation values across all “oculomotor” network (OCM, red), ventral premotor network (vPM, blue), and white matter (WM, cyan) seeds over time for all monkeys (M1-M6, scan 1) with a sliding window of 60s. To the right of each plot shows the frequency distribution of the correlation coefficients for each of the three time series. For scan 2, see Fig. 4.20. Reprinted with permission from Hutchison, Womelsdorf, Gati, Everling & Menon (2012).

Periods of hyper-synchrony were not exclusive to the anesthesia state, as all awake human subjects also exhibited strong network specific synchrony over a period of 12 min (Fig. 4.22; for all subjects see Fig. 4.23). As the time window was increased the effects were no longer evident.

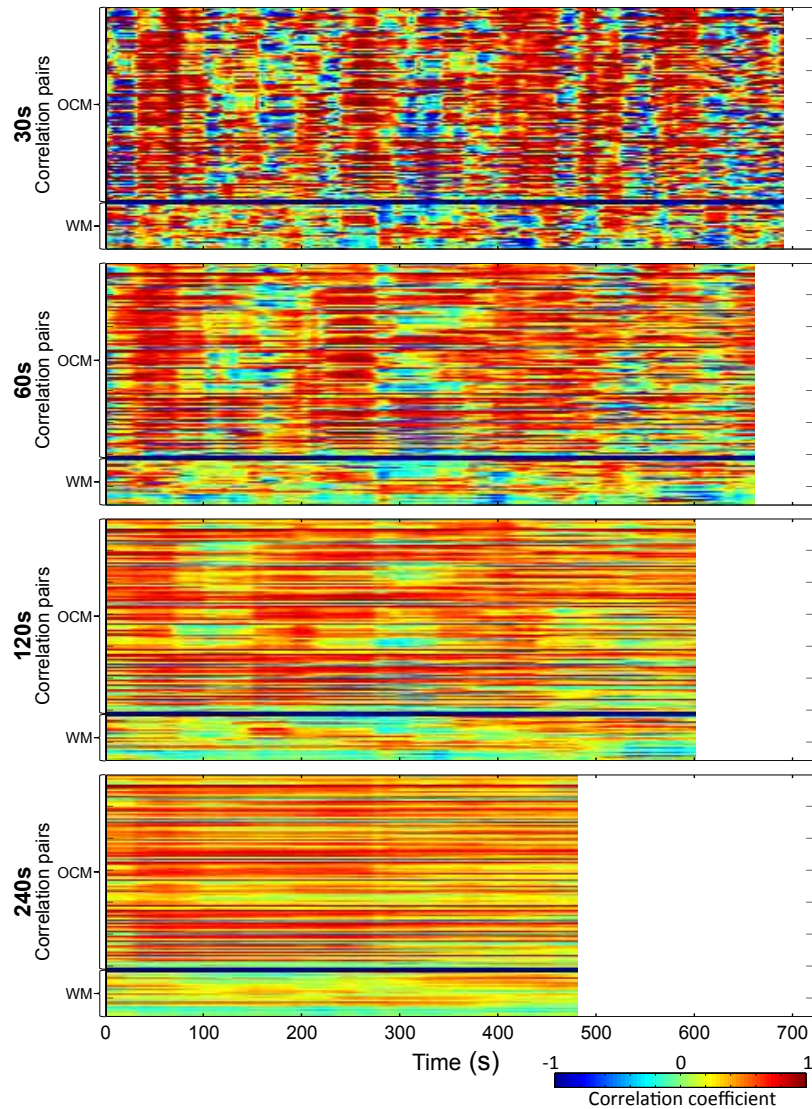


**Figure 4.22. Sliding-window pair-wise correlations of “oculomotor” network seeds over time for a representative awake human subject (S7).** Every vertical line of each image represents the unfolded pair-wise correlation matrix as seen in Fig. 4.09 averaged across 30s (row 1), 60s (row 2), 120s (row 3), and 240s (row 4) windows for the entire scan. Plots for all subjects are shown in Supplementary Fig. 4.23. Reprinted with permission from Hutchison, Womelsdorf, Gati, Everling & Menon (2012).

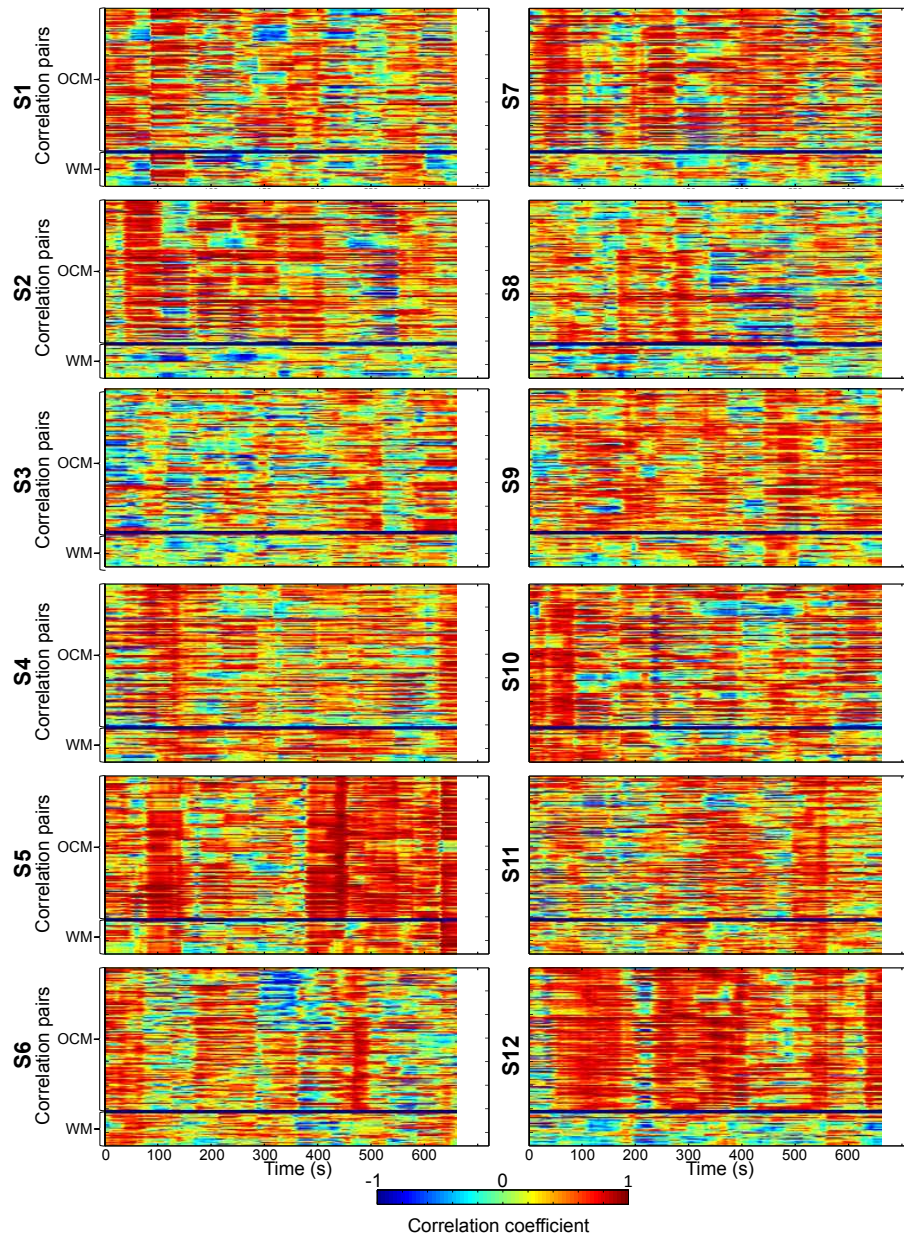


**Figure 4.23. Sliding-window pair-wise correlations of “oculomotor” network (OCM) and white matter (WM) seeds over time for all human subjects (S1-S12).** Every vertical line of each image represents the unfolded pair-wise correlation matrix as seen in Fig. 4.09 averaged across 60s windows for the entire scan. Reprinted with permission from Hutchison, Womelsdorf, Gati, Everling & Menon (2012).

## 4.4 Discussion

### 4.4.1 Dynamic RSN connectivity occurs in the absence of cognition

Ongoing brain activity changes in the absence of stimuli or behaviour, and was historically characterized as background “noise” in both electrophysiological and imaging fields. Evidence from both fields is now changing this view, demonstrating that the spontaneous modulations of activity are highly organized across a range of temporal and spatial scales with profiles and magnitudes similar to task-evoked patterns (for reviews see (Bullock, 2003; Vogels, Rajan, & Abbott, 2005; Ringach, 2009; Sadaghiani et al., 2010; Raichle, 2010).

The primary aim of the current study was to test the hypothesis that stimulus-independent fluctuations of functional connectivity within RSN nodes measured using BOLD-fMRI were not solely a consequence of conscious brain processes (Paus et al., 1997; Mason et al., 2007; Gilbert et al., 2007; Christoff et al., 2009) or subject motion (Van Dijk et al., 2012) during image acquisition, factors that confounded previous studies (Sato et al., 2006; Mantini et al., 2007; Chang & Glover, 2010; Britz et al., 2010; Musso et al., 2010). To eliminate these confounding variables as the origin of the temporal characteristics, we examined the network connectivity patterns over time between nodes of the macaque “oculomotor” (OCM) RSN during anesthesia with isoflurane, thereby precluding such processes related to conscious thought, mind-wandering, memory formation, or changes in arousal and attention (Veselis, 2001; Brown et al., 2010). In addition to the anesthesia, an implanted head post to mount the subject’s head in a stable position prevented any possible movement related artifacts. Under these conditions, a sliding-window correlation analysis revealed that, even in an anesthetized brain state, RSN functional connectivity was dynamically changing across time, a property that could not be captured with whole-scan metrics that only compute the mean connectivity value. Individual seed-pair correlations of the macaque and human OCM RSN showed oscillatory-like behaviour in which the correlation strength fluctuated between strong

positive and strong negative correlations reliably within subjects, and reproducible across subjects and species. Evidenced by the FFT of the correlation time courses, as the window size increased, the amplitude and number of frequency peaks diminished. This effect is the result of averaging the periods of positive and negative synchrony within the same period, effectively canceling out the alternating patterns and eliminating the frequency dynamics. Averaging across longer time windows will result in positive values simply due to the increased amount of time the network seeds are positively correlated compared to being anti-correlated (Fig. 7 and 8, insets). Averaging across the entire scan occasionally failed to detect brain areas that become synchronous with the “core” RSN for brief times throughout the scan, though not consistently enough to survive averaging. This can be seen for example, in the voxel-wise plots (column 2 and 3) of Fig. 5 (as well as the supplementary movies), where at multiple windows such as 268-328s (row 3) and 360-420s (row 5), primary visual cortex (V1) is strongly correlated with the left FEF seed, though does not emerge as a network node in the single subject average (row 6). Additionally, seed-pair correlations at the network level showed periods of strong positive synchronization across the entire network that occurred multiple times throughout the scan in all animals and all human subjects that we have tentatively labelled “hyper-synchronization.” The hyper-synchronous periods were network specific in that the nodes of the OCM and vPM RSNs both exhibited periods of hypersynchrony, albeit at different time points and durations.

Taken together, the findings support each of the three hypotheses investigated. First, in agreement with previous work, RSN connectivity was found to be dynamic over time and functional connectivity profiles dependent upon the temporal scale that was used (Sato et al., 2006; Honey et al., 2007; Majeed, Magnuson, & Keilholz, 2009; Chang & Glover, 2010; de Pasquale et al., 2010; Britz et al., 2010; Musso et al., 2010). Second, the present work offers preliminary evidence that much like RSN organization (Biswal, Yetkin, Haughton, & Hyde, 1995; Beckmann et al., 2005; Vincent et al., 2007; Hutchison et al., 2010, 2011a; Jonckers et al., 2011), dynamic relationships within the networks are also a conserved brain property across mammals. Third, and most importantly, the network dynamics persisted regardless of the use of anesthesia, thereby supporting the notion that RSN connectivity variations are a result of ongoing, spontaneous brain

activity and not solely a consequence of conscious processing. It is important to note that although we identified fluctuating network connectivity in the absence of conscious cognitive processes, we do not intend to exclude ongoing brain dynamics in the participation of cognition and behavior (or conversely, the modulation of spontaneous activity by conscious processes, context, and behavior). In fact, the results from converging methods have implied that the intrinsic neural and hemodynamic fluctuations represent an essential property of normal brain functioning (for reviews see Bullock, 2003; Vogels et al., 2005; Ringach, 2009; Sadaghiani et al., 2010; Raichle, 2010).

#### 4.4.2 Electrophysiological correlates

The periods of metastable RSN synchronization observed in the present study could represent the hemodynamic correlate of “microstates” (Britz et al., 2010; Musso et al., 2010), a fingerprint of specific electrophysiological processes (Lehmann, Faber, Gianotti, Kochi, & Pascual-Marqui, 2006) with power contributions arising from multiple frequency bands (Mantini et al., 2007). Functionally, the microstate is likely reflecting groups of neurons in separate cortical areas linked into a large-scale network that conjointly subserve a unified cognitive, mental, or perceptual function (Felleman & Van Essen, 1991; Friston, 2002; Bressler & Tognoli, 2006; Fuster, 2006). Network areas forming a microstate are thereby assumed to be coordinated with a unique spatio-temporal pattern. Similar to this proposal, the RS-fMRI signals characterize not only a unique spatial distribution, but a multi-component temporal signature (Mantini et al., 2007; Majeed et al., 2009; Hutchison et al., 2010; Baria, Baliki, Parrish, & Apkarian, 2011), albeit at a much lower frequency range (0.01 - 0.1 Hz) owing to convolution with the hemodynamic response function. The observed fluctuation of spatiotemporal connectivity patterns could then represent changing microstates - a cycling of varying network topologies through the brain’s functional repertoire allowing for a plastic and flexible framework necessary for ongoing cognitive processes (Kelso, 1995; Friston, 2000; Rabinovich et al., 2008; Tognoli & Kelso, 2009; Sporns, 2010 p.172).

Previous work across multiple spatial scales and modalities has implicated spontaneous brain activity as a source of variability in evoked responses (Arieli, Sterkin, Grinvald, & Aertsen, 1996; Azouz & Gray, 1999; Fiser, Chiu, & Weliky, 2004; Fox, Snyder, Zacks, & Raichle, 2006b; Becker, Reinacher, Freyer, Villringer, & Ritter, 2011), perception (Sapir, d' Avossa, McAvoy, Shulman, & Corbetta, 2005; van Dijk, Schoffelen, Oostenveld, & Jensen, 2008; Hesselmann et al., 2008b; Sadaghiani et al., 2009), and behaviour (Hesselmann, Kell, & Kleinschmidt, 2008a). Most relevant to the present work, Fox and colleagues (2006a) demonstrated that ongoing activity fluctuations within a widely distributed human RSN (“dorsal motor”) could account for trial-to-trial variability of the evoked hemodynamic responses to a task (finger-related movement). The linear superposition and neuronal basis of this phenomenon was later confirmed by Becker et al. (2011), reinforcing that evoked responses cannot be fully understood in isolation from ongoing activity. The present findings, in addition to the previous work (Sato et al., 2006; Chang & Glover, 2010; de Pasquale et al., 2010), suggest that intra-network RSN connectivity fluctuations might be another key element that may account for parts of the variability of evoked responses, perception, and behaviour. Further, if the spontaneous activity fluctuations are considered as predictive representations as in a Bayesian framework (Pouget, Dayan, & Zemel, 2003; Körding & Wolpert, 2006; Sadaghiani, Hesselmann, Friston, & Kleinschmidt, 2010) in which ongoing cortical activity represents a continuous top-down prediction or expectation, then selecting the correct network state could represent the critical factor for higher-order complex tasks requiring large scale integration of brain areas (Engel, Fries, & Singer, 2001; Buckner & Vincent, 2007).

It is more difficult to speculate on the underlying cause and functional significance of the “hyper-synchronized” periods of both species seen in Fig. 9, 10, and 11. These persisted for tens of seconds and had strong correlation strengths ( $r > 0.6$ ) across all network nodes. Additionally, the confidence values for the strong correlation periods were very high. The lowest confidence values were found when the mean correlation value was near zero. The periods of hyper-synchronization most often occurred independently of other RSNs and WM. The network-specific alternating patterns of enhanced synchrony share similar characteristics with the electrophysiological

‘slow rhythm’ (0.2-0.4 Hz) (Steriade, Contreras, Curró Dossi, & Nuñez, 1993a; Steriade, Nuñez, & Amzica, 1993b; Haider & McCormick, 2009). The slow rhythm oscillates between two different levels of subthreshold membrane potentials. The UP state is distinguished by barrages of both excitatory and inhibitory postsynaptic potentials, and the firing of both excitatory and inhibitory neurons, whereas the DOWN state is characterized by periods of hyperpolarization and quiescence (Steriade et al., 1993b; Contreras, Timofeev, & Steriade, 1996; Stern, Kincaid, & Wilson, 1997; Lampl, Reichova, & Ferster, 1999). Slow rhythms are generated and maintained in distributed populations of neurons throughout the neocortex and engage neurons throughout the brain (Isomura et al., 2006). Studies typically cite their role in coordinating other sleep rhythms (Steriade, Nuñez, & Amzica, 1993c; Contreras, Timofeev, & Steriade, 1996; Achermann & Borbély, 1997) and memory consolidation (Lee & Wilson, 2002; Mölle, Marshall, Gais, & Born, 2004). Given that hyper-synchronization was also observed in awake human RSNs it would suggest that the phenomenon is not a result of anesthesia. The presence and functional relevance of slow rhythms in cortical activation during wakefulness has not yet been fully explored (Destexhe, Hughes, Rudolph, & Crunelli, 2007; Sporns, 2010 p.156). Nir and colleagues (2008) have reported slow (<0.1 Hz) spontaneous fluctuations of neuronal activity (LFP gamma power modulations) in the auditory cortex of awake human subjects. Bilateral single-unit, LFP, and intracranial electrocorticography (ECoG) also revealed significant interhemispheric correlations between the homologous areas that increased during rapid eye movement (REM) and stage 2 sleep (Nir et al., 2008). In a related study, He et al., (2008) compared the “correlation structure” of the sensorimotor network of humans recorded by ECoG and BOLD independently. Slow cortical potentials (<0.5 Hz) were found to best correspond with RS-BOLD fluctuation profiles across wakefulness, slow-wave sleep, and REM sleep, whereas gamma frequency power showed a similar correlation structure albeit only during wakefulness and REM sleep. The results of these studies point towards slow cortical oscillations as a possible electrophysiological correlate of “hyper-synchrony”. Given that the responsiveness of the cortex to sensory stimuli is generally increased during UP states and decreased during DOWN states (Steriade et al., 1993b; Contreras et al., 1996) the slow fluctuations of synchronization (UP states) could represent a

dynamically stable network organization exploited to express selective functional relationships.

The present study only allows us to infer the electrophysiological correlate(s) of the nonstationary relationships and “hyper-synchronization” based on their resemblance to known phenomena. Obtaining direct evidence would require simultaneous electrophysiological and RS-fMRI recordings. Beyond establishing a link between neural activity and the hemodynamic BOLD activity (Logothetis, Pauls, Augath, Trinath, & Oeltermann, 2001), previous work using EEG-fMRI has attempted to directly derive the electrophysiological correlate of RS-fMRI fluctuations (Mantini et al., 2007; Nir et al., 2007; Laufs, 2008, 2010; Shmuel & Leopold, 2008; He, Snyder, Zempel, Smyth, & Raichle, 2008; Britz et al., 2010; Musso et al., 2010; Liu, Zhu, Zhang, & Chen, 2011) and in what may prove synonymous, the hemodynamic manifestations of temporal EEG dynamics (Goldman, Stern, Engel, & Cohen, 2002; Laufs et al., 2003b; Moosman et al., 2003; Sammer et al., 2007; Olbrich et al., 2009; Ritter, Moosmann, & Villringer, 2009; Michels et al., 2010; Wu, Eichele, Calhoun, 2010). It has been established in anesthetized monkeys that slow fluctuations in the power of band-limited oscillations (particularly gamma) can be directly linked to the ongoing RS-fMRI fluctuations (Shmuel & Leopold, 2008). In humans, RSNs were assigned a unique electrophysiological signature that involved a combination of EEG power variations in the delta, theta, alpha, beta, and gamma range (Laufs et al., 2003a; Mantini et al., 2007; for review see Laufs, 2008). This was later confirmed by two independent studies showing that transient multi-frequency EEG events (microstates) can be used as regressors to elicit BOLD activation patterns consistent with at least some RSNs (Britz et al., 2010; Musso et al., 2010). The studies however, did not explore the temporal properties of the within-network connectivity. This presents a promising avenue for future research and will be critical in resolving controversies related to time-scale discrepancies between electrophysiological activity (microstates, slow rhythms, frequency specific power changes) and the RSN fluctuations.

### 4.4.3 Anti-correlations

The role of anti-correlations within RSNs remains unclear and controversial (Fox et al., 2005; Murphy, Birn, Handwerker, Jones, & Bandettini, 2009; Cole, Smith, & Beckmann, 2010), though it has been suggested that they subserve a “differentiating role,” segregating neuronal processes that have competing representations (Fox et al., 2005). In agreement with previous work (Chang & Glover, 2010), the strength of negative correlations was found to depend strongly on the time window used to analyze functional connectivity. Using the whole scan metrics, the correlation coefficients typically do not drop below -0.3, however at shorter time windows, the negative correlations approached -0.8 at high confidence values, suggesting active suppressive interactions between anti-correlated network nodes. Empirical investigations of anti-correlations remain underrepresented in a field that is dominated by interpretations of positive connectivity among seeds, however, the present results calls upon a reevaluation of their possible roles in complex brain networks.

### 4.4.4 Evolutionarily preserved mechanism

Resting-state fluctuations and their assembly into spatial network patterns appear to be a ubiquitous property of mammalian brain organization. Mice, rats, monkeys, and humans (Biswal et al., 1995; Vincent et al., 2007; Lu et al., 2007; Jonckers et al., 2011) all show robust and reproducible RSNs. The present study could now put forward that dynamics within this networks are also a shared feature of mammalian brain systems, at the very least between humans and non-human primates. Brain rhythms and cortical synchrony have been suggested as an indicator of complexity that parallels evolutionary branching; invertebrates lack EEG oscillations, amphibians show cortical coherence albeit less than mammals, and humans seem to possess the greatest range of frequency patterns (Bullock, 2003). Synchronization, network organization, and ongoing fluctuations would then represent an evolved and adaptive mechanism serving “higher-order” cognitive functioning.

RSN networks have been shown to persist under light and deep sleep (Horovitz et al., 2008, 2009), sedation (Greicius et al., 2008), and various forms of anesthesia (Lu et al., 2007; Zhao et al., 2008; Hutchison et al., 2010). This isn't to say however, that quantifiable differences do not exist between the different states. Changes in connectivity have been reported within and across both normal and disease states (Greicius, 2008; Horovitz et al., 2009; Vanhaudenhuyse et al., 2010). This makes direct qualitative comparisons of the anesthetized monkeys and awake human subjects problematic because, although qualitative assessment does indicate preserved temporal characteristics, any variations may not be a result of species difference but a consequence of the anesthesia. The mechanisms of action for isoflurane remain poorly understood, but it has been demonstrated to disrupt functional thalamocortical connectivity (Alkire, Haier, & Fallon, 2000; Steriade, 2001; Arhem, Klement, & Nilsson, 2003), in addition to causing vasodilation that can potentially affect cerebrovascular activity (Farber et al., 1997). The comparatively low dose used in the present work (1%) does not seem to affect spatial RSN properties as our previous work has shown RSNs closely resembling known task-based networks and homologous human RSNs (Hutchison et al., 2011a, 2011b). A greater level of understanding and further experimentation will be necessary to truly elucidate between species differences in dynamics.

#### 4.4.5 Controls and limitations

There has been recent evidence suggesting a possible link between resting-state and spontaneous oculomotor behavior in awake human subjects (Ramot et al., 2011). The authors admittedly could actually not delineate causal relationships between the two phenomenon, i.e. whether the eye movements were controlled by the spontaneous BOLD fluctuations, if the eye movements were actually generated by the fluctuations, or if both were driven by a third, common input. We visually inspected the raw monkey data to determine if there were shifts in eye movements during the resting-state scans of which none were apparent. Importantly, the eyes were kept closed throughout the duration of the scanning. Finally, the vPM network served as an independent control as the

fluctuating dynamics were not correlated with the OCM RSN activity and therefore, would indicate the effects could not solely be a result of residual eye movements.

Heart rate, blood pressure, and breathing rate (monitored for monkeys) were not recorded during image acquisition. This prevents us from modelling the changing physiological parameters in reference to the network fluctuations. However, we do not believe physiological artifacts to be the origin of the RSN dynamics. RS-BOLD signals are dominated by lower frequencies ( $< 0.1$  Hz) with minimal ( $>10\%$ ) contribution of higher frequent cardiac and respiratory oscillations ( $> 0.3$  Hz, higher in the monkey) to the correlation coefficient (Cordes et al., 2001). Contributions from these signals is further diminished through low-pass temporal filtering. Global grey matter (data not shown), white matter, vPM RSN, and OCM RSN were all found to have unique temporal profiles excluding a common artifactual source. Within network seeds also showed unique time-courses and correlation fluctuation profiles suggesting node specific activity. Finally, the findings were reproduced using two different scanners (Seimmas and Agilent), at two different field strengths (3T and 7T), with different acquisition parameters across 2 different species, one of which was anesthetized.

Decreasing the window size will increase the number of spurious correlations that occur when calculating the correlation coefficients over time. This has been shown to change in proportion to the square root of the sampling time (Van Dijk et al., 2009). This is a concern for the present work as the correlation coefficients are compared across window sizes. It was found however, that the highest statistical reliability occurred at the points of highest correlation and the highest variances were found for near-zero correlation values. This was also true of the mean correlation signal in which “hyper-synchronous” states were statistically significant ( $p < 1.7 \times 10^{-4}$ ,  $1.8 \times 10^{-4}$ ,  $2.1 \times 10^{-4}$ ,  $2.8 \times 10^{-4}$ , for 30s, 60s, 120s, and 240s respectively; corrected for multiple comparisons using Bonferroni correction; data not shown). This property was observed across all seeds and subjects. Also, correlations between seed regions are run independently of one another. It is improbable that states of “hypersynchrony” would result from spurious correlations, as these would be randomly distributed across time and not occurring between multiple seed regions simultaneously.

#### 4.4.6 Implications for future work

Current RS-fMRI analysis techniques such as cross-correlation or independent component analysis (both techniques have been previously applied to the current data set, see (Hutchison et al., 2011a, 2011b) assume stationarity of functional connectivity over the entire length of the scan, offering a limited, averaged view of the network relationships. Evidence is now suggesting that these techniques can be insensitive to robust spatiotemporal dynamics of the RSNs (Sato et al., 2006; Mantini et al., 2007; Chang & Glover, 2010; Britz et al., 2010; Musso et al., 2010) that disappear at analysis windows greater than 4 min in length (Van Dijk et al., 2009). The observation of RSN changes does not diminish the significance of studies assuming static network contributions, but suggests that there are statistically reliable and potentially meaningful dynamics that could be examined within these same datasets. This is in addition to new insights that may be gained by examining the transient inclusion of new network nodes into the stereotypical RSN. There is however, one major caveat. For RSNs determined from long observation windows, one can be confident that the static maps reflect all of the “core” nodes in a network. However, RSNs derived from short time windows may not show all nodes in a network as some of these may have transiently zero correlation as shown in our data. Until the nature of these dynamic RSNs are understood, it seems prudent to use observation windows of several minutes to ensure capture all the nodes of a RSN.

The results suggest nonstationary relationships between brain areas; however, the sliding-window technique used to reveal this still assumes stationarity, albeit on a smaller temporal scale. Window sizes below 30s (15 vol) did not result in significant correlations and suggest a minimum window size is necessary. However, more sophisticated complex network measures investigating possible non-linear interactions and their manifestations (Friston, 1997; Werner, 2007), as well as consideration of multiple RSNs will be needed to truly characterize the underlying dynamics and elucidate the processes that govern them.

The time-varying changes of the RSNs may offer insight into the large-scale network behaviour that is difficult to achieve with other methodological approaches that do not share the same level of spatial resolution or brain coverage as fMRI. Additional work will have to focus on identifying activity profiles, transition states, and task-related changes to the dynamic behaviour using novel analysis strategies - particularly at the group level (Sato et al., 2006; Chang & Glover, 2010; Deco, Jirsa, & McIntosh, 2011). RS-fMRI has emerged as a possible diagnostic tool in clinical contexts (Greicius, 2008; Auer, 2008) and, given the wealth of information provided by dynamic alterations and emphasis at the single subject level, presents an exciting future direction for clinical applications.

## 4.5 Conclusions

The present findings indicate that ongoing fluctuations of resting-state functional connectivity are an intrinsic property of mammalian brain organization and not simply a consequence of conscious, cognitive processing. This fundamental feature of temporal brain dynamics may be exploited to assemble and modulate state- or task-dependent representations critical for cognition and behaviour. Multi-modal investigations will be necessary to elucidate the electrophysiological correlates of this phenomenon, but the results suggest that important network information and dynamics are missed when using average functional connectivity as the single network measure.

## 4.6 References

- Achermann, P., & Borbély AA (1997). Low-frequency (< 1 Hz) oscillations in the human sleep electroencephalogram. *Neuroscience*, *81*, 213-222.
- Alkire, M.T., Haier, R.J., & Fallon, J.H. (2000). Toward a unified theory of narcosis: brain imaging evidence for a thalamocortical switch as the neurophysiologic basis of anesthetic-induced unconsciousness. *Conscious Cogn*, *9*, 370-386.

- Amiez, C., Kostopoulos, P., Champod, A-S., & Petrides, M. (2006). Local morphology predicts functional organization of the dorsal premotor region in the human brain. *J Neurosci*, *26*, 2724-2731.
- Arhem, P., Klement, G., & Nilsson, J. (2003). Mechanisms of anesthesia: towards integrating network, cellular, and molecular level modeling. *Neuropsychopharmacology*, *28*, Suppl 1:S40-47.
- Arieli, A., Sterkin, A., Grinvald, A., & Aertsen, A. (1996). Dynamics of ongoing activity: explanation of the large variability in evoked cortical responses. *Science*, *273*, 1868-1871.
- Auer, D.P. (2008). Spontaneous low-frequency blood oxygenation level-dependent fluctuations and functional connectivity analysis of the “resting” brain. *Magn Reson Imaging*, *26*, 1055-1064.
- Azouz, R., & Gray, C.M. (1999). Cellular mechanisms contributing to response variability of cortical neurons in vivo. *J Neurosci*, *19*, 2209-2223.
- Baker, J.T., Patel, G.H., Corbetta, M., & Snyder, L.H. (2006). Distribution of activity across the monkey cerebral cortical surface, thalamus and midbrain during rapid, visually guided saccades. *Cereb Cortex*, *16*, 447-459.
- Baria, A.T., Baliki, M.N., Parrish, T., & Apkarian, A.V. (2011). Anatomical and Functional Assemblies of Brain BOLD Oscillations. *J Neurosci*, *31*, 7910-7919.
- Becker, R., Reinacher, M., Freyer, F., Villringer, A., & Ritter, P. (2011). How ongoing neuronal oscillations account for evoked fMRI variability. *J Neurosci*, *31*, 11016-11027.
- Beckmann, C.F., DeLuca, M., Devlin, J.T., & Smith, S.M. (2005). Investigations into resting-state connectivity using independent component analysis. *Philos Trans R Soc Lond B Biol Sci*, *360*, 1001-1013.
- Bianciardi, M., Fukunaga, M., van Gelderen, P., Horovitz, S.G., de Zwart, J.A., & Duyn, J.H. (2009). Modulation of spontaneous fMRI activity in human visual cortex by behavioral state. *Neuroimage*, *45*, 160-168.
- Biswal, B., Yetkin, F.Z., Haughton, V.M., & Hyde, J.S. (1995). Functional connectivity in the motor cortex of resting human brain using echo-planar MRI. *Magn Reson. Imaging*, *34*, 537-541.
- Bressler, S.L., & Tognoli, E. (2006). Operational principles of neurocognitive networks. *Int J Psychophysiol*, *60*, 139-148.
- Britz, J., Van De Ville, D., & Michel, C.M. (2010). BOLD correlates of EEG topography reveal rapid resting-state network dynamics. *Neuroimage*, *52*, 1162-1170.

- Brown, M.R.G., DeSouza, J.F.X., Goltz, H.C., Ford, K., Menon, R.S., Goodale, M.A., & Everling, S. (2004). Comparison of memory- and visually guided saccades using event-related fMRI. *J Neurophysiol*, *91*, 873-889.
- Brown, M.R.G., Vilis, T., & Everling, S. (2007). Frontoparietal activation with preparation for antisaccades. *J Neurophysiol*, *98*, 1751-1762.
- Brown, E.N., Lydic, R., & Schiff, N.D. (2010). General anesthesia, sleep, and coma. *N Engl J Med*, *363*, 2638-2650.
- Bruce, C.J., & Goldberg, M.E. (1985). Primate frontal eye fields. I. Single neurons discharging before saccades. *J Neurophysiol*, *53*, 603-635.
- Buckner, R.L., & Vincent, J.L. (2007). Unrest at rest: default activity and spontaneous network correlations. *Neuroimage*, *37*, 1091-1096.
- Bullock, T.H. (2003). Have brain dynamics evolved? Should we look for unique dynamics in the sapient species? *Neural Comput*, *15*, 2013-2027.
- Chang, C., & Glover, G.H. (2010). Time-frequency dynamics of resting-state brain connectivity measured with fMRI. *Neuroimage*, *50*, 81-98.
- Christoff, K., Gordon, A.M., Smallwood, J., Smith, R., & Schooler, J.W. (2009). Experience sampling during fMRI reveals default network and executive system contributions to mind wandering. *Proc Natl Acad Sci USA*, *106*, 8719-8724.
- Cole, D.M., Smith, S.M., & Beckmann, C.F. (2010). Advances and pitfalls in the analysis and interpretation of resting-state FMRI data. *Front Syst Neurosci*, *4*, 8.
- Contreras, D., Timofeev, I., & Steriade, M. (1996). Mechanisms of long-lasting hyperpolarizations underlying slow sleep oscillations in cat corticothalamic networks. *J Physiol (Lond)*, *494 (Pt 1)*, 251-264.
- Cordes, D., Haughton, V.M., Arfanakis, K., Carew, J.D., Turski, P.A., Moritz, C.H., Quigley, M.A., & Meyerand, M.E. (2001). Frequencies contributing to functional connectivity in the cerebral cortex in "resting-state" data. *Am J Neuroradiol*, *22*, 1326-1333.
- Damoiseaux, J.S., Rombouts, S.A.R.B., Barkhof, F., Scheltens, P., Stam, C.J., Smith, S.M., & Beckmann, C.F. (2006). Consistent resting-state networks across healthy subjects. *Proc Natl Acad Sci USA* *103*, 13848-13853.
- Deco, G., Jirsa, V.K., & McIntosh, A.R. (2011). Emerging concepts for the dynamical organization of resting-state activity in the brain. *Nat Rev Neurosci*, *12*, 43-56.
- DeSouza, J.F.X., Menon, R.S., & Everling, S. (2003). Preparatory set associated with pro-saccades and anti-saccades in humans investigated with event-related FMRI. *J Neurophysiol*, *89*, 1016-1023.

- Destexhe, A., Hughes, S.W., Rudolph, M., & Crunelli, V. (2007). Are corticothalamic “up” states fragments of wakefulness? *Trends Neurosci*, *30*, 334-342.
- van Dijk, H., Schoffelen, J-M., Oostenveld, R., & Jensen, O. (2008). Prestimulus oscillatory activity in the alpha band predicts visual discrimination ability. *J Neurosci*, *28*, 1816-1823.
- van Dijk, K.R.A., Hedden, T., Venkataraman, A., Evans, K.C., Lazar, S.W., & Buckner, R.L. (2009). Intrinsic Functional Connectivity As a Tool For Human Connectomics: Theory, Properties, and Optimization. *J Neurophys*, *103*, 297-321.
- van Dijk, K.R.A., Sabuncu, M.R., & Buckner, R.L. (2011). The influence of head motion on intrinsic functional connectivity MRI. *Neuroimage*, *59*, 431-8.
- Engel, A.K., Fries, P., & Singer, W. (2001). Dynamic predictions: oscillations and synchrony in top-down processing. *Nat Rev Neurosci*, *2*, 704-716.
- Esposito, F., Bertolino, A., Scarabino, T., Latorre, V., Blasi, G., Popolizio, T., Tedeschi, G., Cirillo, S., Goebel, R., & Di Salle, F. (2006). Independent component model of the default-mode brain function: Assessing the impact of active thinking. *Brain Res Bull*, *70*, 263-269.
- van Essen, D.C., Dickson, J., Harwell, J., Hanlon, D., Anderson, C.H., & Drury, H.A. (2001). An integrated software system for surface-based analyses of cerebral cortex. *J Am Med Inform Assoc*, *8*, 443-459.
- van Essen, D.C. (2004). Surface-based approaches to spatial localization and registration in primate cerebral cortex. *Neuroimage*, *23 Suppl 1*, S97-107.
- van Essen, D.C. (2005). A Population-Average, Landmark- and Surface-based (PALS) atlas of human cerebral cortex. *Neuroimage*, *28*, 635-662.
- Farber, N.E., Harkin, C.P., Niedfeldt, J., Hudetz, A.G., Kampine, J.P., & Schmeling, W.T. (1997). Region-specific and agent-specific dilation of intracerebral microvessels by volatile anesthetics in rat brain slices. *Anesthesiology*, *87*, 1191-1198.
- Felleman, D.J., & Van Essen, D.C. (1991). Distributed hierarchical processing in the primate cerebral cortex. *Cereb Cortex*, *1*, 1-47.
- Fiser, J., Chiu, C., & Weliky, M. (2004). Small modulation of ongoing cortical dynamics by sensory input during natural vision. *Nature*, *431*, 573-578.
- Ford, K.A., Goltz, H.C., Brown, M.R.G., Everling, S. (2005). Neural processes associated with antisaccade task performance investigated with event-related fMRI. *J Neurophysiol*, *94*, 429-440.

- Ford, K.A., Gati, J.S., Menon, R.S., & Everling, S. (2009). BOLD fMRI activation for anti-saccades in nonhuman primates. *Neuroimage*, *45*, 470–476.
- Fox, M.D., Snyder, A.Z., Vincent, J.L., Corbetta, M., Van Essen, D.C., & Raichle, M.E. (2005). The human brain is intrinsically organized into dynamic, anticorrelated functional networks. *Proc Natl Acad Sci USA*, *102*, 9673-9678.
- Fox, M.D., Corbetta, M., Snyder, A.Z., Vincent, J.L., & Raichle, M.E. (2006a). Spontaneous neuronal activity distinguishes human dorsal and ventral attention systems. *Proc Natl Acad Sci USA*, *103*, 10046-10051.
- Fox, M.D., Snyder, A.Z., Zacks, J.M., & Raichle, M.E. (2006b). Coherent spontaneous activity accounts for trial-to-trial variability in human evoked brain responses. *Nat Neurosci*, *9*, 23-25.
- Fox, M.D., & Raichle, M.E. (2007). Spontaneous fluctuations in brain activity observed with functional magnetic resonance imaging. *Nat Rev Neurosci*, *8*, 700-711.
- Fransson, P. (2006). How default is the default mode of brain function? Further evidence from intrinsic BOLD signal fluctuations. *Neuropsychologia*, *44*, 2836-2845.
- Friston, K.J. (1997) Transients, metastability, and neuronal dynamics. *Neuroimage*, *5*, 164-71.
- Friston, K.J. (2000). The labile brain. I. Neuronal transients and nonlinear coupling. *Philos Trans R Soc Lond B Biol Sci*, *355*, 215-236.
- Friston, K.J. (2002). Beyond phrenology: what can neuroimaging tell us about distributed circuitry? *Annu Rev Neurosci*, *25*, 221-250.
- Fuster, J.M. (2006). The cognit: a network model of cortical representation. *Int J Psychophysiol*, *60*, 125-132.
- Gilbert, S.J., Dumontheil, I., Simons, J.S., Frith, C.D., & Burgess, P.W. (2007). Comment on “Wandering minds: the default network and stimulus-independent thought.” *Science* 317:43; author reply 43.
- Goldman, R.I., Stern, J.M., Engel, J. Jr., & Cohen, M.S. (2002). Simultaneous EEG and fMRI of the alpha rhythm. *Neuroreport*, *13*, 2487-2492.
- Greicius, M. (2008). Resting-state functional connectivity in neuropsychiatric disorders. *Curr Opin Neurol*, *21*, 424-430.
- Greicius, M.D., Kiviniemi, V., Tervonen, O., Vainionpää, V., Alahuhta, S., Reiss, A.L., & Menon, V. (2008). Persistent default-mode network connectivity during light sedation. *Hum Brain Mapp*, *29*, 839-847.

- Greicius, M.D., Supekar, K., Menon, V., & Dougherty, R.F. (2009). Resting-state functional connectivity reflects structural connectivity in the default mode network. *Cereb Cortex* 19, 72-78.
- Hagmann, P., Cammoun, L., Gigandet, X., Meuli, R., Honey, C.J., Wedeen, V.J., & Sporns, O. (2008). Mapping the structural core of human cerebral cortex. *PLoS Biology*, 6, e159.
- Haider, B., & McCormick, D.A. (2009). Rapid Neocortical Dynamics: Cellular and Network Mechanisms. *Neuron*, 62, 171-189.
- He, B.J., Snyder, A.Z., Zempel, J.M., Smyth, M.D., & Raichle, M.E. (2008). Electrophysiological correlates of the brain's intrinsic large-scale functional architecture. *Proc Natl Acad Sci USA*, 105, 16039-16044.
- Hesselmann, G., Kell, C.A., Eger, E., & Kleinschmidt, A. (2008a). Spontaneous local variations in ongoing neural activity bias perceptual decisions. *Proc Natl Acad Sci USA*, 105, 10984-10989.
- Hesselmann, G., Kell, C.A., & Kleinschmidt, A. (2008b). Ongoing activity fluctuations in hMT+ bias the perception of coherent visual motion. *J Neurosci*, 28, 14481-14485.
- Honey, C.J., Kötter, R., Breakspear, M., & Sporns, O. (2007). Network structure of cerebral cortex shapes functional connectivity on multiple time scales. *Proc Natl Acad Sci*, 104:10240-10245.
- Honey, C.J., Sporns, O., Cammoun, L., Gigandet, X., Thiran, J.P., Meuli, R., & Hagmann, P. (2009). Predicting human resting-state functional connectivity from structural connectivity. *Proc Natl Acad Sci USA*, 106, 2035-2040.
- Horovitz, S.G., Fukunaga, M., de Zwart, J.A., van Gelderen, P., Fulton, S.C., Balkin, T.J., & Duyn, J.H. (2008). Low frequency BOLD fluctuations during resting wakefulness and light sleep: a simultaneous EEG-fMRI study. *Hum Brain Mapp*, 29, 671-682.
- Horovitz, S.G., Braun, A.R., Carr, W.S., Picchioni, D., Balkin, T.J., Fukunaga, M., & Duyn, J.H. (2009). Decoupling of the brain's default mode network during deep sleep. *Proc Natl Acad Sci*, 106, 11376-11381.
- Hutchison, R.M., Mirsattari, S.M., Jones, C.K., Gati, J.S., & Leung, L.S. (2010). Functional Networks in the Anesthetized Rat Brain Revealed by Independent Component Analysis of Resting-State fMRI. *J Neurophysiol*, 103, 3398-3406.
- Hutchison, R.M., Leung, L.S., Mirsattari, S.M., Gati, J.S., Menon, R.S., & Everling, S. (2011a). Resting-state networks in the macaque at 7T. *Neuroimage*, 56, 1546-1555.

- Hutchison, R.M., Womelsdorf, T., Gati, J.S., Leung, L.S., Menon, R.S., Everling, S. (2011b). Resting-State Connectivity Identifies Distinct Functional Networks in Macaque Cingulate Cortex. *Cereb Cortex*, *in press*.
- Hutchison, R.M., Gallivan, J.P., Culham, J.C., Gati, J.S., Menon, R.S., & Everling, S. (2012). Functional connectivity of the frontal eye fields in humans and macaque monkeys investigated with resting-state fMRI. *J Neurophysiol*, *in press*.
- Isomura, Y., Sirota, A., Ozen, S., Montgomery, S., Mizuseki, K., Henze, D.A., & Buzsáki, G. (2006). Integration and segregation of activity in entorhinal-hippocampal subregions by neocortical slow oscillations. *Neuron*, *52*, 871-882.
- Johnston, K., & Everling, S. (2008). Neurophysiology and neuroanatomy of reflexive and voluntary saccades in non-human primates. *Brain Cogn*, *68*, 271-283.
- Jonckers, E., Van Audekerke, J., De Visscher, G., Van der Linden, A., & Verhoye, M. (2011). Functional Connectivity fMRI of the Rodent Brain: Comparison of Functional Connectivity Networks in Rat and Mouse. *PLoS ONE*, *6*, e18876.
- Kamada, T., & Kawai, S. (1989). An algorithm for drawing general undirected graphs. *Inf Process Lett*, *31*, 7-15.
- Kelly, C., Uddin, L.Q., Shehzad, Z., Margulies, D.S., Castellanos, F.X., Milham, M.P., & Petrides, M. (2010). Broca's region: linking human brain functional connectivity data and non-human primate tracing anatomy studies. *Eur J Neurosci*, *32*, 383-398.
- Kelso, J.A.S. (1995). *Dynamic Patterns: The Self-Organization of Brain and Behavior*. The MIT Press.
- Kiviniemi, V.J., Haanpää, H., Kantola, J-H., Jauhiainen, J., Vainionpää, V., Alahuhta, S., & Tervonen, O. (2005). Midazolam sedation increases fluctuation and synchrony of the resting brain BOLD signal. *Magn Reson Imaging*, *23*, 531-537.
- Klassen, L.M., & Menon, R.S. (2004). Robust automated shimming technique using arbitrary mapping acquisition parameters (RASTAMAP). *Magn Reson Med*, *51*, 881-887.
- Körding, K.P., & Wolpert, D.M. (2006). Bayesian decision theory in sensorimotor control. *Trends Cogn Sci*, *10*, 319-326.
- Koyama, M., Hasegawa, I., Osada, T., Adachi, Y., Nakahara, K., & Miyashita, Y. (2004). Functional magnetic resonance imaging of macaque monkeys performing visually guided saccade tasks: comparison of cortical eye fields with humans. *Neuron*, *41*, 795-807.
- Lampl, I., Reichova, I., & Ferster, D. (1999). Synchronous membrane potential fluctuations in neurons of the cat visual cortex. *Neuron* *22*, 361-374.

- Laufs, H., Krakow, K., Sterzer, P., Eger, E., Beyerle, A., Salek-Haddadi, A., & Kleinschmidt, A. (2003a). Electroencephalographic signatures of attentional and cognitive default modes in spontaneous brain activity fluctuations at rest. *Proc Natl Acad Sci USA*, *100*, 11053-11058.
- Laufs, H., Kleinschmidt, A., Beyerle, A., Eger, E., Salek-Haddadi, A., Preibisch, C., & Krakow, K. (2003b). EEG-correlated fMRI of human alpha activity. *Neuroimage* *19*, 1463-1476.
- Laufs, H. (2008). Endogenous brain oscillations and related networks detected by surface EEG-combined fMRI. *Hum Brain Mapp*, *29*, 762-769.
- Laufs, H. (2010). Multimodal analysis of resting state cortical activity: what does EEG add to our knowledge of resting state BOLD networks? *Neuroimage*, *52*, 1171-1172.
- Lee, A.K., & Wilson, M.A. (2002). Memory of sequential experience in the hippocampus during slow wave sleep. *Neuron*, *36*, 183-1194.
- Lehmann, D., Faber, P.L., Gianotti, L.R.R., Kochi, K., & Pascual-Marqui, R.D. (2006). Coherence and phase locking in the scalp EEG and between LORETA model sources, and microstates as putative mechanisms of brain temporo-spatial functional organization. *J Physiol Paris*, *99*, 29-36.
- Liu, X., Zhu, X-H., Zhang, Y., & Chen, W. (2011). Neural origin of spontaneous hemodynamic fluctuations in rats under burst-suppression anesthesia condition. *Cereb Cortex*, *21*, 374-384.
- Logothetis, N.K., Pauls, J., Augath, M., Trinath, T., & Oeltermann, A. (2001). Neurophysiological investigation of the basis of the fMRI signal. *Nature*, *412*, 150-157.
- Lu, H., Zuo, Y., Gu, H., Waltz, J.A., Zhan, W., Scholl, C.A., Rea, W., Yang, Y., & Stein, E.A. (2007). Synchronized delta oscillations correlate with the resting-state functional MRI signal. *Proc Natl Acad Sci USA* *104*, 18265-18269.
- Luna, B., Thulborn, K.R., Strojwas, M.H., McCurtain, B.J., Berman, R.A., Genovese, C.R., & Sweeney, J.A. (1998). Dorsal cortical regions subserving visually guided saccades in humans: an fMRI study. *Cereb Cortex*, *8*, 40-47.
- Majeed, W., Magnuson, M., & Keilholz, S.D. (2009). Spatiotemporal dynamics of low frequency fluctuations in BOLD fMRI of the rat. *J Magn Reson Imaging*, *30*, 384-393.
- Mantini, D., Perrucci, M.G., Del Gratta, C., Romani, G.L., & Corbetta, M. (2007) Electrophysiological signatures of resting state networks in the human brain. *Proc Natl Acad Sci USA* *104*, 13170-13175.

- Margulies, D.S., Vincent, J.L., Kelly, C., Lohmann, G., Uddin, L.Q., Biswal, B.B., Villringer, A., Castellanos, F.X., Milham, M.P., & Petrides, M. (2009). Precuneus shares intrinsic functional architecture in humans and monkeys. *Proc Natl Acad Sci*, *106*, 20069-20074.
- Mason, M.F., Norton, M.I., Van Horn, J.D., Wegner, D.M., Grafton, S.T., & Macrae, C.N. (2007). Wandering minds: the default network and stimulus-independent thought. *Science*, *315*, 393-395.
- Michels, L., Bucher, K., Lüchinger, R., Klaver, P., Martin, E., Jeanmonod, D., & Brandeis, D. (2010). Simultaneous EEG-fMRI during a working memory task: modulations in low and high frequency bands. *PLoS ONE*, *5*, e10298.
- Mölle, M., Marshall, L., Gais, S., & Born, J. (2004). Learning increases human electroencephalographic coherence during subsequent slow sleep oscillations. *Proc Natl Acad Sci USA*, *101*, 13963-13968.
- Moosmann, M., Ritter, P., Krastel, I., Brink, A., Thees, S., Blankenburg, F., Taskin, B., Obrig, H., & Villringer, A. (2003). Correlates of alpha rhythm in functional magnetic resonance imaging and near infrared spectroscopy. *Neuroimage*, *20*, 145-158.
- Murphy, K., Birn, R.M., Handwerker, D.A., Jones, T.B., & Bandettini, P.A. (2009). The impact of global signal regression on resting state correlations: are anti-correlated networks introduced? *Neuroimage*, *44*, 893-905.
- Musso, F., Brinkmeyer, J., Mobascher, A., Warbrick, T., & Winterer, G. (2010). Spontaneous brain activity and EEG microstates. A novel EEG/fMRI analysis approach to explore resting-state networks. *Neuroimage*, *52*, 1149-1161.
- Nir, Y., Fisch, L., Mukamel, R., Gelbard-Sagiv, H., Arieli, A., Fried, I., & Malach, R. (2007). Coupling between neuronal firing rate, gamma LFP, and BOLD fMRI is related to interneuronal correlations. *Curr Biol*, *17*, 1275-1285.
- Nir, Y., Mukamel, R., Dinstein, I., Privman, E., Harel, M., Fisch, L., Gelbard-Sagiv, H., Kipervasser, S., Andelman, F., Neufeld, M.Y., Kramer, U., Arieli, A., & Fried, I., Malach, R. (2008). Interhemispheric correlations of slow spontaneous neuronal fluctuations revealed in human sensory cortex. *Nat Neurosci*, *11*, 1100-1108.
- Ogawa, S., Menon, R.S., Tank, D.W., Kim, S.G., Merkle, H., Ellermann, J.M., & Ugurbil, K. (1993). Functional brain mapping by blood oxygenation level-dependent contrast magnetic resonance imaging. A comparison of signal characteristics with a biophysical model. *Biophys J*, *64*, 803-812.
- Olbrich, S., Mulert, C., Karch, S., Trenner, M., Leicht, G., Pogarell, O., & Hegerl, U. (2009). EEG-vigilance and BOLD effect during simultaneous EEG/fMRI measurement. *Neuroimage*, *45*, 319-332.

- de Pasquale, F., Della Penna, S., Snyder, A.Z., Lewis, C., Mantini, D., Marzetti, L., Belardinelli, P., Ciancetta, L., Pizzella, V., Romani, G.L., & Corbetta, M. (2010). Temporal dynamics of spontaneous MEG activity in brain networks. *Proc Natl Acad Sci USA*, *107*, 6040-6045.
- Paus, T. (1996). Location and function of the human frontal eye-field: a selective review. *Neuropsychologia*, *34*, 475-483.
- Paus, T., Zatorre, R.J., Hofle, N., Caramanos, Z., Gotman, J., Petrides, M., & Evans, A.C. (1997). Time-Related Changes in Neural Systems Underlying Attention and Arousal During the Performance of an Auditory Vigilance Task. *J Cogn Neurosci*, *9*, 392-408.
- Paxinos, G., Huang, X-F., & Toga, A.W. (1999). The Rhesus Monkey Brain in Stereotaxic Coordinates 1st ed. Academic Press.
- Pouget, A., Dayan, P., & Zemel, R.S. (2003). Inference and computation with population codes. *Annu Rev Neurosci* *26*, 381-410.
- Rabinovich, M.I., Huerta, R., Varona, P., Afraimovich, V.S. (2008). Transient cognitive dynamics, metastability, and decision making. *PLoS Comput Biol*, *4*, e1000072.
- Raichle, M.E. (2010). Two views of brain function. *Trends Cogn Sci*, *14*, 180-190.
- Ramot, M., Wilf, M., Goldberg, H., Weiss, T., Deouell, L.Y., & Malach R. (2011). Coupling between spontaneous (resting state) fMRI fluctuations and human oculo-motor activity. *Neuroimage*, *58*, 213-225.
- Ringach, D.L. (2009). Spontaneous and driven cortical activity: implications for computation. *Curr Opin Neurobiol* *19*, 439-444.
- Ritter, P., Moosmann, M., & Villringer, A. (2009). Rolandic alpha and beta EEG rhythms' strengths are inversely related to fMRI-BOLD signal in primary somatosensory and motor cortex. *Hum Brain Mapp*, *30*, 1168-1187.
- Sadaghiani, S., Hesselmann, G., & Kleinschmidt, A. (2009). Distributed and antagonistic contributions of ongoing activity fluctuations to auditory stimulus detection. *J Neurosci* *29*, 13410-13417.
- Sadaghiani, S., Hesselmann, G., Friston, K.J., & Kleinschmidt, A. (2010). The relation of ongoing brain activity, evoked neural responses, and cognition. *Front Syst Neurosci*, *4*, 20.
- Sammer, G., Blecker, C., Gebhardt, H., Bischoff, M., Stark, R., Morgen, K., & Vaitl, D. (2007). Relationship between regional hemodynamic activity and simultaneously recorded EEG-theta associated with mental arithmetic-induced workload. *Hum Brain Mapp*, *28*, 793-803.

- Sapir, A., d'Avossa, G., McAvoy, M., Shulman, G.L., & Corbetta, M. (2005). Brain signals for spatial attention predict performance in a motion discrimination task. *Proc Natl Acad Sci USA*, *102*, 17810-17815.
- Sato, J.R., Junior, E.A., Takahashi, D.Y., de Maria Felix, M., Brammer, M.J., & Morettin, P.A. (2006). A method to produce evolving functional connectivity maps during the course of an fMRI experiment using wavelet-based time-varying Granger causality. *Neuroimage* *31*, 187-196.
- Shirer, W.R., Ryali, S., Rykhlevskaia, E., Menon, V., Greicius, M.D. (2012). Decoding subject-driven cognitive States with whole-brain connectivity patterns. *Cereb Cortex*, *22*, 158-165.
- Shmuel, A., & Leopold, D.A. (2008). Neuronal correlates of spontaneous fluctuations in fMRI signals in monkey visual cortex: Implications for functional connectivity at rest. *Hum Brain Mapp*, *29*, 751-761.
- Smith, S.M., Fox, P.T., Miller, K.L., Glahn, D.C., Fox, P.M., Mackay, C.E., Filippini, N., Watkins, K.E., Toro, R., Laird, A.R., & Beckmann, C.F. (2009). Correspondence of the brain's functional architecture during activation and rest. *Proc Natl Acad Sci USA*, *106*, 13040-13045.
- Sporns, O. (2010). *Networks of the Brain* 1st ed. The MIT Press.
- Squire, L., & Zola-Morgan, S. (1991). The medial temporal lobe memory system. *Science*, *253*, 1380 -1386.
- Steriade, M., Contreras, D., Curró Dossi, R., & Nuñez, A. (1993a). The slow (< 1 Hz) oscillation in reticular thalamic and thalamocortical neurons: scenario of sleep rhythm generation in interacting thalamic and neocortical networks. *J Neurosci*, *13*, 3284-3299.
- Steriade, M., Nuñez, A., & Amzica, F. (1993b). A novel slow (< 1 Hz) oscillation of neocortical neurons in vivo: depolarizing and hyperpolarizing components. *J Neurosci*, *13*, 3252-3265.
- Steriade, M., Nuñez, A., & Amzica, F. (1993c). Intracellular analysis of relations between the slow (< 1 Hz) neocortical oscillation and other sleep rhythms of the electroencephalogram. *J Neurosci*, *13*, 3266-3283.
- Steriade, M. (2001). Impact of network activities on neuronal properties in corticothalamic systems. *J Neurophysiol*, *86*, 1-39.
- Stern, E.A., Kincaid, A.E., & Wilson, C.J. (1997). Spontaneous subthreshold membrane potential fluctuations and action potential variability of rat corticostriatal and striatal neurons in vivo. *J Neurophysiol*, *77*, 1697-1715.

- Sun, F.T., Miller, L.M., Rao, A.A., & D'Esposito, M. (2007). Functional connectivity of cortical networks involved in bimanual motor sequence learning. *Cereb Cortex* 17, 1227-1234.
- Tognoli, E., & Kelso, J.A.S. (2009). Brain coordination dynamics: true and false faces of phase synchrony and metastability. *Prog Neurobiol* 87, 31-40.
- Vanhaudenhuyse, A., Noirhomme, Q., Tshibanda, L.J-F., Bruno, M-A., Boveroux, P., Schnakers, C., Soddu, A., Perlberg, V., Ledoux, D., Brichant, J-F., Moonen, G., Maquet, P., Greicius, M.D., Laureys, S., & Boly, M. (2010). Default network connectivity reflects the level of consciousness in non-communicative brain-damaged patients. *Brain* 133, 161-171.
- Veselis, R.A. (2001). Anesthesia--a descent or a jump into the depths? *Conscious Cogn* 10, 230-235.
- Vincent, J.L., Patel, G.H., Fox, M.D., Snyder, A.Z., Baker, J.T., Van Essen, D.C., Zempel, J.M., Snyder, L.H., Corbetta, M., & Raichle, M.E. (2007). Intrinsic functional architecture in the anaesthetized monkey brain. *Nature*, 447, 83-86.
- Vogels, T.P., Rajan, K., & Abbott, L.F. (2005). Neural network dynamics. *Annu Rev Neurosci*, 28, 357-376.
- Werner, G. (2007). Metastability, criticality and phase transitions in brain and its models. *Biosystems* 90, 496-508.
- Wu, L., Eichele, T., & Calhoun, V.D. (2010). Reactivity of hemodynamic responses and functional connectivity to different states of alpha synchrony: a concurrent EEG-fMRI study. *Neuroimage*, 52, 1252-1260.
- Wurtz, R.H., Goldberg, M.E. (1989). The neurobiology of saccadic eye movements. Amsterdam: Elsevier.
- Zhao, F., Zhao, T., Zhou, L., Wu, Q., & Hu, X. (2008). BOLD study of stimulation-induced neural activity and resting-state connectivity in medetomidine-sedated rat. *NeuroImage* 39, 248-260.

## Chapter 5 <sup>7</sup>

### 5 General discussion

“The greatest challenge today, not just in cell biology and ecology but in all of science, is the accurate and complete description of complex systems. Scientists have broken down many kinds of systems. They think they know most of the elements and forces. The next task is to reassemble them, at least in mathematical models that capture the key properties of the entire ensembles.” (Wilson, 1998, p. 85 as cited in Strogatz, 2001).

Early theoretical accounts of brain function emphasized aspects of localization and functional segregation, establishing the foundation of modern neuroscience. Current work, however, is now focusing extensively on the structural and functional interactions between brain areas – “reassembling” the individual elements within a complex network framework. The topology of nodes at multiple levels is not random, but organized according to an efficient topology that combines efficient local information processing with efficient global information integration. Emergent and nonlinear dynamics arise from this connectivity architecture and the multi-scale network organization facilitates all adaptive behavior and cognitive processing. Resting-state fMRI affords a non-invasive method capable of exploring the topology of functional brain networks and has revealed that the human brain is composed of multiple spatially distributed, but functionally linked brain regions referred to as resting-state networks (RSNs).

The identification of RSNs is only a preliminary step in elucidating the complex nature of human brain mechanisms. In addition to discovering the neural origins underlying the spontaneous activity measured with resting-state fMRI and quantification of disease-related changes in experimentally controlled animal models, comparative

---

<sup>7</sup> Portions of this chapter have been published in Hutchison, R.M., & Everling, S. (2012). Monkey in the middle: Why non-human primates are needed to bridge the gap in resting-state investigations. *Frontiers in Neuroanatomy*. *Under review*.

studies are needed to explore the evolution and generalizability of the RSNs' spatial and temporal properties. The present work represents the first step towards this goal.

The aim of the current thesis was to characterize the functional network architecture and dynamics of the rat and macaque brains using a methodology that could allow direct cross-species comparisons with humans. Assessment of potential large-scale homologies represents an essential step in the validation of rats and macaques as animal models that span multiple physiological and pathological uses. Chapter 2 and 3 examined the spatiotemporal characteristics of anesthetized rats and macaques, respectively, using RS-fMRI. ICA, an exploratory analysis technique, was utilized to reveal multiple independent functional networks, circumventing limitations associated with previous seed-based approaches. Using a network identified in Chapter 3, Chapter 4 investigated the role of cognitive processing in dynamic changes in functional connectivity of both macaques and humans. The results supported several hypotheses showing that functional relationships are: not static; not solely a consequence of conscious processes; and an evolutionarily preserved aspect of brain function.

## 5.1 Comparative biology

Beyond the intrinsic motivation to explore and classify species, comparative biology can reveal important insights into the evolution of brain organization. By determining which features are conserved across species it can indicate brain regions and patterns that have a basic functional and/or developmental role. The results can also help validate extrapolated findings derived from the use of animal models that afford a greater range of experimental manipulations not practical in humans. Different species, including humans, have evolved by a repeated branching of lineages. Comparative studies typically focus on evaluating the divergence and similarity of characteristics between species of different branches. Divergence is a specialization that has evolved and is unique to a species or grouping of species, for example, the language capabilities in humans. Similar characteristics typically fall within two categories: homologies and homoplasies (also referred to as analogies). A homologue is “the same organ in different animals under

every variety of form and function,” (Owen, 1843). This could, for example, describe a bat's wing and a human hand that have a common underlying structure of bones and muscles. A homoplastic structure is “a part or organ in one animal that has the same function as another part or organ in a different animal” though the similarities between organisms are not present in the last common ancestor of the taxa being considered, but rather are the result of parallel or convergent evolution (Owen, 1843). An example of a homoplastic trait would be the wings of a bat and a butterfly.

Rats and primates diverged over 80 million years ago and the last common ancestor of humans and macaques dates back to more than 25 million years ago (Fig. 5.1, top). Determining the relationships among cortical areas and networks between these species can be difficult because they differ in both brain (Fig. 5.1, bottom and Fig. 5.2) and body size, the relationship of which is nonlinear (Van Dongen, 1998). Over this duration, brain regions could duplicate, fuse, reorganize, or expand, changing the proportions of different regions as well as its microstructure and connectivity (Hill et al., 2010; Sereno & Tootell, 2005). It is these changes that are believed to be related to the extensive differences in behavioural and cognitive capacities between the three species. The task of comparison is made more difficult because the measurement techniques are often different between species. RS-fMRI circumvents this final limitation and provides a more direct tool for cross-species comparisons

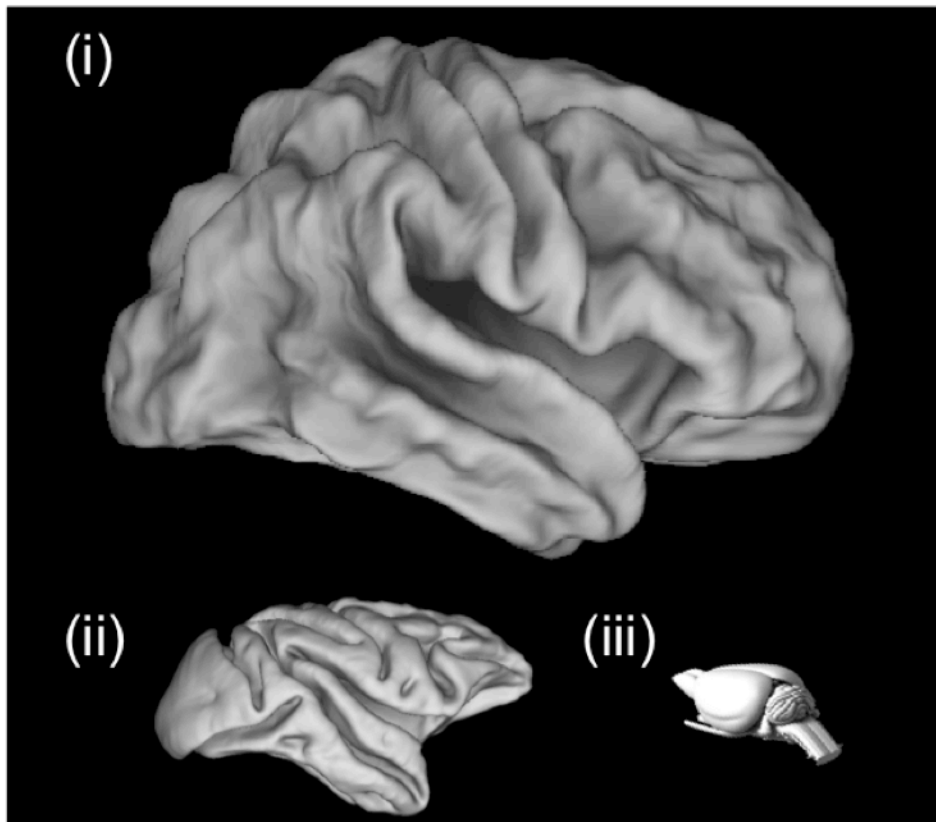
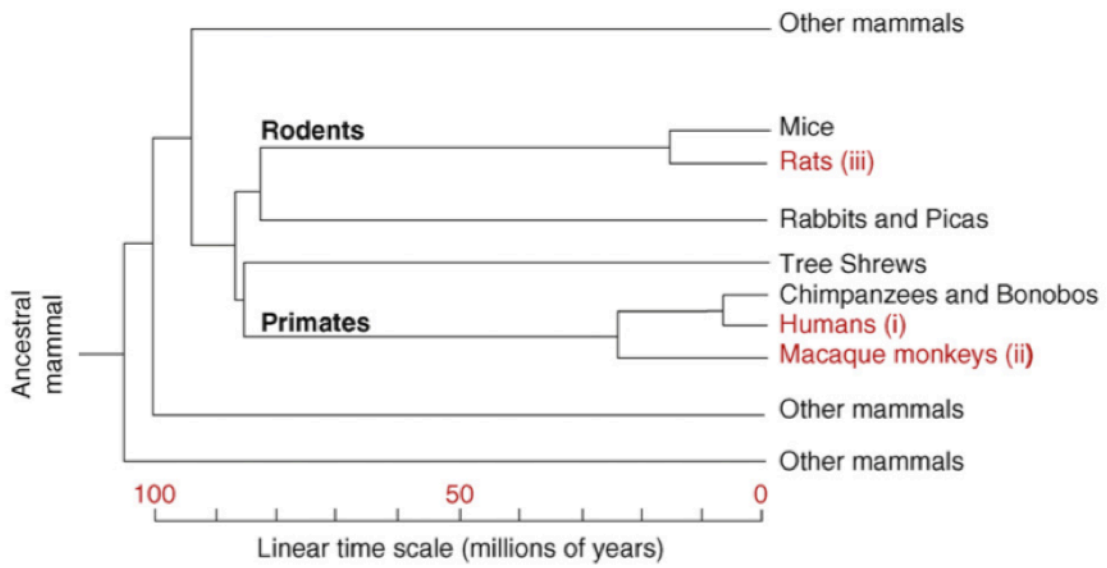


**Figure 5.1.** Simplified cladogram of mammals, indicating the divergence times of selected groups. Time scale in millions of years before the present. The encephalization quotient indicates the deviation of the brain size of a species from brain size expected on the basis of a 'standard' species of the same taxon, in this case of the cat. Modified with permission from Wise, 2008. The bottom panel displays the cortical surfaces of the highlighted species.

Animal taxa	Brain weight (in g) <sup>a</sup>	Encephalization quotient <sup>b,c</sup>	Number of cortical neurons (in millions) <sup>d</sup>
Whales	2600–9000	1.8	
False killer whale	3650		10 500
African elephant	4200	1.3	11 000
Man	1250–1450 <sup>e</sup>	7.4–7.8	11 500
Bottlenose dolphin	1350	5.3	5800
Walrus	1130	1.2	
Camel	762	1.2	
Ox	490	0.5	
Horse	510	0.9	1200
Gorilla	430 <sup>e</sup> –570	1.5–1.8	4300
Chimpanzee	330–430 <sup>e</sup>	2.2–2.5	6200
Lion	260	0.6	
Sheep	140	0.8	
Old world monkeys	41–122	1.7–2.7	
Rhesus monkey	88	2.1	480
Gibbon	88–105	1.9–2.7	
Capuchin monkeys	26–80	2.4–4.8	
White-fronted capuchin	57	4.8	610
Dog	64	1.2	160
Fox	53	1.6	
Cat	25	1.0	300
Squirrel monkey	23	2.3	480
Rabbit	11	0.4	
Marmoset	7	1.7	
Opossum	7.6	0.2	27
Squirrel	7	1.1	
Hedgehog	3.3	0.3	24
Rat	2	0.4	15
Mouse	0.3	0.5	4

**Figure 5.2. Brain weight, encephalization quotient and number of cortical neurons in selected mammals.** Modified with permission from Roth & Dicke, 2005. Data calculated from Jerison, 1973; Russell, 1979; Haug, 1987.

## 5.2 Homologous connectivity patterns

The analysis of the networks of the rat using RS-fMRI in Chapter 2 revealed multiple networks composed of contralateral homologues (Fig. 2.1). The implication of which is that the synchronous hemodynamic fluctuations are reflecting ongoing electrical synchronization between the areas with similar functional attributes. This finding has since been reproduced in awake (Liang, King, & Zhang, 2011) and medetomidine-anesthetized (Jonckers, Van Audekerke, De Visscher, Van der Linden, & Verhoye, 2011); Fig. 5.3) rats. Similar network topology in what may be regarded as lower-order networks has also been observed in mice (Jonckers et al., 2011) and songbirds (Jonckers, Denolf, De groof, & Van der Linden, 2011b). Primates show similar patterns for sensory and motor networks (Fig. 5.4) and interhemispheric synchronization is also evident in newborn infants (Fransson et al., 2007; Gao et al., 2009). Taken together the results suggest that interhemispheric synchronization of LFFs is phylogenetically preserved across all mammalian species and may underlie a rudimentary aspect of brain function. As discussed in Chapter 2, coherent integration of cognition and behavior is dependent upon constant inter-hemispheric communication (Compton, 2002). This is especially critical for creating a unified representation of world (Houzel, Carvalho, & Lent, 2002), movement coordination (Gerloff & Andres, 2002), attentional processing (Banich, 1998), pooling processing resources (Liederman, 1998), and parallel processing (Compton, 2002).

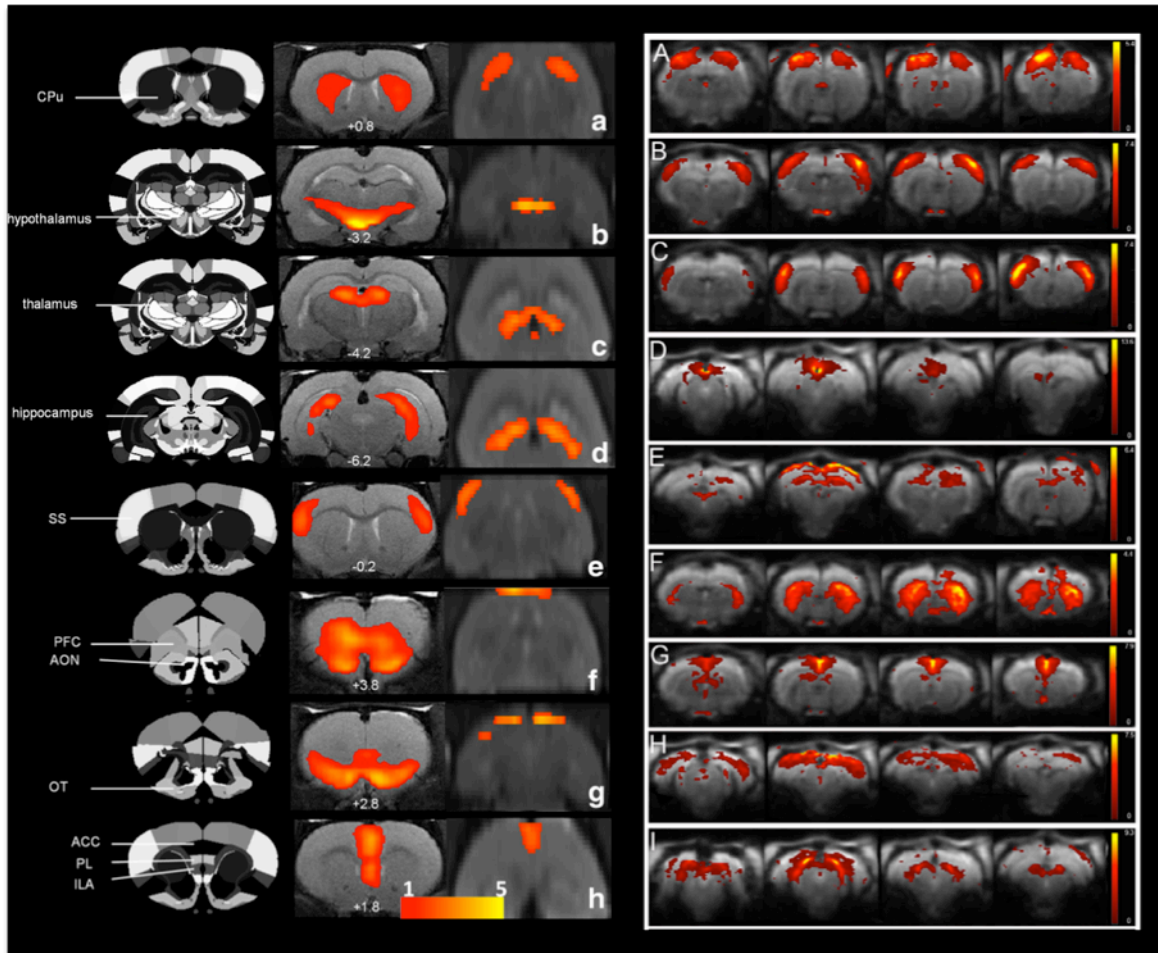


**Figure 5.3. Resting-state networks of the awake (left column) and medetomidine-anesthetized (right column) rat.** Both studies utilized ICA to show bilaterally homologous networks through cortical and subcortical structures. Reproduced with permission from Liang et al., 2011; Jonckers et al., 2011.

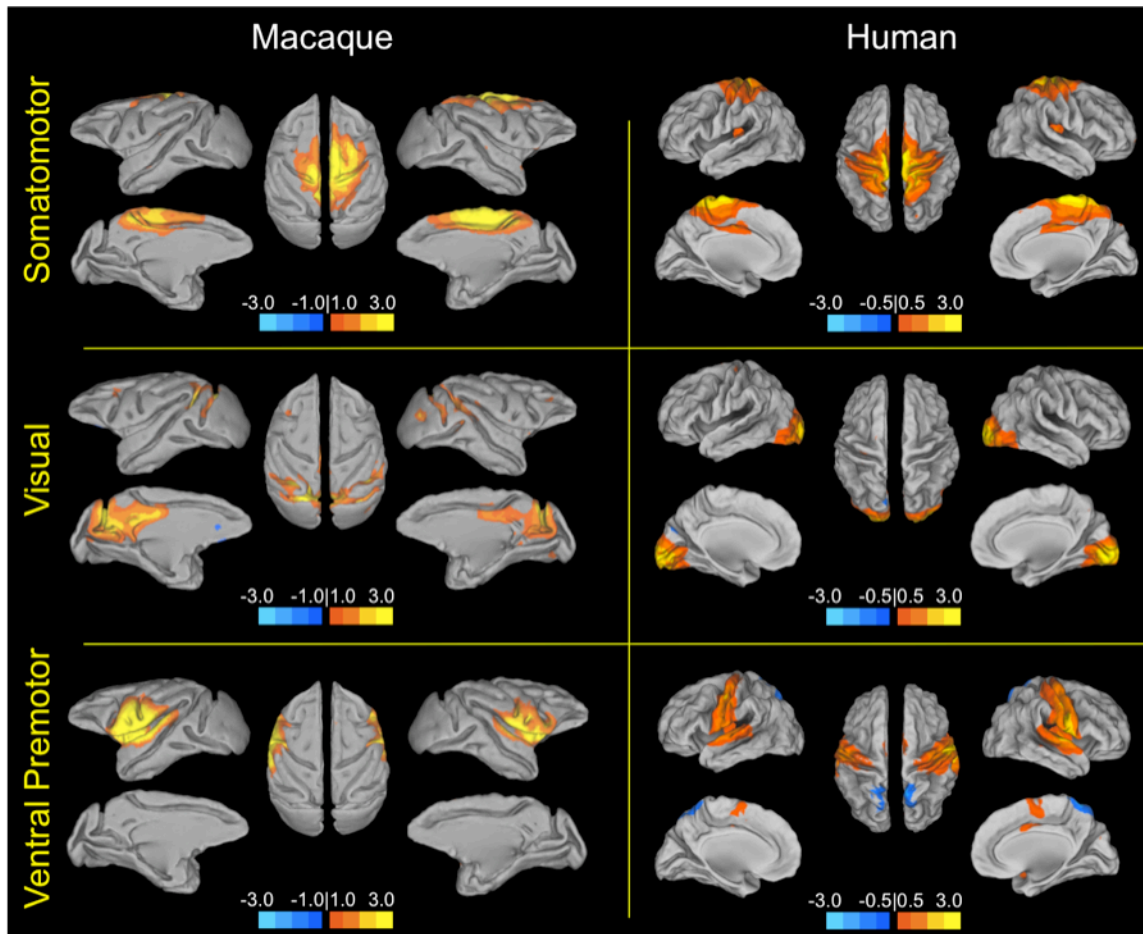


**Figure 5.4. Sensory and motor resting-state networks of the macaque (left column) and human (right column) showing connectivity between bilateral homologues.** Macaque networks reproduced with permission from Hutchison et al., 2011a. Human connectivity maps (N = 12) derived from ICA of Chapter 4 data.

The importance of interhemispheric communication is further highlighted when examining disease states. For example, when compared with normal controls or language-delayed subjects, children with autism show significantly weaker RS-fMRI interhemispheric correlations across multiple bilateral homologues including the inferior frontal gyrus and superior temporal gyrus - areas associated with language production and comprehension (Dinstein et al., 2011). Further, the strength of interhemispheric synchronization is positively correlated with verbal ability and negatively correlated with autism severity. This allowed the authors to identify autistic children with a sensitivity and specificity of 72% and 84%, respectively suggesting that weak interhemispheric neural synchronization is a notable characteristic of autism. The cause of the connectivity disruption remains to be determined, but the authors suggest that it could result from a combination of “abnormal [structural] connectivity, synaptic function, excitation-inhibition balance, local neural network structure/function, and so forth” (Dinstein et al., 2011).

Thus far, most of the reported RSNs of the rat (as well as mice and songbirds) have been primarily limited to connections between interhemispheric homologues, particularly when examined using ICA. Seed region analysis has revealed more distributed networks though these are typically much “noisier” and do not share the same level of robustness and reproducibility as observed in the distributed networks seen in both humans and macaques. Liang and colleagues (2011) have applied graph metrics to examine inter-RSN topology, revealing a broad grouping of the rat RSNs into clusters /modules (Fig. 5.5A). These were classified as 1) a cortical ribbon module that included bilateral dorsal olfactory bulb, motor cortex, somatosensory cortex, insular cortex, and visual cortex (Fig. 5.5B); 2) a module comprising the olfactory system, PFC, ACC, CPu, posterior somatosensory cortex, thalamus, hypothalamus, hippocampus, and auditory cortex that the authors speculate is involved in the integration of sensory input, cognitive processing, and output (Fig. 5.5C); and 3) a limbic/autonomic module consisting of the PFC, insular cortex, amygdala, hypothalamus, and auditory cortex (Fig. 5.5D).

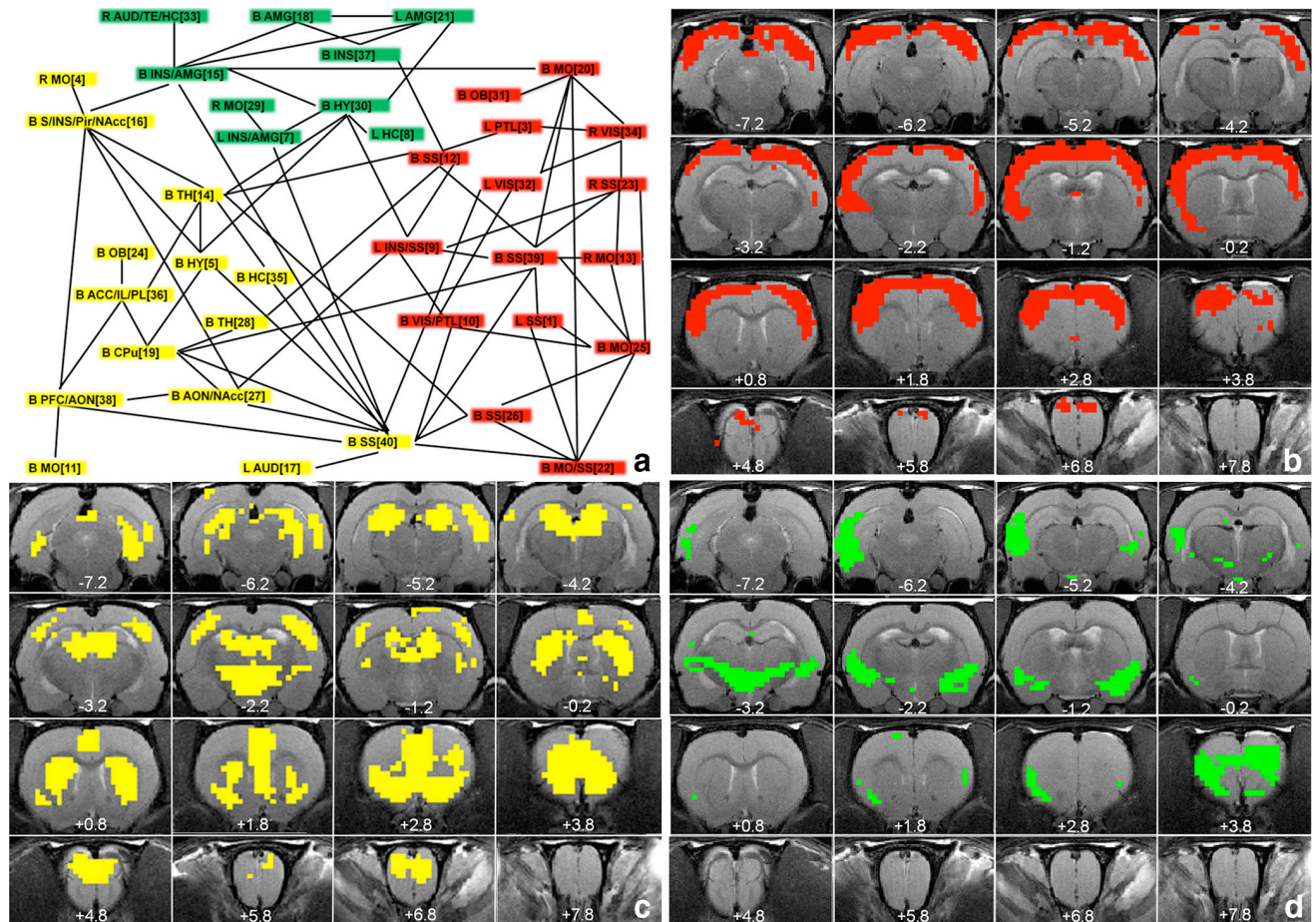


**Figure 5.5. Segregation of the whole-brain network of the awake rat brain.** a, The global functional network constructed based on significant intercomponent connections. Each colored box represents an ICA component labeled with its corresponding anatomy and the ICA number. Each line represents a significant connection between two components. Nodes within the same module are displayed in the same color (red, green, and yellow). Three modules were obtained by the spectral partitioning algorithm. B, Bilateral; L, left; R, right; AMG, amygdala; INS, insula; NAcc, nucleus accumbens; MO, motor cortex; HC, hippocampus; HY, hypothalamus; OB, olfactory bulb; Pir, piriform cortex; PTL, parietal cortex; S, septum; TE, temporal cortex; TH, thalamus; VIS, visual cortex. b– d, Community structures of the whole-brain network revealed by spectral partitioning. b, The first module is dominated by cortical ribbon. c, The second module is highlighted by the olfactory pathway and its interaction with PFC, and the integration of other sensory input, cognitive processing, and output in cortical and subcortical regions like thalamus and hippocampus. d, The third module includes regions important for emotional and autonomic functions such as amygdala, insular cortex, PFC, and hypothalamus. The same colors are used in b, c, and d as those in a. Distance to bregma (in millimeters) is labeled at the bottom of each image. Reprinted with permission from Liang et al., 2011.

The organization of the RSNs into modules, however, is still a far departure from the distributed within network connectivity seen in primate species. RSNs of humans and macaques are much more spatially distributed across cortical and subcortical areas. Even the aforementioned bilateral sensory and motor networks tend to encompass larger extents of cortex and in humans, multiple discrete functional and anatomical areas (e.g. Fig. 5.4, cingulate connectivity in human premotor RSN). Many task-based studies of rats also do not report networks beyond uni- or bilateral activation of specific areas though there have been reports of more distributed task- and electrically- evoked networks (Zhao, Zhao, Zhou, Wu, & Hu, 2008). Therefore, it appears that the minimal synchronization across multiple structures in the rat brain could reflect limited ongoing “higher-order” processing such as spontaneous cognition or predictive processing (further discussed in section 5.4) and represent a less evolved form of network topology.

### 5.2.1 Fronto-parietal networks

Homologous networks between macaques and humans are described in Chapter 3 and some of these networks are directly compared in Fig. 5.6 (with putative functional labels). Apparent is the presence of lateralized, fronto-parietal networks in the human whose potential homologue in the macaque is symmetric. The networks have been implicated in cognitive attentional and oculomotor processes as well as memory and language functions (Beckmann et al., 2005; Jafri et al., 2008; Smith et al., 2009). The asymmetry in correlation patterns between left and right hemispheres might reflect stronger lateralization in humans than in monkeys. This is consistent with the general evolution to increased functional specialization in humans. Recently, event-related fMRI showed strong contralateral activations in monkeys, which were significantly weaker in putative human homologues, while the asymmetry between the hemispheres was stronger (Kagan, Iyer, Lindner, & Andersen, 2010). Fronto-parietal connectivity was further explored in a seed-region analysis of the same human and monkey data set (Hutchison et al., 2012b). As expected, there were consistent ipsilateral functional connections of the frontal eye fields with fronto-parietal cortical areas across both species. These included the intraparietal sulcus, dorsolateral prefrontal cortex, anterior cingulate cortex, and

supplementary eye fields (Fig 5.7). The use of cortical surface-based transformation of connectivity maps between species further corroborated the remarkable ipsilateral organization of the FEF functional connectivity (Fig. 5.8). The analysis also revealed greater lateralization of connectivity with the FEF in both hemispheres in humans than in monkeys, corroborating the findings of the ICA. Overall, the results indicate an evolutionarily preserved fronto-parietal system, but also presents the opportunity to investigate the evolutionary predecessor of the lateralized human networks

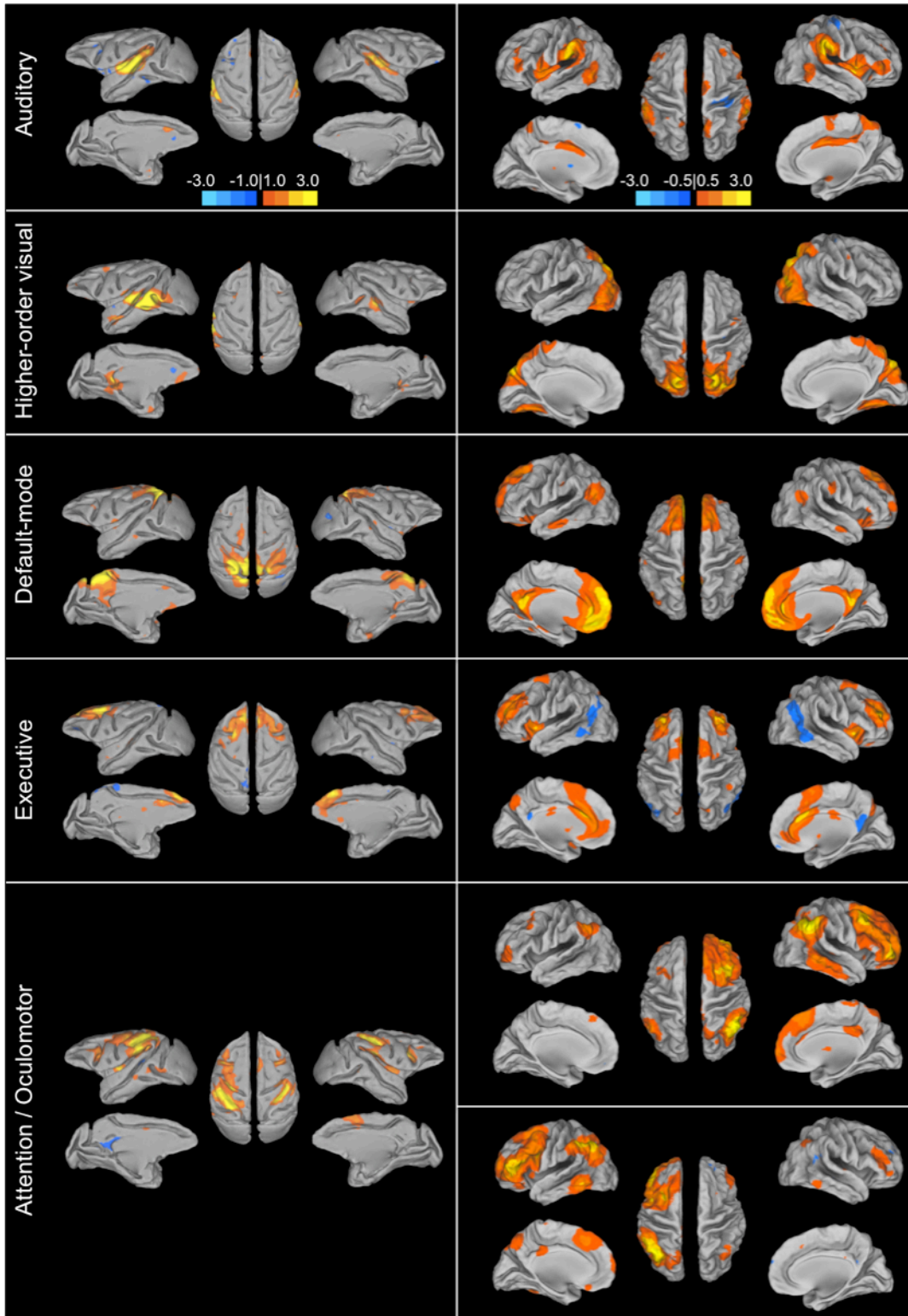


**Figure 5.6. Homologous higher-order resting-state networks of the macaque (left column) and human (right column).** Putative functional roles of the networks are indicated on the left. Macaque networks modified with permission from Hutchison et al., 2011a. Human connectivity maps (N = 12) derived from ICA of Chapter 4 data.

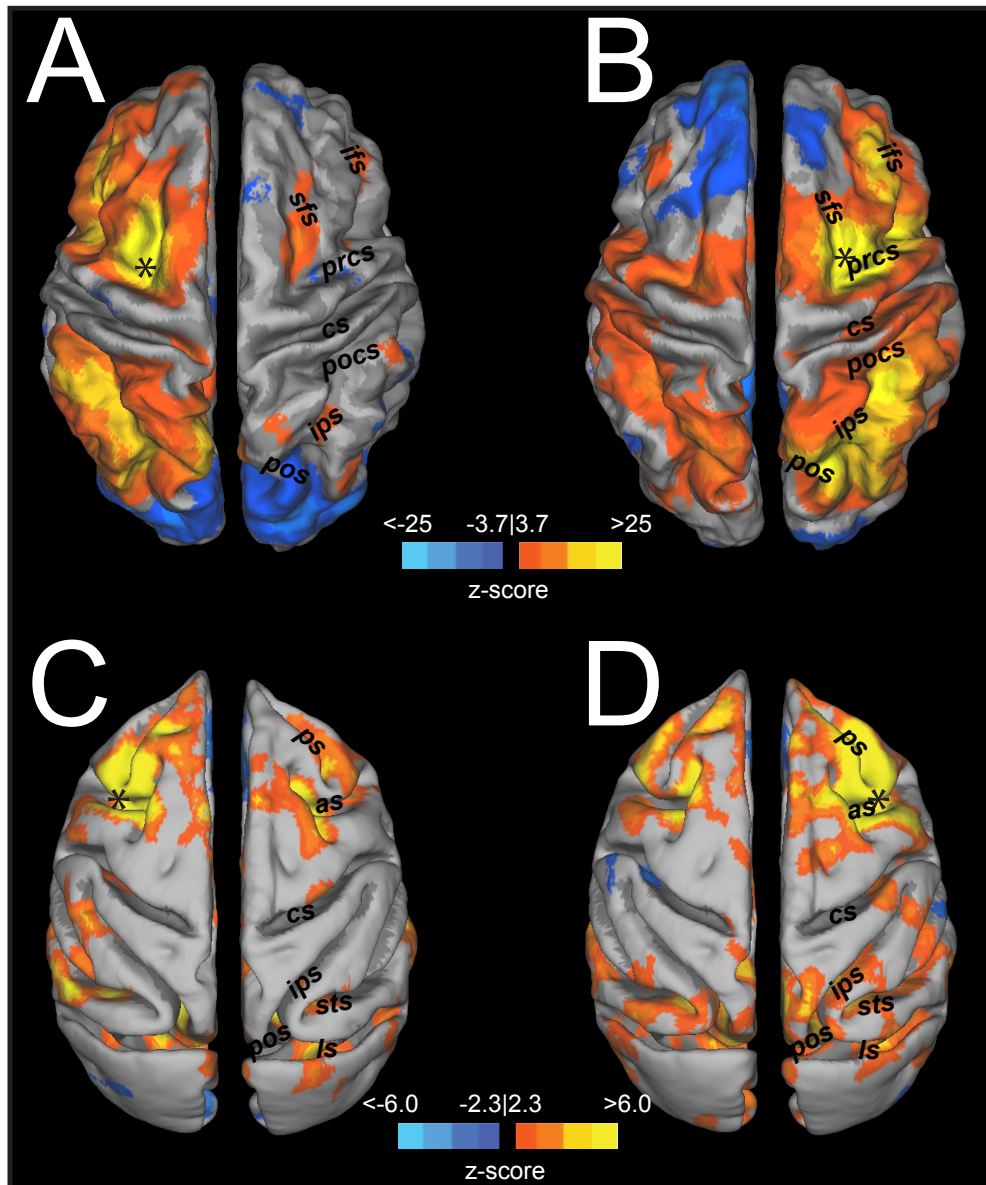


**Figure 5.7. Bilateral functional connectivity of FEF seeds in humans (A,B) and macaque monkeys (C,D).** Dorsal view of the left and right hemisphere in humans ( $N = 12$ ) for left (A) and right (B) hemisphere seeds. Thresholded z-score maps normalized to the space of the PALS-B12 template (Van Essen 2005) are overlaid. Dorsal view of the left and right hemisphere in macaques ( $N = 6$ ) for left (C) and right (D) hemisphere seeds. Thresholded z-score maps normalized to the space of the F99 template (Van Essen 2004) are overlaid. Note that the thresholded z-scores differ between human and monkey maps. Black asterisks indicate the location of the FEF seeds. as, arcuate sulcus; cs, central sulcus; ifs, inferior frontal sulcus; ls, lunate sulcus; mfs, middle frontal sulcus; pos, parieto-occipital sulcus; pocs, posterior central sulcus; prcs, precentral sulcus; ps, principal sulcus.; sfs, superior frontal sulcus; sts, superior temporal sulcus.. Reprinted with permission from Hutchison et al., 2012b.

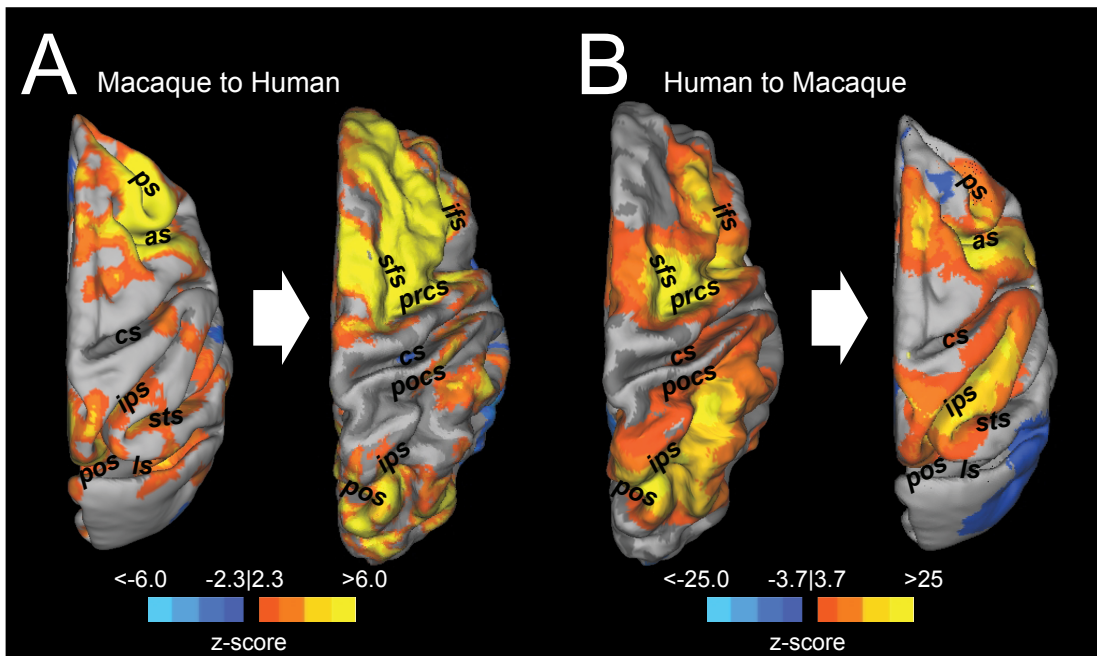


**Figure 5.8. Registration of resting-state functional connectivity maps between macaques and humans.** (A) Dorsal view of the macaque (left) and human (right) cortical surface. Superimposed are the thresholded z-score maps of macaques normalized to the F99 macaque brain (left) and transformed to the space of the human PALS-B12 template (right). (B) Dorsal view of the human (left) and macaque (right) cortical surface. Superimposed are the thresholded z-score maps of humans normalized to the PALS-B12 human template (left) and transformed to the space of the F99 macaque template (right). as, arcuate sulcus; cas, calcarine sulcus; cs, central sulcus; ifs, inferior frontal sulcus; lus, lunate sulcus; mfs, middle frontal sulcus; pos, parieto-occipital sulcus; pocs, posterior central sulcus; prcs, precentral sulcus; ps, principal sulcus; sfs, superior frontal sulcus; sts, superior temporal sulcus. Reprinted with permission from Hutchison et al., 2012b.

The results also highlight an important distinction between ICA and seed based approaches. The left and right human FEF maps closely resemble the left- and right-lateralized fronto-parietal networks revealed using ICA (Beckmann, DeLuca, Devlin, & Smith, 2005; Damoiseaux et al., 2006; Jafri, Pearlson, Stevens, & Calhoun, 2008; Liao et al., 2009; van den Heuvel, Mandl, & Hulshoff Pol, 2008). However, the networks are not identical and positively connected areas such as the central sulcus, postcentral sulcus, and precuneus are not included in the ICA lateralized networks even when ICA is applied to the current human data set (Fig. 5.7). Negatively connected areas are also absent. When ICA was applied to the current macaque data (Chapter 3), multiple independent resting-state networks were found including a bilateral fronto-parietal network. Similar to what was observed in human subjects, the seed-based FEF network also encompassed regions associated with other resting-state networks such as the precentral-temporal and posterior-parietal networks including the precuneus. Negative correlations were again absent. A direct comparison of group ICA-derived and seed-based connectivity measures is not straightforward, owing to the differences in preprocessing (prewhitening and dimensionality reduction versus confound regression) and their underlying theory (Joel, Caffo, van Zijl, & Pekar, 2011). ICA also requires a prediction about the number of underlying sources in the data and increasing this model order can split a network into smaller sub-networks (Abou-Elseoud et al., 2010; Smith et al., 2009). Therefore, ICA and seed-based RS-fMRI analysis are both useful in examining RS-fMRI functional connectivity but differ in the types of questions they can answer.

### 5.2.2 Default-mode network

The most commonly investigated and perhaps most controversial network is the default-mode network (DMN). In humans, it bilaterally encompasses the posterior cingulate (PCC) / retrosplenial cortex (Rsp) / precuneus (PGm), ventral and dorsal medial prefrontal cortex, inferior parietal lobule, lateral temporal cortex, and hippocampal formation (see Fig. 5.6). The DMN reduces its activity during goal-directed behavior and has been implicated in a range of functions including self-referential thought, both internal and external monitoring, memory consolidation, supporting consciousness, and

daydreaming, among others (Mason et al., 2007; Raichle and Snyder, 2007; Buckner et al., 2008, 2008). Given its potential role in oft-labeled “human” processes, assessing its presence in other species is of great interest.

Most resting-state investigations using seed-based or ICA approaches have not reported a potential homologue for the DMN in the rat. Recently, however, two separate reports have supported a DMN-like network in the rat brain (Upadhyay et al., 2011; Lu et al., 2012). Both of these studies converged on a similar, though not identical topology patterns. Upadhyay and coworkers found that a seed placed in the anterior cingulate cortex of awake animals showed bilateral connectivity with Rsp/PCC, parietal cortex, and the hippocampus. Lu et al., using ICA of anesthetized rats (dexmedetomidine and isoflurane), found a network comprising bilateral orbital, prelimbic, cingulate (Cg1/Cg2), retrosplenial cortex, rostral, and dorsal posterior parietal cortex, perirhinal, entorhinal and temporal association cortical regions (TeA) as well as the hippocampus. Many of the structures are the same between studies though notably absent in the published study by Upadhyay et al. is the occipital and prelimbic cortex, thought to be rat representations of the prefrontal cortex.

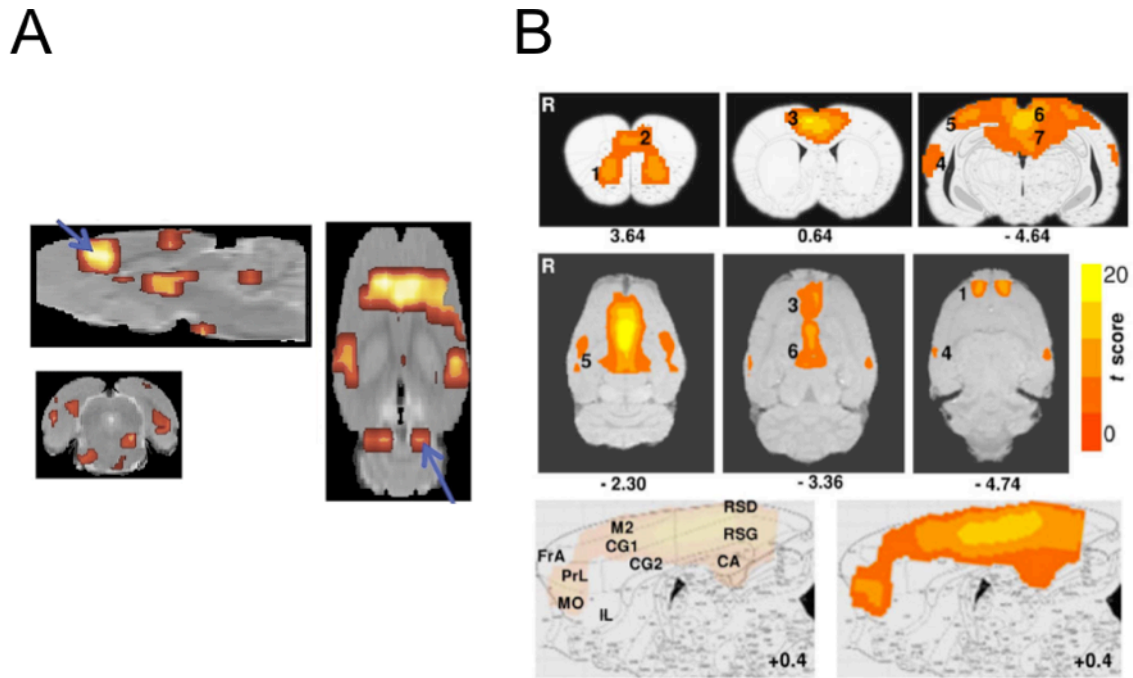


**Figure 5.9. Potential default-mode network homologue in (A) awake and (B) anesthetized rats.** Modified with permission from (A) Upadhyay et al., 2011); (B) Lu et al., 2011.

These results raise a number of interesting questions. Could this network represent a precursor to the primate DMN? What is its functional role? Before these questions can be addressed it will first be essential to determine the validity of these findings. It is unclear why previous reports did not reveal the same network when using ICA at multiple model orders at single and group levels. As mentioned, a distributed network at rest is also not typical of most reported RSNs in rat investigations. Finally, by definition, the DMN activity should decrease during task performance and this functional role will have to be addressed.

The identification of a DMN in nonhuman primates remains equivocal, though a rough consensus is beginning to emerge (Fig. 5.10). Vincent and colleagues first reported a potential candidate for a homologous macaque DMN (Fig. 5.10A). An anatomically placed seed in the posterior midline encompassing areas of the PCC (areas 23 and 31) and a portion of the PGm (area 7m) of isoflurane anesthetized macaques was found to be functionally connected with lateral temporoparietal cortex (including area 7a and superior temporal gyrus) and posterior parahippocampal cortex. There were also strong correlations with the dorsal medial prefrontal cortex (dmPFC; area 9) though there is considerable overlap with the anterior cingulate cortex (area 24c). Using the same dataset, Margulies and colleagues showed that the heterogeneous features of the posteromedial cortex could be revealed using RS-fMRI and that connectivity profiles are greatly dependent upon the selection of the seed region within its individual subunits (Rsp. PCC, PGm) (Margulies et al., 2009). Seeds restricted to the PCC (area 23/31) most closely resembled that of the previous study and possessed characteristic human DMN nodes (Fig. 5.10B). There were however, notable differences as the ventral medial PFC (vmPFC; areas 10m, 32, and 14r), dorsolateral prefrontal cortex (dlPFC), and inferior parietal lobule were functionally connected to the PCC seed where as lateral temporoparietal cortex and hippocampal formation connectivity were absent. Their results also advanced the idea that the PGm is not in fact a component of the DMN (Buckner et al., 2008). A third study of the same isoflurane anesthetized monkeys using a PCC/Rsp seed defined from a posterior parahippocampal cortex (PPHC) connectivity map revealed a combination of areas from the previous studies albeit with limited dlPFC connectivity (Vincent et al., 2010); Fig. 5.10C). A separate seed-region based

investigation of three isoflurane anesthetized macaques did not corroborate the potential homologous cortical areas as medial frontal, dorsal frontal and hippocampal regions were absent from a posteromedial cortex seed (Teichert et al., 2010); Fig. 5.10D). Given the dependency on the seed location shown in the aforementioned studies - a finding that has been observed in humans (Cole et al., 2010) - it is possible the seed encompassed a large proportion of the PGM.

To avoid the constraints of seed selection, we followed in the path of many human investigations and implemented ICA with a low model order (Chapter 3; (Hutchison et al., 2011a). The closest qualitative component matching a potential DMN homologue contained the PGM with some extension into the PCC, areas PG and PE of the parietal cortex, and unilateral vmPFC (area 14r and 10m) and ACC area 24a/c (Fig. 5.10E). Given the previous results and significant portions of the DMN architecture that are missing, this more likely reflects a combination of the PGM sensorimotor and cognitive networks (Margulies et al., 2009). To rule out issues with the quality of our data or confound variables, we have since placed a midline spherical seed (radius = 1.5 mm) in the PCC (area 23/31). The results show homologous areas across all nodes of the human DMN (Hutchison et al., unpublished data; Fig. 5.10F) and taken with the other studies most likely represents the full DMN homologue of the macaque. Future investigation and application of ICA will be necessary to explain why this DMN component does not emerge in either group or single subject ICA (Moeller et al., 2009; Hutchison et al., 2011a) as it is very robustly identified in human studies.

Most recently, a meta-analysis of fMRI data collected from ten awake monkeys performing tasks showed a network of regions that decreased in activity when the task demands shifted from a passive task to externally oriented processing (Mantini et al., 2011) – a defining feature of the human DMN. The network included medial, cingulate, parietal, and prefrontal regions (Fig. 5.10G) that demonstrate substantial spatial overlap with our PCC seed-based network with the exclusion of lateral temporoparietal cortex and the hippocampal formation. The findings further corroborate this as the monkey equivalent of the human DMN. It is important to consider that within the same paper however, seeding areas within nodes of the network in awake fixating monkeys (N = 4)

did not reproduce the identical network, though seeding the area 31 produced the closest qualitative match (Fig. 5.10H). Taken together, there does seem to be a general consensus as to a homologous DMN and its components in the macaque that can be revealed with resting-state approaches. For it to become a dependent variable in experimental manipulations, future work examining both physiological and methodological variables will be needed to explain the lack of robustness within and across studies.

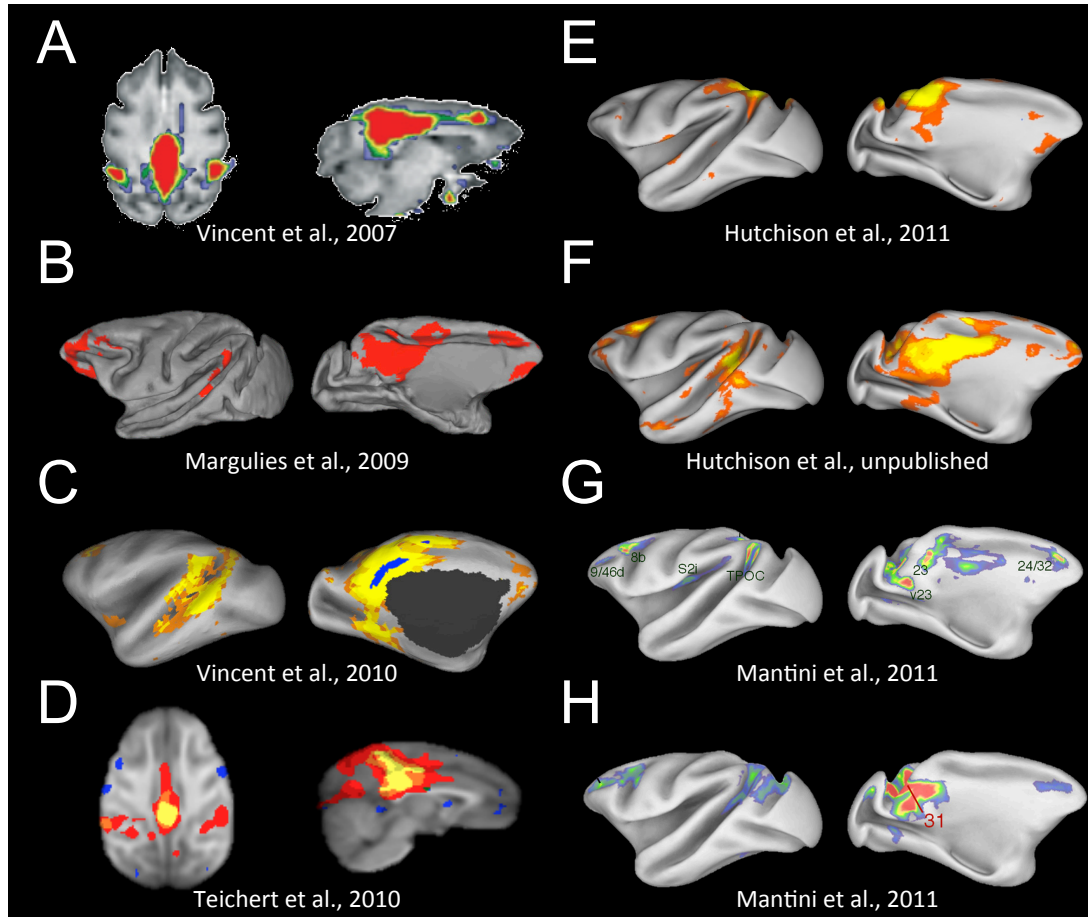


**Figure 5.10. Potential default-mode network homologue of the macaque across multiple studies.** See text for description. Modified with permission from (A) Vincent et al., 2007; (B) Margulies et al., 2009; (C) Vincent et al., 2010; (D) Teichert et al., 2010; (E) Hutchison et al., 2011; (F) Hutchison et al., 2011; (G,H) Mantini et al., 2011. Reproduced with permission from Hutchison & Everling, 2012.

### 5.2.3 Expanding network investigations

The examination of functional homologous connectivity patterns between species with RS-fMRI is not limited to the comparison of the 8-10 most commonly reported networks as these primary RSNs do not represent the extent of large-scale networks in the human or nonhuman primate brain. Unique connectivity profiles have been reported when using both hypothesis driven (Krienen and Buckner, 2009; Vincent et al., 2010; Mars et al., 2011) and exploratory (Damoiseaux et al., 2006; Moeller et al., 2009; Liao et al., 2009; Hutchison et al., 2011a) techniques. RS-fMRI offers an excellent opportunity to examine functional subunits or parcellation within structures. As mentioned above, distinct patterns of functional connectivity were demonstrated within the posteromedial cortex of both species, with each subdivision suggesting a discrete functional role (Margulies et al., 2009). A similar analysis procedure has been used to delineate subdivisions of the ACC. Margulies and coworkers (2007) placed spherical seeds throughout the caudal, rostral, and subgenual ACC in human subjects (Fig. 5.11, left panel). They found that posterior seeds were positively correlated with cortical motor-related areas and anti-correlated with posterior and subgenual cingulate. More anterior seeds showed strong positive correlations with PPC and dlPFC. The ventral ACC was positively correlated with insular cortex. These functional connectivity patterns were consistent with the popular model that proposes a distinction between a dorsal cognitive and a ventral affective ACC subdivision (Bush et al. 2000). Recently, we performed a similar analysis in macaque monkeys and humans (Hutchison et al., 2011b); Fig. 5.11). We found that the functional connectivity of the ACC varied systematically along the rostral/caudal and dorsal/ventral axis, thereby confirming previous anatomical tracer and lesion studies in monkeys (Pandya et al. 1981; Vogt and Pandya 1987; Barbas et al. 1999; Rudebeck et al. 2006). We were able to delineate several subdivisions and identified separate primary networks within the ACC. The functional connectivity maps of individual seeds showed a remarkable similarity with those found by Margulies et al. (2007) in humans. In particular, we were able to identify macaque ACC seeds that corresponded to the motor, cognitive, and limbic subdivisions (Fig. 5, right panel). These two studies demonstrate that RS-fMRI is a useful tool for comparative mapping of brain networks in humans and non-human macaques.

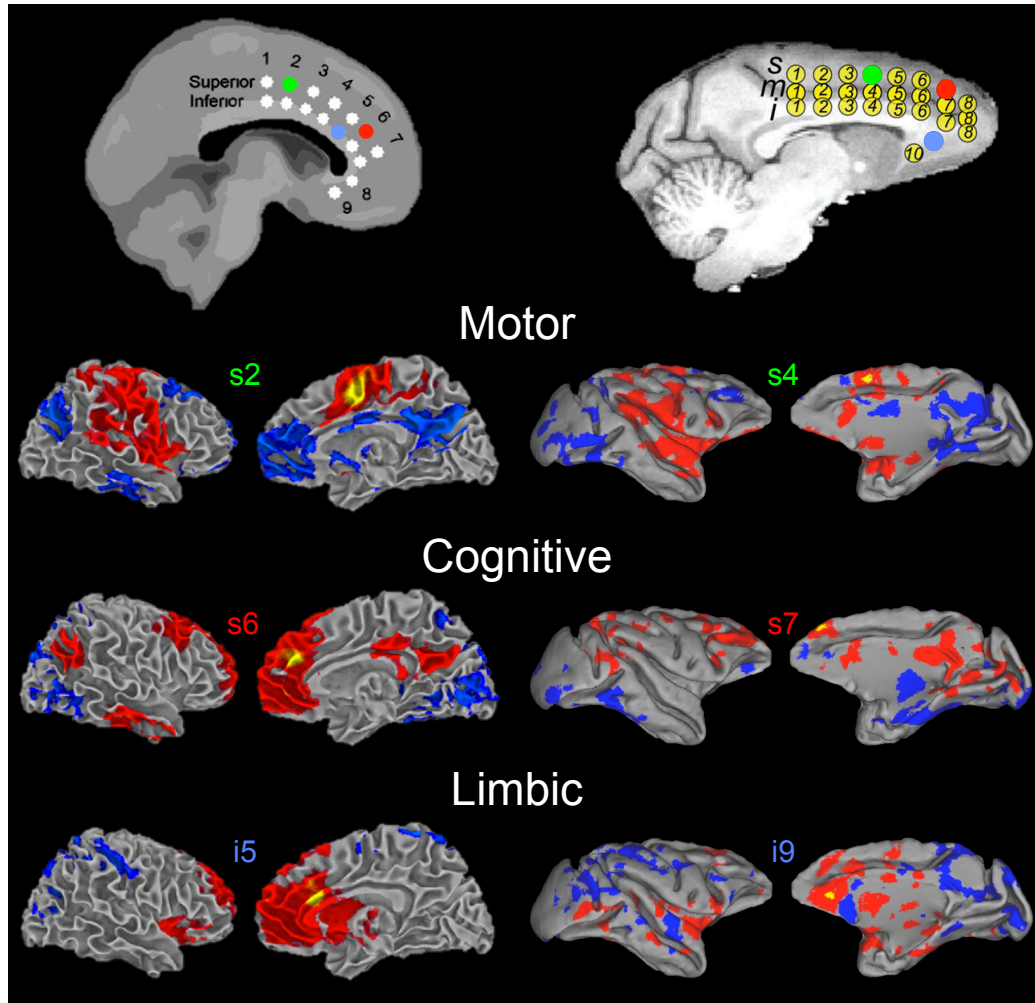


**Figure 5.11. Homologous functional subdivisions of the anterior cingulate cortex.** Functional connectivity profiles of seed regions within the anterior cingulate cortex are shown for the human (left column) and macaque (right column). Seed locations are shown on the standard MNI and F99 brains for the humans and monkeys, respectively (top). Putative functional roles are labeled. Modified with permission from Margulies et al., 2007; Hutchison et al., 2011b. Reproduced with permission from Hutchison & Everling, 2012.

## 5.2.4 Summary of comparative biology

The brain topology of a species is the product of evolutionary changes driven by a diverse range of internal and external selection pressures. Universal properties commonly emerge such as high efficiency of information transfer for low physical connection cost found in small world networks (Bullmore & Sporns, 2009; Sporns, 2010) are good examples. That is not to say that all brains are organized in the same fashion. The specific development and arrangement of neurons across multiple scales vary greatly between species that are not simply a product of increased size. The conclusions of the present thesis in regards to homologous organization is that as brain complexity increases, bringing with it a more diverse repertoire of cognitive and behavioural states, new RSN topology develops (Fig. 5.12). All three species examined demonstrate robust interhemispheric communication and this seems to represent the most fundamental large-scale network structure. More sentient species such as the macaque and human show distributed networks encompassing multiple brain areas beyond contralateral homologues. Hierarchical evaluation of such networks does however, show that the homologous structures are most strongly connected and can represent subsystems within the larger network. Presumably these networks, whose cost in terms of wiring and development is high, evolved to facilitate greater information integration, and computation. At the highest complexity level, humans demonstrate robust lateralization of the distributed fronto-parietal RSNs, a property not found in non-human primate species and suggests that this specialization is a further adaption necessary for human-specific behaviours such as language. Taken together, the results suggest that RS-fMRI is well suited for the examination of the evolution of brain networks and evaluation of homologies between species. Within the networks examined, both rats and monkeys can provide suitable models to address research questions not possible in humans though the appropriate level of network complexity must be taken into consideration.

	Bilateral RSNs	Distributed RSNs	Lateralized RSNs
Humans	●	●	●
Macaques	●	●	
Rats	●		

Figure 5.12. Summary of findings.

### 5.3 The relationship between function and structure revisited

As outlined in the introduction (Section 1.7.4), there are a number of open questions regarding the potential relationship between functional connectivity, measured as the temporal relationships between brain regions, and the underlying structural connectivity that represents the anatomical white matter fiber tracts. Simulated and empirical investigations of humans have suggested an overall good correspondence between the two (Damoiseaux & Greicius, 2009; Greicius, Supekar, Menon, & Dougherty, 2009), although clear discrepancies have emerged. The few case studies examining congenital or surgical alteration of the callosal fiber connections have also produced mixed results (Johnston, Vaishnavi, et al., 2008; Quigley et al., 2003; Tyszka, Kennedy, Adolphs, & Paul, 2011; Uddin et al., 2008). There are two limiting factors when using human subjects that will prevent an adequate understanding of the relationship and as such the issue will have to be addressed with an animal model. The first is that thus far, most empirical studies have examined structural connectivity derived from diffusion MRI methodologies (Greicius et al., 2009; Hagmann et al., 2008; Honey et al., 2009). These techniques can provide evidence about major white matter pathways, but methodological limitations do not allow precise delineation of the origins, crossings, and terminations of pathways, thereby restricting the interpretation of results. Invasive tracer studies carried out in non-human primates remains the gold standard for uncovering the precise information concerning the origins and terminations of white matter connections. The first qualitative comparisons of functional resting-state connectivity maps and structural connectivity maps derived from experimental tracer studies in the macaque demonstrated remarkable consistency between the patterns (Margulies, Vincent, et al., 2009; Vincent et al., 2007), Fig. 5.13). In fact, the finding of the macaque tracing results can be accurately extrapolated to predict human functional connectivity patterns (Kelly et al., 2010; Margulies, Vincent, et al., 2009).

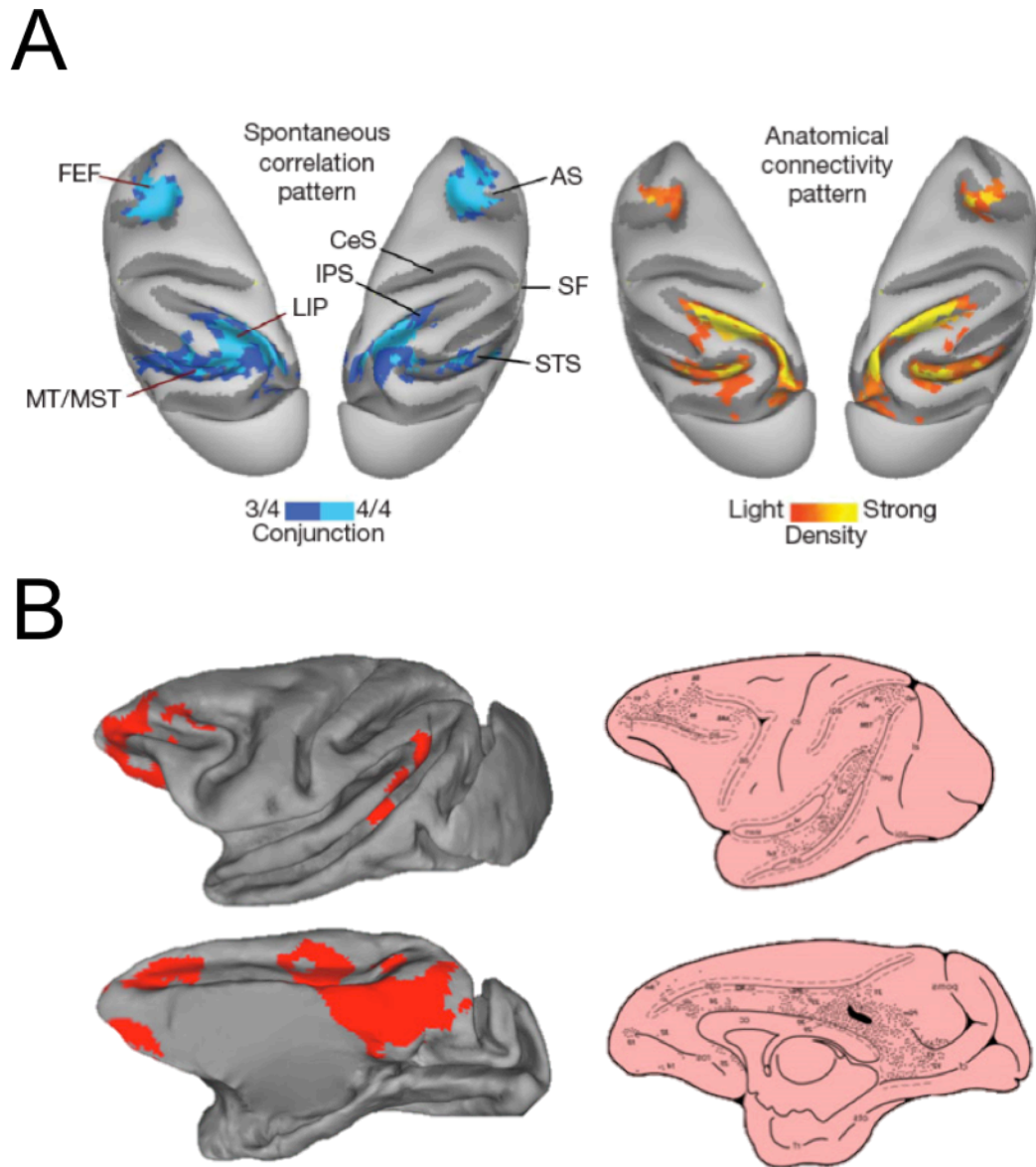


**Figure 5.13. Overlap of functional and structural connectivity patterns in the macaque.** Modified with permission from Vincent et al., 2007; Margulies et al., 2009.

To allow for a more quantitative assessment of functional/structural relationships it is necessary to examine the correspondence beyond single areas. Recent work has compared macaque RS-fMRI connectivity to structural connectivity derived from macaque axonal tract tracing studies contained within the CoCoMac database (Adachi et al., 2011). CoCoMac is a systematic record of the known wiring of the primate brain containing details of hundreds of tracing studies in their original descriptions (Stephan et al., 2001). The primary finding of this work was that functional connectivity between areas with no direct structural connection is driven by common afferents and common efferents (as opposed to serial relays). The work however, did not attempt to explore the overall correspondence between the connectivity types and was limited to unilateral visual and sensorimotor areas in two monkeys. My collaborative work directly addressed this limitation. Eighty-two cortical regions of interest were selected (41 per hemisphere) within the CoCoMac database creating a structural connectivity matrix of the relative strengths of connections between the origin (source) and termination (target) of the axonal fibers (Fig. 5.14A). Pairwise correlations were performed across timeseries derived from the same ROIs in the functional data (Fig. 5.14B). There was an overall high cosine similarity (0.69), a measure of correspondence between the two matrices that could also be examined individually for sources (range = 0.39 – 0.85) and targets (range = 0.20 – 0.86). The results also demonstrated that the strength of functional connectivity was proportional to the strength of anatomical connection, albeit as shown in previous reports, functional connections did exist between regions that had no direct anatomical connection.

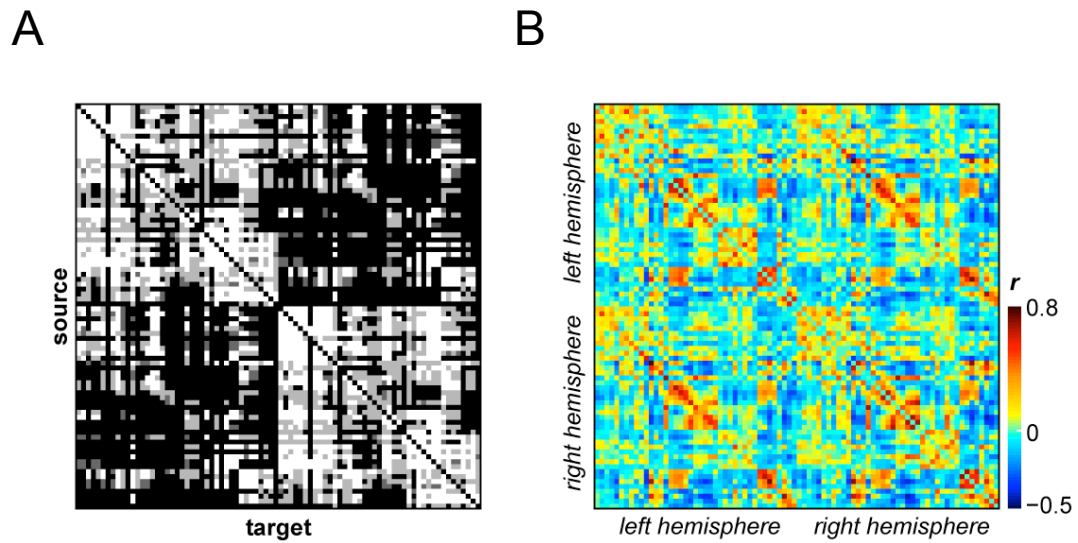


**Figure 5.14. Overlap of functional and structural connectivity.** (A) Structural connectivity matrix derived from the CoCoMac database. Strong (white), moderate (light grey), weak (dark grey) and no (black) anatomical connections are indicated. (B) Functional connectivity correlation matrix of 82 cortical seed regions averaged across 6 monkeys. Matrices are organized generally from anterior to posterior regions, for left then right hemispheres. Reprinted with permission from Shen et al., 2012.

The macaque model has also allowed for the controlled evaluation of fiber pathway contribution to functional connectivity through surgical manipulation. As stated, there are inconsistent results when examining patients with agenesis or resection of the corpus callosum. A case study of a 6-year-old child following resection of the corpus callosum (Johnston et al., 2008) and of a small cohort (N = 3) of patients with agenesis (Quigley et al., 2003) found significantly decreased functional connectivity between the neocortices. However, contradictory reports from a patient (age = 73) who underwent complete forebrain commissurotomy (Uddin et al., 2008) and a sample (N = 8) of patients with complete agenesis of the corpus callosum (Tyszka et al., 2011) found preserved bilateral connectivity. In response to these discrepancies, that are possibly related to compensatory mechanisms occurring over time, Crosson et al., (2011) scanned monkeys (N= 4) before and after surgical transection of the forebrain commissures (including the body and genu of the corpus callosum, anterior commissure, and splenium including the hippocampal commissure). There were significantly decreased interhemispheric correlations between pre- and post- operative scans across multiple bilateral homologues. Overall, the strong positive similarity values between functional and structural connectivity matrices and the loss of interhemispheric correlations following surgical resection of the tracts suggest that the two measures are intricately related. The correspondence between the two measures is not, however, 1:1 as evidenced by the less than perfect correlation and presence of correlations in the absence of direct connections.

## 5.4 Function of spontaneous fluctuations and synchronization

Spontaneous activity and dynamic network relationships have emerged as a common theme when studying the brain across multiple spatial and temporal scales in both animals and humans and likely represent a fundamental property of brain organization (Friston, 2000; Kelso, 1995; Rabinovich, Huerta, Varona, & Afraimovich, 2008; Sporns, 2010). The disproportionate metabolic cost driving spontaneous activity further substantiates its role in brain function. Beyond their underlying activity and mechanisms, most likely a complex manifestation of the underlying electrical activity (Britz, Van De Ville, & Michel, 2010; Laufs, 2008; Mantini, Perrucci, Del Gratta, Romani, & Corbetta, 2007; Musso, Brinkmeyer, Mobascher, Warbrick, & Winterer, 2010; Nir et al., 2008; Shmuel & Leopold, 2008), the specific role of low frequency BOLD fluctuations and their synchronization remains unclear though there have been several hypotheses (Fox & Raichle, 2007).

One suggestion is that the observed temporal correlations between fMRI time-series of anatomically separated regions at rest represent a record or memory of previous use. Within this framework, regions that are modulated together in a task-dependent manner will subsequently “wire” together via synaptic plasticity/potentialiation. At rest, the functional architecture will then continue to reflect the intrinsic energy demands of neuron populations that had fired together with a common functional purpose and possibly maintain the structural and functional integrity of networks. Evidence showing a high degree of overlap between resting- and task- based networks (Esposito et al., 2006; Fransson, 2006; Sun, Miller, Rao, & D’Esposito, 2007) and subsequent alteration of resting-state connectivity following intense training/learning (Lewis, Baldassarre, Committeri, Romani, & Corbetta, 2009) supports this view.

It has also been suggested that BOLD correlations could represent the coordination of spontaneous neuronal patterns that organize or coordinate the activity of neurons. Regions that commonly work in concert will then exhibit synchronous temporal patterns. Fox and Raichle (2007) equate the idea to the temporal binding hypothesis albeit

on a “much slower, broader, and more permanent scale.” However, empirical evidence supporting this notion is still in its infancy.

A third idea, and in the author’s opinion the most compelling, is that the spontaneous fluctuations and their dynamic network manifestations represent predictions about expected use. Correlation patterns are then a calculated assumption about the brain regions that are likely to be used together in the future. Both theoretical (Friston, Glaser, et al., 2002; Friston, Penny, et al., 2002) and empirical (Körding & Wolpert, 2006; Pouget, Dayan, & Zemel, 2003; Sadaghiani, Hesselmann, Friston, & Kleinschmidt, 2010) studies have provided support for a Bayesian perspective of brain function. That is, the ongoing selection of optimal statistical inferences that are continuously informed by prior probabilities which is akin to forms of top down processing. In a recent review, Buckner and Vincent (2007) argue that:

“future oriented processes are the majority of the brain’s function. Perhaps our recent evolutionary adaptations, having largely solved surviving the moment, now include a great deal of neural resources dedicated to surviving future moments. That is, while we spend critical moments engaging the environment to solve immediate tasks, we spend most of our time directed away from the environment in processing modes that consolidate the past, stabilize brain ensembles, and prepare us for the future.” (Buckner & Vincent, 2007, p. 1095)

The brains of most species, especially primates, must allow the individual to implement different behaviors under different environmental contingencies to accommodate a wide variety of goals. The time for perception, integration, and decision processes to take place can extend beyond the available time window to make an appropriate response, and in some circumstances lead to death of the individual (e.g. when failing to quickly decide to run from a predator). Predictive processing can significantly decrease the time and available metabolic resources needed to integrate the information for these tasks and allow for a faster and more accurate response. Within the context of this thesis, the predictions about upcoming use/need could result in a greater probability of certain network configurations emerging. This concept is also intricately linked to the observed

spontaneous cycling of network topology demonstrated in Chapter 4. The fluctuating configurations could reflect the updating of predictions, and may also serve a functional role in that changing metastable states allows the brain to better respond to changing internal or external demands that are the critical factor for higher-order complex tasks requiring large-scale integration of brain areas (Buckner & Vincent, 2007; Engel et al., 2001). Deco and coworkers have compared the phenomenon to a tennis player awaiting a serve. Preemptively, a player makes small hops to the left and to the right so as to be able to react more quickly to the incoming ball than would be possible from a static position (Deco, Jirsa, McIntosh, Sporns, & Kötter, 2009). Finally, it is important to note that each of these three hypotheses are not mutually exclusive and it is most likely the case that spontaneous activity is shaped by all three at any given time.

## 5.5 Anesthesia and States

A large proportion of the resting-state investigations of animals have utilized anesthesia as a method to eliminate motion effects, physiological stress, and training requirements. As outlined throughout this review, RSNs have been found in rodents and macaques despite the use of various types of anesthesia. In rodents, these have included alpha-chloralose (Lu et al., 2007; Majeed et al., 2009), medetomidine (Zhao et al., 2008; Pawela et al., 2008, 2010; Magnuson et al., 2010), ketamine (Hutchison et al., 2010), and isoflurane (Kannurpatti et al., 2008; Hutchison et al., 2010; van Meer et al., 2010; Wang et al., 2011; Liu et al., 2011). Isoflurane represents the most commonly used anesthetic in monkeys (Vincent et al., 2007; Shmuel and Leopold, 2008; Teichert et al., 2010; Mars et al., 2011; Hutchison et al., 2011a,b) though propofol (Matsui et al., 2011; Adachi et al., in press) and a combination of ketamine and medetomidine (Moeller et al., 2009) have been used successfully. Despite convergence of results across anesthesia types and even with awake animals (Zhang et al., 2010b; Liang et al., 2011; Mantini et al., 2011) it is incorrect to say that quantifiable differences do not exist between the different states (Lu et al., 2007; Moeller et al., 2009; Williams et al., 2010; Wang et al., 2011). The mechanisms of action of many anesthetics remain poorly understood, but certainly modulate neural activity and consequently influence the cerebral blood flow if not

effecting blood flow directly. Isoflurane in particular has been shown to disrupt functional thalamocortical connectivity (Alkire et al., 2000; Steriade, 2001; Arhem et al., 2003) in addition to causing vasodilation that can affect cerebrovascular activity (Farber et al., 1997; White and Alkire, 2003; Schlünzen et al., 2006). The effects could be manifested as changes in the correlation strength, localization, or inclusion of distributed nodes within specific networks (Vincent et al., 2007; Lu et al., 2007; Wang et al., 2011; Liu et al., 2011). Anesthesia can also limit longitudinal studies in cases such as alpha-chloralose that require animal sacrifice or recoverable anesthetics that require a necessary interval between scanning sessions. Finally, there are concerns of possible drug interactions when studying pharmacological interventions.

Despite the disadvantages, the utility of anesthesia should not be understated. Beyond allowing extended, motion-free acquisition in naive animals, anesthesia experimentation can serve to explore the fundamental physiological relationships underlying spontaneous fluctuations and functional connectivity by exploiting their unique mechanisms of action and effect on neural activity, neurovascular coupling, and vascular reactivity. Further, anesthesia can eliminate conscious processes such as passive mind wandering, active monitoring, memory formation, or changes in attention and arousal during image acquisition that may confound certain experiments (Hutchison et al., 2012a). Reciprocally, there is the potential to explore the mechanisms that account for the anesthesia's diverse effects on memory, pain, and consciousness. While the use of anesthesia in human research is possible (Greicius et al., 2008) it is severely limited and provides an additional need for animal investigations.

## 5.6 Future Directions

The work presented in this thesis represents the first steps upon which multiple research directions can now be developed. It is with the knowledge of the normal brain topology and dynamics of the rat and monkey models that experimental manipulations can be characterized providing new and valuable insights in how the human brain operates across multiple states.

Homologous spatial and temporal brain properties establish the suitability of the rat and macaque as models of human brain organization and can extend the application of animal RS-fMRI investigations to the exploration controlled disease models. These can explore the spectrum of neurological and psychiatric diseases such as schizophrenia, Alzheimer's disease, epilepsy, among others that are accompanied by abnormal functional disruptions (Auer, 2008; Greicius, 2008) and have a developed animal equivalent. Following the determination of causal relationships between the disease and altered connectivity patterns, the animal models will allow the assessment of early diagnostic biomarkers and the development of better drug treatments. In a similar manner, functional or structural changes can be induced with temporary or permanent lesions using techniques such as cooling loops (Koval et al., 2011), muscimol injections (Dias et al., 1995; Shi et al., 1998), tissue ablation (Rushworth et al., 2003), or optogenetics (Han et al., 2009; Diester et al., 2011). These changes can disrupt local and distributed topology such as small-world topology, particularly when targeting central or provincial hubs. Taken further, longitudinal studies of these animals offer the opportunity to investigate the timecourse of network plasticity in response to the alterations of brain organization. Longitudinal studies are also critical to allow comparison of the network development in humans (Fransson et al., 2009; Fransson et al., 2007) to that of other species.

The spatial connectivity patterns of RSN nodes can provide future electrophysiological targets that could potentially reveal new functional representations. The multimodal approach would first identify brain areas functionally connected to a region of interest using RS-fMRI. Depth electrodes can then be placed based upon the resulting maps to identify the functional properties of cells within that area. My current collaborative work has already begun exploring the functional role of cingulate areas identified as part of the macaque oculomotor RSN shown in Chapter 3 and 4 (Babapoor-Farrokhran, Hutchison, Gati, Menon, & Everling, 2011). Another particularly exciting avenue of future research is the use of multi-site depth recordings combined with simultaneous whole-brain fMRI. Though technically difficult, this will allow for more accurate identification of the neural origins of spontaneous BOLD activity as well as offer insight to the electrophysiological correlates of the dynamic patterns and

hypersynchronization observed in Chapter 4. Like the work described in this thesis, this should be first conducted in anesthetized animals before examining task-related modulation of the dynamic patterns. A greater focus on awake animals (Liang et al., 2011; Mantini et al., 2007) will also serve avoid the potential confounding effects of the anesthetic agents. It will also likely be the case that simultaneous depth recordings and fMRI in animal models will be necessary to reveal the origin and potential functional role of anticorrelated areas – a phenomenon reported throughout this thesis. Anticorrelations can occur within or between RSNs and the temporally consistent negative correlations are most often observed between regions lacking direct anatomical connections (Shen et al., 2012). Whether this often neglected connectivity type represents a form of temporal segregations (Fox et al., 2005) or a manifestation of noise-driven transitions between different metastates (Deco et al., 2009) could provide further insights into ongoing brain organization.

From an analytical standpoint the techniques used in this thesis represent a simplified approach for examining a very complex system. Certain properties of the networks are not taken into account when modeling the system. For instance, there is an implicit assumption of uniformity across the nodes (brain regions) and the connections between them. However, it is known that cell type, density, and configurations vary greatly region by region and the connections between the regions can have different weights, directions, conduction times, and signs (excitatory/inhibitory). Chapter 4 also outlined that the dynamic connections most likely are a manifestation of a nonlinear system that will require measures beyond simple correlations or measures of statistical independence. Therefore, future research will be needed to better take into account the diverse and complex functional and structural architectures as well as better address the interactions between both can shape the other. Finally, the effects of movement, vasomotion, cardiac, and respiratory factors and their contribution to the spontaneous signals need to be further investigated.

## 5.7 Conclusions

The mammalian brain is compilation of functional and structural networks across multiple spatial scales. These networks work in concert to support the diverse range of cognitive processes necessary for the selection and implementation of appropriate behaviours essential for the survival and reproductive success of the individual and by extension, the species. The bulk of the metabolic resources in the brain are not, however, allocated for the implementation of the immediate behaviour, but instead to the ongoing brain activity necessary for consolidating, maintaining, and predicting internal and external representations (configurations) over much longer time scales. Resting-state fMRI has provided a methodology capable of exploring this fundamental, yet overlooked, attribute of brain organization. The present work revealed that network topology and the reciprocal temporal features are ubiquitous across mammalian species as well as the presence of homologous network architecture. The results also show that with increasing brain complexity more distributed network patterns emerge and as well as lateralized organization in humans. From an applied research perspective, the findings support the use of animal models for the study of network disruptions in disease and exploration of the true underpinnings of the RS-fMRI signal. The applications and future avenues of research extending from the present thesis are broad and will aid in our understanding of study of large-scale brain function.

## 5.8 References

- Abou-Elseoud, A., Starck, T., Remes, J., Nikkinen, J., Tervonen, O., & Kiviniemi, V. (2010). The effect of model order selection in group PICA. *Hum Brain Mapp*, *31*, 1207–1216.
- Adachi, Y., Osada, T., Sporns, O., Watanabe, T., Matsui, T., Miyamoto, K., & Miyashita, Y. (2011). Functional Connectivity between Anatomically Unconnected Areas Is Shaped by Collective Network-Level Effects in the Macaque Cortex. *Cereb Cortex*, *in press*.
- Alkire, M. T., Haier, R. J., & Fallon, J. H. (2000). Toward a unified theory of narcosis: brain imaging evidence for a thalamocortical switch as the neurophysiologic basis of anesthetic-induced unconsciousness. *Consci Cogn*, *9*, 370–386.

- Arhem, P., Klement, G., & Nilsson, J. (2003). Mechanisms of anesthesia: towards integrating network, cellular, and molecular level modeling. *Neuropsychopharmacol*, 28 Suppl 1, S40–47.
- Auer, D. P. (2008). Spontaneous low-frequency blood oxygenation level-dependent fluctuations and functional connectivity analysis of the “resting” brain. *Magn Reson Imag*, 26, 1055–1064.
- Babapoor-Farrokhran, S., Hutchison, R.M., Gati, J.S., Menon, R.S., Everling, S. Resting-state fMRI as a tool to localize putative saccade-related brain areas in nonhuman primates. Program No. 272.06. 2011 Neuroscience Meeting Planner. Washington, DC: Society for Neuroscience, 2011. Online.
- Banich, M. T. (1998). The missing link: the role of interhemispheric interaction in attentional processing. *Brain Cogn*, 36, 128–157.
- Beckmann, C. F., DeLuca, M., Devlin, J. T., & Smith, S. M. (2005). Investigations into resting-state connectivity using independent component analysis. *Phil Trans R Soc B: Biol Sci*, 360, 1001-1013.
- Britz, J., Van De Ville, D., & Michel, C. M. (2010). BOLD correlates of EEG topography reveal rapid resting-state network dynamics. *NeuroImage*, 52, 1162–1170.
- Buckner, R. L., Andrews-Hanna, J. R., & Schacter, D. L. (2008). The brain’s default network: anatomy, function, and relevance to disease. *Ann NY Acad Sci*, 1124, 1–38.
- Buckner, R. L., & Vincent, J. L. (2007). Unrest at rest: default activity and spontaneous network correlations. *NeuroImage*, 37, 1091–1096.
- Bullmore, E., & Sporns, O. (2009). Complex brain networks: graph theoretical analysis of structural and functional systems. *Nat Rev Neurosci*, 10, 186–198.
- Cole, D. M., Smith, S. M., & Beckmann, C. F. (2010). Advances and pitfalls in the analysis and interpretation of resting-state FMRI data. *Front Syst Neurosci*, 4, 8.
- Compton, R. J. (2002). Inter-hemispheric interaction facilitates face processing. *Neuropsychol*, 40, 2409–2419.
- Croxson, P.L, O'reilly, J.X, Sallet J., Noonan, M.P., Mars, R.B., Browning, P.G., Miller, K.L., Rushworth, M.F., Baxter, M.G. Alterations in resting-state network activity following complete commissurotomy in macaque monkeys. Program No. 405.17. 2011. Neuroscience Meeting Planner. Washington, DC: Society for Neuroscience, 2011. Online
- Damoiseaux, J S, Rombouts, S. A. R. B., Barkhof, F., Scheltens, P., Stam, C. J., Smith, S. M., & Beckmann, C. F. (2006). Consistent resting-state networks across healthy subjects. *Proc Natl Acad Sci U S A*, 103, 13848–13853.

- Damoiseaux, Jessica S, & Greicius, M. D. (2009). Greater than the sum of its parts: a review of studies combining structural connectivity and resting-state functional connectivity. *Brain Struct Funct*, *213*, 525–533.
- Deco, G., Jirsa, V., McIntosh, A. R., Sporns, O., & Kötter, R. (2009). Key role of coupling, delay, and noise in resting brain fluctuations. *Proc Natl Acad Sci U S A*, *106*, 10302–10307.
- Dias, E. C., Kiesau, M., & Segraves, M. A. (1995). Acute activation and inactivation of macaque frontal eye field with GABA-related drugs. *J Neurophys*, *74*, 2744–2748.
- Dinstein, I., Pierce, K., Eyster, L., Solso, S., Malach, R., Behrmann, M., & Courchesne, E. (2011). Disrupted neural synchronization in toddlers with autism. *Neuron*, *70*, 1218–1225.
- Esposito, F., Bertolino, A., Scarabino, T., Latorre, V., Blasi, G., Popolizio, T., Tedeschi, G., et al. (2006). Independent component model of the default-mode brain function: Assessing the impact of active thinking. *Brain Res Bull*, *70*, 263–269.
- Farber, N. E., Harkin, C. P., Niedfeldt, J., Hudetz, A. G., Kampine, J. P., & Schmeling, W. T. (1997). Region-specific and agent-specific dilation of intracerebral microvessels by volatile anesthetics in rat brain slices. *Anesthesiology*, *87*, 1191–1198.
- Fox, M. D, Snyder, A. Z., Vincent, J. L., Corbetta, M., Van Essen, D. C., & Raichle, M. E. (2005). The human brain is intrinsically organized into dynamic, anticorrelated functional networks. *Proc Natl Acad Sci U S A*, *102*, 9673-9678.
- Fox, Michael D, & Raichle, M. E. (2007). Spontaneous fluctuations in brain activity observed with functional magnetic resonance imaging. *Nat Rev Neurosci*, *8*, 700–711.
- Fransson, P., Skiöld, B., Engström, M., Hallberg, B., Mosskin, M., Aden, U., Lagercrantz, H., et al. (2009). Spontaneous brain activity in the newborn brain during natural sleep-an fMRI study in infants born at full term. *Ped Res*, *66*, 301-305.
- Fransson, P., Skiöld, B., Horsch, S., Nordell, A., Blennow, M., Lagercrantz, H., & Aden, U. (2007). Resting-state networks in the infant brain. *Proc Natl Acad Sci U S A*, *104*, 15531.
- Fransson, P. (2006). How default is the default mode of brain function? Further evidence from intrinsic BOLD signal fluctuations. *Neuropsychol*, *44*, 2836–2845.
- Friston, K. J. (2000). The labile brain. I. Neuronal transients and nonlinear coupling. *Phil Trans R Soc Lon B, Biol Sci*, *355*, 215–236.

- Friston, K. J., Glaser, D. E., Henson, R. N. A., Kiebel, S., Phillips, C., & Ashburner, J. (2002). Classical and Bayesian inference in neuroimaging: applications. *NeuroImage*, *16*, 484–512.
- Friston, K. J., Penny, W., Phillips, C., Kiebel, S., Hinton, G., & Ashburner, J. (2002). Classical and Bayesian inference in neuroimaging: theory. *NeuroImage*, *16*, 465–483.
- Gao, W., Zhu, H., Giovanello, K. S., Smith, J. K., Shen, D., Gilmore, J. H., & Lin, W. (2009). Evidence on the emergence of the brain's default network from 2-week-old to 2-year-old healthy pediatric subjects. *Proc Natl Acad Sci U S A*, *106*, 6790–6795.
- Gerloff, C., & Andres, F. G. (2002). Bimanual coordination and interhemispheric interaction. *Acta Psychologica*, *110*, 161–186.
- Greicius, M. (2008). Resting-state functional connectivity in neuropsychiatric disorders. *Curr Opin Neurol*, *21*, 424–430.
- Greicius, M. D., Supekar, K., Menon, V., & Dougherty, R. F. (2009). Resting-state functional connectivity reflects structural connectivity in the default mode network. *Cereb Cortex*, *19*, 72–78.
- Greicius, Michael D., Kiviniemi, V., Tervonen, O., Vainionpää, V., Alahuhta, S., Reiss, A. L., & Menon, V. (2008). Persistent default-mode network connectivity during light sedation. *Hum Brain Mapp*, *29*, 839–847.
- Hagmann, P., Cammoun, L., Gigandet, X., Meuli, R., Honey, C. J., Wedeen, V. J., & Sporns, O. (2008). Mapping the structural core of human cerebral cortex. *PLoS Biology*, *6*, e159.
- Han, X., Qian, X., Bernstein, J. G., Zhou, H.-H., Franzesi, G. T., Stern, P., Bronson, R. T., et al. (2009). Millisecond-timescale optical control of neural dynamics in the nonhuman primate brain. *Neuron*, *62*, 191–198.
- Haug, H. (1987) Brain sizes, surfaces, and neuronal sizes of the cortex cerebri: a stereological investigation of man and his variability and a comparison with some mammals (primates, whales, marsupials, insectivores, and one elephant). *Am. J. Anat.* *180*, 126-142.
- Hill, J., Inder, T., Neil, J., Dierker, D., Harwell, J., & Van Essen, D. (2010). Similar patterns of cortical expansion during human development and evolution. *Proc Natl Acad Sci U S A*, *107*, 13135–13140.
- Honey, C. J., Sporns, O., Cammoun, L., Gigandet, X., Thiran, J. P., Meuli, R., & Hagmann, P. (2009). Predicting human resting-state functional connectivity from structural connectivity. *Proc Natl Acad Sci U S A*, *106*, 2035-2040.

- Houzel, J.-C., Carvalho, M. L., & Lent, R. (2002). Interhemispheric connections between primary visual areas: beyond the midline rule. *Braz J Med Biol Res*, *35*, 1441–1453.
- Hutchison, R. M., Mirsattari, S. M., Jones, C. K., Gati, J. S., & Leung, L. S. (2010). Functional Networks in the Anesthetized Rat Brain Revealed by Independent Component Analysis of Resting-State fMRI. *J Neurophys*, *103*, 3398–3406.
- Hutchison, R. M., Leung, L. S., Mirsattari, S. M., Gati, J. S., Menon, R. S., & Everling, S. (2011). Resting-state networks in the macaque at 7 T. *NeuroImage*, *56*, 1546–1555.
- Hutchison, R. M., Womelsdorf, T., Gati, J. S., Leung, L. S., Menon, R. S., & Everling, S. (2011). Resting-State Connectivity Identifies Distinct Functional Networks in Macaque Cingulate Cortex. *Cereb Cortex*.
- Hutchison RM, Womelsdorf T, Gati JS, Everling S, Menon RS. (2012a). Resting-state networks show dynamic functional connectivity in awake humans and anesthetized macaques. *Hum Brain Mapp. In press*.
- Hutchison RM, Gallivan JP, Culham JC, Gati JS, Menon RS, Everling S. (2012b). Functional connectivity of the frontal eye fields in humans and macaque monkeys investigated with resting-state fMRI. *J Neurophysiol. In press*.
- Jafri, M. J., Pearlson, G. D., Stevens, M., & Calhoun, V. D. (2008). A method for functional network connectivity among spatially independent resting-state components in schizophrenia. *Neuroimage*, *39*, 1666–1681.
- Jerison, H.J. (1973) *Evolution of the Brain and Intelligence*, Academic Press.
- Joel, S. E., Caffo, B. S., van Zijl, P. C. M., & Pekar, J. J. (2011). On the relationship between seed-based and ICA-based measures of functional connectivity. *Magn Res Med*, *66*, 644–657.
- Johnston, J. M., Vaishnavi, S. N., Smyth, M. D., Zhang, D., He, B. J., Zempel, J. M., Shimony, J. S., et al. (2008a). Loss of resting interhemispheric functional connectivity after complete section of the corpus callosum. *J Neurosci*, *28*, 6453–6458.
- Jonckers, E., Van Audekerke, J., De Visscher, G., Van der Linden, A., & Verhoye, M. (2011). Functional Connectivity fMRI of the Rodent Brain: Comparison of Functional Connectivity Networks in Rat and Mouse. *PLoS ONE*, *6*, e18876.
- Jonckers, P. Denolf, G. De groof, A. & Van der linden. Resting state fMRI of the songbird brain: Functional connectivity of the song control system. Program No. 538.02. 2011 Neuroscience Meeting Planner. Washington, DC: Society for Neuroscience, 2011. Online.

- Kagan, I., Iyer, A., Lindner, A., & Andersen, R. A. (2010). Space representation for eye movements is more contralateral in monkeys than in humans. *Proc Natl Acad Sci U S A*, *107*, 7933–7938.
- Kannurpatti, S. S., Biswal, B. B., Kim, Y. R., & Rosen, B. R. (2008). Spatio-temporal characteristics of low-frequency BOLD signal fluctuations in isoflurane-anesthetized rat brain. *NeuroImage*, *40*, 1738–1747.
- Kelly, C., Uddin, L. Q., Shehzad, Z., Margulies, D. S., Castellanos, F. X., Milham, M. P., & Petrides, M. (2010). Broca's region: linking human brain functional connectivity data and non-human primate tracing anatomy studies. *Eur J Neurosci*, *32*, 383–398.
- Kelso, J. A. S. (1995). *Dynamic Patterns: The Self-Organization of Brain and Behavior*. The MIT Press.
- Körding, K. P., & Wolpert, D. M. (2006). Bayesian decision theory in sensorimotor control. *Trends Cogn Sci*, *10*, 319–326.
- Koval, M. J., Lomber, S. G., & Everling, S. (2011). Prefrontal cortex deactivation in macaques alters activity in the superior colliculus and impairs voluntary control of saccades. *J Neurosci*, *31*, 8659–8668.
- Krienen, F. M., & Buckner, R. L. (2009). Segregated fronto-cerebellar circuits revealed by intrinsic functional connectivity. *Cereb Cortex*, *19*, 2485–2497.
- Laufs, H. (2008). Endogenous brain oscillations and related networks detected by surface EEG-combined fMRI. *Hum Brain Mapp*, *29*, 762–769.
- Lewis, C. M., Baldassarre, A., Committeri, G., Romani, G. L., & Corbetta, M. (2009). Learning sculpts the spontaneous activity of the resting human brain. *Proc Natl Acad Sci U S A*, *106*, 17558–17563.
- Liang, Z., King, J., & Zhang, N. (2011). Uncovering intrinsic connective architecture of functional networks in awake rat brain. *J Neurosci*, *31*, 3776–3783.
- Liao, W., Mantini, D., Zhang, Z., Pan, Z., Ding, J., Gong, Q., Yang, Y., et al. (2009). Evaluating the effective connectivity of resting state networks using conditional Granger causality. *Biol Cybern*, *102*, 57–69.
- Liederman, J. (1998). The dynamics of interhemispheric collaboration and hemispheric control. *Brain Cogn*, *36*, 193–208.
- Liu, X., Zhu, X.-H., Zhang, Y., & Chen, W. (2011). Neural origin of spontaneous hemodynamic fluctuations in rats under burst-suppression anesthesia condition. *Cereb Cortex*, *21*, 374–384.
- Lu, H., Zou, Q., Gu, H., Raichle, M. E., Stein, E. A., & Yang, Y. (2012). Rat brains also have a default mode network. *Proc Natl Acad Sci U S A* *109*, 3979–3984.

- Lu, H., Zuo, Y., Gu, H., Waltz, J. A., Zhan, W., Scholl, C. A., Rea, W., et al. (2007). Synchronized delta oscillations correlate with the resting-state functional MRI signal. *Proc Natl Acad Sci U S A*, *104*, 18265–18269.
- Magnuson, M., Majeed, W., & Keilholz, S. D. (2010). Functional connectivity in blood oxygenation level-dependent and cerebral blood volume-weighted resting state functional magnetic resonance imaging in the rat brain. *J Magn Res Imag*, *32*, 584–592.
- Majeed, W., Magnuson, M., & Keilholz, S. D. (2009). Spatiotemporal dynamics of low frequency fluctuations in BOLD fMRI of the rat. *J Magn Reson Imag*, *30*, 384–393.
- Mantini, Dante, Gerits, A., Nelissen, K., Durand, J.-B., Joly, O., Simone, L., Sawamura, H., et al. (2011). Default mode of brain function in monkeys. *J Neurosci*, *31*, 12954–12962.
- Mantini, D., Perrucci, M. G., Del Gratta, C., Romani, G. L., & Corbetta, M. (2007). Electrophysiological signatures of resting state networks in the human brain. *Proc Natl Acad Sci U S A*, *104*, 13170–13175.
- Margulies, D. S., Vincent, J. L., Kelly, C., Lohmann, G., Uddin, L. Q., Biswal, B. B., Villringer, A., et al. (2009). Precuneus shares intrinsic functional architecture in humans and monkeys. *Proc Natl Acad Sci U S A*, *106*, 20069–20074.
- Mars, R. B., Jbabdi, S., Sallet, J., O'Reilly, J. X., Croxson, P. L., Olivier, E., Noonan, M. A., et al. (2011). Diffusion-Weighted Imaging Tractography-Based Parcellation of the Human Parietal Cortex and Comparison with Human and Macaque Resting-State Functional Connectivity. *J Neurosci*, *31*, 4087–4100.
- Mason, M. F., Norton, M. I., Van Horn, J. D., Wegner, D. M., Grafton, S. T., & Macrae, C. N. (2007). Wandering minds: the default network and stimulus-independent thought. *Science*, *315*, 393–395.
- Matsui, T., Tamura, K., Koyano, K. W., Takeuchi, D., Adachi, Y., Osada, T., & Miyashita, Y. (2011). Direct Comparison of Spontaneous Functional Connectivity and Effective Connectivity Measured by Intracortical Microstimulation: An fMRI Study in Macaque Monkeys. *Cereb Cortex*, in press.
- Moeller, S., Nallasamy, N., Tsao, D. Y., & Freiwald, W. A. (2009). Functional connectivity of the macaque brain across stimulus and arousal states. *J Neurosci*, *29*, 5897–9509.
- Musso, F., Brinkmeyer, J., Mobascher, A., Warbrick, T., & Winterer, G. (2010). Spontaneous brain activity and EEG microstates. A novel EEG/fMRI analysis approach to explore resting-state networks. *NeuroImage*, *52*, 1149–1161.

- Nir, Y., Mukamel, R., Dinstein, I., Privman, E., Harel, M., Fisch, L., Gelbard-Sagiv, H., et al. (2008). Interhemispheric correlations of slow spontaneous neuronal fluctuations revealed in human sensory cortex. *Nat Neurosci*, *11*, 1100–1108.
- Owen, R. Lectures on the comparative anatomy and physiology of the invertebrate animals, delivered at the Royal College of Surgeons. (1843). London: Longman, Brown, Green and Longmans.
- Pawela, C. P., Biswal, B. B., Cho, Y. R., Kao, D. S., Li, R., Jones, S. R., Schulte, M. L., et al. (2008). Resting-state functional connectivity of the rat brain. *Magn Reson Med*, *59*, 1021–1029.
- Pawela, C. P., Biswal, B. B., Hudetz, A. G., Li, R., Jones, S. R., Cho, Y. R., Matloub, H. S., et al. (2010). Interhemispheric neuroplasticity following limb deafferentation detected by resting-state functional connectivity magnetic resonance imaging (fcMRI) and functional magnetic resonance imaging (fMRI). *NeuroImage*, *49*, 2467–2478.
- Pouget, A., Dayan, P., & Zemel, R. S. (2003). Inference and computation with population codes. *Ann Rev Neurosci*, *26*, 381–410.
- Quigley, M., Cordes, D., Turski, P., Moritz, C., Haughton, V., Seth, R., & Meyerand, M. E. (2003). Role of the corpus callosum in functional connectivity. *Am J Neurorad*, *24*, 208-212.
- Rabinovich, M. I., Huerta, R., Varona, P., & Afraimovich, V. S. (2008). Transient cognitive dynamics, metastability, and decision making. *PLoS Comput Bio*, *4*, e1000072.
- Raichle, M. E., & Snyder, A. Z. (2007). A default mode of brain function: a brief history of an evolving idea. *NeuroImage*, *37*, 1083–1090.
- Roth, G., Dicke, U. (2005). Evolution of the brain and intelligence. *Trends Cogn Sci*, 9250-257.
- Rushworth, M. F. S., Hadland, K. A., Gaffan, D., & Passingham, R. E. (2003). The effect of cingulate cortex lesions on task switching and working memory. *J Cogn Neurosci*, *15*, 338–353.
- Russell, S. (1979) Brain size and intelligence: a comparative perspective. In *Brain, Behavior and Evolution* (Oakley, D.A. and Plotkin, H.C., eds), pp. 126–153, Methuen 180, 126–142.
- Sadaghiani, S., Hesselmann, G., Friston, K. J., & Kleinschmidt, A. (2010). The relation of ongoing brain activity, evoked neural responses, and cognition. *Front Syst Neurosci*, *4*, 20.

- Schlünzen, L., Cold, G. E., Rasmussen, M., & Vafaei, M. S. (2006). Effects of dose-dependent levels of isoflurane on cerebral blood flow in healthy subjects studied using positron emission tomography. *Acta Anaesthesiologica Scandinavica*, *50*, 306–312.
- Sereno, M. I., & Tootell, R. B. H. (2005). From monkeys to humans: what do we now know about brain homologies? *Curr Opin in Neurobio*, *15*, 135–144.
- Shen, K., Bezgin, G., Hutchison, R.M., Gati, J., Menon, R., McIntosh, A.R., Everling, S. Resting-state connectivity reflects underlying anatomical structure in the macaque cortex. Organization for Human Brain Mapping, June 2012.
- Shi, D., Friedman, H. R., & Bruce, C. J. (1998). Deficits in smooth-pursuit eye movements after muscimol inactivation within the primate's frontal eye field. *J Neurophys*, *80*, 458–464.
- Shmuel, A., & Leopold, D. A. (2008). Neuronal correlates of spontaneous fluctuations in fMRI signals in monkey visual cortex: Implications for functional connectivity at rest. *Hum Brain Mapp*, *29*, 751–761.
- Smith, S. M., Fox, P. T., Miller, K. L., Glahn, D. C., Fox, P. M., Mackay, C. E., Filippini, N., et al. (2009). Correspondence of the brain's functional architecture during activation and rest. *Proc Natl Acad Sci U S A*, *106*, 13040–13045.
- Sporns, O. (2010). *Networks of the Brain* (1st ed.). The MIT Press.
- Stephan, K. E., Kamper, L., Bozkurt, A., Burns, G. A., Young, M. P., & Kötter, R. (2001). Advanced database methodology for the Collation of Connectivity data on the Macaque brain (CoCoMac). *Phil Trans R Soc L B, Biol Sci*, *356*, 1159–1186.
- Steriade, M. (2001). Impact of network activities on neuronal properties in corticothalamic systems. *Journal of Neurophysiology*, *86*(1), 1–39.
- Strogatz, S. H. (2001). Exploring complex networks. *Nature*, *410*, 268–276.
- Sun, F. T., Miller, L. M., Rao, A. A., & D'Esposito, M. (2007). Functional connectivity of cortical networks involved in bimanual motor sequence learning. *Cereb Cortex*, *17*, 1227–1234.
- Teichert, T., Grinband, J., Hirsch, J., & Ferrera, V. P. (2010). Effects of heartbeat and respiration on macaque fMRI: Implications for functional connectivity. *Neuropsychologia*, *48*, 1886–1894.
- Tyszka, J. M., Kennedy, D. P., Adolphs, R., & Paul, L. K. (2011). Intact bilateral resting-state networks in the absence of the corpus callosum. *J Neurosci*, *31*, 15154–15162.

- Uddin, L. Q., Mooshagian, E., Zaidel, E., Scheres, A., Margulies, D. S., Kelly, A. M. C., Shehzad, Z., et al. (2008). Residual functional connectivity in the split-brain revealed with resting-state functional MRI. *Neuroreport*, *19*, 703–709.
- Upadhyay, J., Baker, S. J., Chandran, P., Miller, L., Lee, Y., Marek, G. J., Sakoglu, U., et al. (2011). Default-mode-like network activation in awake rodents. *PloS ONE*, *6*, e27839.
- van den Heuvel, M., Mandl, R., & Hulshoff Pol, H. (2008). Normalized cut group clustering of resting-state fMRI data. *PloS ONE*, *3*, e2001.
- Van Dongen, P.A.M. (1998). Brain size in vertebrates. In *The Central Nervous System of Vertebrates* (Vol. 3) (Nieuwenhuys, R. et al., eds), pp. 2099–2134, Springer Berlin.
- van Meer, M. P. A., van der Marel, K., Otte, W. M., Berkelbach van der Sprenkel, J. W., & Dijkhuizen, R. M. (2010). Correspondence between altered functional and structural connectivity in the contralesional sensorimotor cortex after unilateral stroke in rats: a combined resting-state functional MRI and manganese-enhanced MRI study. *J Cereb Blood Flow Metab*, *30*, 1707–1711.
- Vincent, J. L., Kahn, I., Van Essen, D. C., & Buckner, R. L. (2010). Functional Connectivity of the Macaque Posterior Parahippocampal Cortex. *Journal of Neurophysiology*, *103*, 793–800.
- Vincent, J. L., Patel, G. H., Fox, M. D., Snyder, A. Z., Baker, J. T., Van Essen, D. C., Zempel, J. M., et al. (2007). Intrinsic functional architecture in the anaesthetized monkey brain. *Nature*, *447*, 83–86.
- Wang, K., van Meer, M. P. A., van der Marel, K., van der Toorn, A., Xu, L., Liu, Y., Viergever, M. A., et al. (2011). Temporal scaling properties and spatial synchronization of spontaneous blood oxygenation level-dependent (BOLD) signal fluctuations in rat sensorimotor network at different levels of isoflurane anesthesia. *NMR in Biomedicine*, *24*, 61–67.
- White, N. S., & Alkire, M. T. (2003). Impaired thalamocortical connectivity in humans during general-anesthetic-induced unconsciousness. *NeuroImage*, *19*, 402–411.
- Wise, S.P. (2008). Forward frontal fields: phylogeny and fundamental function. *Trends Neurosci*, *31*, 599-608.
- Williams, K. A., Magnuson, M., Majeed, W., LaConte, S. M., Peltier, S. J., Hu, X., & Keilholz, S. D. (2010). Comparison of alpha-chloralose, medetomidine and isoflurane anesthesia for functional connectivity mapping in the rat. *Magnetic Resonance Imaging*, *28*(7), 995–1003. doi:10.1016/j.mri.2010.03.007
- Wilson, E. O. (1998). *Consilience: The Unity of Knowledge* (1st ed.). Knopf.

- Zhang, N., Rane, P., Huang, W., Liang, Z., Kennedy, D., Frazier, J. A., & King, J. (2010). Mapping resting-state brain networks in conscious animals. *J Neurosci Methd*, *189*, 186–196.
- Zhao, F., Zhao, T., Zhou, L., Wu, Q., & Hu, X. (2008). BOLD study of stimulation-induced neural activity and resting-state connectivity in medetomidine-sedated rat. *NeuroImage*, *39*, 248–260.

## Appendix A: Documentation of Ethics Approval.



01.01.11

**\*This is the 2nd Renewal of this protocol**

\*A Full Protocol submission will be required in 2013

Dear Dr. **Everling**

Your Animal Use Protocol form entitled:

### **Role of Frontal Cortex in Cognitive Control**

has had its yearly renewal approved by the Animal Use Subcommittee.

This approval is valid from **01.01.11 to 01.01.12**

The protocol number for this project remains as **2008-125**

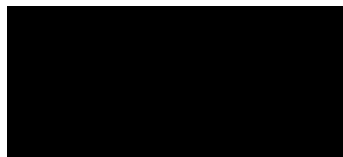
1. This number must be indicated when ordering animals for this project.
2. Animals for other projects may not be ordered under this number.
3. If no number appears please contact this office when grant approval is received.  
If the application for funding is not successful and you wish to proceed with the project, request that an internal scientific peer review be performed by the Animal Use Subcommittee office.
4. Purchases of animals other than through this system must be cleared through the ACVS office. Health certificates will be required.

#### **REQUIREMENTS/COMMENTS**

Please ensure that individual(s) performing procedures on live animals, as described in this protocol, are familiar with the contents of this document.

**The holder of this *Animal Use Protocol* is responsible to ensure that all associated safety components (biosafety, radiation safety, general laboratory safety) comply with institutional safety standards and have received all necessary approvals. Please consult directly with your institutional safety officers.**

c.c. B. Soper



#### **The University of Western Ontario**

Animal Use Subcommittee / University Council on Animal Care  
Health Sciences Centre, ● London, Ontario ● CANADA – N6A 5C1  
PH: 519-661-2111 ext. 86770 ● FL 519-661-2028 ● www.uwo.ca / animal



### Use of Human Participants - Ethics Approval Notice

**Principal Investigator:** Prof. Jody Culham  
**Review Number:** 13507  
**Review Level:** Delegated  
**Approved Local Adult Participants:** 400  
**Approved Local Minor Participants:** 0  
**Protocol Title:** Neural Coding Within Human Brain Regions Involved in Grasping and Reaching  
**Department & Institution:** Psychology, University of Western Ontario  
**Sponsor:** Natural Sciences and Engineering Research Council  
 Canadian Institutes of Health Research

**Ethics Approval Date:** September 20, 2011                      **Expiry Date:** March 31, 2016  
**Documents Reviewed & Approved & Documents Received for Information:**

Document Name	Comments	Version Date
Revised Study End Date		
Revised UWO Protocol	Revised methodology and hypotheses, change to 3 Tesla scanner, increase in number of participants to 400	
Revised Letter of Information & Consent	August 2011	

This is to notify you that The University of Western Ontario Research Ethics Board for Health Sciences Research Involving Human Subjects (HSREB) which is organized and operates according to the Tri-Council Policy Statement: Ethical Conduct of Research Involving Humans and the Health Canada/CIH Good Clinical Practice Practices: Consolidated Guidelines; and the applicable laws and regulations of Ontario has reviewed and granted approval in the above referenced revision(s) or amendment(s) on the approval date noted above. The membership of this REB also complies with the membership requirements for REBs as defined in Division 5 of the Food and Drug Regulations.

The ethics approval for this study shall remain valid until the expiry date noted above assuming timely and acceptable responses to the HSREB's periodic requests for surveillance and monitoring information. If you require an updated approval notice prior to that time you must request it using the UWO Updated Approval Request Form.

Members of the HSREB who are named as investigators in research studies, or declare a conflict of interest, do not participate in discussions related to, nor vote on, such studies when they are presented to the HSREB.

HSREB is registered with the U.S. Department of Health & Human Services under the IRB

Officer to Contact for Further Information

<input checked="" type="checkbox"/> Justice Sutherland (justice@uwo.ca)	<input type="checkbox"/> Grace Kelly (grace.kelly@uwo.ca)	<input type="checkbox"/> Sinaad Walcott (sinaad@uwo.ca)
--	--	--

This is an official document. Please retain the original in your files.

**The University of Western Ontario**  
 Office of Research Ethics

Support Services Building Room 5150 • London, Ontario • CANADA - N6G 1G9  
 P1: 519-661-3036 • F: 519-850-2466 • ethics@uwo.ca • www.uwo.ca/research/ethics



October 26, 2007

**\*This is the Original Approval for this protocol\***  
 \*A Full Protocol submission will be required in 2011\*

Dear Dr. Leung:

Your Animal Use Protocol form entitled:  
 fMRI and Neurophysiology During Seizure and Theta Rhythm  
 Funding Agency CIHR - 60433

has been approved by the University Council on Animal Care. This approval is valid from **October 26, 2007 to October 31, 2008**. The protocol number for this project is **2007-085-10**.

1. This number must be indicated when ordering animals for this project.
2. Animals for other projects may not be ordered under this number.
3. If no number appears please contact this office when grant approval is received.  
 If the application for funding is not successful and you wish to proceed with the project, request that an internal scientific peer review be performed by the Animal Use Subcommittee office.
4. Purchases of animals other than through this system must be cleared through the ACVS office. Health certificates will be required.

**ANIMALS APPROVED FOR 1 YR.**

Species	Strain	Other Detail	Pain Level	Animal # Total for 1 Year
Rat	Long Evans	250-400 gm Male	D	15
Rat	Sprague Dawley	200-350 gm Male	D	15

**STANDARD OPERATING PROCEDURES**

Procedures in this protocol should be carried out according to the following SOPs. Please contact the Animal Use Subcommittee office (661-2111 ext. 86770) in case of difficulties or if you require copies.  
 SOP's are also available at <http://www.uwo.ca/animal/acvs>  
 310 Holding Period Post-Admission  
 320 Euthanasia  
 321 Criteria for Early Euthanasia/Rodents

**REQUIREMENTS/COMMENTS**

Please ensure that individual(s) performing procedures on live animals, as described in this protocol, are familiar with the contents of this document.

## Appendix B: Permissions from Publishers


The American Physiological Society  
INTEGRATING THE LIFE SCIENCES FROM MOLECULE TO ORGANISM

[Home](#) | [Members Only](#) | [Search](#) | [About APS](#) | [Store](#) | [FASEB Member Directory](#)

[the-aps.org](#) > [publications](#) > [instructions for preparing your manuscript](#) > [copyright and permissions](#)

- Advertising ▾
- Awards ▾
- Careers/Mentoring ▾
- Chapters ▾
- Committees ▾
- Education ▾
- Meetings ▾
- Membership ▾
- News Archives ▾
- Press Room ▾
- Science Policy ▾
- Publications ▾
- Sections & Groups ▾
- Sites of Interest ▾
- Trainees ▾

### Copyright

The Mandatory Submission Form serves as the Society's official copyright transfer form. (Forms customized to your manuscript will become available on completion of the submission process; check the [Info Page of the journal](#) to which you are submitting, for blank forms.) The APS Journals are copyrighted for the protection of authors and the Society.

### Rights of Authors of APS Articles

For educational purposes only, authors may make copies of their own articles or republish parts of these articles (e.g., figures, tables), without charge and without requesting permission, provided that full acknowledgement of the source is given in the new work. Also, authors may e-mail a PDF of their article to fellow researchers for educational purposes. However, authors may not post a PDF of their published article on any website; instead, links may be posted to the article on the APS journal website where it resides. Posting of articles or parts of articles is restricted and subject to the conditions below.

### Rights of Authors for Reuse of Content from their Articles

**Theses and dissertations.** APS permits whole published articles to be reproduced without charge in dissertations, which may be posted to these repositories. Full citation is required.

**Open courseware.** Articles, or parts of articles, may be posted to a public access courseware website. Permission must be requested from the APS. A copyright fee will apply during the first 12 months of the article's publication by the APS. The APS requires full citation for all permissions granted.

**Institutional websites.** The author's published article (in whole or in part) may not be posted to an institutional website, neither at the institutional nor departmental level. This exclusion includes, but is not limited to, library websites and national government websites. Instead, a link to the article on the APS journal website should be used. (See also the APS Policy on Funding Agencies, below.)

**Institutional repositories (non-theses).** The author's published article (in whole or in part) may not be posted to any institutional repository. This exclusion includes, but is not limited to, library repositories and national government repositories. Instead, a link to the APS journal website should be used. (See also the APS Policy on Funding Agencies, below.)

**Author's article in presentations.** Authors may use their articles (in whole or in part) for presentations (e.g., at meetings and conferences). These presentations may be reproduced (e.g., in monographs) on any type of media including, but not limited to, CDs, DVDs, and flash drives, for educational use only in materials arising from the meeting or conference such as the proceedings of a meeting or conference. A copyright fee will apply if there is a charge to the user or if the materials arising are directly or indirectly commercially supported.

**Reuse in another journal before final publication is prohibited.** Permission for reuse of an article (whether in whole or in part) in another publication is restricted to the final published version of the article. If an article is currently published on the APS "publish ahead of print" website (Articles in PresS), then the author must wait to request permission to reuse the article, or any part of the article, until such time when the article appears in final-published form on the APS journal website.

Authors who do not have access to a subscription and/or who are not APS members may

- purchase the article through the pay-per-view option, or
- purchase a Toll-Free Link from APS, which will allow them to post a link to the APS journals website (directly to the article) enabling unlimited free downloads for any user accessing the article via this Toll-Free Link.

### Organizations Requesting Permission to Reuse the Work of Others for Educational Purposes

APS grants permission for free use of our articles (in whole or in part) in educational materials provided

- there is no charge or fee for those materials, and/or
- those materials are not directly or indirectly commercially supported.

If a fee is charged or the materials are commercially supported, a fee will be assessed when permission is granted.

### Translation of a Figure or Table into another Language

9650 Rockville Pike  
Bethesda, MD  
20814-3991  
USA

301-634-7164  
301-634-7241 fax  
webmaster@the-aps.org  
Copyright © 2008

**ELSEVIER** Home Products Alerts User Resources About Us Support & Contact Elsevier Websites

Search Knowledgebase [Advanced Search](#)

Send to Friend | Print

### WHAT RIGHTS DO I RETAIN AS AN AUTHOR?

As an author, you retain rights for a large number of author uses, including use by your employing institute or company. These rights are retained and permitted without specific permission from Elsevier. These include:

- the right to make copies of the article for your own personal use, including for your own classroom teaching use;
- the right to make copies and distribute copies (including through e-mail) of the article to research colleagues, for the personal use by such colleagues (but not on systematically, e.g. via an e-mail list or list serve);
- the right to post a pre-print version of the article on Internet web sites including electronic pre-print servers, and to retain indefinitely such version on such server our information on [electronic pre-prints](#) for a more detailed discussion on these points);
- the right to post a revised personal version of the text of the final article (to reflect changes made in the peer review process) on the author's personal or institute server, with a link to the journal home page (on [elsevier.com](#));
- the right to present the article at a meeting or conference and to distribute copies of such paper or article to the delegates attending the meeting;
- for the author's employer, if the article is a 'work for hire', made within the scope of the author's employment, the right to use all or part of the information in (an article for other intra-company use (e.g. training);
- patent and trademark rights and rights to any process or procedure described in the article;
- the right to include the article in full or in part in a thesis or dissertation (provided that this is not to be published commercially);**
- the right to use the article or any part thereof in a printed compilation of works of the author, such as collected writings or lecture notes (subsequent to publication the journal); and the right to prepare other derivative works, to extend the article into book-length form, or to otherwise re-use portions or excerpts in other works acknowledgement of its original publication in the journal.

Other uses by authors should be authorized by Elsevier through the **Global Rights Department** (for addresses see [Obtaining Permissions](#)), and authors are encourage know of any particular needs or requirements.

**Related Answers**

- [Where do I go if I'm an Author?](#)
- [Careers & Jobs at Elsevier](#)
- [Buying an E-Book](#)



ELSEVIER [Home](#) | [Elsevier Websites](#) | [Privacy Policy](#) | [Terms and Conditions](#) | [Feedback](#) | [Site Map](#) | [A Reed Elsevier Company](#)

Copyright © 2010 Elsevier B.V. All rights reserved.

**WILEY ONLINE LIBRARY**

LOGIN

Enter e-mail address  NOT REGISTERED ?  
 Enter password  FORGOTTEN PASSWORD ?  
 REMEMBER ME INSTITUTIONAL LOGIN >

Home > Neuroscience > Journal Home

## HUMAN BRAIN MAPPING

Human Brain Mapping

Copyright © 2012 Wiley Periodicals Inc.

Edited By: Peter T. Fox and Jack L. Lancaster  
 Impact Factor: 5.107  
 ISI Journal Citation Reports © Ranking: 2010: 2/14 (Neuroimaging); 5/111 (Radiology Nuclear Medicine & Medical Imaging); 38/237 (Neurosciences)  
 Online ISSN: 1097-0193

Permissions

**\*PLEASE NOTE: If the links highlighted here do not take you to those web sites, please copy and paste address in your browser.**

**Permission to reproduce Wiley journal Content:**

Effective immediately, requests to reproduce material from John Wiley & Sons journal content are being handled through the Rightslink® online service. Wiley no longer accepts requests or forms for Wiley journal content sent via email, fax or mail.

**Simply follow the steps below to obtain permission via the Rightslink® system:**

- Locate the article you wish to reproduce on Wiley Online Library (<http://onlinelibrary.wiley.com>)
- Navigate to the abstract page.
- Click on the 'Request Permissions' link, under the 'ARTICLE TOOLS' menu
- Follow the online instructions and select your requirements from the drop down options and click on 'quick price' to get a quote
- Create a RightsLink® account to complete your transaction (and pay, where applicable)
- Read and accept our Terms & Conditions and Download your license
- For any technical queries please contact [customer-care@copyright.com](mailto:customer-care@copyright.com)
- For further information and to view a Rightslink® demo please visit [www.wiley.com](http://www.wiley.com) and select Rights & Permissions.

**AUTHORS -** If you wish to reuse your own article (or an amended version of it) in a new publication of which you are the author, editor or co-editor, prior permission is not required (with the usual acknowledgements). However, a formal grant of license can be downloaded free of charge from Rightslink if required.

Photocopying

TRAINING AND TUTORIALS  
 Self-paced tutorials available 24/7

WILEY SCIENCE JOBS  
 Search thousands of jobs on the Wiley Job Network

Brain and Behavior



SINAUER ASSOCIATES, Inc. • Publishers • P.O. Box 407 • Sunderland, MA 01375-0407

Telephone: (413) 549-4300  
Fax: (413) 549-1118  
E-mail: orders@sinauer.com

PERMISSIONS AGREEMENT

April 19, 2012

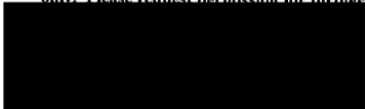
Permission granted to:  
R. Matthew Hutchison



Material to be reproduced:  
Huettel et al: *Functional magnetic Resonance Imaging, First Edition*  
Figure 1.7, page 10

To be reproduced in the work:  
R. Matthew Hutchison's PhD Thesis entitled "Brain connectivity studied by fMRI: homologous network organization in the rat, monkey, and human" to be published by Western University

Sinauer Associates owns copyright to the material described above and hereby grants permission for the one-time use of the material as specified, and for nonexclusive world rights provided that full and appropriate credit is given to the original source and that the work is for NON-COMMERCIAL use only. Please request permission for further use in subsequent editions, translations, or revisions of



Permissions Coordinator

April 19, 2012  
Date

Please acknowledge your acceptance of these terms by signing one copy of this form and returning it to Sinauer Associates. Permission Agreement is not valid until signed by applicant and received by Sinauer Associates.



April 19, 2012  
Date

**jn permissions** jnpermissions@sfn.org via uwo.ca Apr 8 (7 days ago) ☆ ↶ ↷

to Matthew ▾

Dear R. Matthew Hutchison,

Permission is granted at no cost, both online and in print to include the following article "Mantini D, Gerits A, Nelissen K, Durand JB, Joly O, Simone L, Sawamura H, Wardak C, Orban GA, Buckner RL, Vanduffel W. J Neurosci. 2011; Default mode of brain function in monkeys. Sep 7;31(36):12954-62. and publish it in your dissertation, both online and print. Please make sure to add proper citation.

As for publishing in a special issue in Frontiers in Neuroanatomy, I can't tell who the publisher is. If the publisher is a for-profit publisher, then there will be a \$70.00 charge for a onetime use of each figure you reuse from the article listed below in a book chapter. We do not process these fees directly, but you can request permission online through the Copyright Clearance Center: <http://www.copyright.com/>

If an original author is directly involved in this reuse or if I am mistaken regarding non-profit status, you may email me for direct, no-fee permission.

Also, if the figures will be changed in anyway, permission is needed by the original authors. Any subsequent editions, ancillaries and other derivative works, in any form or medium, in all languages, will need to contact SFN to seek approval. Please make sure proper citation is used to cite original source.

Please contact CCC if you have trouble with the site or payment. You may contact us if you have any further questions regarding use.

Respectfully,  
Jackie Perry  
Editorial Manager, SFN

Rightslink® by Copyright Clearance Center https://s100.copyright.com/AppDispatchServlet



[Home](#) [Account Info](#) [Help](#)



**Title:** Evolution of the brain and intelligence  
**Author:** Gerhard Roth,Ursula Dicke  
**Publication:** Trends in Cognitive Sciences  
**Publisher:** Elsevier  
**Date:** May 2005  
Copyright © 2005, Elsevier

Logged in as:  
R. Matthew Hutchison  
Account # 1  
3000513222

**Order Completed**  
Thank you very much for your order.

This is a License Agreement between R. Matthew Hutchison ("You") and Elsevier ("Elsevier"). The license consists of your order details, the terms and conditions provided by Elsevier, and the [payment terms and conditions](#).

[Get the printable license.](#)

License Number	2890071140201
License date	Apr 15, 2012
Licensed content publisher	Elsevier
Licensed content publication	Trends in Cognitive Sciences
Licensed content title	Evolution of the brain and intelligence
Licensed content author	Gerhard Roth,Ursula Dicke
Licensed content date	May 2005
Licensed content volume number	9
Licensed content issue number	5
Number of pages	8
Type of Use	reuse in a thesis/dissertation
Portion	figures/tables/illustrations
Number of figures/tables /illustrations	1
Format	both print and electronic
Are you the author of this Elsevier article?	No
Order reference number	Brain connectivity studied by fMRI: homologous network organization in the rat, monkey and human
Title of your thesis/dissertation	
Expected completion date	Jul 2012
Estimated size (number of pages)	300
Elsevier VAT number	GB 494 6272 12
Permissions price	0.00 USD
VAT/Local Sales Tax	0.0 USD / 0.0 GBP
Total	0.00 USD



RightsLink®

Home Account Info Help



**Title:** Resting-State Connectivity Identifies Distinct Functional Networks in Macaque Cingulate Cortex

**Author:** R.Matthew Hutchison, Thilo Womelsdorf, Joseph S. Gati, L.Stan Leung, Ravi S. Menon, Stefan Everling

**Publication:** Cerebral Cortex

**Publisher:** Oxford University Press

**Date:** 08/11/2011

Copyright © 2011, Oxford University Press

Logged in as:  
R. Matthew Hutchison

[Logout](#)

**Order Completed**

Thank you very much for your order.

This is a License Agreement between R. Matthew Hutchison ("You") and Oxford University Press ("Oxford University Press"). The license consists of your order details, the terms and conditions provided by Oxford University Press, and the [payment terms and conditions](#).

[Get the printable license.](#)

License Number 2873720845461  
 License date Mar 21, 2012  
 Licensed content Oxford University Press  
 publisher  
 Licensed content Cerebral Cortex  
 publication  
 Licensed content title Resting-State Connectivity Identifies Distinct Functional Networks in Macaque Cingulate Cortex  
 Licensed content author R.Matthew Hutchison, Thilo Womelsdorf, Joseph S. Gati, L.Stan Leung, Ravi S. Menon, Stefan Everling  
 Licensed content date 08/11/2011  
 Type of Use Thesis/Dissertation  
 Requestor type Academic/Educational institute  
 Format Print and electronic  
 Portion Figure/table  
 Number of figures/tables 1  
 Will you be translating? No  
 Author of this OUP article Yes  
 Order reference number  
 Title of your thesis / dissertation Brain connectivity studied by fMRI: homologous network organization in the rat, monkey and human  
 Expected completion date Jul 2012  
 Estimated size(pages) 300

**Rights and Permissions**

**Copyright and License to Publish**

Beginning with articles submitted in Volume 106 (2009) the author(s) retains copyright to individual articles, and the National Academy of Sciences of the United States of America retains an exclusive license to publish these articles and holds copyright to the collective work.

Volumes 90–105 (1993–2008), copyright © by the National Academy of Sciences. Volumes 1–89 (1915–1992), the author(s) retains copyright to individual articles, and the National Academy of Sciences holds copyright to the collective work.

The PNAS listing on the Sherpa RoMEO publisher copyright policies & self-archiving detail pages can be found [here](#).

**Rights and Permissions**

- Author Rights and Permissions
- FAQ
- Requests for Permission to Reprint
- Requests for Permission to Photocopy

**1 Requests for Permission to Reprint**

Requests for permission should be made in writing. For the fastest response time, please send your request via e-mail to [PNASPermissions@pnas.edu](mailto:PNASPermissions@pnas.edu). If necessary, requests may be faxed to 1-202-334-2739 or mailed to:

PNAS Permissions Editor  
 700 11th Street, NW  
 Suite 450  
 Washington, DC 20001 USA  
 Phone 1-202-334-2679

Anyone may, without requesting permission, use original figures or tables published in PNAS for noncommercial and educational use (i.e., in a review article, in a book that is not for sale) provided that the original source and the applicable copyright notice are cited.

For permission to reprint material in volumes 1–89 (1915–1992), requests should be addressed to the original authors, who hold the copyright. The full journal reference must be cited.

For permission to reprint material in volumes 90–105 (1993–2008), requests must be sent via e-mail, fax, or mail and include the following information about the original material:

1. Your full name, affiliation, and title
2. Your complete mailing address, phone number, fax number, and e-mail address



RightsLink®

- [Home](#)
- [Account Info](#)
- [Help](#)



**Title:** Cytoarchitecture and cortical connections of the posterior cingulate and adjacent somatosensory fields in the rhesus monkey  
**Author:** R.J. Morecraft, P.B. Cipolloni, K.S. Stilwell-Morecraft, M.T. Gedney, D.N. Pandya  
**Publication:** Journal of Comparative Neurology  
**Publisher:** John Wiley and Sons  
**Date:** Jan 26, 2004  
 Copyright © 2003 Wiley-Liss, Inc.

Logged in as:  
 R. Matthew Hutchison  
 Account #: 3000513222

[LOGOUT](#)

**Order Completed**

Thank you very much for your order.

This is a License Agreement between R. Matthew Hutchison ("You") and John Wiley and Sons ("John Wiley and Sons"). The license consists of your order details, the terms and conditions provided by John Wiley and Sons, and the [payment terms and conditions](#).

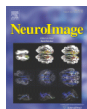
[Get the printable license.](#)

License Number	2874860370419
License date	Mar 23, 2012
Licensed content publisher	John Wiley and Sons
Licensed content publication	Journal of Comparative Neurology
Licensed content title	Cytoarchitecture and cortical connections of the posterior cingulate and adjacent somatosensory fields in the rhesus monkey
Licensed content author	R.J. Morecraft, P.B. Cipolloni, K.S. Stilwell-Morecraft, M.T. Gedney, D.N. Pandya
Licensed content date	Jan 26, 2004
Start page	37
End page	69
Type of use	Dissertation/Thesis
Requester type	University/Academic
Format	Print and electronic
Portion	Figure/table
Number of figures/tables	1
Original Wiley figure/table number(s)	Panel of Figure 5.
Will you be translating?	No
Order reference number	
Total	0.00 USD



RightsLink®

- [Home](#)
- [Account Info](#)
- [Help](#)



**Title:** Mapping the functional connectivity of anterior cingulate cortex  
**Author:** Daniel S. Margulies, A.M. Clare Kelly, Lucina Q. Uddin, Bharat B. Biswal, F. Xavier Castellanos, Michael P. Milham  
**Publication:** NeuroImage  
**Publisher:** Elsevier  
**Date:** 15 August 2007  
 Copyright © 2007, Elsevier

Logged in as:  
 R. Matthew Hutchison

[LOGOUT](#)

**Order Completed**

Thank you very much for your order.

This is a License Agreement between R. Matthew Hutchison ("You") and Elsevier ("Elsevier"). The license consists of your order details, the terms and conditions provided by Elsevier, and the [payment terms and conditions](#).

[Get the printable license.](#)

License Number	2873720087534
License date	Mar 21, 2012
Licensed content publisher	Elsevier
Licensed content publication	NeuroImage
Licensed content title	Mapping the functional connectivity of anterior cingulate cortex
Licensed content author	Daniel S. Margulies, A.M. Clare Kelly, Lucina Q. Uddin, Bharat B. Biswal, F. Xavier Castellanos, Michael P. Milham
Licensed content date	15 August 2007
Licensed content volume number	37
Licensed content issue number	2
Number of pages	10
Type of Use	reuse in a thesis/dissertation
Portion	figures/tables/illustrations
Number of figures/tables /illustrations	1
Format	both print and electronic
Are you the author of this Elsevier article?	No
Will you be translating?	No
Order reference number	
Title of your thesis/dissertation	Brain connectivity studied by fMRI: homologous network organization in the rat, monkey and human
Expected completion date	Jul 2012



RightsLink®

- [Home](#)
- [Account Info](#)
- [Help](#)



**Title:** Effects of heartbeat and respiration on macaque fMRI: Implications for functional connectivity  
**Author:** Tobias Teichert, Jack Grinband, Joy Hirsch, Vincent P. Ferrera  
**Publisher:** Neurophysiologia  
**Date:** June 2010  
 Copyright © 2010, Elsevier

Logged in as:  
 R. Matthew Hutchison  
 Account #: 3000513222

[LOGOUT](#)

**Order Completed**

Thank you very much for your order.

This is a License Agreement between R. Matthew Hutchison ("You") and Elsevier ("Elsevier"). The license consists of your order details, the terms and conditions provided by Elsevier, and the [payment terms and conditions](#).

[Get the printable license.](#)

License Number	2874051088638
License date	Mar 22, 2012
Licensed content publisher	Elsevier
Licensed content publication	Neurophysiologia
Licensed content title	Effects of heartbeat and respiration on macaque fMRI: Implications for functional connectivity
Licensed content author	Tobias Teichert, Jack Grinband, Joy Hirsch, Vincent P. Ferrera
Licensed content date	June 2010
Licensed content volume number	48
Licensed content issue number	7
Number of pages	9
Type of Use	reuse in a thesis/dissertation
Portion	figures/tables/illustrations
Number of figures/tables /illustrations	1
Format	both print and electronic
Are you the author of this Elsevier article?	No
Will you be translating?	No
Order reference number	
Title of your thesis/dissertation	Brain connectivity studied by fMRI: homologous network organization in the rat, monkey and human
Expected completion date	Jul 2012



RightsLink®

- [Home](#)
- [Account Info](#)
- [Help](#)



RightsLink®

- [Home](#)
- [Account Info](#)
- [Help](#)

**Title:** Intrinsic functional architecture in the anaesthetized monkey brain  
**Author:** Ed Bullmore and Olaf Sporns  
**Publisher:** Nature Reviews Neuroscience  
**Date:** Feb 4, 2009  
 Copyright © 2009, Rights Managed by Nature Publishing Group

Logged in as:  
 R. Matthew Hutchison  
 Account #: 3000513222

[LOGOUT](#)

**Order Completed**

Thank you very much for your order.

This is a License Agreement between R. Matthew Hutchison ("You") and Nature Publishing Group ("Nature Publishing Group"). The license consists of your order details, the terms and conditions provided by Nature Publishing Group, and the [payment terms and conditions](#).

[Get the printable license.](#)

License Number	289060637942
License date	Apr 15, 2012
Licensed content publisher	Nature Publishing Group
Licensed content publication	Nature Reviews Neuroscience
Licensed content title	Complex brain networks: graph theoretical analysis of structural and functional systems
Licensed content author	Ed Bullmore and Olaf Sporns
Licensed content date	Feb 4, 2009
Type of Use	reuse in a thesis/dissertation
Volume number	10
Issue number	3
Requester type	academic/educational
Format	print and electronic
Portion	figures/tables/illustrations
Number of figures/tables /illustrations	1
High-res required	no
Figures	Table 1
Author of this NPG article	no
Your reference number	
Title of your thesis / dissertation	Brain connectivity studied by fMRI: homologous network organization in the rat, monkey and human
Expected completion date	Jul 2012



RightsLink®

[Home](#) [Account Info](#) [Help](#)


**Title:** Exploring complex networks  
**Author:** Steven H. Strogatz  
**Publication:** Nature  
**Publisher:** Nature Publishing Group  
**Date:** Mar 8, 2001  
 Copyright © 2001, Rights Managed by Nature Publishing Group

Logged in as:  
 R. Matthew Hutchison  
 Account #: 3000513222

[Logout](#)
**Order Completed**

Thank you very much for your order.

This is a License Agreement between R. Matthew Hutchison ("You") and Nature Publishing Group ("Nature Publishing Group"). The license consists of your order details, the terms and conditions provided by Nature Publishing Group, and the [payment terms and conditions](#).

[Get the printable license.](#)

License Number	2890060807248
License date	Apr 15, 2012
Licensed content publisher	Nature Publishing Group
Licensed content publication	Nature
Licensed content title	Exploring complex networks
Licensed content author	Steven H. Strogatz
Licensed content date	Mar 8, 2001
Type of Use	reuse in a thesis/dissertation
Volume number	410
Issue number	6825
Requestor type	academic/educational
Format	print and electronic
Portion	figures/tables/illustrations
Number of figures/tables/illustrations	2
Figures	Figure 1 and Figure 2
Author of this NPG article	no
Your reference number	
Title of your thesis / dissertation	Brain connectivity studied by fMRI: homologous network organization in the rat, monkey and human
Expected completion date	Jul 2012
Estimated size (number of pages)	300
Total	0.00 USD



RightsLink®

[Home](#) [Account Info](#) [Help](#)


**Title:** Spontaneous fluctuations in brain activity observed with functional magnetic resonance imaging  
**Author:** Michael D. Fox and Marcus E. Raichle  
**Publication:** Nature Reviews Neuroscience  
**Publisher:** Nature Publishing Group  
**Date:** Sep 1, 2007  
 Copyright © 2007, Rights Managed by Nature Publishing Group

Logged in as:  
 R. Matthew Hutchison  
 Account #: 3000513222

[Logout](#)
**Order Completed**

Thank you very much for your order.

This is a License Agreement between R. Matthew Hutchison ("You") and Nature Publishing Group ("Nature Publishing Group"). The license consists of your order details, the terms and conditions provided by Nature Publishing Group, and the [payment terms and conditions](#).

[Get the printable license.](#)

License Number	2890061038259
License date	Apr 15, 2012
Licensed content publisher	Nature Publishing Group
Licensed content publication	Nature Reviews Neuroscience
Licensed content title	Spontaneous fluctuations in brain activity observed with functional magnetic resonance imaging
Licensed content author	Michael D. Fox and Marcus E. Raichle
Licensed content date	Sep 1, 2007
Type of Use	reuse in a thesis/dissertation
Volume number	8
Issue number	9
Requestor type	academic/educational
Format	print and electronic
Portion	figures/tables/illustrations
Number of figures/tables/illustrations	1
High-res required	no
Figures	Figure 1
Author of this NPG article	no
Your reference number	
Title of your thesis / dissertation	Brain connectivity studied by fMRI: homologous network organization in the rat, monkey and human



RightsLink®

[Home](#) [Account Info](#) [Help](#)


**Title:** Centenary of Brodmann's map (mdash) conception and fate  
**Author:** Karl Zilles and Katrin Amunts  
**Publication:** Nature Reviews Neuroscience  
**Publisher:** Nature Publishing Group  
**Date:** Jan 4, 2010  
 Copyright © 2010, Rights Managed by Nature Publishing Group

Logged in as:  
 R. Matthew Hutchison  
 Account #: 3000513222  
[LOGOUT](#)

**Order Completed**

Thank you very much for your order.

This is a License Agreement between R. Matthew Hutchison ("You") and Nature Publishing Group ("Nature Publishing Group"). The license consists of your order details, the terms and conditions provided by Nature Publishing Group, and the [payment terms and conditions](#).

[Get the printable license.](#)

License Number	2890061270740
License date	Apr 15, 2012
Licensed content publisher	Nature Publishing Group
Licensed content publication	Nature Reviews Neuroscience
Licensed content title	Centenary of Brodmann's map (mdash) conception and fate
Licensed content author	Karl Zilles and Katrin Amunts
Licensed content date	Jan 4, 2010
Type of Use	reuse in a thesis/dissertation
Volume number	11
Issue number	2
Requestor type	academic/educational
Format	print and electronic
Portion	figures/tables/illustrations
Number of figures/tables/illustrations	1
High-res required	no
Figures	Figure 2
Author of this NPG article	no
Your reference number	
Title of your thesis / dissertation	Brain connectivity studied by fMRI: homologous network organization in the rat, monkey and human
Expected completion date	Jul 2012
Estimated size (number of pages)	300



RightsLink®

[Home](#) [Account Info](#) [Help](#)


**Title:** Complex network measures of brain connectivity: Uses and interpretations  
**Author:** Mikail Rubinov, Olaf Sporns  
**Publication:** NeuroImage  
**Publisher:** Elsevier  
**Date:** September 2010  
 Copyright © 2010, Elsevier

Logged in as:  
 R. Matthew Hutchison  
 Account #: 3000513222  
[LOGOUT](#)

**Order Completed**

Thank you very much for your order.

This is a License Agreement between R. Matthew Hutchison ("You") and Elsevier ("Elsevier"). The license consists of your order details, the terms and conditions provided by Elsevier, and the [payment terms and conditions](#).

[Get the printable license.](#)

License Number	2890070132019
License date	Apr 15, 2012
Licensed content publisher	Elsevier
Licensed content publication	NeuroImage
Licensed content title	Complex network measures of brain connectivity: Uses and interpretations
Licensed content author	Mikail Rubinov, Olaf Sporns
Licensed content date	September 2010
Licensed content volume number	52
Licensed content issue number	3
Number of pages	11
Type of Use	reuse in a thesis/dissertation
Portion	figures/tables/illustrations
Number of figures/tables/illustrations	1
Format	both print and electronic
Are you the author of this Elsevier article?	No
Will you be translating?	No
Order reference number	
Title of your thesis / dissertation	Brain connectivity studied by fMRI: homologous network organization in the rat, monkey and human
Expected completion date	Jul 2012
Estimated size (number of pages)	300
Elsevier VAT number	GB 494 6272 12
Permissions price	0.00 USD
VAT/Local Sales Tax	0.0 USD / 0.0 GBP

Rightslink® by Copyright Clearance Center

https://s100.copyright.com/AppDispatchServlet



Home Account Info Help



**Title:** Forward frontal fields: phylogeny and fundamental function  
**Author:** Steven P. Wise  
**Publication:** Trends in Neurosciences  
**Publisher:** Elsevier  
**Dates:** December 2008  
 Copyright © 2008, Elsevier

Logged in as:  
 R. Matthew Hutchison  
 Account #: 3000513222  
 LOGOUT

**Order Completed**

Thank you very much for your order.

This is a License Agreement between R. Matthew Hutchison ("You") and Elsevier ("Elsevier"). The license consists of your order details, the terms and conditions provided by Elsevier, and the [payment terms and conditions](#).

[Get the printable license.](#)

License Number	2890070282277
License date	Apr 15, 2012
Licensed content publisher	Elsevier
Licensed content publication	Trends in Neurosciences
Licensed content title	Forward frontal fields: phylogeny and fundamental function
Licensed content author	Steven P. Wise
Licensed content date	December 2008
Licensed content volume number	31
Licensed content issue number	12
Number of pages	10
Type of Use	reuse in a thesis/dissertation
Portion	figures/tables/illustrations
Number of figures/tables/illustrations	1
Format	both print and electronic
Are you the author of this Elsevier article?	No
Will you be translating?	No
Order reference number	
Title of your thesis/dissertation	Brain connectivity studied by fMRI: homologous network organization in the rat, monkey and human
Expected completion date	Jul 2012
Estimated size (number of pages)	300
Elsevier VAT number	GB 494 6272 12
Permissions price	0.00 USD
VAT/Local Sales Tax	0.0 USD / 0.0 GBP

1 of 2

12-04-15 3:01 AM

Rightslink® by Copyright Clearance Center

https://s100.copyright.com/AppDispatchServlet



Home Account Info Help



**Title:** Functional connectivity in the motor cortex of resting human brain using echo-planar mri  
**Author:** Bharat Biswal, F. Zerrin Yetkin, Victor M. Haughton, James S. Hyde  
**Publication:** Magnetic Resonance in Medicine  
**Publisher:** John Wiley and Sons  
**Dates:** Nov 21, 2005  
 Copyright © 1995 Wiley-Liss, Inc., A Wiley Company

Logged in as:  
 R. Matthew Hutchison  
 Account #: 3000513222  
 LOGOUT

**Order Completed**

Thank you very much for your order.

This is a License Agreement between R. Matthew Hutchison ("You") and John Wiley and Sons ("John Wiley and Sons"). The license consists of your order details, the terms and conditions provided by John Wiley and Sons, and the [payment terms and conditions](#).

[Get the printable license.](#)

License Number	2890070810496
License date	Apr 15, 2012
Licensed content publisher	John Wiley and Sons
Licensed content publication	Magnetic Resonance in Medicine
Licensed content title	Functional connectivity in the motor cortex of resting human brain using echo-planar mri
Licensed content author	Bharat Biswal, F. Zerrin Yetkin, Victor M. Haughton, James S. Hyde
Licensed content date	Nov 21, 2005
Start page	537
End page	541
Type of use	Dissertation/Thesis
Requestor type	University/Academic
Format	Print and electronic
Portion	Figure/table
Number of figures/tables	1
Original Wiley figure/table number(s)	3
Will you be translating?	No
Order reference number	
Total	0.00 USD

[ORDER MORE](#) [CLOSE WINDOW](#)

Copyright © 2012 Copyright Clearance Center, Inc. All Rights Reserved. [Privacy statement](#).  
 Comments? We would like to hear from you. E-mail us at [customercare@copyright.com](mailto:customercare@copyright.com)

1 of 2

12-04-15 3:10 AM

## Curriculum Vitae

---

**Date of Birth:** 11<sup>th</sup> January 1985

**Nationality:** Canadian

**Tel:** X.XXX.XXX.XXX

**Fax:** X.XXX.XXX.XXXX

**Email:** XXXXXXXX@uwo.ca

---

### Research Interests

- Mapping large-scale brain networks using resting-state functional MRI
- Characterizing network homologies between humans and animal models
- Exploring the alteration of functional brain connectivity in disease states
- Applications of multivariate analysis techniques
- Investigating the functional role of coherent neural oscillations

### Education

2007 – 2012

**Ph.D. Neuroscience**

University of Western Ontario, Canada

Thesis Title: *Brain connectivity studied by fMRI: Homologous network organization in the rat, monkey, and human*

Supervisors: Dr. L.S. Leung & Dr. S.M. Mirsattari

2003 – 2007

**B.Sc. with Honors in Physiology and Psychology**

University of Western Ontario, Canada

### Honors and Awards

2012 – 2015

Canadian Institute of Health Research (CIHR) Fellowship Award  
(\$45,000 per annum)

2012

Graduate Thesis Research Award (\$1500)

2010 – 2013

Natural Sciences and Engineering Research Council (NSERC) Award  
PGS-D (\$21,000 per annum)

2011, 2012

Academic All-Canadian Award

2009 – 2010

Ontario Graduate Scholarship for Sciences and Technology  
(\$15,000 per annum)

2007 – 2012

Western Graduate Research Scholarship (\$8,300 per annum)

2003 – 2007

Dean's Honors List in Science

2003

University of Western Ontario Entrance Award (\$2,500)

## Publications and Presentations

### Journal articles published/in press (10)

**Hutchison, R.M.**, Everling, S. 2012. Monkey in the middle: Why non-human primates are needed to bridge the gap in resting-state investigations. *Frontiers in Neuroanatomy*. *In press*.

**Hutchison, R.M.**, Gallivan, J.P., Gati, J.S., Menon, R.S., Everling, S. 2012. Functional connectivity of the frontal eye fields in humans and macaque monkeys investigated with resting-state fMRI. *Journal of Neurophysiology*, *in press*.

**Hutchison, R.M.**, Womelsdorf, T, Gati, J.S., Everling, S., Menon, R.S. 2012 Resting-state networks show dynamic functional connectivity in awake humans and anesthetized macaques. *Human Brain Mapping*, *in press*.

Wang, Z., Norton, L., **Hutchison, R.M.**, Ives, J.R., Mirsattari, S.M. 2012. Spontaneous EEG-functional MRI in mesial temporal lobe epilepsy: implications for the neural correlates of consciousness. *Epilepsy Research and Treatment*, 2012, 385626.

Norton, L., **Hutchison, R.M.**, Young, G.B., Sharpe, M., Lee, D., Mirsattari, S.M. 2012. Disruptions of functional connectivity in default mode network predict outcome of comatose patients. *Neurology*, 78, 175-181.

Kaping, D., Vinick, M., **Hutchison, R.M.**, Everling, S., Womelsdorf, T. 2011. Specific contributions of ventromedial frontal, anterior cingulate and lateral prefrontal cortex for attentional selection and stimulus valuation. *PLoS Biology*, 9: e1001224.

*\*Featured as the journal editor's selection: Weaver, J. 2011. How the brain homes in on valuable objects. PLoS Biology 9: e10012284.*

**Hutchison, R.M.**, Womelsdorf, T., Gati, J.S., Leung, L.S., Menon, R.S., Everling, S. 2011. Resting-state connectivity identifies distinct functional networks in macaque cingulate cortex. *Cerebral Cortex*, doi: 10.1093/cercor/bhr181.

**Hutchison, R.M.**, Leung, L.S., Mirsattari, S.M., Gati, J.S., Menon, R.S., Everling S., 2011. Resting-state networks in the macaque at 7 T. *NeuroImage* 56, 1546-1555.

*\*Featured as the journal cover image.*

**Hutchison, R.M.**, Mirsattari, S.M., Jones, C.K., Gati, J.S., Leung, L.S., 2010. Functional networks in the anesthetized rat brain revealed by independent component analysis of resting-state fMRI. *Journal of Neurophysiology* 103, 3398-3406.

**Hutchison, R.M.**, Chidiac, P., Leung, L.S., 2009. Hippocampal long-term potentiation is enhanced in urethane-anesthetized RGS2 knockout mice. *Hippocampus* 19, 687-691.

### **Journal articles in revision/under review (1)**

Shen, K., Bezgin, G., **Hutchison, R.M.**, Gati, J., Menon, R., Everling, S., McIntosh, A.R. Anatomical architecture supports functional community structure in the macaque cortex.

### **Invited Talks (3)**

**Hutchison, R.M.** Monkeying around: Resting-state fMRI investigations of the macaque. Harvard University, MA, USA, June 2012.

**Hutchison, R.M.** Functionally connected: Network organization of the rat, monkey, and human. *Johns Hopkins University, MD, USA, Nov 2011.*

**Hutchison, R.M.** The intrinsic properties of the brain: The resting-state AND The convergence of art and science. *University of Western Ontario, ON, Canada, Oct 2011.* Invited speaker for Subtle Technologies, “The Art and Science of Brain Imaging” workshop.

### **Presentations and Posters (14)**

**Hutchison, R.M.**, Gallivan, J.P., Culham, J.C., Gati, J.S., Menon, R.S., Everling, S. Functional connectivity of the frontal eye fields in humans and macaque monkeys investigated with resting-state fMRI. Biennial Conference on Resting State Brain Connectivity, Sept 2012.

**Hutchison, R.M.**, Gallivan, J.P., Culham, J.C., Gati, J.S., Menon, R.S., Everling, S. Homologous functional connectivity architecture of the monkey and human saccade-related networks. Society for Neuroscience, Oct 2012.

Shen, K., Bezgin, G., **Hutchison, R.M.**, Gati, J., Menon, R., Everling, S. McIntosh, A.R. Anatomical connectivity supports functional community structure in macaque cortex. Society for Neuroscience, Oct 2012.

Shen, K., Bezgin, G., **Hutchison, R.M.**, Gati, J., Menon, R., McIntosh, A.R., Everling, S. Resting-state connectivity reflects underlying anatomical structure in the macaque cortex. *Organization for Human Brain Mapping, June 2012.*

**Hutchison, R.M.**, Womelsdorf, T., Gati, J.S., Menon, R.S., Everling, S. Dynamic resting-state correlations in anesthetized macaques. *Society for Neuroscience, Nov 2011.*

Babapoor-Farrokhran, S., **Hutchison, R.M.**, Gati, J.S., Menon, R.S., Everling, S. Resting-state fMRI as a tool to localize putative saccade-related brain areas in nonhuman primates. *Society for Neuroscience, Nov 2011.*

**Hutchison, R.M.**, Leung, L.S., Mirsattari, S.M., Gati, J.S., Menon, R.S., Everling S. Functional networks in the macaque brain revealed by independent component

analysis of resting-state fMRI. *International Society for Magnetic Resonance in Medicine*, May 2011.

**Hutchison, R.M.**, Gati, J.S., Leung, L.S., Menon, R.S., Everling, S. Mapping the functional connectivity of the ACC in the non-human primate. *Society for Neuroscience*, Nov 2010.

Norton, L., **Hutchison, R.M.**, Lee, D., Sharpe, M., Young, G.B., Mirsattari, S.M. An fMRI study of the Default Mode Network Connectivity in Comatose Patients. *The Association for the Scientific Study of Consciousness*, June 2010.

**Hutchison, R.M.**, Mirsattari, S.M., Jones, C.K., Gati, J.S., Leung, L.S. Functional connectivity of the anesthetized rat brain. *International Society for Magnetic Resonance in Medicine*, May 2010.

**Hutchison, R.M.**, Mirsattari, S.M., Leung, L.S. Functional activation and connectivity associated with the hippocampal theta rhythm. *The American Epilepsy Society*, Dec 2008.

**Hutchison, R.M.**, Mirsattari, S.M., Leung, L.S. Functional activation and connectivity associated with the hippocampal theta rhythm. *Society for Neuroscience*, Nov 2008.

**Hutchison, R.M.** Simultaneous EEG-fMRI: Applications for epilepsy research. *Epilepsy Research Day*, London Health Sciences Centre, Jun 2008.

**Hutchison, R.M.** Converging Operations and the use of simultaneous multimodal techniques. *Western Research Forum*, Western University, Mar 2008.

## Teaching Experience

2010 – 2011	Lecturer and teaching assistant
2009 – 2010	Neuroscience 9500: Principles of Neuroscience Dept. of Neuroscience Graduate-level research course Lectured as part of a multi-professor format, wrote and graded tests, and taught tutorial component of the course.
2008 – 2009	Teaching assistant
2007 – 2008	Psychology 2800E: Research Methods Dept. of Psychology Independently taught and graded laboratory component of the course.

## Other Scientific Activities and Contributions

Ad-hoc reviewer of submitted manuscripts for Journal of Neuroscience (1), Human Brain Mapping (1), NeuroImage (2), and European Journal of Neuroscience (1).

Ad-hoc co-reviewer of submitted manuscripts for Nature Neuroscience (1), Journal of Neuroscience (4), Cerebral Cortex (2), NeuroImage (1), and Human Brain Mapping (1).

Member of the Society for Neuroscience (SFN) and the International Society for Magnetic Resonance in Medicine (ISMRM).

Lead member of Canadian Research Chair student selection committee (Apr 2011).

Work featured in the online edition of Scientific American (July 2011).

Journal article featured on the cover of NeuroImage (June 2011).

Work featured on the cover of Science News (Dec 2009).

### **Supervision and Mentoring**

2012 – present     *Justin Arcaro*  
Master's student in neuroscience graduate program

2011 – present     *Sahand Babapoor-Farrokhran*  
Ph.D. candidate in neuroscience graduate program

## **Personal Activities and Accomplishments**

### **Athletics**

Western University varsity wrestling team (2009 – 2012)

Leyshon trophy (2012): Most dedicated team member.

1<sup>st</sup> Colour Award (2011, 2012).

Provincial team champions (2012).

Coaching and competing in mixed martial arts (2000 – present).